SOIL STRUCTURE AND TENSILE STRENGTH IN RELATION TO THE MICROTOPOGRAPHY OF SOIL FRACTURE SURFACES

A thesis presented in fulfilment of the requirements for

the Degree of Doctor of Philosophy,

Faculty of Agricultural Science,

The University of Adelaide

by

CAMERON DOUGLAS GRANT

Department of Soil Science

Waite Agricultural Research Institute

The University of Adelaide

FEBRUARY 1989.

Table of Contents

Table of Contents (cont'd.)

Table of Contents (cont'd.)

List of Figures

List of Figures (cont'd)

List of Figures (cont'd)

List of Figures (cont'd)

List of Figures (cont'd)

List of Tables

List of Tables (cont'd)

List of Tables (cont'd)

List of Tables (cont'd)

List of Plates

List of Appendices

SUMMARY

Tillage for the preparation of seedbeds in dryland agriculture is a major problem worldwide, and involves the management of brittle fracture of unsaturated soils to minimize cloddiness and deep compaction. Management of brittle fracture is particularly important, for example, in tropical regions where flooded rice crops are often grown in rotation with a dryland crop each year. The transition of soil from the puddled state, after rice harvest, to a friable state for establishment of the dryland crop is extremely difficult because it requires the soil to be dried out to a considerable extent prior to tillage. This may take weeks or even months.

While many soils have severe tillage problems, there are some soils (grouped with the Vertisols, and located mainly in India, Australia and Africa) which have the natural capacity to crumble into a friable state after only a few wetting and drying cycles. This ability of soils to crumble naturally is termed "self-mulching". No single property, or single combination of properties has been identified which is responsible for this phenomenon. Other soil may also possess some potential for natural regeneration of structure in compacted and damaged non-vertisols. Even if the self-mulching process cannot be exactly imitated in non-vertisols, if it were at least possible to induce 'problem soils' to crack extensively, the energy needed for their cultivation could be reduced significantly.

Cracks such as those produced during drying or cultivation of soil involve brittle fracture under tensile stress. Thus, an understanding and ability to characterize the mechanism of such failure should increase the possibility that cracking can be enhanced by suitable management techniques. Brittle fracture is controlled by the distribution of microscopic flaws in the soil. These flaws can be air-filled pores, micro-cracks, organic and inorganic inclusions, and other irregularities in the soil matrix. Management practices that influence the dispersion of flaw strengths in the soil may also affect the brittle behaviour of the soil under tensile

stresses. Controlled rapid wetting, for example, has recently been shown to induce anisotropic cracking in soil, which strongly affects its tensile strength.

The theoretical understanding of brittle fracture is further advanced than our ability to characterize it. This is partly because the methods currently in use (eg. %size-stability, friability, etc.) remain time-consuming and tedious to perform. Simpler methods for measuring the effects of different management practices on brittle fracture of soils would therefore be quite useful.

The objectives of this study were therefore to:

(1) develop and interpret a new method for characterizing brittle fracture of soils under tensile stress, using soils subject to a range of different soil management practices common in Southern Australia, and to

(2) investigate, further, the phenomenon of mellowing in poorly structured soils, through rapid wetting, in order to better understand the applicability of previously published results to soil-water-conditions found in the field.

(1). Development of a Method to Characterize Brittle Fracture:

The idea is investigated that an applied tensile stress will cause unsaturated soil to fracture along a pathway determined by the dispersion of weakest internal flaw strengths. It is proposed that any failure surface produced under tensile stress contains a blueprint of the fracture pathway, and that the topography of this surface contains clues regarding the spatial distribution of the soil's internal flaws. The topography of soil fracture surfaces is therefore a measure of this dispersion of strengths. Soils were fractured under indirect tension and cross-sectional profiles of the fracture surfaces were analysed at a resolution of 0.1mm. Two different techniques were developed for this purpose: (i) a single-transect method and (ii) a multiple-transect method, both of which produced essentially the same information.

Techniques investigated for analysing the topographical transect data included (i) Fourier spectral analysis, (ii) Semi-variogram analysis, and (iii) Rugosity analysis. Rugosity analysis was found to be the most informative technique. The rugosity of a linear transect across a soil fracture surface is defined as the standard deviation of the difference between the surface-elevation and the running-mean-surface-elevation.

Theory on the spatial distribution of flaws and cracks in relation to the soil water content and suction is presented and related to the fracture surface rugosity. It is shown that there is a linear relationship between the soil water content at time of tensile failure and the spatial distribution of flaws in the soil (measured by fracture surface rugosity). In this context, the flaws in unsaturated, uncemented soils are simply the air-filled pores.

The effects of calcium and organic matter (which are important to soil workability) on the fracture surface rugosity were also investigated. It was found that the amount of applied calcium was negatively correlated with the fracture surface rugosity, and reasons for this are discussed. Organic matter was found to have a variable effect on the rugosity, depending on whether the water content at the time of fracture was above or below the lower plastic limit.

(2) Investigation of Mellowing

The role of water in the mellowing (or weakening by wetting and/or drying) of soils is investigated in two main studies. One study looks at the relative significance of air entrapment versus uneven swelling on the tensile strength of moulded soils having different clay contents and mineralogies. The study was conducted using a combination of different environmental air pressures, as well as polar and non-polar wetting fluids. On the basis of measured wetting rates and tensile strengths, it was found that air entrapment on its own did not generate sufficient stresses during wetting to initiate cracking. Furthermore, differential swelling on its own had limited ability to initiate

cracking and its effects appeared to be related to clay and organic matter contents. Most significant was the finding that a synergistic effect existed between air entrapment and differential swelling such that when both processes acted together, cracking and a major reduction in tensile strength of moulded soils occurred.

The other study reports on the use of different initial water contents and wetting rates to examine the limiting conditions associated with the mellowing process. Tensile strengths and fracture surface rugosities are measured and discussed in relation to microcracking in moulded soils. New terminology is introduced to describe the rate of wetting needed to induce mellowing. It was found that rapid wetting was capable of inducing microcracking in soils even when the initial soil water matric potential was as high as only -1 to -1.5 MPa (10-15 bar). Implications for soil and water management are briefly considered. Visual and analytical evidence from photographs and computer images indicates that internal microcracking is almost always detectable whenever the wetting rate is sufficiently high to reduce the soil tensile strength.

STATEMENT

This thesis contains no material which has been accepted for the award of any other degree or diploma in any university. To the best of the author's knowledge and belief, this thesis contains no material previously published or written by another person, except where due reference is made in the text of the thesis.

I consent to this thesis being made available for photocopying and loan.

CAMERON DOUGLAS GRANT

February, 1989.

Acknowledgements

A. Research Support

I would like to thank my supervisors, Dr. A.R. Dexter, and Professor J.M. Oades (Department of Soil Science) for their unqualified support throughout my research program. They provided very helpful discussion and direction in all of my research, and also valuable administrative support, especially during my application for research scholarships every year.

I would also like to thank Dr. R.S. Murray (Director's Research Unit, Waite Institute), and Dr. B. Jakobsen (Department of Soil Science) for their guidance and helpful discussion during numerous stages of the program. I am also grateful to Professor B.D. Kay (Chairman, Department of Land Resource Science, University of Guelph, Canada) who offered helpful criticism during the writing of this thesis, while he was on study-leave at the Waite.

I thank Dr. C. Huang (C.S.I.R.O. Division of Environmental Mechanics, Canberra) for his co-operation and help in conducting the laser-scanning experiments and in organizing the transfer of data from Canberra to Adelaide for analysis. I also thank Mr. T. Hancock (Biometry Section, Waite Institute) for the numerous occasions on which he clarified issues on the statistical analysis of my data. Mr. S. Eckert (Biometry Section, Waite Institute) helped in computer programming which enabled me to analyse the laser data on the VAX-system in Adelaide.

Thanks are also due to the indispensable Mr. P. Brown (Department of Soil Science, Waite Institute) who meticulously produced the diagrams for this thesis, and who also provided invaluable computer-programming assistance and help in the laboratory at various stages of the program. Mrs. A. Waters (Department of Soil Science) did all the organic carbon analyses and also the B.E.T. surface areas of the soils used in this program, for which I thank her. Thanks also go to Mr. D. Greguric (Department of Soil Science) who assisted with field sampling and computer scanning of some of the fracture surfaces. The photographs in this thesis were prepared by Mr. A Dunbar, Mr. B.A. Palk and Miss C. Clark.

Professor Y. Horikawa (Department of Agricultural Chemistry, Kochi University, Japan) kindly translated from Japanese into English, several important papers on the rapid wetting of paddy soils, for which I am grateful. I am also indebted to Dr. W.D. Kemper (Director, Snake River Conservation Research Centre, USDA-ARS, Kimberley, Idaho, USA) who supplied the Portneuf soil used in SECTION 7, and who also offered helpful advice for some of the experiments in SECTION 6.

I would like to thank Mrs. J. Ditchfield (Department of Soil Science) for her help in typing numerous manuscripts, as well as applications for travel funding, and also the staff of the Department for the wide range of support offered throughout my studies.

B. Financial Support

I am grateful to the Natural Sciences and Engineering Research Council of Canada for the award of a postgraduate scholarship for the period mid-1985 to mid-1988, which enabled me to study in Australia. I am also grateful to the University of Adelaide for providing an Adelaide University Postgraduate Research Award for the period mid-1988 to early-1989, which allowed me to finish my studies.

Invaluable financial support for travel and accommodation was provided by several organizations listed below, which made it possible for me to participate in conferences, and to conduct research at other institutions. I am very grateful to the following organizations:

1.(a) The Canadian Society of Soil Science, and
(b) the Waite Agricultural Research Institute (Research Committee) for funds to attend the 13th Congress of the International Society of Soil Science, Hamburg, West Germany. August, 1986.

2. Department of Soil Science (Waite Institute) for funds to attend the Australian Society of Soil Science (Riverina Branch) Conference, Deniliquin, N.S.W. May, 1987.

3. C.S.I.R.O. Division of Environmental Mechanics, Canberra, for travel funds to Canberra and for use of their laser-scanning device and computer facilities, September, 1987.

4. (a) The Australian Society of Soil Science, and
(b) the Department of Soil Science (Waite Institute) for funds to attend the Australian Society of Soil Science Inc., National Soils Conference, Canberra, A.C.T. May, 1988.

C. Other Support

Finally, I would like to offer special thanks to Rosie (and Barney), and also the people at Maughan Church, Adelaide Central Mission, for their patience and invaluable support, without which this study would not have been possible.

Section 1. INTRODUCTION

The preparation of seedbeds for dryland cropping is a worldwide problem. It is an expensive operation in terms of time, energy and money, and unless it is conducted when soil conditions are suitable, it can also be an inefficient and sometimes wasted effort. Good management of dryland tillage involves the timing of cultivation to match the most suitable soil water conditions, which lead to maximum brittle fracture (Kuipers, 1980; Warkentin, 1982). Unfortunately, the range of suitable water conditions within which tillage operations can be effective is only partly sensitive to soil management practices, and is mainly set by the prevailing climatic and environmental conditions, leaving little room for error (Dexter, 1988a). It is therefore important to understand the role that natural forces can play in the preparation of seedbeds.

In colder regions of the world for example, (Canada and Northern Europe) spring tillage operations are best conducted during a relatively short period, before which the soil is either frozen or else too wet to till (Bullock, et al, 1988), and after which the soil becomes too dry to till and the remaining available growing season becomes too short for crop production (Grevers and Bomke, 1986). If tillage operations are performed outside the optimum period, compaction problems can occur (Fippin, 1910; Monnier and Goss, 1987) and the resulting soil tilths are often very rough and cloddy (Low, 1972; Greenland, 1977). Thorough drying can sometimes reduce compaction problems (McGowan et al, 1983), but only in fine textured soils. Where freezing occurs extensively over winter, frost is sometimes relied upon to 'undo' some of the compaction problems at depth created by untimely tillage and heavy agricultural machinery (Gill, 1971; Håkansson and Danfors, 1981; Håkansson, 1985; Håkansson et al, 1987). It has been found by Voorhees (1983) and Kay et al (1985), however, that deep freezing even in 'frost susceptible' soils (cf. Penner, 1968) is not capable of reducing high bulk densities in fine textured soils in southern Canada. Kay et al (1985) found that ice lenses,

which formed over winter, introduced significant porosity only while the soil remained frozen. In spring, the soils quickly reconsolidated upon thawing, and bulk densities below the top few centimetres returned to near-pre-freezing values. Hence although freezing may be helpful in breaking up puddled soil (Koenigs, 1963) and surface clods (Salter, 1925; Kemper et al, 1987), it cannot be regarded as a panacea for poor soil management in these colder parts of the world.

In arid and semi-arid regions of the world, the soil is often tilled in the air-dry state which results in the formation of large, dense and hard clods. Seedbed preparation on these clod-forming soils (which have been estimated by Wolf and Luth (1977) to comprise approximately one third of the total tilled area of the world) requires much more energy than on soils in more temperate climates (Hadas and Wolf, 1983). Furthermore, tillage of these soils accelerates the decomposition of organic matter, which is quite low to begin with (Greacen, 1983), and this in turn reduces the structural stability of seedbed aggregates (Tisdall and Oades, 1979, 1980a,b, 1982), which makes them even more difficult to work.

Tillage is also a problem in tropical regions, particularly where rice-based cropping systems are dominant, (I.R.R.I., 1978; Bolton and De Datta, 1979). In these regions, two types of tillage operations are performed , both having opposing functions (Fagi and De Datta, 1983). The first type of tillage operation, puddling, is conducted when the soil is saturated and therefore destroys the soil structure (Bodman and Rubin, 1948; Sanchez, 1979). This reduces percolation and conserves water for transplanting and production of rice (Sanchez, 1973). The second type of tillage operation, which follows the rice harvest, is intended to regenerate soil aggregates from the puddled, (or moulded) state in order to make a seedbed for a subsequent dryland grain crop, such as sorghum or maize (Hundal and De Datta, 1984). The transition from lowland rice production to dryland crop production presents a huge problem because it requires that the soil be dried down to at least the lower plastic limit before tillage (Dexter, 1979; Ojeniyi and Dexter, 1979) which may take weeks or even months (Fujioka and Sato, 1968a,b; Sharma and De Datta,

1986). Where resources and technology are limiting factors, there is an urgent need to develop techniques to help farmers make a successful transition between wetland rice and upland crops with minimum use of mechanical energy (Mandal, 1984; U.S.D.A., 1985).

While many soils have severe tillage problems,as outlined above, it is known that some rice-producing soils in Southeast Asia, are capable of forming an aggregated state naturally during drying (Moormann and Van Breemann, 1978; Greenland, 1981). In addition, the self-mulching soils (cf. Blackmore, 1981)of the Darling Downs in Queensland, Australia are famous for their ability to regenerate a granular structure after only a few wetting and drying cycles (Coughlan et al, 1973; Coughlan, 1984). Although these soils are mainly vertisols, they do not share a narrow range of common features that adequately explains the basis for their unusual behaviour (Hubble, 1984; Probert, et al, 1987). With this in mind, it was thought that there exists some potential for the natural regeneration of cracks in compacted, cloddy and moulded soils that are not vertisolic in nature. Even if the self-mulching process cannot be exactly imitated in non-vertisolic soils, the formation of extensive cracking in these soils prior to their cultivation would markedly reduce the energy required to work them. In connection with this idea, there have been a few studies (eg. Peterson, 1943; Telfair et al, 1957) which indicate that there is some potential for structure regeneration in degraded non-vertisolic soils, and several recent studies (eg. Dexter, 1983; Dexter et al, 1984; McKenzie and Dexter, 1985) have indicated that mellowing (or reduction in tensile strength) of moulded, oven-dry soils can be induced through rapid wetting. Little is known yet, however, about the limiting conditions associated with mellowing of moulded soils under field conditions.

Possible solutions to the problems outlined above require an understanding of the phenomenon of brittle fracture, under tensile stresses, which have considerable agronomic importance. Tensile stresses in unsaturated soils are created during tillage operations (Koolen and Kuipers, 1983; Dexter and Woodhead, 1985; Stafford and Geikie, 1987) and they control the degree of fragmentation and crumbling which

results (Braunack and Dexter, 1978). Tensile stresses are also active in crack formation during drying of surface soils (Johnson and Hill, 1944; Johnson, 1962; Sharma and Verma, 1977) and clays (Towner, 1987a,b and 1988), and also of subsoils (White, 1966; 1967). The tensile strength of soil crusts often controls seedling emergence and crop productivity (Richards, 1953; Hanks and Thorp, 1957; Arndt, 1965). For brittle materials, when at least one of the principal stresses is compressive, shear processes are subsidiary to tensile stresses (Ingles and Lafeber, 1967). Tensile failure of aggregates and clods can therefore result indirectly from the application of compressive stresses (Dexter, 1988b).

The measurement of brittle fracture and tensile strength of soils has been the subject of studies by Marshall and Quirk (1950), Braunack et al (1979) and Snyder and Miller (1985). Each of these has made a major contribution to our theoretical understanding of brittle fracture in unsaturated soils. Methods for measuring the effects of different management practices on brittle fracture, however, remain time-consuming and tedious, and there is considerable room for improvement.

The objectives of this study were therefore to:

(1) develop and interpret a new method for quantifying structural features that influence brittle fracture of unsaturated soils under tensile stress, using soils subject to a range of different soil management practices common in Southern Australia, and to

(2) investigate, further, the phenomena of mellowing in poorly-structured soils through rapid wetting, in order to better understand the applicability of previous results to soil water conditions found in the field.

Section 2. LITERATURE REVIEW

2.1 Introduction

The literature reviewed in this section is related almost entirely to the tensile strength of unsaturated soils. Tensile strength, which is a well-defined physical property of matter, measures the true and apparent intergranular cohesion forces that bind soil particles together. The term 'cohesion', however, has several (somewhat related) meanings in the engineering, soil mechanics and soil science literature. This review first defines the meaning of soil cohesion as it will be used in this study, and then outlines the most important mechanisms of soil cohesion, and also the role of flaws and cracks as they relate to the brittle fracture of soils. The literature reviewed forms the background for the studies undertaken in this thesis, and will be restricted mainly to work published up until mid-1985, when this research project began. Reference to more recent literature is omitted except in cases where (i) the present author had access to draft-copies of manuscripts that have since been published, or where (ii) the reader is directed to recent advances on subjects of related, but peripheral interest to this study.

2.2 Soil Cohesion

'Cohesion' is considered to be a basic mechanical property of soils (Koolen and Vaandrager, 1984). In the engineering literature cohesion is designated '**c**', according to the theories of Coulomb, Hvorslev and Mohr, and is used to describe the τ-intercept of a plot of shear strength, τ, against the stress, σ, acting normally to the shear plane as determined from shear tests (Jumikis, 1984). Cohesion in this sense, is the component of the shear strength of soil that is independent of the normal stress on the shear plane (Rowe, 1962). The physical significance of the term '**c**', however, is a bit unclear, because it is not independent of ϕ, the angle of internal friction (Winterkorn, 1955). One of the principal advantages of the term, '**c**', is that it can be visualized mathematically, as the shear stress necessary to cause soil failure at zero

normal external load (Hillel, 1980). It is also considered to be a constant for soil material in a specified state (Towner and Childs, 1972).

Use of the term 'cohesion', **c**, in these contexts is misleading, but it is mathematically convenient for isolating the contribution of friction to the shear strength in different soils. Hillel (1980) has suggested that the term 'cohesiveness' is more appropriate for describing the τ-intercept, and that 'cohesion' should refer only to the well defined cases of 'true' and 'apparent' cohesion. 'True cohesion' is due to the intermolecular attraction of soil particles for one another throughout the soil mass, and 'apparent' (or temporary) cohesion is due to the binding action of the soil mass by the action of soil water films (Jumikis, 1984). The temporary nature of apparent cohesion is reflected in the fact that at saturation, apparent cohesion is reduced to zero. True and apparent cohesion increase with increasing amounts of finer-sized particles. The magnitude of cohesion is therefore very considerable in fine-grained soils (hence the term 'cohesive' soils) and almost negligible in sandy ('cohesionless') soils (Stauffer, 1927; Nichols, 1931).

Measurement of 'cohesiveness' from Mohr-Coulomb theory is accomplished using shear tests with $\sigma_1 > \sigma_2 = \sigma_3$, where σ_1 is the major principal stress (applied axially), and where σ_2 and σ_3 are the hydrostatically applied radial stresses. The soil fails along shear planes, but because two physical properties of the soil are involved in the failure (i.e. friction and cohesion), interpretation of results in terms of other basic parameters is difficult (Ingles and Frydman, 1963). Measurements of tensile strength, on the other hand, are independent of sliding and frictional forces (Ingles, 1962c), so are ideal for determining true and apparent cohesion in soils. Interpretation of results in terms of other basic soil properties is also much simpler because only one physical property is being measured (Ingles and Frydman, 1963).

Numerous attempts have been made to relate soil 'cohesiveness' , **c**, from unconfined compression tests, to the true cohesion as measured by tensile strength tests (Vomocil and Waldron, 1962; Ingles and Frydman, 1966; Douglas, 1967; Vomocil and Chancellor, 1967; Mullins and Panayiotopoulos, 1984; and Koolen and

Vaandrager, 1984). The relationship as developed by Koolen and Vaandrager (1984) is summarized below. They relate the results of shear, tensile and compressive tests in terms of their relative positions in the coordinate space defined by critical state soil mechanics, **CSSM** (cf. Kurtay and Reece, 1970; Hettiarachi and O'Callaghan, 1980).

Consider first the test for shear failure of a confined soil sample. A relatively dense cylinder of soil is hydrostatically loaded in a standard 'triaxial' cell (where the intermediate and minor principal stresses are equal: $\sigma_2 = \sigma_3 = 0$). The soil cylinder is then loaded axially, so that the major principal stress, σ_1, increases until plastic failure results. Repeated loading for increasing values of σ_3 is done until an envelope of Mohr circles is defined, from which one can determine the values of cohesiveness, **c**, and the angle of internal shearing resistance or friction, ϕ. The loading paths of the triaxial shearing tests end at the shear failure surface in the orthogonal (σ_{mean}, τ_{max}, f_t)-**CSSM**-co-ordinate space, where $\sigma_{mean} = (\sigma_1+\sigma_2+\sigma_3)/3$, $\tau_{max} = (\sigma_1-\sigma_3)/2$, and f_t is equal to the total porosity.

By contrast to the triaxial shearing tests, tensile tests are conducted on relatively brittle soil samples and the tensile strength, σ_t, is determined (either directly or indirectly) by the maximum force at fracture divided by the cross-sectional area of the soil. Loading paths of tensile tests end at the brittle failure surface in the **CSSM** co-ordinate space.

In a transition region between the shear loading paths and the tensile-loading paths lie the compression-loading paths. Unconfined compressive strengths, σ_c, are determined by axial loading of soil cylinders and the loading paths ending both at the shear-plane failure surface and the brittle failure surface in the **CSSM** co-ordinate space.

For shear failure, the stress conditions at the moment of failure are:

$$\sigma_1 = \sigma_3 \tan^2\left(45^\circ + \frac{\phi}{2}\right) + 2c \tan\left(45^\circ + \frac{\phi}{2}\right) \qquad [2\text{-}1]$$

In an unconfined compression test, $\sigma_3 = 0$, so at failure the compressive strength, σ_c, is simply the applied axial load, σ_1. Hence,

$$\sigma_c = 2c \tan(45^\circ + \frac{\phi}{2}) \qquad [2\text{-}2]$$

Taking an average value of $\phi = 35^\circ$, the cohesiveness, **c**, becomes approximately:

$$c = \frac{\sigma_c}{4} \qquad [2\text{-}3]$$

It is known from the work of Griffith (1924) that the compressive strength of many materials is eight times larger, on average, than the tensile strength. That is,

$$\sigma_t = \frac{\sigma_c}{8} \qquad [2\text{-}4]$$

It can therefore be inferred from equations **[2-3]** and **[2-4]** that the tensile strength (or 'cohesion') is approximately half the value of the 'cohesiveness', **c**:

$$\sigma_t = \frac{c}{2} \qquad [2\text{-}5]$$

Equation **[2-5]** gives only a 'ball-park' estimate of the relationship between 'true' (and 'apparent') 'cohesion', as measured by tensile strength, σ_t, and the 'cohesiveness', **c**, of soil. In view of the difficulty in interpreting the physical significance of 'cohesiveness', the term 'cohesion', in the remainder of this thesis, will be used mainly in reference to the tensile strength of soils.

2.3 Mechanisms of Soil Cohesion

Particles of various sizes and shapes are held together in compound units (eg. domains, aggregates and clods) by several different binding mechanisms. Each operates over one or more magnitudes of scale and each imparts some degree of cohesive strength to the soil (Hillel, 1980), whether it be permanent or temporary cohesive strength (Winterkorn, 1942). Mechanisms responsible for cohesion between particles include surface interactions (Quirk, 1963; Rengasamy et al, 1984), organic and inorganic

cementation (Gifford and Thran, 1974), water films (i.e. surface tension and negative pressures; Gill, 1959; Kemper and Rosenau, 1984), and biological entanglement by, for example, fungal hyphae (Clough and Sutton,1976), and roots (Greenland et al, 1962; Clarke et al, 1967; Tisdall and Oades, 1979). The biological-cohesion mechanism will not be dealt with in this review, mainly because there has been virtually no quantitative work done on the cohesive strength imparted to the soil by fungal hyphae. Only indirect work has been done, all in reference to the water stability of soil aggregates (Martin, 1945; Harris et al, 1963 ,1964; Aspiras et al, 1971) Furthermore, most of the studies involving plant roots (eg. Waldron, 1977; Waldron and Dakessian, 1981) have concentrated on the increased shearing resistance of soils due to roots, rather than on the effects on tensile cohesion of the soil. Considerable visual evidence exists to suggest that microflora and roots could affect the tensile strength of soils (eg. see Figure 3 in Hubble and Chapman, 1946; also Plate 1 in Bond and Harris, 1964). To the authors knowledge, however, no direct measurements of the tensile strengths of roots and microflora (eg. fungal hyphae) and their effects on the tensile strength of soils have yet been published. The present review of mechanisms responsible for interparticle cohesion will therefore restrict itself to (1) surface interactions, (2) cementation, and (3) water films, only.

2.3.1 Interparticle Cohesion due to Surface Interactions

Interactions between particle surfaces which lead to cohesion can be either electromagnetic or electrostatic in nature. These forces are much weaker than the covalent and ionic bonds that are responsible for interparticle cementation (Ingles, 1962a), and yet they are important as sources of attraction between clay particles and between liquids and solids (Mitchell, 1976).

2.3.1.1 Electromagnetic Attractive Forces

The electromagnetic attractive forces (van der Waals forces) are fluctuating, dipole forces which exist between all particles of matter regardless of surface charge

(Mitchell, 1976) and electrolyte concentration (Murray and Quirk, in press). They arise between atoms and molecules at particle surfaces that approach each other, because of temporary imbalances in electron density around atomic nuclei within the particles. The electron imbalance causes weak, instantaneous dipoles to develop, and the oppositely charged ends of these dipoles attract each other. The bonding strength of these fluctuating dipoles is an order of magnitude weaker than that of permanent dipoles (Hallet et al, 1977), that are involved, for example, in hydrogen bonding.

Several theories exist to explain the inverse power relationship that exists between interparticle cohesion due to van der Waals forces and particle separation distance. The theories vary with the geometry of adjacent particles (i.e. whether the approaching particles are three-dimensional molecules, or two dimensional, flat parallel plates, or flat plates approaching three-dimensional molecules, like spheres). The equations describing the forces of cohesion due to van der Waals forces are outlined for special cases in Ingles (1962c) and in Mitchell (1976). The attractive energy is approximately inversely related to the sixth or seventh power of the separation distance between atoms or molecules (Arnold, 1978).

Although van der Waals forces are individually rather weak, they are non-directional and additive between atoms (Murray and Quirk, in press). This means that the average bonding capacity due to van der Waals forces between two particles is based on the summation of the attractive energy between all molecular pairs in the particles. As a consequence, their attractive force decreases less rapidly with particle separation distance than do permanent dipole bonds (Arnold,1978). The overall cohesive strength between particles due to these forces, however, can only be developed at distances of particle separation less than 260 nm (Ingles, 1962c) and van der Waals cohesive forces (of any significance) do not exist beyond a separation distance of approximately 100nm in most soils, and reach maximum values for separations of less than only 2-3 nm (MacEwen, 1948,1954; Ingles, 1964). Nonetheless, these forces should not be disregarded because they affect flocculation of colloids and possibly the strength of bonds holding microaggregates together (Murray and Quirk, in press).

2.3.1.2 Electrostatic Attractive Forces

The nature of electrostatic forces (also called Coulombic forces) is usually repulsive, as between like-charges, but can also be attractive, as between unlike charges (Hallett et al, 1977). Repulsive electrostatic forces arise from either the overlapping of electron clouds of adjacent particles at close range, or from the overlapping of like-charged ions in the diffuse electrical double layers of approaching clay particles (Ingles, 1962c).

Attractive electrostatic forces occur in situations where differences exist in the electrostatic charge between adjacent surfaces of soil particles. For example, the net charge on the planar surfaces of most clay particles is negative, whereas at their edges it is often positive, especially in kaolinitic clay minerals (Mitchell, 1976). Hence the particle edges can be attracted to the plane particle surfaces (Quirk, 1960), thereby causing flocculation into a 'cardhouse' structure (see Figure 7 of Schofield and Samson;1954, or Figure 5.13 in Hillel; 1980).

Cations tend to be attracted to negatively-charged particle surfaces, and anions tend to be repelled. A diffuse electrical 'double' layer of ions therefore forms at the solid-liquid interface, and this reduces the repulsive forces between like-charged particles. The extent to which the repulsive forces between particles is reduced by the ions in the diffuse double layer depends on the properties of the ions, namely their size, valence, hydration energy, polarizability and on their concentration in the bulk solution (Ingles, 1962c). Ions having greater positive charge per unit hydrated radius will generally neutralize a greater amount of negative (repulsion) charge per unit volume, and therefore encourage flocculation to occur and thus slightly increase the cohesion between particles. For example, the charge per unit hydrated radius, which may be estimated using the valence divided by the hydrated radius of the ion, is greater for the calcium ion, Ca^{2+}, $\left(\frac{2^+}{0.96nm}\right)$ whereas it is much smaller for the sodium ion, Na^+, $\left(\frac{1^+}{(0.56 \text{ to } 0.79nm)}\right)$, (Mitchell, 1976).

The attractive potential energy, E, between a single negatively charged clay plate and cations in the double layer of a dilute solution is described (Ingles, 1962c) by the relation

$$E = \frac{\Phi\ ze}{D\ h} \qquad [2\text{-}6]$$

where Φ= charge density of particle surface

z= valence of double layer cations

D= dielectric constant of fluid medium

h= separation distance

e= unit electronic charge

For very close approach (< 1 nm) of two parallel clay plates whose double layers overlap (eg. during drying), the electric field is no longer homogeneous and is considered as a group of point charges (Bolt and Koenigs, 1972). An attractive interaction energy known as **'Madelung Attraction'** exists in this situation and it is responsible for bonding between individual clay crystals, causing them to form stacks and clusters or domains (Koenigs, 1963). It results from extensive interaction between electrical fields surrounding ions and the negative charge sites within clay crystals. The mutual potential energy of attraction in the overlapping Stern layers diminishes rapidly when the distance between plates exceeds that between ions (1.0-1.4 nm) (Koenigs, 1963). The energy can be approximately calculated by the method of Madelung (1918) as:

$$E = \left(\frac{2(\Phi^2 ez)^{1/2}}{D}\right) \exp\left(-2\pi h \left(\frac{\Phi}{ez}\right)^{1/2}\right) \qquad [2\text{-}7]$$

where the symbols are the same as for equation **[2-6]**, after MacEwen (1954). Stern layer interactions will not be considered further in this review because they do not relate to the work of this thesis.

The above two equations probably contribute to the basis for the strong correlation (usually linear; Ingles, 1962c) that exists between cation exchange capacity (Φ in equation **[2- 6]**) and the tensile cohesive strength of clays (Tschebotarioff et al, 1953; Ingles and Frydman, 1966).

The balance between forces of attraction and forces of repulsion results in either dispersion or flocculation, as shown in Figure **2- 1**. The repulsion energy between particles is very sensitive to electrolyte concentration, valence of cations, the dielectric constant of the medium, as well as the pH. The attraction energy, on the other hand, is sensitive only to changes in temperature and the dielectric constant (Mitchell, 1976).

It should be noted that interparticle cohesion due to the surface interactions discussed above are most significant in soils dominated by very fine (usually flat and parallel) particles, which have a large area per unit mass. Double layer phenomena exert a much smaller influence on the strength of soils composed predominantly of clay minerals having low surface area (Ingles, 1964). In coarser textured soil (silts and sands) cementation processes contribute much more to cohesive strength.

2.3.2 Interparticle Cohesion due to Cementation

In many cases, the strength in soils develops as a result of either naturally occurring or added cementing materials, which bind particles together and which may make their surfaces at the points of contact inaccessible to water (Denisov and Reltov, 1961) This section presents some of the ideas behind the mechanisms of cementitious bond formation as well as theory on the tensile strength associated with cementitious bonding in soils.

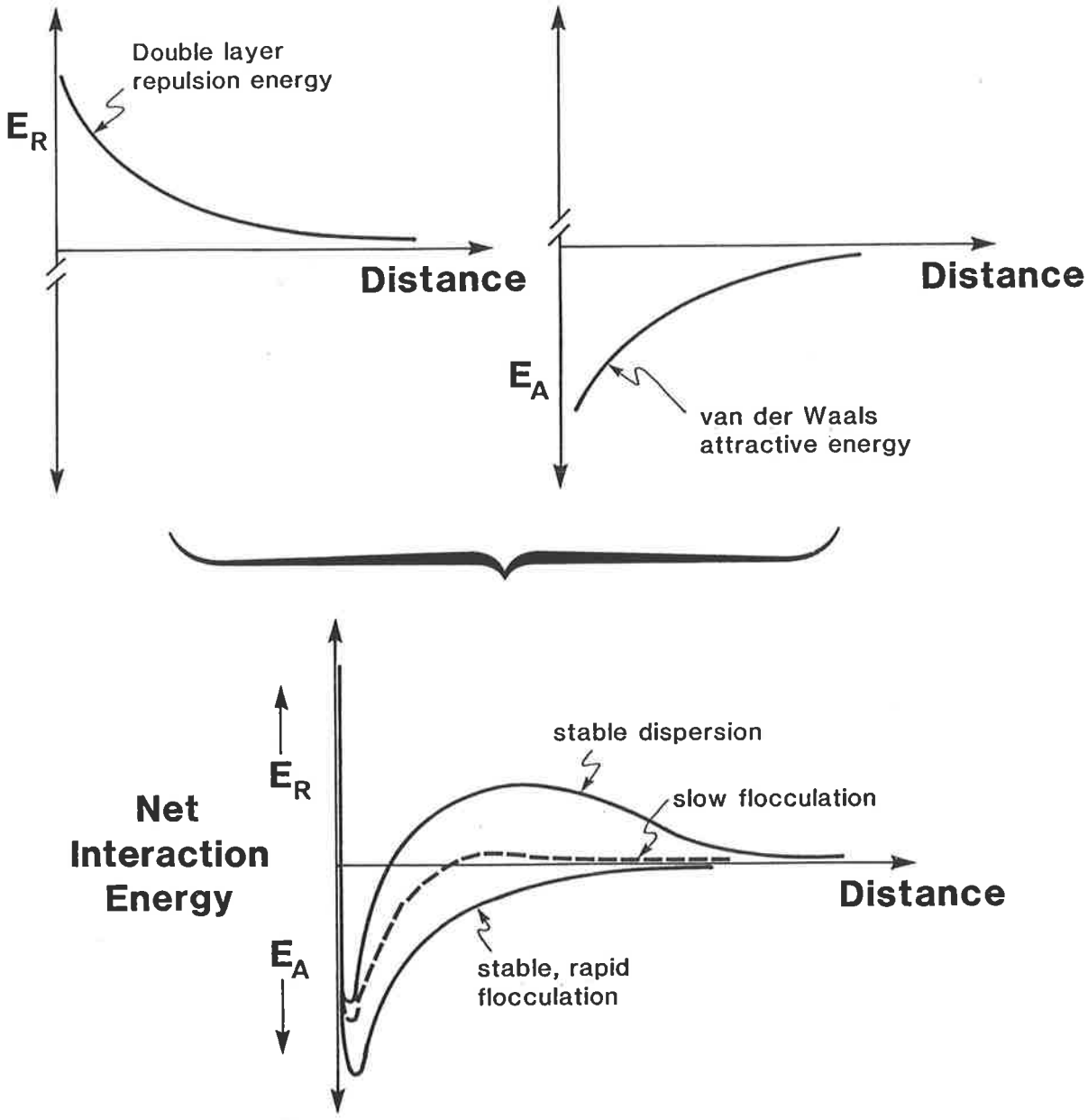

Figure 2-1. Energies of repulsion, E_R, attraction, E_A, and net interaction energy associated with dispersion and flocculation of flat (parallel) plates (re-drawn from Figure 7.17 of Mitchell, 1976).

2.3.2.1 Formation of Cementitious Bonds

Inorganic cementitious bonds can form as a result of chemical degradation of the clay lattice as well as the silica in soils due to the addition of soil stabilizers such as calcium chloride, calcium carbonate, or calcium silicate ('cement'), all of which are alkalis (Ingles, 1962b, 1970). Inorganic bonds can also form due to the selective precipitation of dissolved silica or other slightly soluble solutes (Mitchell, 1976) occurring naturally in the soil (Kemper and Rosenau, 1984). Organic cementitious bonds can form naturally (Chatterjee and Jain, 1970) or by the addition of polysaccharides (eg. Martin, 1946) and polymers like polyvinyl alcohol or PVA (see for example, Oades, 1976). These bonds, however, are much weaker than inorganic bonds, and consist mainly of weak electrostatic bonds, hydrogen bonds and chelation associated with polycations near particle surfaces (Ingles, 1968). The strength imparted to soil aggregates by these organic bonds comes mainly from the formation of interdomainal links, and is usually temporary due to the oxidation of the organic substrate by soil microbes (Tisdall and Oades, 1982; Oades, 1984). Furthermore, cementitious bonds due to polymers such as PVA, once broken will not reform, so their strength-value is easily lost (Ingles, 1968) when the soil is disturbed, say during tillage operations.

Inorganic cementation can induce both short-term as well as long- term cohesion. The sequence of reactions associated with stabilization using calcium compounds involves the slow dissolution of the salt containing the calcium and the diffusion-dependent transfer of calcium to the clay surface exchange sites (Ingles, 1962b). The exchange of calcium for other ions at the clay surface induces flocculation (weak bonding), and has only a small effect on the strength of the soil (Ingles, 1968). If calcium hydroxide is used, the calcium and hydroxide ions diffuse into the silicate structures of clays, and cause degradation of the clay structure by hydrolysing Si-O-Si bonds. The reactions produce very insoluble polymeric calcium silicates which act as cement for longer term stabilitzation. The extent to which strength-increases occur depends on (1) the reactions taking place ubiquitously and

(2) there being a sufficient number of close inter-particle contacts to enable cementitious bridges to form (Ingles, 1962b). The role of $CaCO_3$ as a cement in agricultural soils is discussed by Hadas and Wolf (1984b).

The formation of inorganic bonds due to site-selective precipitation of solutes at particle-to-particle contacts has been described by Kemper and Rosenau (1984). Precipitation of minute quantities of silica, calcium carbonate and other slightly soluble compounds in the soil solution occurs during slow drying of the soil (Gerard et al, 1962; Gerard, 1965).

Particle to particle contact points (concave surfaces) offer positions of lower thermodynamic free energy than other (flat or convex) surfaces, and this makes the contact points preferred sites for selective precipitation (Kemper and Rosenau, 1984). Once precipitation begins, the solubility of the precipitate decreases rapidly relative to that of the ions and particles still in solution. The difference in solubility establishes a concentration gradient (the driving force) between the particles in solution and the precipitate, which leads to the growth of the precipitate in contact points at the expense of the particles in solution (Hunter, 1987). This phenomenon, known as **Ostwald Ripening** is based on the relation described by the Gibbs-Thomson equation (after Kahlweit, 1975):

$$\{c_s(r) - c_s(\infty)\} = c_s(\infty)\, \exp\{(\frac{a}{r}) - 1\} \qquad [2\text{-}8]$$

which can be approximated to within about 1% accuracy over the range $0.85 < \frac{a}{r} < 1.15$ by the relation:

$$\{c_s(r) - c_s(\infty)\} = c_s(\infty)(\frac{a}{r}) \qquad [2\text{-}9]$$

where $a=\frac{2\sigma V_m}{\nu RT}$, $c_s(r)$ and $c_s(\infty)$ are the solubilities of particles of sizes r and ∞ respectively, σ is the interfacial tension between the particles and water, V_m the molar volume of the precipitate, ν is the number of dissociation products of the precipitate, R is the ideal gas constant and T is the absolute temperature.

The concentration gradient described in equations **[2- 8]** and **[2- 9]** causes soluble compounds to diffuse toward the particle-contact points, and so long as there is sufficient water in the soil to allow continuity of water films, the precipitation will continue and the cementitious bonds will grow stronger. Although the limiting thickness of water films necessary to enable this process to continue in agricultural soils is uncertain, diffusion slows down considerably at low water contents (Porter et al, 1960; Van Shaik et al, 1966). Nonetheless, Kemper and Rosenau (1984) found that increases in strength continued to occur over a period of years, (age hardening), even at air-dry water contents. It was assumed in the studies of Kemper and Rosenau (1984) that water in the air dry soil existed only in single layers. Whether it is possible for the Ostwald ripening phenomenon to be responsible for "the migration of bonding components" reported by Kemper and Rosenau (1984) has not yet been determined. Thixotropic age hardening described, for example, by Blake and Gilman (1970) and Utomo and Dexter (1981a) could presumably occur simultaneously and even augment cementation processes, particularly at intermediate water contents (close to the lower plastic limit).

2.3.2.2 Tensile Strength of Cementitious Bonds in Soils

The overall effectiveness of cementitious (chemical) bonds for imparting strength to the soil is a function of (1) the separate cohesive strengths of both the soil particles (substrate) and the cement, (2) the adhesive strength of the cement-to-substrate bond (i.e. whether the bond is covalent or ionic, the latter being weaker), and (3) the area of contact between cement and substrate (Ingles, 1962c). Naturally occurring inorganic cements in soils include silica (Gifford and Thran, 1974), as well as oxides and oxyhydroxides of iron, aluminum and manganese (Deshpande et al, 1964; Giovanni and Sequi, 1976) and calcite (Uehara and Jones, 1974). The effects of various different cementitious substances on soil cohesion have been studied by numerous authors (eg. Puri et al, 1940; Arca and Weed, 1966).

If cements occur extensively enough to form a continuous matrix throughout the soil, the tensile strength of the soil will simply be the tensile strength of the cement. If, as is usually the case in agricultural topsoils, cementing occurs only sparsely throughout the soil, then the tensile strength of the soil is influenced by many factors. The most important factors influencing the overall strength in this case are the number (Kemper, 1958) and the area of cement-to-substrate contacts (Ingles, 1962c). The more contacts and the more extensive the area of cementation, the greater will be the tensile strength of the soil.

A mechanistic theory of tensile strength in soils due to cementitious bonding is outlined by Ingles (1962c) and is of sufficient relevance to this thesis to warrant its presentation in some detail here.

Important assumptions are made regarding the cement and the substrates involved in cementitious bonding, namely that there exists:

(1) random and isotropic distribution of cementitious bonds in the soil (i.e. no crusts or layers).

(2) random distribution of particle sizes within both the substrate and the cement, and

(3) the same effective bonding forces everywhere which can be considered as overall 'average' bonding forces.

While these assumptions allow for homogeneous macroscopic behaviour, the microscopically heterogenous nature of granular materials prevents the occurrence of failure along a straight, 'ideal' plane, exactly perpendicular to the applied tensile stress. Instead, the bulk strength of the soil and the fracture pathway depends upon which type of bond is broken under tensile stress. Blakey (1964) pointed out that failure can occur within the cement (or substrate) itself, or alternatively failure can occur at the cement-substrate interface (Figure 2- 2). When bond strengths between soil particles are *weaker* than within soil particles, a crack will occur along the circumference of the soil particles (through cement, or along cement/substrate interface). When bond strengths between particles are *greater* than within particles,

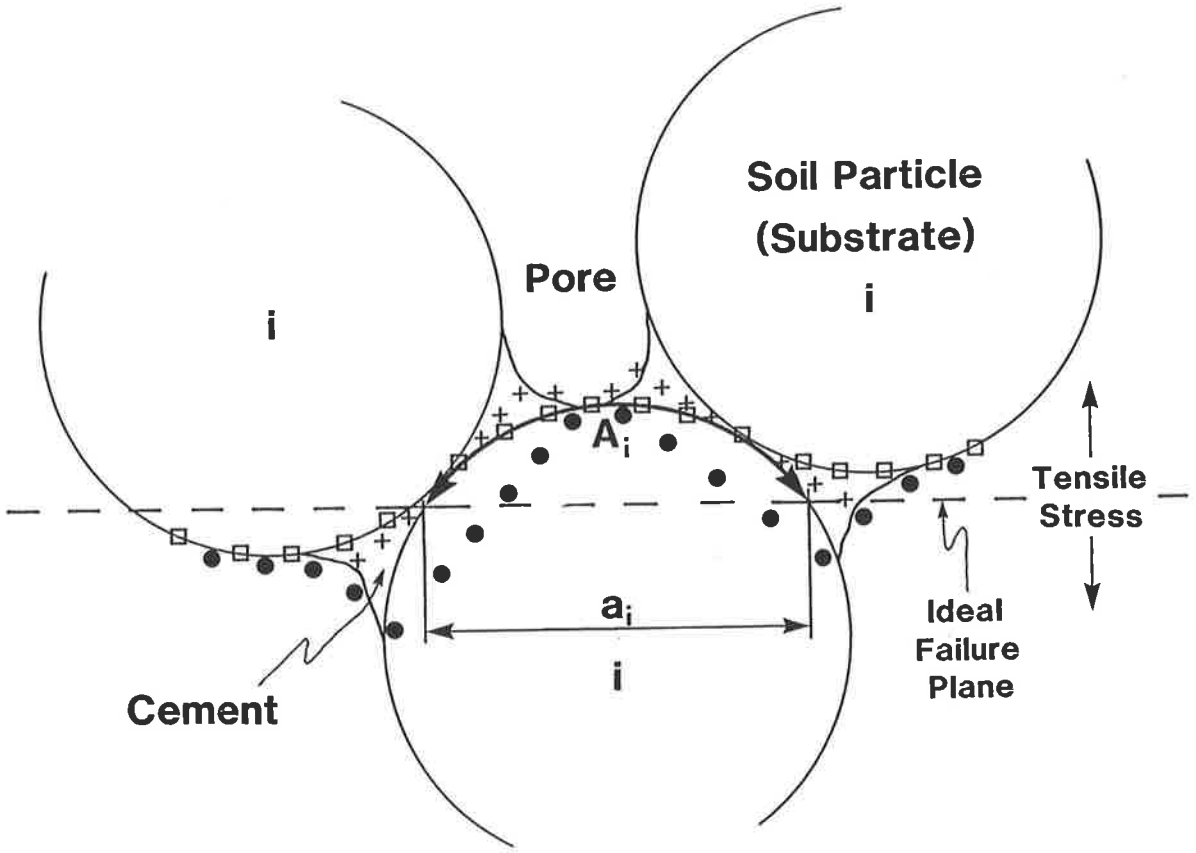

KEY TO REAL FAILURE PATHWAYS

+ + + + within cement

● ● ● ● within substrate

□ □ □ □ along cement/substrate interface

Figure 2-2. Ideal and real failure pathways between cemented, spherical soil particles due to an applied tensile stress (re-drawn from Figure 10 of Ingles, 1962c).

on the other hand, a crack will occur through the particles themselves (Ingles and Lafeber, 1967).

First consider the case where failure under tensile stress occurs within the cement (or within the substrate) itself. If a_i is the area of soil particle, **i**, that is intersected by an 'ideal' tensile failure plane, if **n** is the number of particles intersected, **f** is the porosity, and if **e** is the voids ratio,
then the total intersected area, $\sum_{i=1}^{n} a_i$, across the soil sample can be equated to the porosity and voids ratio in the equation:

$$\sum_{i=1}^{n} a_i = 1 - f, \qquad \text{where } f = \frac{e}{(1+e)} \qquad [2\text{-}10]$$

or

$$\sum_{i=1}^{n} a_i = \frac{1}{(1+e)} \qquad [2\text{-}11]$$

If the average number of particle to particle contacts (bonds) per unit particle-surface area is **p**, and if the average bond strength at each particle contact point is **P**, then it is possible to equate the bulk tensile strength per unit cross-sectional area, σ_t, as the product of the average bond strength, the density of contact-points and the area:

$$\sigma_t = P \sum_{I=1}^{n} (a_I)\ p \qquad [2\text{-}12]$$

or

$$\sigma_t = P \left(\frac{1}{(1+e)}\right) p \qquad [2\text{-}13]$$

A value for **p** can be assigned using knowledge about the geometry of the component particles, specifically the coordination number of the particles, **k**, and the total surface area of each particle, A_i, from the relation:

$$p = \left(\frac{nk}{\sum_{i=1}^{n} A_i}\right) \qquad [2\text{-}14]$$

Substitution of **p** from **[2-14]** into **[2-13]** gives:

$$\sigma_t = \frac{nPk}{(1+e)\sum_{i=1}^{n} A_i} \qquad [2\text{-}15]$$

The value for A_i, of course, depends on the geometry of the individual particles. For equal-sized spheres of diameter, **d**, ($A_{sphere} = \pi d^2$), the tensile strength can be calculated as:

$$\sigma_t = \frac{Pk}{\pi d^2 (1+e)} \qquad [2\text{-}16]$$

For an isotropic and random assemblage of rods of diameter, **d**, and length, *l*, the tensile strength can be calculated as:

$$\sigma_t = \frac{Pk}{\pi d (l + \frac{d}{2})(1+e)} \qquad [2\text{-}17]$$

And for an isotropic, random assemblage of cubes having length of sides, *l*, the tensile strength can be calculated as:

$$\sigma_t = \frac{Pk}{6 l^2 (1+e)} \qquad [2\text{-}18]$$

It can be seen from equations **[2-16]**, **[2-17]**, and **[2-18]** that for similar-sized particles, an assemblage of equal-sized spheres will generally have greater tensile strength than an assemblage of equal-sized rods, and even greater tensile strength than an assemblage of equal-sized cubes. Estimates of the variables in these equations require some knowledge about either the void ratio, **e**, or the mean particle coordination number, **k**. Work on the correlation between the coordination number of lead-shot and its porosity for different types of packing has been done by Smith et al (1929), Graton and Fraser (1935) and Deresiewicz (1958). If **e** is known, an approximate value of **k** can be calculated from the relation after Smith et al (1929):

$$k = \frac{\pi (1+e)}{e} = \frac{\pi}{f} \qquad [2\text{-}19]$$

An estimate of **P**, the average bond strength per contact point, is more difficult, and involves knowledge of the tensile strength of the cement itself, σ_c (or of the substrate, σ_s, if failure predominates in the substrate rather than in the cement), as well as the volume of the cement. Values of σ_c and σ_s may already be known, or else may be measured experimentally. (For example, Gifford and Thran (1974) measured the tensile strength of silica bonds formed between paired glass beads, and found them to range between 180 and 830 kPa). Estimates of the volume of cement per unit contact point, **v**, can be made using information on the average particle radius, **R**, and using the theory of capillary condensation around a single contact point. As shown by Kruyer (1958), the volume of cement, **v**, is

$$v = f(\phi) 2\pi R^3 \qquad [2\text{-}20]$$

where $f(\phi)$ is described by a trigonometric function of the angle, ϕ, (in arc units) subtended by the point where two (spherical) particles meet and the point where the liquid cement surface meets the sphere, as well as the contact angle, θ_c, between the cement and the particle surface, (Figure 2-3) viz:

$$f(\phi) = (1-\cos\phi)^2 \left[1+\tan(\theta_c+\phi)\left\{(1-\cos\phi)\tan(\theta_c+\phi)+\sin\phi\right\}\right] - (1-\cos\phi)^2\left[(1-\cos\phi)\tan(\theta_c+\phi)+\sin\phi\right]\left(\frac{\pi/2-\theta_c-\phi}{\cos^2(\theta_c+\phi)}\right) \qquad [2\text{-}21]$$

For known values of ϕ, the geometry of the cement may be calculated from

$$R\sin\phi = \alpha \cosh\left(\frac{R-\cos\phi}{\alpha}\right) \qquad [2\text{-}22]$$

where α = smallest radius of cement fill (see Figure 2-3). So if tensile failure occurs within the cement (rather than in the particle), **P** can be estimated as

$$P = \sigma_c \pi \alpha^2 \qquad [2\text{-}23]$$

For failure within the particle ($\alpha' = R\sin\phi$), the average bond strength per contact point, P', now becomes:

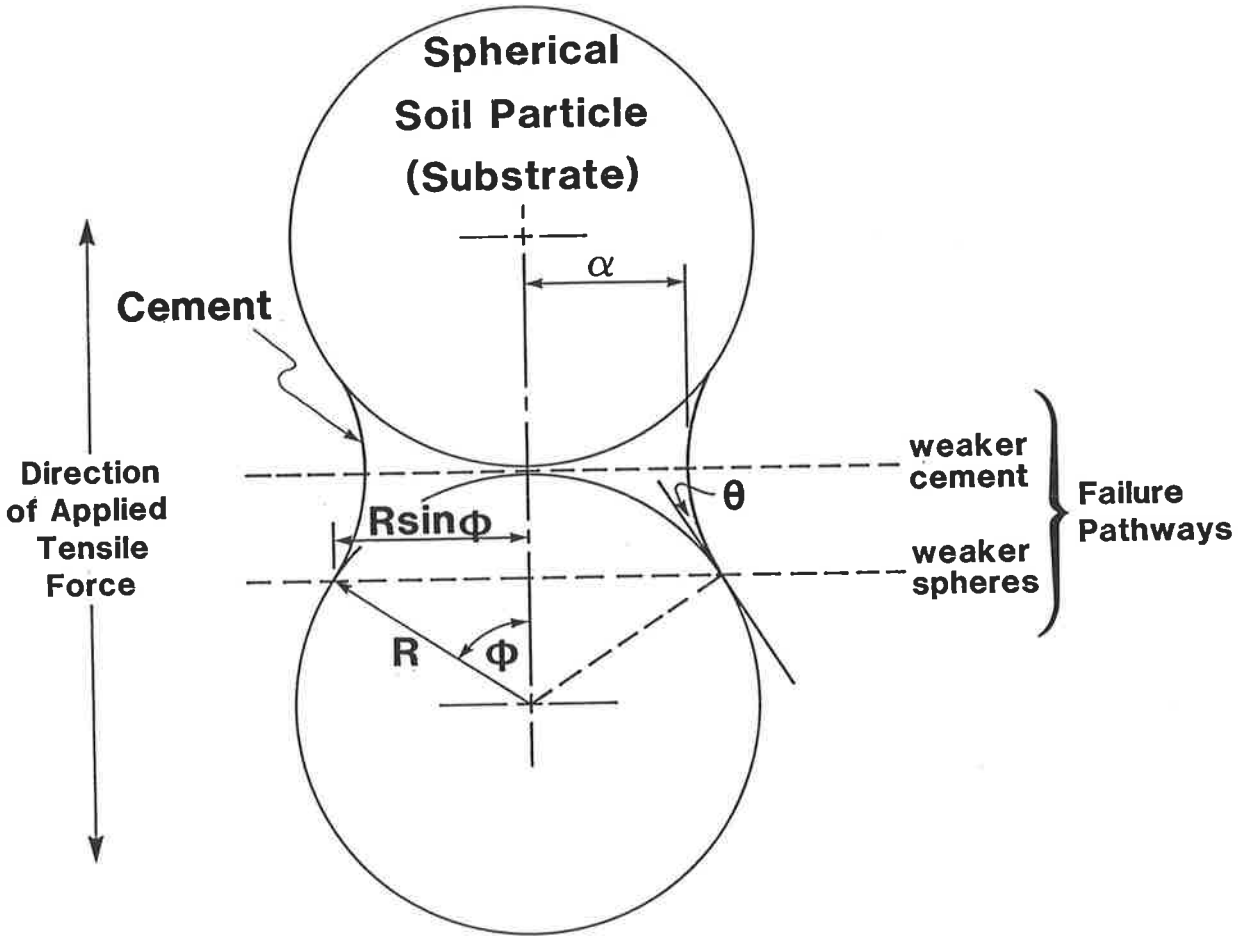

Figure 2-3. Potential tensile failure pathways (through cement or substrate) between two cemented, spherical particles, illustrating the variables needed to calculate the volume of cement holding the particles together (re-drawn from Figure 11 of Ingles, 1962c, and Figure 1 of Kruyer, 1958).

$$P' = \sigma_s \pi \alpha'^2 \qquad [2\text{-}24]$$

If failure occurs at the cement-particle interface, on the other hand, the interfacial contact area between cement and substrate replaces the radius of the cement bridge, α, used in equations [2-22], [2-23], and [2-24]. The area can be measured using a microscope, or it can be calculated based on the geometry of the system, so the average bond strength per contact point, P'', becomes:

$$P'' = \sigma_i \left(\frac{\sin\phi}{\phi} \right) 2\pi R^2 (1 - \cos\phi) \qquad [2\text{-}25]$$

The estimates of tensile strength based on Ingles' theory assumes that the cementitious bonds form a solid, continuous, cylindrical bridge between soil particles. In cases where the bridges are hollow rather than solid, however, as Gifford and Thran (1974) found with silica bonds between glass beads, estimates of tensile strength using the equations outlined above will be too high.

Kemper et al (1974) found, in agreement with Ingles (1962c), that the tensile strength of soil crusts was directly related to the number of particle-to-particle contacts (cf. equation [2-15], this thesis), the strength of individual bonds (cf. equations [2-23], [2-24], and [2-25], this thesis), but also the particle shape. These three factors are all a function of the particle size distribution in soils, and the combined effect on soil strength can be seen in Figure 2-4. Different combinations of particle sizes in synthetically mixed soils shows that the strength of soils dominated by clay-size particles is often, but not always (eg. Ibanga et al, 1980), at least an order of magnitude greater than that for sand-size particles (Kemper et al, 1974). Using different mixtures of sand, silt and clay, Chepil (1955), Gerard (1965) and Aylmore and Sills (1978), also found an inverse relationship between the effective diameter of soil particles and soil strength (as measured by the modulus of rupture technique of Richards, 1953). This is because for bonding between particles to occur, the particles must be brought into close proximity to one another at many places. If the particles are mainly small sized, the soil will have a large surface area, which increases the

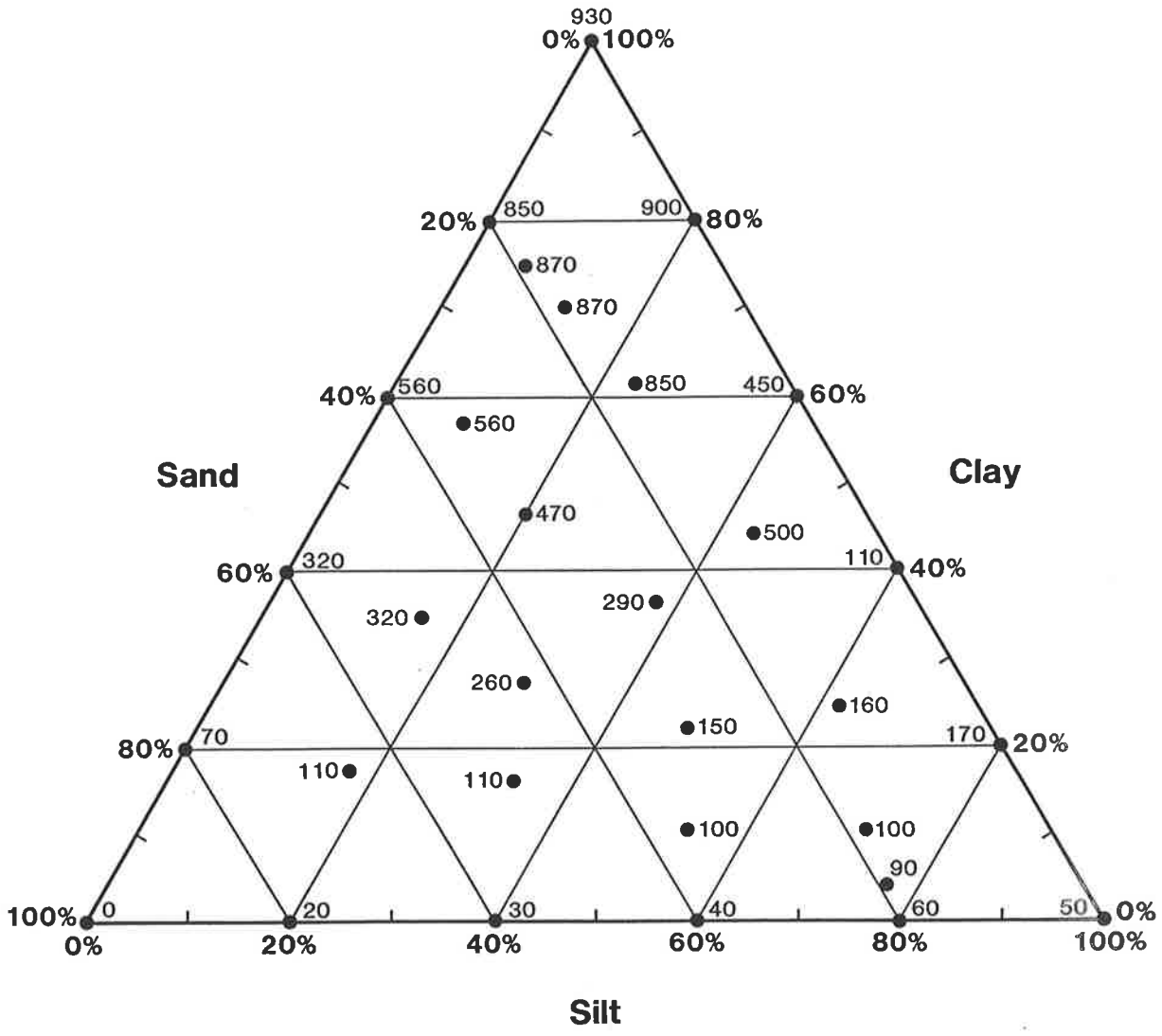

Figure 2-4. Textural triangle showing modulus of rupture (kPa) beside each point for 31 different mixtures of particle sizes (after Figure 4-1 of Kemper et al, 1974).

likelihood of particles making a large number of contacts with one another (Uehara and Jones, 1974).

2.3.3. Interparticle Cohesion Due to Water Films

2.3.3.1 Haines and Fisher (H-F) Theory

It has long been recognized (eg. Haines, 1925; Fisher, 1926 & 1928) that a significant temporary cohesive strength exists in uncemented, moist soils as a result of the surface tension and capillary forces associated with lenticular, or interparticle water films (Ingles, 1962c) throughout the soil matrix. Both forces require the presence of a gas/liquid/solid interface, and so do not exist in saturated soils.

The basis for cohesion due to surface tension in unsaturated soils is as follows. The denser side of a gas/liquid interface is continuously 'trying' to contract, because there is a greater intermolecular attraction among subsurface liquid molecules than there is among liquid molecules at the gas/liquid interface (Hillel, 1980). The resulting excess energy of liquid molecules at the interface relative to that in the bulk is called surface energy or surface tension (Hallett et al, 1977). The tendency for the surface to contract at all times exerts a net compressive force on particles that are in connection with each other through a continuous film of water. Adhesion between soil particles and water molecules (eg. see Fountaine, 1954; Winterkorn, 1955) ensures that the soil particles are pulled together. Surface tension acts along the entire length of an air/water interface. Considering the simple case of two particles connected by a capillary wedge of water (Figure 2-5), Fisher (1926) showed that the cohesive force, F_{ST}, due to surface tension between two spherical, incompressible particles is

$$F_{ST} = 2\pi r \sigma_w \qquad [2\text{-}26]$$

where r = radius of capillary wedge at (by convention) the pore neck,

$2\pi r$ = length of the air/water interface,

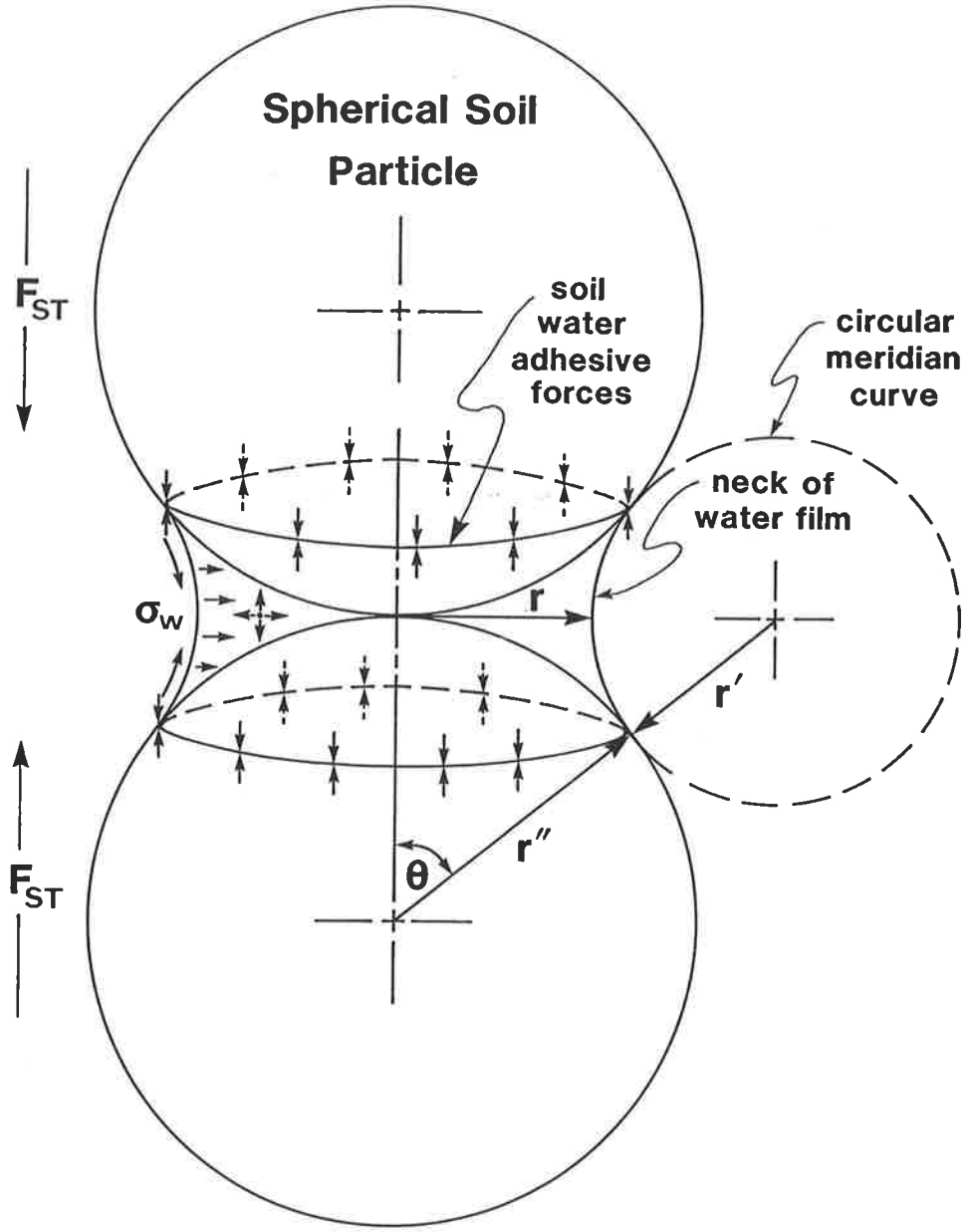

Figure 2-5. Two spherical soil particles held together by a capillary wedge of water, showing the particle radius, r", and the two principle radii of curvature of the water film, r' and r. Arrows on left hand side indicate net direction of compressive force, F_{ST}, due to surface tension of water, σ_w.

σ_w= surface tension of air/water interface.

Cohesion due to capillary forces is a function of the contact angle that develops between liquid and solid at the gas/liquid/solid interface. Different contact angles arise due to the different affinities that liquid molecules have for solid molecules. The contact angle controls the curvature of the gas/liquid interface at the solid surface. Liquids having contact angles between 0° and 90° are considered to 'wet' the solid surface, thus leading to the 'capillary rise' phenomenon. A curved meniscus forms, and is concave with respect to the gas phase. The curvature of the meniscus, $\frac{1}{r}$, increases in smaller pores.

When considering the curvature of a meniscus between two spherical particles (as opposed to the meniscus within a capillary tube) there are two principal radii affecting the shape of the meniscus, and so the 'total curvature' must be considered. The total curvature of a surface is a measure of the extent to which the surface departs from being a plane. A curved surface having two principal radii, (see **r** and **r'**, in Figure **2-5**) has total curvature **K**, defined as:

$$K = \left(\frac{1}{r'} - \frac{1}{r}\right) \qquad [2\text{-}27]$$

By convention (Mualem and Morel-Seytoux, 1979) the value of either **r'** or **r** takes a positive sign if the centre of curvature lies within the phase at higher pressure (gas-side of the meniscus), and is negative otherwise. Attempts have been made (eg. Carman, 1941) to replace **K** with a more general estimate of curvature that is not limited to regular shapes in real soils.

In unsaturated soils, the contact angle between water and solid particles is often assumed to be negligibly small (0°), and the phenomenon of curvature of the meniscus results in a pressure difference across the air/water interface, the lower pressure existing on the convex side of the meniscus (Hillel, 1980). That is, the liquid pressure under the meniscus is lower than atmospheric pressure. Water is therefore

drawn (or 'pushed') into the soil pores until the phase pressure difference due to capillarity is exactly counter-balanced by the hydrostatic pressure of the water 'columns' which develop in the matrix of soil pores. When the contact angle is greater than zero (but less than 90°), the radius of curvature increases. Referring to Figure 2-5, the cohesive force due to capillarity (or phase pressure deficit), F_c, was calculated by Fisher (1926) to be

$$F_c = \pi r^2 \sigma_w K \qquad [2\text{-}28]$$

or

$$F_c = \pi r^2 \sigma_w \left(\frac{1}{r'} - \frac{1}{r}\right) \qquad [2\text{-}29]$$

The forces of surface tension and capillarity are additive, and the total combined cohesive force, F_t, due to water films was expressed by Fisher (1926) as

$$F_t = 2\pi r \sigma_w + \pi r^2 \left(\frac{1}{r'} - \frac{1}{r}\right) \sigma_w \qquad [2\text{-}30]$$

which, with knowledge of the particle sizes, reduces to

$$F_t = \frac{2\pi r'' \sigma_w}{1 + \tan \frac{\theta}{2}} \qquad [2\text{-}31]$$

where r'' is the particle radius and θ is the angular radius of the wedge of water connecting the particles (see Figure 2-5).

Counteracting the cohesive force holding particles together, (due to surface tension and capillarity) is the pressure between rigid primary particles at points of contact. If a tensile stress is applied to an aggregate of unsaturated soil, the compressive stress on the particles due to water films is correspondingly relieved, yet not overcome. Fisher (1926) described the cohesive force of water films in unsaturated soil aggregates to be the tensile stress required to just overcome the compressive stress on the soil particles. For tensile stresses less than this, the soil aggregate behaves as a rigid particle.

Far more sophisticated models on the theory of capillarity and surface tension have since been proposed for various limited cases (eg. de Bisschop and Rigole, 1982; Zasandzinski et al, 1987; and Bayramli et al, 1987). The limitations that the Haines and Fisher (H-F) models have in predicting the tensile strength of real soils, however, makes the more sophisticated versions of limited use. Despite its weaknesses, the H-F approach is still instructive in the study of cohesion due to water films in natural soils as recognized by Aitchison (1961) in a study on effective stresses in unsaturated nonuniform soils. For example, if one equates F_t from equation **[2-30]** with **P** from equation **[2-15]**, its substitution for **P** in equation **[2-15]** yields an expression which is similar to that of Ingles (1962c) for the tensile strength of capillary-bound aggregates:

$$\sigma_t = \left(\frac{nk\sigma_w}{(1+e)\sum_{i=1}^{n}(A_i)} \right) \left(2\pi r + \pi r^2 \left(\frac{1}{r'} - \frac{1}{r} \right) \right) \qquad [2-32]$$

Cohesion occurs only at interparticle contact points, and so this equation emphasizes the importance of the number, **n**, of these contacts per unit area of the ideal tensile failure plane in determining the contribution of water films to tensile strength.

Waldron et al (1961) used H-F theory to study the water retention properties of glass beads (which simulate ideal, rigid, spherical particles). They found that upon desorption of initially saturated systems, the measured water contents were much higher than calculated values. They concluded that the difference between experimental and theoretical water contents could still be used as an estimate of the contribution of adsorption forces (as compared to capillary forces). The difference supposedly represents the quantity of water not contributing to soil cohesion. Snyder and Miller (1985), however, challenged the results of Waldron et al(1961) on the basis that although the water contents of Waldron et al, were too high to be accounted for by capillarity, they were also too high to be accounted for by adsorption. They suggested

that the time allowed for equilibrium water contents to be established in the glass beads was probably too short. According to this suggestion, the water contents would eventually drop to within H-F predictions given sufficient time.

Kemper and Rosenau (1984) made approximate estimates of soil cohesion using calculations of (1) surface tension cohesion, P_{ST}, separately from (2) hydraulic-phase-pressure-difference cohesion, P_H, in moulded soils. Estimates of cohesion due to surface tension, upon desorption, were made assuming (i) spherical shape of all empty pores, and (ii) all empty pores had an air/water interface around their entire circumference that exerted a tension. Hence each pore of radius, r_i, in a plane through the middle of that pore contributed an amount equal to $2\sigma_w \pi r_i$ to the cohesion of the sample. (σ_w, in this case, is the surface tension of the air/water interface, as described in equation **[2-26]**). Cohesion due to surface tension could therefore be estimated over a given range of suctions by multiplying the number of pores drained, N_i, by $2\sigma_w \pi r_i$. The value of N_i can be estimated by dividing the change in volumetric water content between two suctions, ($\Delta\theta = \theta_1 - \theta_2$, assuming no anisotropy), by the area of an average-size pore, of radius $\bar{r}_i$, corresponding to the two suctions where $\bar{r}_i$ is defined as $\bar{r}_i = \frac{(r_i + r_{i+1})}{2}$.

$$N_i = \frac{\Delta\theta_i}{\pi \bar{r}_i^2} \qquad [2\text{-}33]$$

Hence the surface tension cohesion, P_{ST}, is calculated as

$$P_{ST} = \left(\sum_{i=1}^{n} \frac{\Delta\theta_i}{\pi \bar{r}_i^2} \right) 2\pi \bar{r}_i \sigma_w \qquad [2\text{-}34]$$

or

$$P_{ST} = 2\sigma_w \left(\sum_{i=1}^{n} \frac{\Delta\theta_i}{\bar{r}_i} \right) \qquad [2\text{-}35]$$

Estimates of cohesion due to the hydraulic-phase-pressure-difference, P_H, were made simply by multiplying the gauge pressure (or the measured suction pressure, P_a-P_w) by the volumetric water content, θ, thus:

$$P_H = \theta\ (P_a - P_w) \qquad [2\text{-}36]$$

where P_a and P_w are the air and water pressures respectively.

The two separate estimates of soil cohesion due to water films (P_{ST} and P_H) were compared to values of tensile strength measured on two different soils (see results for Portneuf and Billings soils in Figure 2-6). The calculated values of P_H were generally higher than the measured tensile strengths, and at lower water contents the values of P_{ST} were also higher. The total estimate of cohesion due to water (i.e. $P_{ST} + P_H$) would be even higher still compared to the measured tensile strength, but the point they were trying to make was that in the Portneuf and Billings soils, P_{ST} and P_H were at least large enough to account for the measured tensile strength. Two possibilities were suggested to explain why P_{ST} and P_H overestimated the actual tensile strengths of the soils:

(1) The calculated estimates of cohesion were based on a model of spherical pores. If the soils had contained an ideal distribution of isotropically oriented, spherical particles, the estimated and measured values might have been closer. The presence of microcracks, however, plus the differences in the particle sizes, shapes and arrangements (Winterkorn, 1955; Jaeger, 1956), caused the soil to fail at lower tensile stresses than calculated.

(2) The calculated estimates of cohesion were made on the assumption that all empty pores contained a circumferential air/water interface wherein surface tension forces predominated. The presence of pore water that is adsorbed only on particle surfaces (rather than at particle contact points) contributes nothing to soil cohesion,

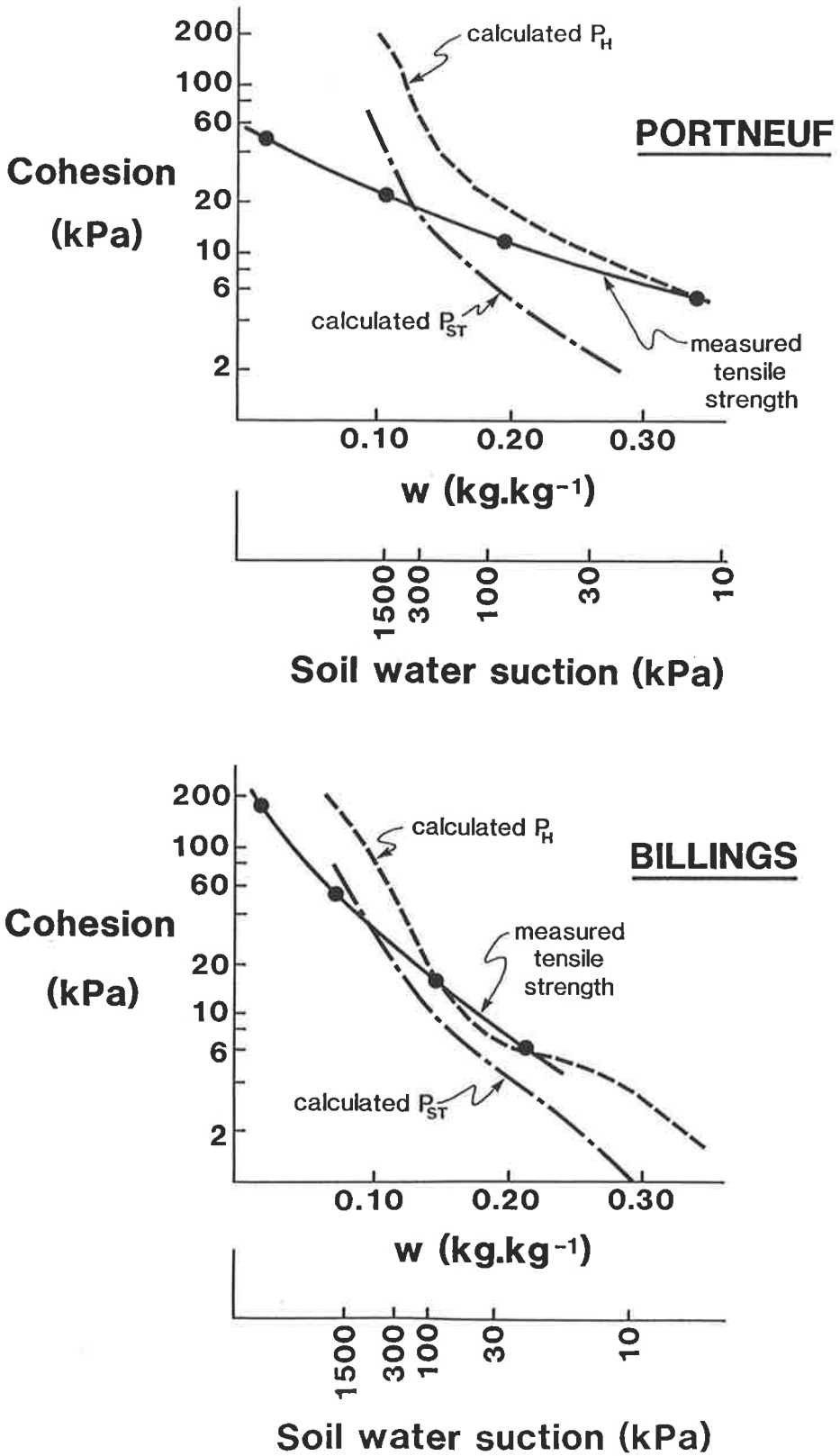

Figure 2-6. Comparison of estimated cohesion due to water films (P_{ST} & P_H) with measured tensile strengths for Portneuf and Billings soils (re-drawn from Kemper and Rosenau, 1984).

and hence reduces the tensile strength of real soils below the predicted values.

2.3.3.2 H-F Theory Modified

Snyder and Miller (1985) point out the most significant limitations of H-F theory, and indicate some reasons why it often over-estimates the tensile strength of real soils. First of all, H-F theory is most applicable to (i) materials of low specific surface area (eg. rigid spheres) and to (ii) unsaturated soils at relatively high water contents. In these two cases, the gauge-pressure reading is equal to the hydrostatic pressure or the matric potential ($-\rho gh$). The theory begins to fail, however, in (i) relatively dry soils, where adsorption of water becomes significant (Bouyoucos, 1925), and in (ii) soils of high surface activity, and also in (iii) soils exhibiting non-water cohesion (i.e. cementation). In these three cases, a significant proportion of the water does not contribute anything to soil cohesion, and the gauge pressure does not reflect the hydrostatic pressure.

With these limitations in mind,Snyder and Miller (1985) present a comprehensive theory of tensile strength due to capillarity, which is based upon Aitchison's modification of the H-F model as well as on ***similar media*** theory (after Miller and Miller, 1956). Their theory is of sufficient importance to the present thesis that it will be outlined here (equations **[2- 37]** to **[2- 50]** below) in some detail.

Consider a model of unsaturated soil particles having cross sectional area, **A**, which is exposed to a constant normal stress, σ, in the z-direction (Figure **2- 7**) . (The use of the symbol σ for stress in this context should not be confused with σ_w, the surface tension of water, used in previous equations). The soil particles are traversed by any (wavy) plane, **B**, which passes between the soil particles at their contact points, thereby defining the projected areas of particle contact, A_p, water phase, A_w, and air phase, A_a. The circumferences of the projected air/water interfaces have total length, **P**. Water and air exist in the pores at gauge pressures of u_w and u_a, respectively. The value of u_a is often the atmospheric pressure, which is greater than

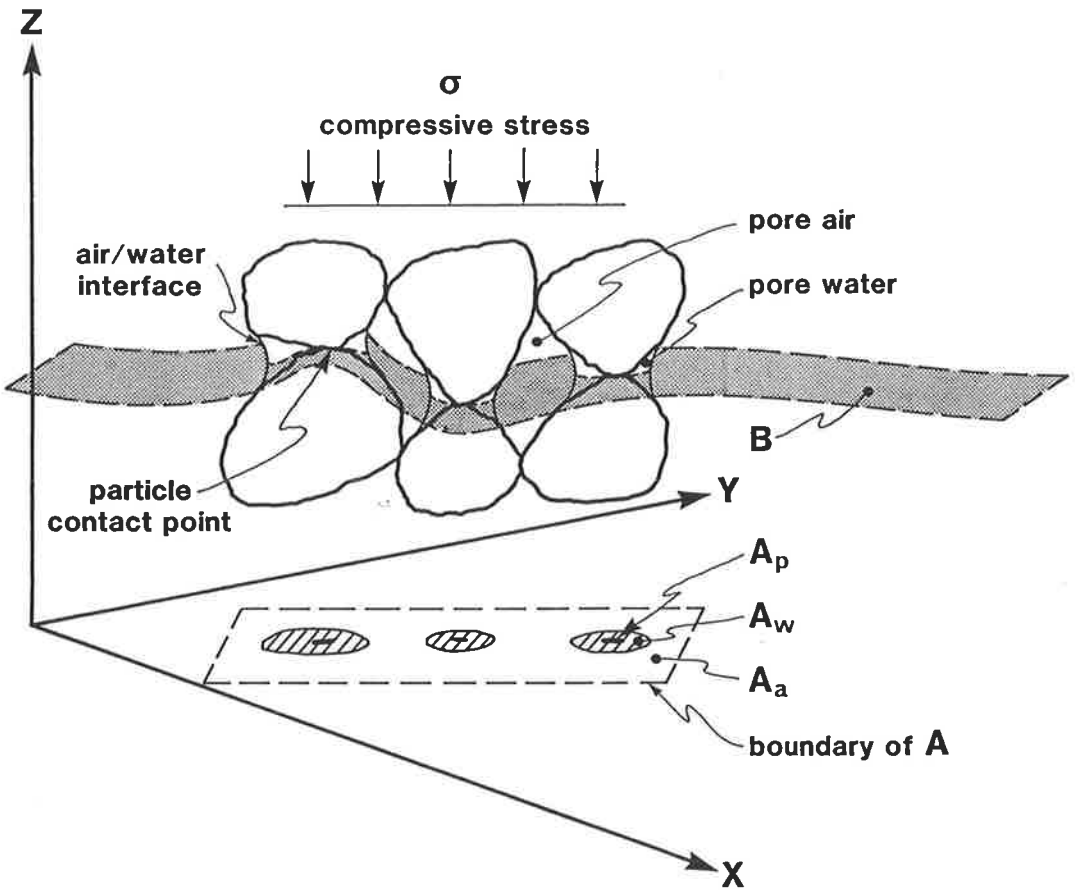

Figure 2-7. Unsaturated soil element having the projected boundary, A, traversed by an imaginary, wavy plane, B (re-drawn from Snyder and Miller, 1985).

u_w in unsaturated soils. Consequently, the quantity (u_a-u_w) is therefore referred to as the relative pressure or the pressure deficiency of the pore water(Aitchison, 1957). A surface tension, γ, (equivalent to σ_w in equation **[2-26]** this thesis), acts tangentially to the air/water interface.

Balancing forces in the z-direction results in the relation:

$$\sigma A = F_p + A_w u_w + A_a u_a - \gamma \int_0^P \mathbf{i} \cdot \mathbf{j} \, dt \qquad [2\text{-}37]$$

where F_p= the z-component of total interparticle contact forces acting across the wavy plane **B**.

A_w= area of water intersecting **B**.

A_a= area of air intersecting **B**

$\gamma \int_0^P \mathbf{i} \cdot \mathbf{j} \, dt$= the z-component of surface tension force.

$\mathbf{i}$= the unit vector in z-direction.

$\mathbf{j}$= the unit vector tangent to the air/water interface and perpendicular to an incremental segment, **dt**, along the air/water interface intersecting **B**.

Dividing left and right hand sides of equation **[2-37]** by the total area, **A**, gives an expression in terms of stresses:

$$\sigma = \frac{F_p}{A} + \frac{A_w u_w}{A} + \frac{A_a u_a}{A} - \frac{\gamma}{A} \int_0^P \mathbf{i} \cdot \mathbf{j} \, dt \qquad [2\text{-}38]$$

The term $\frac{F_p}{A}$ is the average interparticle, or effective stress. Replacing A_a with its identity $(A_a = A - A_p - A_w)$ gives the expression:

$$\sigma = \frac{F_p}{A} + \frac{A_w(u_w-u_a)}{A} + \frac{u_a(A-A_p)}{A} - \frac{\gamma}{A} \int_0^P \mathbf{i} \cdot \mathbf{j} \, dt \qquad [2\text{-}39]$$

If we now group together on the right hand side all the terms associated with the soil water, the result is the expression:

$$\frac{F_p}{A} + u_a\left(1-\frac{A_p}{A}\right) - \sigma = \frac{A_w(u_a-u_w)}{A} + \frac{\gamma}{A}\int_0^P \mathbf{i}\cdot\mathbf{j}\, dt \qquad [2\text{-}40]$$

Defining a dimensionless parameter χ as:

$$\chi = \frac{A_w}{A} + \frac{\gamma}{A(u_a-u_w)}\int_0^P \mathbf{i}\cdot\mathbf{j}\, dt \qquad [2\text{-}41]$$

and substituting it into equation [2-40] gives:

$$\frac{F_p}{A} + u_a\left(1-\frac{A_p}{A}\right) - \sigma = \chi(u_a-u_w) \qquad [2\text{-}42]$$

Similitude concepts can be used to show that the value of χ is a constant for ***similar*** soils in ***similar*** states. That is, χ is constant in soils dominated by capillary phenomena, and which are also geometrically identical except in size scale, λ, (Miller and Miller, 1956). For ***similar*** soils, therefore, the following can be said about the variables comprising χ in equation [2-41]:

$$\begin{aligned} A_w &= K_1 \lambda^2 \\ A &= K_2 \lambda^2 \\ P &= K_3 \lambda \\ dt &= \lambda dk \\ (u_a-u_w) &= K_4 \frac{\gamma}{\lambda} \end{aligned} \qquad [2\text{-}43]$$

where K_1, K_2, K_3, and K_4 are constants. The value of **dk** is a constant representing an incremental section of the air/water interface. Substitution of equation **[2-43]** into equation **[2-41]** gives an expression which reduces to a series of constants:

$$\chi = \frac{K_1\lambda^2}{K_2\lambda^2} + \left(\frac{\gamma \int_0^{K_3\lambda} \mathbf{i}\cdot\mathbf{j}\,\lambda\, d\,k}{K_2\lambda^2 \frac{K_4\gamma}{\lambda}} \right) \qquad [2-44]$$

This implies, as stated above, the constancy of the value of χ for similar soils. When the geometry of the solid skeleton is also considered to be constant, then the value of χ depends only on **s**, the degree of pore saturation. The degree of pore saturation is defined as:

$$s = \frac{\theta}{f} \qquad [2-45]$$

where θ is the volumetric water content and **f** is the total porosity (Green and Ampt, 1911; Skempton, 1961). The value of χ will be unity at saturation, where θ=**f**, as shown below, and it will be zero in dry soil, where θ=0, (Olson, 1963). At intermediate water contents, however, χ is in general, not precisely equal to **s** (Donald, 1961; Groenevelt and Kay, 1981). The value of χ will be influenced by the soil structure, the wetting history and the stress history of the soil (Bishop, 1961). It is also possible that in sandy loam soils containing significant amounts of clay and silt-sized particles (yet insufficient amounts to bridge gaps between sand grains) that much of the water, upon drying will be held in the finer material on grain surfaces, away from contact points. The water held in this finer material contributes nothing to the tensile strength of the bulk soil, and therefore χ will be less than **s** below a certain degree of saturation (Mullins and Panayiotopoulos, 1984). There are also conditions

where χ may be greater than **s**, but for the purposes of this review, however, it will simply be assumed that χ is at least approximately a single-valued function of **s**.

Assuming that the contact area between particles, A_p, is negligible, equation **[2-42]** can be rearranged to solve for the effective stress, σ',(where $\sigma' = \frac{F_p}{A}$) as follows (after Bishop, 1961):

$$\sigma' = (\sigma - u_a) + \chi (u_a - u_w) \qquad [2-46]$$

In equation **[2-46]** the term $(\sigma - u_a)$ is equivalent to the applied stress, while the term $(u_a - u_w)$ is equivalent to the pore water pressure, or the equilibrium liquid pressure (Groenevelt and Kay, 1981). Both terms in equation **[2-46]** are stated with reference to the air pressure in the soil pores, u_a , which is usually atmospheric, and therefore negligible, which reduces equation **[2-46]** to:

$$\sigma' = \sigma - \chi u_w \qquad [2-47]$$

When the soil is saturated, the z-component of the surface tension force ($\gamma \int_0^P \mathbf{i} \cdot \mathbf{j} \lambda \, dt$ in equation **[2-41]**) becomes zero, which reduces χ to:

$$\chi = \frac{A_w}{A} \qquad [2-48]$$

which is approximately equal to unity, as already mentioned above. Substitution of χ=1 into equation **[2-47]** results in Terzaghi's equation for effective stress in saturated soils (Skempton, 1960):

$$\sigma' = \sigma - u_w \qquad [2-49]$$

Fisher (1926) described the cohesive force of water films in unsaturated ideal soil to be the tensile stress required to just overcome the compressive stress on the

soil particles. This means that at failure, the effective stress is $\sigma' = 0$, which if applied to equation [2-46], gives the result at failure that

$$\chi = -\frac{(\sigma - u_a)}{(u_a - u_w)} \qquad [2-50]$$

where the numerator and denominator of equation [2-50] represent (1) the critical tensile strength and (2) the pore water pressure deficiency, respectively, after Fisher (1926).

Because χ depends solely on the degree of pore saturation, **s**, equation [2-50] indicates that the ratio $-\frac{(\sigma - u_a)}{(u_a - u_w)}$ is also a function of only **s**. Hence, once χ is known for a soil, the tensile stress $(\sigma - u_a)$ necessary to cause failure can be calculated with knowledge of $(u_a - u_w)$.

Calculation of χ can be done, assuming that $(u_a - u_w)$ is equivalent to the measured soil water matric potential at equilibrium, by using the relation:

$$\chi = s + \frac{0.3}{(u_a - u_w)} \int_{i=s}^{1.0} (u_a - u_w)_i \, d s_i \qquad [2-51]$$

where s_i and $(u_a - u_w)_i$ are the pore saturation and pore water pressure deficiency, respectively, at any point **i** between **s** and complete saturation (**s=1.0**).

Despite their contributions to improving capillary cohesion theory, however, Snyder and Miller (1985) note that the major limitation of H-F theory for real soils lies in the assumption that tensile stresses are uniformly distributed throughout the soil and that no stress-concentrations exist. This leads to the very important subject of how various flaws, zones of weakness and cracks affect the distribution of tensile stresses in the soil and ultimately how they influence the brittle fracture of unsaturated soils.

2.4 Flaws and Cracks and the Brittle Fracture of Unsaturated Soils

2.4.1 Background

The importance of flaws and cracks in determining the mechanical strength of soils exposed to tillage was recognized many years ago by Fippin (1910) and by Russell (1938). Fippin concluded that "the contraction of the water film is the primary force and it acts in conjunction with lines of weakness to bring about granulation. Anything which produced a line of weakness in the soil mass would determine the location of a crack". Russell observed that "the units out of which several types of large aggregates in virgin soils are built are merely a smaller version of the large aggregates", which is what Grant et al (1985) concluded using a micropenetrometer, and which supports the contention that the soil structure is hierarchical in nature (Dexter, 1988a). Russell (1938) also observed that fracture during tillage occurred along lines of weakness in the soil and he noted that the higher mechanical strength of moulded aggregates over that of natural field aggregates of the same size "was probably due to their being more uniform than the field aggregates." Russell's observations were very important because they implied that irregularities (eg. cracks and different sized pores) in the soil structure are significant strength-determining factors. That is, strength depends on the weakest points in the soil (Kuipers, 1984).

This practical result was recognized independently at about the same time in the coal industry (eg. Bennett, 1936; Bennett et al, 1941; Brown, 1941; Bennett and Brown, 1941), and was followed up by Marshall and Quirk (1950) using agricultural soils. Marshall and Quirk used a drop-shatter test (recently refined by Hadas and Wolf, 1984a), which caused soil clods to fracture along natural cleavage planes. Marshall and Quirk defined the percent size-stability of soil clods, $\%SIZE_{stab}$, to be:

$$\%SIZEstab = \left(\frac{\sum_{i=1}^{n} \frac{X_i}{N}}{X_o} \right) \times 100 \qquad [2\text{-}52]$$

where X_i= diameter of ith clod-size category
X_o= diameter of original clod prior to fracture
N= number of size categories.

They further defined a complementary term "friability" as ($100 - \%SIZE_{stab}$), which was an attempt to quantify the general definition of friability, viz: the "liability to break or crumble into smaller pieces when subjected to handling" (Gilmore and Nichols, 1937). Marshall and Quirk found the important result using blocks made of plaster-of-Paris and sand that the energy required "to reduce all fragments to less than half the original size was approximately doubled as the block size was decreased from 2 to 1 inch and again from 1 to 0.5 inch". That is, they found that larger aggregates fracture more easily than smaller aggregates, and this has also been reported by Winterkorn (1955) and Gill and McCreery (1960). The results of Marshall and Quirk were evaluated by Ingles (1963) who used probability theory to predict the breakage process.

The inverse relationship between tensile strength and aggregate size was also found by Rogowski and Kirkham (1976). They suggested that as the size of soil unit increases from, say, clay films (eg. Dowdy and Larson, 1971), to soil aggregates (eg. Rogowski et al, 1968), to compressed cores of soil aggregates (Farrell, et al, 1967; Williams et al, 1967), the work needed for fracture would decrease, because larger soil units have a greater statistical chance of containing a severe flaw.

2.4.2 Theory of Brittle Fracture

A statistical crack theory for the tensile strength of soils has since been developed by Braunack et al (1979). They indicated that if a compressive force is applied across the poles of a relatively dry aggregate ($w <$ lower plastic limit), strain energy will be reversibly stored until a sufficiently large tensile stress is developed. When this happens brittle fracture occurs by the activation of one or more flaws in the aggregate, and strain energy is irreversibly released with the formation of a new fracture surface.

There are many different types and strengths of flaws distributed throughout granular materials, like soil aggregates and clays (Ingles and Lafeber, 1966). These flaws include small and large pores, cracks, holes, inclusions and surface flaws, as well as differences in material composition. The latter type of flaw is particularly relevant to the strength of concretes and stabilized soils (eg. Jones and Kaplan, 1957; Ingles and Frydman, 1966; Perry and Gillott, 1977). The term "flaw strength" will often be used here to indicate the level of mechanical stress at which a flaw will grow irreversibly leading to failure. Braunack et al (1979) pointed out that the nature and severity of flaws is more varied in natural soils than in artificial soils, which is consistent with the finding of Sideri (1936) that "the most stable arrangement of particles is the homogeneous one", and explains the higher mechanical strength of moulded soils over natural field aggregates reported by Russell (1938).

The theory of brittle fracture developed by Braunack et al (1979) assumes that fracture occurs by the activation and spreading of a single (most severe) crack, though they acknowledge that the concatenation of a combination of cracks can also occur prior to failure, as shown by Brace and Bombolakis (1963). At a critical tensile stress, the most severe flaw (or most severe concentration of stresses around a flaw) spreads causing fracture. This implies that the tensile strength of the soil is of a statistical nature, which is dependent upon the random distribution of the most severe flaws. If the most severe flaws are uniformly distributed throughout the soil, then the soil strength is volume-dependent. Rogowski and Kirkham (1976) were therefore correct in suggesting that larger aggregates fail at lower applied stresses simply on the basis that they stand a greater chance of containing a severe flaw than do smaller aggregates. The relationship between the volume of a soil unit, **V**, and its tensile strength, **S**, is presented in Braunack et al (1979) and Utomo and Dexter (1981b) as:

$$\log_e S = -k \log_e V + A \qquad [2\text{-}53]$$

where $A = \log_e\{S_o V_o^k \Gamma[1+k]\}$, which is the intercept, or the extrapolated estimate of tensile strength of 1 m^3 of bulk soil.

S_o and V_o = strength and volume, respectively of the basic structural elements comprising the aggregates.

Γ = tabulated Gamma function

k = slope of the log(strength)-log(volume) curve, and a measure of the dispersion of flaw strengths within the soil.

The term **k** in equation **[2-53]** is referred to as the soil friability (Utomo and Dexter, 1981b), and it measures how readily large clods tend to break under stress into smaller soil units of greater relative stability. Friability, **k**, is the quantitative expression of the concept of "grades of durability" introduced by Nikiforoff (1941), wherein the lowest grade of durability occurs when the strength within aggregates is the same as the strength between aggregates. In the theory of Braunack et al (1979), large **k**-values (eg. $0.25 < k < 0.40$) indicate a wide dispersion of flaw strengths, meaning that more severe flaws exist in the larger structural units. Small **k**-values on the other hand (eg. $k< 0.05$) indicate a narrow dispersion of flaw strengths with the consequence that the tensile strength of the larger units does not differ markedly from that of the smaller ones (eg. Hadas and Wolf, 1984b). Virgin, well structured soils are quite friable and tend to have large **k**-values (Shanmuganathan and Oades, 1983a). This is because the bonds holding particles together within aggregates are much stronger than the inter-aggregate bonds (Martin, et al, 1955), hence rupture of these weak inter-aggregate links usually yields smaller aggregates of greater cohesive strength (Ingles, 1962a).

2.4.3 Griffith Theory

2.4.3.1 Behaviour of a Single Crack

Brittle fracture in the presence of micro- and macroscopic flaws has been studied widely in the engineering literature in an attempt to explain the large discrepancy between experimentally measured tensile strengths of brittle materials and the theoretical estimates based on intermolecular cohesive forces. The mathematical basis for the failure of materials around flaws was established by Inglis in 1913, who investigated the stresses due to the presence of an elliptical hole in a

brittle, non-ductile plate. Based on Inglis's solution of the equations of elasticity in elliptic coordinates, Griffith (1921, 1924) calculated the theoretical critical (or breaking) stress for a material (containing an elliptical crack) exposed to a uniform tensile stress. He considered the summation of (1) the applied normal stresses, (2) the elastic strain energy of the plate, and (3) the surface energy of the crack, or the energy needed for creating new surface area in his computations in his well known equation:

$$\sigma_c = \left(\frac{2ET}{\pi C}\right)^{1/2} \qquad [2\text{-}54]$$

where σ_c is the component of the applied stress that is normal to the major axis of the elliptical crack (Figure 2-8), **2C** is the length of the major axis of the elliptical crack, and **E** and **T** are, respectively, the Young's modulus and surface tension of the material. He found that the maximum tensile stress, σ_m, occurs at the sharpest edge of an incipient elliptical crack (where the radius of curvature, ρ, is very small), and also that σ_m is often many times larger than the critical applied stress, σ_c. The value of σ_m approaches the theoretical molecular cohesive strength of the material, and is calculated as:

$$\sigma_m = 2\sigma_c \left(\frac{C}{\rho}\right)^{1/2} \qquad [2\text{-}55]$$

or

$$\frac{\sigma_m}{\sigma_c} = 2\left(\frac{C}{\rho}\right)^{1/2} \qquad [2\text{-}56]$$

provided that $C >>> \rho$. This gives the important result that the ratio $\frac{\sigma_m}{\sigma_c}$ is only a function of the geometry of the crack, and is independent of either the crack volume or the elastic constants of the material. The lowest possible value that $\frac{\sigma_m}{\sigma_c}$ can take is approximately 2, and it rapidly increases for more elliptic cracks, becoming huge for extremely sharp cracks (Snyder and Miller, 1985).

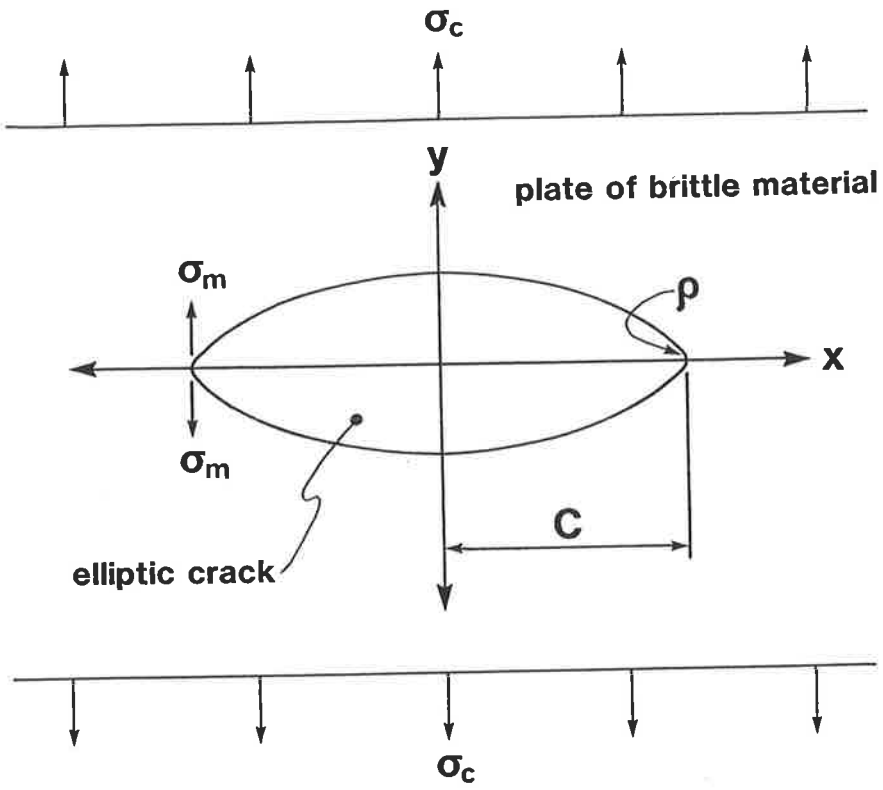

Figure 2-8. Two-dimensional representation of an elliptical crack having the major axis of semi-length, C, with radius of curvature, ρ, showing the critical applied normal tensile stress, σ_c, and the maximum normal tensile stress, σ_m.

Griffith-theory, as outlined in equations **[2-54]** to **[2-56]** is best suited to brittle materials like glass or ceramics, where minimal deformation occurs during fracture. In some materials, however, plastic deformation can take place during fracture (for example, in metals). The surface tension term, **T**, is unsuitable in these cases, and needs to be replaced with a quantity that reflects the fact that considerable energy is absorbed by slight plastic flow in the brittle-fracture zone (Winne and Wundt,1958). Hence for materials that exhibit plastic deformation, the stress for crack propagation, σ_c, is calculated from:

$$\sigma_c = \left(\frac{GE}{\pi C}\right)^{1/2} \qquad \text{(for plane stress)} \qquad \textbf{[2-57]}$$

and

$$\sigma_c = \left(\frac{GE}{\pi(1-\nu^2)\,C}\right)^{1/2} \qquad \text{(for plane strain)} \qquad \textbf{[2-58]}$$

where **G** is the strain energy release rate or the quantity of stored elastic strain energy released from a cracking sample due to extension of the advancing crack by a unit of new surface area, ν is the dimensionless Poisson's ratio (or the reciprocal of the ratio of elongation under stress along one axis to the corresponding contraction along orthogonal axes). Values of ν range from 0.5 for cases where the volume remains constant, down towards zero for materials that do not contract laterally when under longitudinal strain. The Poisson's ratio in soils is a function of the porosity, **f**, and the degree of saturation, **s** (Hillel, 1980), and is typically around $\nu = 0.25$.

The significance of "Griffith" cracks in brittle and granular materials is illustrated in Table **2-1**, which lists the tensile strengths for different soil materials and for chemically bonded and crystalline materials. In Table **2-1**, crystalline materials tend to be strongest, although the presence of microcracks in glass reduces the tensile strength by at least two orders of magnitude. The tensile strength of clay films (Dowdy and Larson, 1971) is comparable to that of aged (flawed) glass, and it is at least an order of magnitude greater than that of soil aggregates and soil cores, which are full of flaws. The measured strength of the clay films in this case is less than the theoretical strength (Table **2-1**), probably due to "secondary aggregation and non-

Table 2-1

Material	Tensile Strength (kPa)	Reference
glass	1.3×10^7 (calculated*)	Griffith (1924)
	1.8×10^5 (measured)	"
quartz fibre	1.0×10^6	Jaeger (1956)
aged glass	6.0×10^4	"
limestone	4.0×10^3	"
sandstone	2.0×10^3	"
sodium-saturated montmorillonite, clay films, water content=0.02	4.0×10^4 (calculated*)	Dowdy & Larson (1971)
	1.2×10^4 (measured)	"
air-dry natural aggregates of 4mm diameter:		
-Luton silty clay	2.1×10^3	Rogowski et al (1968)
-Kenyon loam	7.9×10^2	"
-Hagener fine sand	53	"
natural aggregates at-153 MPa potential:		
-Allora Soil:		
(58% < 2µm;1.2-2.0mm diam.)	1.4×10^3	Braunack et al (1979)
(" ;2.0-4.0mm diam.)	9.5×10^2	"
(" ;4.0-6.7mm diam.)	4.1×10^2	"
-Urrbrae Soil:		
(17% < 2µm;1.2-2.0mm diam.)	89	"
(" ;2.0-4.0mm diam.)	76	"
(" ;4.0-6.7mm diam.)	70	"
pressed cores of red-brown earth (Parafield loam); water content = 0.02	1.6×10^2	Farrell et al (1967)

*Calculated values are based on the cohesive forces between molecules (based on heats of vapourization) whereas others are measured experimentally

Table **2-1**. Range of tensile strengths for various engineering and soil materials.

ideal arrangements of cohesion-giving water films" (Winterkorn, 1955). Particle size distribution and shape influence the packing arrangement of particles, (Dexter and Tanner, 1972) and therefore the extent and severity of flaws, as implied by the data of Rogowski et al (1968) in Table **2-1**, although other factors may also be important. Clays tend to have smaller pores of more uniform size distribution and therefore have fewer sites for the propagation of severe flaws (eg. Luton silty clay). Loam soils, on the other hand, have a wider range of particle sizes and hence a less uniform pore size distributions (and therefore greater chance for a severe flaw to exist; eg. Kenyon Loam, Hagener Fine Sand). The effect of aggregate volume on the presence of flaws is also shown in Table **2-1** by the data of Braunack et al (1979). Larger aggregates are invariably shown to be weaker than smaller aggregates.

2.4.3.2 Growth and Arrest of Cracks

Ingles and Lafeber (1967) outlined the following criteria for growth and arrest of pre-existing and stress-induced cracks. Defects in granular materials cause stress concentrations, the magnitudes of which are controlled by the geometry of the defect and by the applied stresses. Cracks can also be stress-induced depending on the distribution of bond-strengths in the material (c.f. Section **2.3.2.2**). In a homogeneous material under an applied stress, cracks smaller than a critical size will remain stable, while larger cracks will propagate to a rapid and well-defined fracture according to equations **[2-54]** to **[2-58]**. A growing crack can meet impediments, however, which cause it to change direction and thereby raise the value of σ_c. Cracks propagating under external compressive stresses follow the direction of the major principal stress, rather than the major axis of the initial crack.

Growing cracks can also be arrested, in particular when they encounter phase-changes of much different elastic moduli. If the Young's modulus suddenly increases, a crack can be stopped or deflected. If the Young's modulus decreases, on the other hand, the energy of crack-propagation can be dissipated in deformation of the weaker phase. A finer grain size, for instance, can arrest a crack, but only if the pores in the finer

material are extremely small by comparison; otherwise stress-concentrations will quickly occur and the crack will continue.

2.4.3.3 Theoretical Limitations

Griffith-theory has been modified and extended for various materials (eg. Irwin, 1957; Berry, 1960a,b; Craggs, 1960; Stroh, 1960; Kaplan, 1961; and Lachenbruch, 1961). It has also been criticized and yet widely applied by many researchers (eg. Smekal, 1936; Gramberg, 1966; Brace and Bombolakis, 1963; Keer, 1966). The most significant limitations of Griffith-theory (as outlined in equations **[2-54]** to **[2-56]**) for real soils have been summarized by Snyder and Miller (1985) as follows. The theory in its present form is limited to sharp, flat cracks, which are by no means the only kinds of pores in real soils. It also requires knowledge of the lengths of cracks, **C**, as well as the Young's modulus of the soil, E, both of which are extremely difficult to measure, and which change with water content and bulk density (Briones and Uehara, 1977a,b). Furthermore, an estimate of **T** is needed, and although in relatively wet soils, the surface tension of water (σ_w in equation **[2-26]**) can be substituted as an estimate for T in equation **[2-54]**, it is unsuitable for drier soils.

2.4.4 Griffith and H-F Theory Combined

The most recent attempt to make Griffith-theory useful in real soils is the work of Snyder and Miller (1985) who combined Griffith criteria with H-F theory to predict the conditions for tensile failure in unsaturated soils.. They argued that because the stress concentration ratio, $\frac{\sigma_m}{\sigma_c}$, is a unique function of the crack geometry (cf. equation **[2-56]**), it is possible that $\frac{\sigma_m}{\sigma_c}$ is also unique for a given crack shape in ***similar*** soils. This means that $\frac{\sigma_m}{\sigma_c}$ is a scalable parameter, and Snyder and Miller use this concept to link $\frac{\sigma_m}{\sigma_c}$ with the parameter χ, thus defining a unique relationship

between tensile strength, soil water matric suction (u_a-u_w) and the degree of pore saturation, **s**, for ***similar*** soils.

They considered two different unsaturated granular systems: one unflawed (containing no cracks), the other containing flaws or cracks. Tensile failure in the unflawed system is governed by χ (a single-valued function of the degree of pore saturation, **s**) according to equation **[2-50]**, which is simply an extension of H-F theory for cohesion due to water films. The effective and applied stresses will be everywhere the same in the unflawed soil system for any plane perpendicular to the applied stress.

By contrast, the stresses in the flawed system will not be everywhere the same, rather a maximum tensile stress $(\sigma\text{-}u_a)_m$ will exist at the apex of any flaw or crack. The value of $(\sigma\text{-}u_a)_m$ is related to $(\sigma\text{-}u_a)$ by some proportionality constant, **f**, which is controlled by the shape of the flaw or crack. This shape is of course unknown, but it will be a function of the degree of pore saturation in ***similar*** soils. Hence Snyder and Miller define the ratio of the maximum tensile stress and the applied tensile stress in cracked soils to be:

$$\frac{(\sigma - u_a)_m}{(\sigma - u_a)} = f(s) \qquad \textbf{[2-59]}$$

which is analogous to equation **[2-56]**, where $f(s)$ denotes a proportionality factor accounting for crack shape and its dependence on **s**. Solving for the maximum tensile stress at the crack edge, $(\sigma\text{-}u_a)_m$, gives:

$$(\sigma - u_a)_m = f(s)\ (\sigma - u_a) \qquad \textbf{[2-60]}$$

As in the unflawed soil, failure occurs when the effective stresses in the system are reduced to zero. Hence $(\sigma\text{-}u_a)_m$ is not a soil constant, and it must vary to satisfy the condition that the effective stress at the edge of a crack drops to zero at failure. This means that, in the same way that equation **[2-50]** applies to unflawed soils at failure, we can say for flawed soils that:

$$\chi = \frac{-(\sigma - u_a)_m}{(u_a - u_w)} \qquad [2-61]$$

which can be related to the applied stress, $(\sigma - u_a)$, by substituting equation **[2-60]** into equation **[2-61]**, to obtain the relation:

$$\frac{\chi}{f(s)} = \frac{-(\sigma - u_a)}{(u_a - u_w)} \qquad [2-62]$$

where χ and $f(s)$,independently, are both functions of the degree of pore saturation, **s**. According to equation **[2-62]** the ratio of the tensile strength to the soil-water matric potential in cracked soils should be constant in different soils (of ***similar*** pore space configuration) at the same value of **s**. This is true so long as the cracks in the different soils are ***similar*** in shape.

For saturated soils, $\frac{\chi}{f(s)} = 1.0$, regardless of the presence or absence of cracks, because at failure, all the tensile stresses are carried by the water. In unsaturated soils, tensile stress-concentrations occur as described in equation **[2-59]**, and the ratio of $\frac{\chi}{f(s)}$ will be less than 1.0, but can vary widely. Low values of $\frac{\chi}{f(s)}$ can occur in dry soil (small χ) and/or in soils containing sharp cracks (large $f(s)$). The maximum possible value of $\frac{\chi}{f(s)}$ is 0.5, which corresponds to the largest possible value of χ (unity, in nearly-saturated soils) and the smallest possible value of $f(s)$, which is approximately 2 (in air-filled, spherical flaws). This result has great practical significance because it means that the tensile strength of soils containing flaws and cracks that are draining, must be less than or equal to (but not greater than) approximately half the value of the soil-water matric potential $(u_a - u_w)$.

Verification of the theory of Snyder and Miller (1985) is given in Figure 2-9, for which the $\frac{\text{tensile strength}}{\text{matric potential}}$ ratio (or $\frac{\chi}{f\ (s)}$), based only on H-F theory (i.e. Aitchison's model, assuming no cracks; $f(s)$=1.0) are far too high (upper dashed line, with $\frac{\chi}{f\ (s)} = \chi$). A more realistic theoretical upper limit is shown by the lower dashed line for $\frac{\chi}{f\ (s)} = \frac{\chi}{2}$, which applies to spherical cracks. Note that the maximum possible value of $\frac{\chi}{f\ (s)}$, 0.5, is approached only at saturation (s=1.0). Hence all values for unsaturated real soils fall below $\frac{\chi}{f\ (s)}$ = 0.5. For moulded soils, the theoretical prediction is quite reasonable, but for aggregated soil, the theory over-estimates the experimental results. The reason for the difference between puddled and aggregated soils is that nearly all the water in the puddled soils contributes toward the tensile strength, whereas only the water at interaggregate contact points contributes to cohesion in aggregated soils. Intra-aggregate water will contribute nothing to the tensile strength, yet it will be counted in the value of s, and this causes the line for aggregated soil to be 'pushed' lower than the theoretical upper limit.

The theory of Snyder and Miller (1985) applies to the failure of uncemented, unsaturated (desorbed) soils under tensile stress (eg. shrinkage stresses or mechanical stresses due to tillage). Tensile failure occurs along the weakest flaws once the ratio of the tensile stress over the pore water matric potential reaches a critical value which is controlled by the degree of pore saturation. This gives important clues about the mechanics of brittle fracture in unsaturated soils. Initiation of failure in unsaturated soil will occur either (1) in only a few isolated places, or else (2) in many places at once. Soils having mainly small (saturated) pores and cracks (eg. poorly structured heavy clay soils, and soil crusts) will tend to fracture in only a few isolated places between larger, drained, pores where $\frac{\chi}{f\ (s)} << 1$, rather than

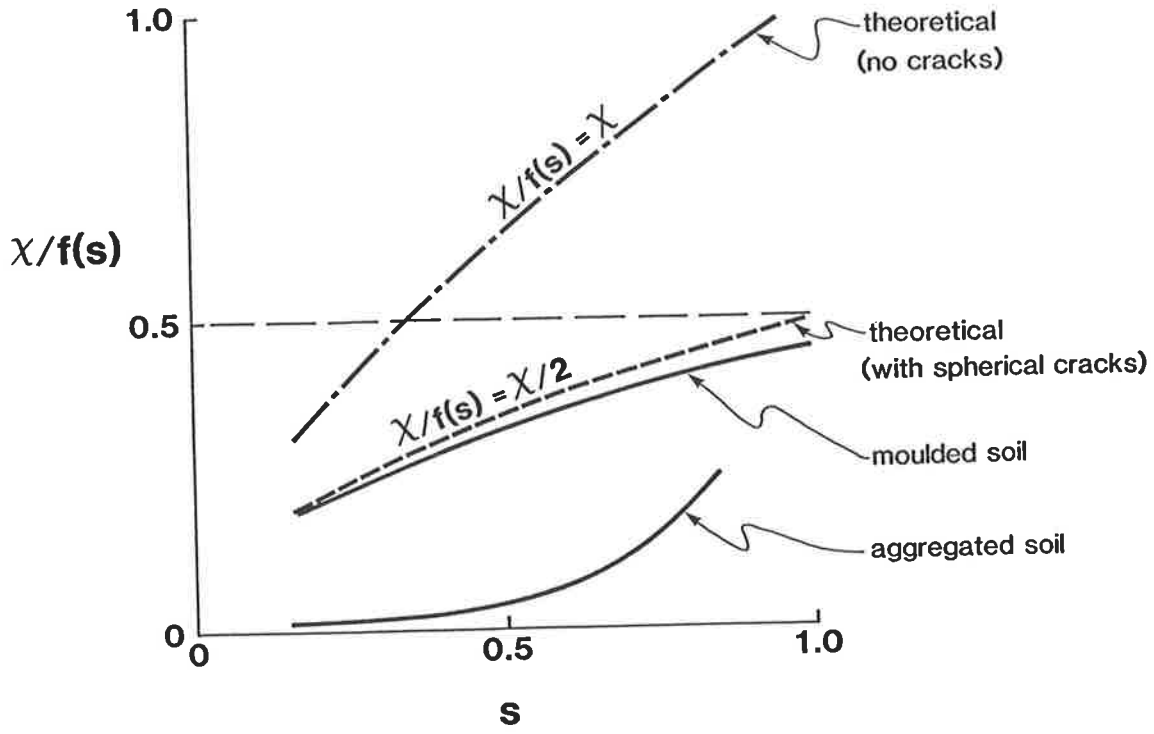

Figure 2-9. Plots of $\frac{\chi}{f(s)}$, or $\frac{-(\sigma - u_a)}{(u_a - u_w)}$, versus the degree of pore saturation, s, for theoretical (no cracks compared with spherical cracks) and real (moulded compared with aggregated) soils. Lines are sketched from the data of Figure 5 of Snyder and Miller (1985).

between smaller saturated pores where $\frac{\chi}{f(s)} = 1$. By contrast, coarse textured and well aggregated soils, (which have a high proportion of unsaturated pores, and correspondingly low values of $\frac{\chi}{f(s)}$) will tend to fracture at many points in the soil mass, resulting in friable tilths.

2.4.5 Practical Significance

Flaws and cracks in the soil contribute to the development of structure (Sleeman, 1962) and its heterogeneity (Larson and Allmaras, 1971) and are the result of many different factors (Heinonen, 1982). These factors include wetting and drying (Coughlan and Fox, 1977; Tessier et al, 1980; Utomo and Dexter, 1981c; Dexter, 1983; McKenzie and Dexter, 1985), freezing and thawing (Czeratzki and Frese, 1958; Utomo and Dexter, 1981b; Kay et al, 1985), the accumulation and decomposition of organic matter (Emerson, 1973; Oades, 1984), the presence of flocculating cations such as calcium (Loveday and Scotter, 1966), the activity of roots (Sequi, 1978; Misra et al, 1986), and earthworms (Barley, 1959; 1961; McKenzie and Dexter, 1988a,b), and tillage (Koolen and Kuipers, 1983).

This review, while recognizing the importance of freezing, thawing and biological activity, will be restricted to aspects of brittle fracture associated with water, organic matter and calcium.

2.4.5.1 Soil Water and Brittle Fracture

The role of static water content in the formation of soil aggregates was investigated many years ago by Vilensky and Germanova (1934), McHenry and Russell (1943) and by Vilensky (1937, 1940, and 1945). The results of Vilensky's investigations form the famous ' **Vilensky's Principle**' which states that there exists a water content for each soil, where optimum crumb formation occurs, and that at this water content crumbs formed have their maximum water stability and cohesion.

This water content is the **'moisture of aggregation'** or the **'moisture of structure development'** , and corresponds approximately to the lower plastic limit of the soil, or possibly a little drier (Hénin, 1936). This accords with the results of Arndt (1964) and also of Dexter (1979) and Ojeniyi and Dexter (1979) who found that maximum fragmentation of soil clods occurred at a water content of 0.9 times the lower plastic limit (**PL**). Much more energy is required to accomplish the same degree of soil fragmentation if tillage occurs at water contents significantly drier than 0.9**PL** (Russell, 1938), and if tillage is performed at much higher water contents, shearing dominates failure (Spoor and Godwin, 1979), and the soil becomes very cloddy upon drying. Boekel (1959; 1965; 1979) outlined an important relationship describing the "soil structure capacity" (= workability) as a function of the soil consistency limits of Atterberg (1911) in relation to the water content at field capacity, **FC**, (considered to be 10 kPa suction). For fine textured soils, he defined the ratio of the water content at the lower plastic limit (**PL**) to the water content at field capacity, **FC**. He found that if $\frac{PL}{FC}$ was much less than 1.0, soil workability was poor, whereas it was better for soils having $\frac{PL}{FC}$ greater than or equal to 1.0. In the case of coarse textured soils (which may be non-plastic) he defined the ratio of the water content at the upper plastic limit (**LL**) to the water content at field capacity, **FC**. Soil workability was found to be best when $\frac{LL}{FC} >> 1.0$ (eg. 1.5), whereas dispersion resulted when $\frac{LL}{FC}$ was less than or equal to 1.0. These ratios correlated quite well in his study with visual estimates of soil structure and soil cohesion (eg. see Figure 1 in Boekel, 1965). Another version of this approach was given by Greacen (1960) who combined Atterberg limits with water contents at different suctions to obtain an expression for the equivalent strength of soils.

The static water content of the soil also affects the recovery of soil cohesion (or age hardening) after tillage or disturbance (Blake and Gilman, 1970; Utomo and Dexter, 1981a,d; Molope, et al, 1985; Davies, 1985). Maximum age hardening occurs at water contents surrounding the lower plastic limit. If the soil is considerably drier than the **PL** (eg. air dry), cohesion-recovery due to thixotropic

processes is almost negligible (Mitchell, 1960), because the water films become too thin to allow significant particle rearrangement and migration of cementing substances (Kemper and Rosenau, 1984). At very high water contents, age hardening is also negligible, because there is insufficient particle-to-particle contact to allow strength recovery (See **Section 2.3.2**).

In addition to the effects of static water content discussed above, the influence of rapid changes in water content (i.e. wetting and drying) on the stability, the microfabric and the brittle fracture of soils is also quite significant (Utomo and Dexter, 1982; Dalrymple and Jim, 1984). It is known, for example, that aggregation can occur naturally in some soils during drying (Moormann and van Breeman, 1978) due to normal shrinkage and the development of internal tensile stresses, which cause cracks (Dexter and Woodhead, 1985). Wetting on the other hand also generates significant stresses (Emerson, 1979), and recent studies indicate that rapid wetting is the major cause of mellowing and strength-anisotropy of artificially compacted soils (Dexter, 1983; McKenzie and Dexter, 1985). Mellowing can be considered as partial slaking, wherein the soil is weakened by the introduction of micro-cracks yet does not completely fall apart. It was indicated by Mazurak (1950) that the effects of wetting and drying on aggregate stability "probably depend on the method of wetting more than upon the mere repetition of drying and wetting of the soils". The present review will therefore concentrate mainly on the role of rapid wetting.

Mellowing occurs when microcracks pervade the soil during rapid wetting (Dexter, et al, 1984) and this enables fragmentation to occur more easily during tillage (Yoder, 1936; Utomo and Dexter, 1981c). Mellowing of soil by wetting, however, is thought to occur only when the soil is initially very dry (McGeorge, 1937; Sanchez, 1973). It has been found by Sato (1969) and Nagahori and Sato (1970; 1974) that mellowing can occur in rice-producing clay soils submerged in water, only when the initial matric potential is drier than -1MPa. Soil aggregates that are initially wetter have already experienced considerable crystalline swelling and many of the pores are water-filled. This reduces the slaking effects of further wetting

(Dettmann, 1958; Emerson, 1977) when exposed to water at near-zero potentials.

The soil water content immediately prior to wetting is very important in the slaking process (Russell and Tamhane, 1940; Cernuda et al, 1954). For example, lower soil aggregate stabilities in wet sieving analyses have been found by Kemper and Rosenau (1984) as the soil water content, **w**, prior to immersion decreased in the range **w**=0.34 (high stability) down to **w**=0.02 (low stability). Panabokke and Quirk (1957) found that the initial soil water content influenced aggregate cohesion and stability through its effect on the wetting rate, noting that "planes of failure are set up" during rapid wetting. In their study, the response of macroaggregates (5-10 mm diameter) to rapid wetting, however, was different from that of microaggregates (0.05 mm diameter). The macroaggregates experienced greater structural breakdown when wetted from increasingly drier initial water contents, whereas the microaggregates were more stable. They attributed the higher stability of the microaggregates to "the protective action of entrapped air which prevents direct contact of the water with some of the colloidal interfaces". This result was also observed by Kolodny and Joffe (1939) and by Mazurak (1950).

As indicated by the results of Panabokke and Quirk (1957) with microaggregates, entrapped air may not necessarily be a destructive agent. If the cohesive strength of the soil is large in relation to the magnitude of the air pressure (as it might be in some calcium-stabilized soils), the entrapped air may greatly reduce the water permeability, especially into pores of intermediate size (Christiansen, 1944; Pillsbury and Appleman, 1945; Smith and Browning, 1946; Collis-George and Bond, 1981). Under these circumstances, however, there is also the possibility that water will eventually reduce the cohesive strength of the soil to below the pressure of the entrapped air, at which point the soil system 'bursts' or 'explodes' (Winterkorn, 1942; Dixit and Awasthi, 1971; Stroosnyder and Koorevaar, 1972).

This phenomenon has been expressed in the form of an equation by Concaret (1967):

$$s = C - P_i \qquad [2-63]$$

where **s** is the stability condition (either slaked or stable) determined by the balance between **C**, the cohesive (tensile) strength and P_i, the internal pressure of the entrapped air. An aggregate remains stable when $C > P_i$ (Bonneau and Levy, 1982). The point at which slaking occurs was expressed by McKenzie and Dexter (1985) as:

$$P_i - C = 0 \qquad [2-64]$$

which is equivalent to $s = 0$ in equation [2-63] The air pressure, P_i, may be calculated as follows (after Concaret, 1967):

$$P_i = \frac{2T \cos\alpha}{R} \qquad [2-65]$$

where **T** is the surface tension of water in contact with air, α is the contact angle between water and soil, and **R** is the radius of the soil pore. A detailed discussion of this phenomena is given in Bolt and Koenigs (1972). The effect of α on soil cohesion has been investigated by Robinson and Page (1950) and by Chassin (1979) using different organic compounds, but it is often assumed that $\alpha = 0^\circ$ in most soils (Panabokke and Quirk, 1957; Quirk and Panabokke, 1962).

Aggregate disruption during rapid wetting is also influenced by differential swelling (Emerson, 1964), although there is conflicting evidence in the literature about the relative significance of swelling versus air entrapment in the slaking process. Russell and Tamhane (1940) looked at the water stability of oven dried, and field-moist aggregates having different organic matter contents and wetted by immersion, by capillarity or under vacuum. Their results strongly implicated air entrapment in the slaking process. Smith and Browning (1946) also demonstrated (with photographs and percolation rates) the physical disruption of soil structure by the explosive action of air entrapped in clods and aggregates. They found that the structural damage due to entrapped air was greatest in intermediate-sized pores of silty and well-aggregated clay subsoils. They pointed out, however, that even under vacuum, whenever the soil was saturated for long periods (8-40 days), structural deterioration also occurred, and this was due to continuous swelling and dispersion of the clay fraction. Emerson and Grundy (1954) wetted columns of air-dried loam soil

aggregates, with and without evacuation, for different wetting periods. They concluded that structural degradation of the aggregates was due mainly to entrapped air and stated that non-uniform swelling of the clay fraction contributed very little to the loss of cohesion.

Brewer and Blackmore (1956), by contrast, found that the role of entrapped air in aggregate breakdown during rapid wetting of various clays was negligible relative to that of other forces. For one of their clays, only 20% of the total aggregate breakdown could be attributed to the effects of entrapped air. The rate and extent of slaking in most of their soils was related to swelling and its interaction with the soil fabric. The amount and degree of optical orientation of clay in the undisturbed agggregates was found to be critical. Soils with highly oriented, continuous clay-coatings on aggregates and in pores tended to breakdown faster and more completely than those with weakly oriented and less continuous coatings. They proposed that the directed forces of swelling exerted by highly oriented clay-coatings were more effective in breaking down aggregates than the random forces exerted by weakly oriented clay coatings. Weakly oriented clay was said to exert forces in all directions upon wetting "so that the resultant force tending to cause disruption will be small".

Dettmann (1958) also concluded that rapid swelling was the major cause of slaking, based first upon the fact that slaking of dry clay flakes occurred both at atmospheric pressure and under vacuum. Secondly, she found that slaking of clay flakes was prevented if swelling was induced slowly and uniformly by first exposing the clay to humid air for a few minutes prior to flooding. Third, when swelling did not occur, neither did slaking. Fourth, in apparent contrast to the findings of Brewer and Blackmore (1956), clay systems that were highly orientated experienced less violent disruption during flooding. Dettmann argued that "a perfectly packed array of uniform plates expanding rapidly in one direction..." could maintain its identity. In a random, less densely packed clay system, however, "the impulsive swelling forces could produce turning moments that could be disruptive". If wetting occurred slowly, on the

other hand, "local forces might be locally dissipated by relative motion of the particles into positions in which the stress is relieved but coherence is maintained".

Air entrapment was considered minor by Dettmann (1958), except during rapid flooding where she suggested that its effects would be augmented by temperature rises occurring by the release of the heat of wetting. Collis-George and Lal (1971) also claimed that entrapped air did not cause structural breakdown of oven dried aggregates. They too commented on the significance of the heat of wetting, released during infiltration, on aggregate collapse.

Panabokke and Quirk (1957) found that macro-aggregates (5-10 mm diameter) of an Urrbrae red-brown earth remained stable when wetted under vacuum, yet slaked at atmospheric pressure. The pressure of entrapped air which builds up ahead of a rapidly-advancing wetting front, and the diminished internal cohesion of the wet soil (Emerson, 1955) were considered the main reasons behind the slaking. To elucidate the role of reduced internal cohesion due to swelling with water, Panabokke and Quirk (1957) wetted aggregates with ethyl alcohol, which has a lower dielectric constant than water. (Ethyl alcohol is still a polar liquid, however, so would not stop all swelling, but its use would cause much less swelling than water; it would thus allow relatively higher attractive forces to be maintained among the clay plates than with water). They found that the aggregates remained stable when immersed in ethyl alcohol and assumed that any swelling of the clay fraction due to ethyl alcohol must have been internally accommodated within the aggregates.

With aggregates from their clay soils, however, Panabokke and Quirk (1957) found that slaking occurred when wetting was done with water, even under vacuum. Slaking also occurred when wetting was done at atmospheric pressure with ethyl alcohol, so air entrapment may have been involved. Differential swelling, nonetheless, was considered to have been the main mechanism responsible for breakdown of the clay aggregates. It was pointed out, however, that the rate of swelling may be more important than the total amount of swelling. The Wiesenboden used in Panabokke and Quirk's study had greater total swelling than the other two clay soils and yet was more

stable when immersed in water. The greater stability was speculated to be related to the Wiesenboden's high organic matter content, which may have reduced the wetting rate, but no data were reported on rates of wetting.

Although a consensus on the relative significance of air entrapment versus differential swelling could not be found in the literature, the two processes certainly occur at the same time (Bonneau and Levy, 1982). Thus, Bolt and Koenigs (1972) predicted that "an aggregate destroyed by air explosion will slake and thus become better accessible for the swelling action of water on the fractured elements".

2.4.5.2 Calcium and Brittle Fracture

The incorporation of calcium (as carbonate or sulfate) to hard-setting soils (in particular, to those under irrigation) has long been known to reduce dispersion and crusting, and thereby increase seedling emergence (Davidson and Quirk, 1961; Bennett et al, 1964; Bakker et al, 1973; Gobran et al, 1982; Rengasamy, 1983). It is also known to increase the soil friability, **k**, especially after numerous wetting and drying cycles (Shanmuganathan and Oades, 1983b).

The improvements in friability and soil structure caused by additions of calcium are mainly associated with a combination of (i) increased electrolyte concentrations in the soil solution, which induces flocculation of clay, and (ii) a reduction in the E.S.P., or exchangeable sodium percentage (i.e. exchange of calcium ions for sodium ions on clay surfaces) which reduces swelling and dispersion (Quirk and Schofield, 1955; Loveday, 1974, 1976). Changes in friability due to the addition of calcium compounds are responsible for improving the soil workability (Loveday et al, 1970), and reducing the modulus of rupture (c.f. Richards, 1953) of hard-setting soils (Aylemore and Sills, 1982). The effects on structure, however, are not always long-lasting (Chartres et al, 1985), especially under irrigated conditions (eg. Loveday, 1976). Periodic applications of calcium (eg. every few years) are therefore usually recommended to maintain the flocculation and reduced-dispersion effects (Shanmuganathan and Oades, 1983b).

Although it is known that the distribution of cracks in drying soil is controlled to a large extent by the nature of the exchangeable cations (Wolkewitz, 1958), most of the research looking at soil cracking has concentrated on macroscopic crack patterns (eg. Sleeman, 1963; O'Callaghan and Loveday, 1973), and little is known about the effects of calcium on microscopic flaws.

2.4.5.3 Organic Matter and Brittle Fracture

It has long been recognised that soils high in organic matter (eg. virgin soils and old pastures) have a well-aggregated structure when tilled (Russell, 1938; Low, 1955), and have higher infiltration rates and greater cohesion or resistance to dispersion (Emerson, 1954a; Greacen, 1958; Clapp and Emerson, 1965a,b). They also usually have lower bulk densities and breaking strengths (Williams et al, 1967; Hamblin and Davies, 1977). Organic matter is involved in binding aggregates of all sizes through a range of bonding mechanisms (Tisdall and Oades, 1982). For example, polysaccharides are particularly important for stabilizing microaggregates, and are produced as mucilages by plant roots, bacteria, fungi and algae (Mehta et al, 1960; Oades, 1984). It was suggested by Quirk and Panabokke (1962) that organic matter preferentially strengthens macropores against failure. This seems likely because the need for aerobic environments restricts most of the biota involved in polysaccharide production to relatively coarse soil pores along with roots (Adu and Oades, 1981a,b; Foster, 1981), which are considered to be zones of relative weakness in the soil (Oades, 1986) and which could be potential sites for crack propagation when tensile stresses are applied.

Organic matter strongly influences the wetting rate (Emerson, 1954b), the water-holding capacity (Hayes and Swift, 1978), and the plastic behaviour of the soil. For example, soils high in organic carbon have higher plastic limits (Mitchell, 1976) and can therefore be tilled at considerably higher water contents than other soils. Organic matter also influences aggregate formation and the shapes of particles produced by tillage (Dexter, 1985). For example, Chapman (1927) described the fracture

characteristics of air-dried clods from soils having high and low organic carbon (**OC**) contents as (italics mine):

> "All crumbs of the *low-**OC*** plot bore sharp edges and were inclined to break in two directions or when deviating from this, break with a chonchoidal fracture. These crumbs appear more like minerals or other substances of nearly constant chemical composition throughout their mass.
> In the case of the *high-**OC*** plot the crumbs were rounded and irregular, far more granular in structure than the *low-**OC*** plot."

More recently, Davis and Dexter (1972), Kousaka et al (1981) and Dexter (1985) have given quantitative information on aggregate shape which supports Chapman's observations. Dexter(1985) found a positive linear relationship between the roundness of Australian and Dutch soil aggregates and the soil organic matter content using the method of Fourier curvature spectra. Aggregates of low organic matter content were much more angular in shape.

2.5 Summary of Literature and Areas Needing Research

In summary, this review indicates that tensile strength is a measure of the true and apparent soil cohesion. Tensile stresses are active during soil drying and are responsible for incipient cracks, which are particularly relevant to the brittle fracture of unsaturated soils exposed to tillage.

Different mechanisms of cohesion pertain to different shapes and sizes of soil particles and aggregates. Particle-surface interactions are active cohesive agents between flat clay 'plates' over very short distances. Once two surfaces are separated by more than about 0.3 nm, only relatively weak physical forces (non-chemical bonding) are available to maintain cohesion. The further apart, the weaker the cohesive forces (Ingles and Lafeber, 1967), and the more significant are the phase and strength discontinuities in granular masses at very small scales. Water films and various cementing agents are also active in cohesion, but over a much wider range of particle sizes. Cohesion due to roots and fungal hyphae is active at a very large scale (up to several centimetres). The mechanisms which influence the response of soils to tillage

operations are those which operate at relatively large scales. Hence methods which assess interparticle cohesion at a scale of micrometres (eg. % dispersion) cannot predict the way in which unsaturated soil will respond to tillage operations.

The tensile strength imparted to the soil by (1) cements and (2) water is a function of the degree of contact generated between particles. (1) In the case of interparticle cementation, the area of contact between cement and substrate is important, the strength of the cement itself, and the nature of the cement-substrate bonding are also important. Much is known about the strength-inducing properties of cements such as calcium carbonate and gypsum, particularly in reference to the stabilization of granular materials exposed to huge compressive loads (eg. foundations, airstrips, embankments and roads). In agricultural soils, considerable work has also been done to improve the friability of dispersive and hard-setting soils, especially those under irrigation. (2) In the case of water in unsaturated soils, it is the degree of pore saturation that is important, because it controls the effective stresses between soil particles. The tensile strength imparted to unsaturated soil by water films plays a major role in determining the aggregate-size distribution and friability of the soil in response to tillage operations. Methods of assessing the response of unsaturated (and stabilized) soils to compressive and tensile stresses (eg. % size stability of dry clods, friability of soil tilths) although informative, are extremely time-consuming and tedious, however, particularly at different water contents. Simpler, more rapid and direct methods of looking at the structure of soils in response to tensile stresses are needed.

The heterogeneity (flaws and cracks) introduced to the soil by various bonding mechanisms makes the brittle fracture of unsaturated soils a rather complex process, and one which is very difficult to model. Prediction of the tensile stress needed to cause failure must take into account the criteria of Griffith theory. It has been shown in this review of the literature, however, that even Griffith theory on its own is inadequate, and that models which combine Griffith-theory with Haines-Fisher theory predict ma closely the measureable tensile strengths of uncemented, unsaturated soils.

According to the model of Snyder and Miller (1985), the initiation of failure should occur in either only a few places, or else many places at once, depending on the structural condition of the soil and the degree of pore saturation. This idea holds the potential for assessing the effects of different management practices on soil structure, but as indicated above, current methods for assessing brittle fracture are very difficult. Much work needs to be done in this area.

Ingles and co-workers, and Gramberg (1966) have done a considerable amount of work on the tensile strength of stabilized granular materials and rocks. They made qualitative observations directly on fracture surfaces, which suggest a possible means of assessing the mechanism of initiation of brittle fracture in soils. Their observations form the basis for many of the investigations outlined in this thesis.

The role of water in the brittle fracture of soils is outlined in this review, and special attention is paid to the behaviour of the soil at particular water contents, such as the Atterberg consistency limits and the field capacity. These affect the way in which soils crumble under tensile stresses. The quantitative extent to which the soil water content and the rate of wetting influence the distribution of flaws in the soil needs investigation, particularly in relation to the mellowing process. The effects of swelling versus air entrapment during rapid wetting have been discussed widely in the literature, mainly in reference to the stability of soil aggregates. There is controversy in the literature about the relative significance of these two destructive mechanisms on soil cohesion (tensile strength) mainly because the effects have not been quantified very clearly. Very little quantitative work has been done on the contribution of these two mechanisms to the mellowing process in structurally damaged, (or uniformly moulded) soils. The problem of quantifying these two mechanisms in moulded soils will form the basis for a number of studies in this thesis.

The roles of calcium and of organic matter in brittle fracture of soils have been discussed in this review mainly in reference to their effects on soil structure, friability and workability. Considerable descriptive work has been done with calcium on macroscopic cracking, but there is much quantitative work to be done before we

understand how microscopic cracking affects the brittle fracture of agricultural soils. Similarly, much work has been done looking at the effects of organic matter on soil strength, structure and workability, and yet no simple relationships seem to exist. Organic matter exerts control over the water content and plastic behaviour of the soil as well, and these in turn control the strength and workability. Research is needed to elucidate the interactive roles of organic carbon, particularly as they relate to brittle fracture of soils.

SECTION 3. SOIL FRACTURE SURFACES

3.1 Introduction

The tensile strength and the mechanics behind brittle fracture of unsaturated soil control the ease with which soil can be tilled, the patterns of cracking induced by wetting and drying cycles, and the resulting soil structures. This is appreciated in the drop-shatter test for soils (eg. Marshall and Quirk, 1950; Hadas and Wolf, 1984a) and also in the measurement of soil friability (eg. Braunack et al, 1979). These methods take advantage of two important facts: first, that brittle fracture of soil is influenced by the presence of microscopic and macroscopic flaws, and second that soil structure is hierarchical in nature (Hadas, 1987), wherein each structural group is composed of groups of lower structural order (Grant et al, 1985). Structural units of low hierarchical order (eg. small aggregates) usually have greater tensile strength relative to the structural units of higher order (eg. larger aggregates) (Ingles, 1962c; Rogowski and Kirkham, 1976; Braunack et al, 1979). The principal disadvantage, however, which limits the efficacy of current techniques in studies on the brittle fracture of unsaturated soil, is the laborious procedures involved in their measurement. New techniques are needed, which incorporate the same sort of information as these two methods, but which are much simpler to measure. The work reported here is an attempt to satisfy this need.

3.2 Background and Hypothesis

Snyder and Miller (1985) concluded that tensile failure in uncemented, unsaturated soil occurs along the weakest flaws in the soil once the ratio (tensile strength): (matric potential) reaches a critical value. It was suggested from their work that initiation of failure in unsaturated soil will occur either in a few isolated places or else in a large number of places at once, depending on the structure of the soil. Soils having small (saturated) pores and cracks (eg. soil crusts, poorly structured soils, and heavy clay soils) will tend to fracture in only a few isolated

places between larger, drained pores (not between smaller saturated pores). Soils containing mainly large (i.e. unsaturated) pores and cracks (eg. sandy soils and well-aggregated soils) will tend to fracture at many points in the soil mass. These suggestions complement the drop-shatter and the friability techniques in that they predict tensile failure is controlled by flaws and cracks and also by the nature of the structural hierarchy.

The fracture pathway is determined by the distribution (random, or otherwise) of the weakest flaws. If the weakest flaws are distributed at close range to one another, then when a sufficiently large tensile stress is applied across some plane in the soil, fracture occurs along a relatively straight pathway about that plane, simply by connecting these closely-spaced flaws. If the weakest flaws are widely spaced, on the other hand, then fracture must occur along a more jagged pathway about the tensile stress plane.

The failure surfaces produced under tensile stress should contain a 'blueprint' of the surface of the fracture pathway. Visual examination of tensile fracture surfaces can reveal much about the internal structure of different granular materials (see for example McDonald and Julian, 1966; also Figures 17, 18 and 31 in Gramberg, 1966; and Figures 11 to 14 in Ingles and Lafeber, 1967). In particular, the topography, or relief of the fracture surface should contain clues regarding the spatial distribution of the soil's internal weakest flaws. On this basis, it was proposed that soils with weakest flaws at close range to one another will produce relatively smooth fracture surfaces, while soils containing sparsely-distributed flaws will probably produce more jagged, or rugose fracture surfaces. The rugosity, or the degree of brokenness (Bernard, 1986) of a fractured soil surface is proposed to be directly related to the spacing between weakest flaws in the soil.

3.3. Spectral Analysis and the Nature of Soil Fracture Surfaces

The question first arises as to how the rugosity of fracture surfaces should be characterised to effectively describe the spacing between weakest flaws, and that is the

subject of the work that follows. One approach to characterising the rugosity of soil fracture surfaces is to quantify the spatial variability of the surface elevation along a transect across the soil surface. This can be accomplished by the use of variance spectra, autocorrelograms, or alternatively by the use of semi-variograms, (eg. Campbell, 1978). Variance spectra have been used by Davis and Dexter (1972) to characterize aggregate shapes and to characterize the surface relief of tilled soils (Dexter, 1977). Comprehensive reviews on the application of these geostatistical techniques to problems in soil science have been published relatively recently (eg. Trangmar et al., 1985; Webster, 1985), the theory for which is based on the notion of regionalised variables, as introduced by Matheron (1963).

In communications engineering, tools such as Fourier spectral analysis have been widely used to study the periodicity of wave forms in time (eg. Blackman and Tukey, 1958; Jenkins and Watts, 1968). The reason for its popular use is that data which exhibit periodicity are most simply described in terms of frequency, **f**, or wavelength, λ. Fourier analysis enables the transformation of these data from the time domain to functions of frequency or wavelength. The calculations associated with the transformation treat time and space analogously, hence Fourier analysis can often be applied to many spatial data series (Webster, 1977). It follows that the application of Fourier analysis to soil fracture surfaces may be expected to reveal something about the magnitude and spatial distribution of the weakest flaws in the soil.

There are, however, numerous problems involved with the indiscriminate use of Fourier techniques on any series of spatial observations. Among the problems are (1) assumptions of constant periodicity, (2) aliasing due to sampling at frequencies higher than the cut-off (or Nyquist) frequency, and (3) unidentifiable harmonics in the data. The first two problems are widely recognized in soil science (see for example, Green, 1967) and in most cases can be avoided through correct transformation and handling of the data series. The third problem, which is less well known but more serious, relates to the structural nature, or morphology, of the soil features being studied, and is not easily compensated for.

The morphology (eg. smooth, and angular or abrupt) of the features on a soil fracture surface gives important clues about the sizes and shapes of the underlying features around which fracture occurs (Marshall and Quirk, 1950). For instance, if the features are smooth and continuous, such as shown in Figure **3- 1a**, then the dominant wavelength, λ, from a spectral analysis of a transect of elevation across the fracture surface would likely correspond closely with the diameter (D_1) of the soil aggregates or features comprising the soil clod. Spectral analysis, in this case, could be quite a powerful tool for characterising the dominant aggregate size, or the spacing of the weakest flaws. If on the other hand, the topography of a soil fracture surface contains sharp, or abrupt or angular features as shown in Figure **3- 1b**, the aggregate diameter, D_2, corresponds poorly with the wavelength, λ, that would be revealed in a spectral analysis. In fact, λ, from Figure **3- 1b** could be as large as $2D_2$, and would therefore give misleading information.

An additional problem of spectral analysis in relation to fracture surface morphology is that waves which deviate significantly from a pure sine wave tend to exhibit the properties of a discontinuous wave (eg. square wave). The Fourier series representation of such a wave involves a large number of harmonics (component sine or cosine waves) to accurately specify their shape. For example, a symmetric square wave (Figure **3- 2c**) can be described as the summation of a fundamental sine wave and its odd harmonics in the Fourier series:

$$f(\Omega x) = A\{\cos\Omega x - \frac{1}{3}\cos 3\Omega x + \frac{1}{5}\cos 5\Omega x - \frac{1}{7}\cos 7\Omega x + \ldots\} \quad [3-1]$$

where **A** is the amplitude (Figures **3- 2a,b**), and $\Omega = \frac{2\pi}{\lambda}$. The fundamental sine wave of this Fourier series accounts for much of the variance. The harmonics, but especially the next (third) harmonic, account for the rest of the variance. Hence in cases where both large and small angular features are present (as in Figure **3-3**) the variance from the harmonics of the large soil features can overwhelm the fundamentals of the smaller-scale soil features present. The power spectrum under these circumstances

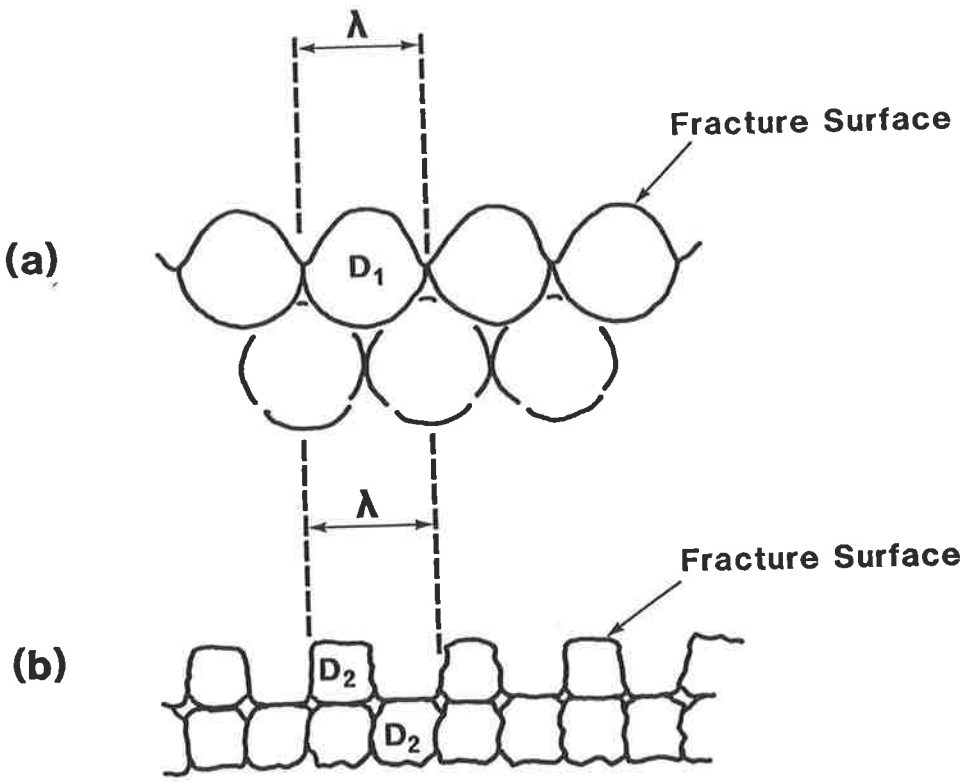

Figure 3-1. Shapes of soil fracture surfaces. (a) smooth, sinusoidal surface where λ is similar to D_1. (b) angular or abrupt surface where λ and D_2 are significantly different.

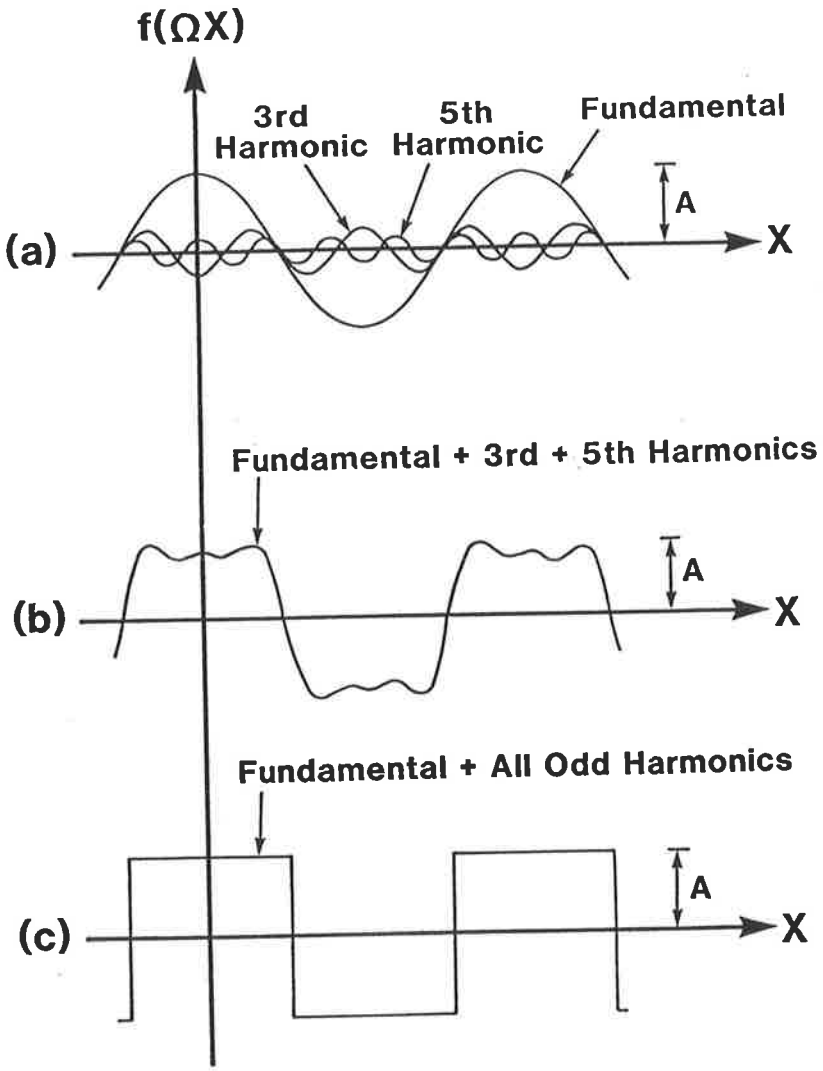

Figure 3-2. Plots of (a) some of the component sine waves (harmonics) of a symmetric square wave, superimposed on one another (b) composite wave of the fundamental, third harmonics; as higher harmonics are added, the composite wave becomes more and more like the (c) symmetric square wave.

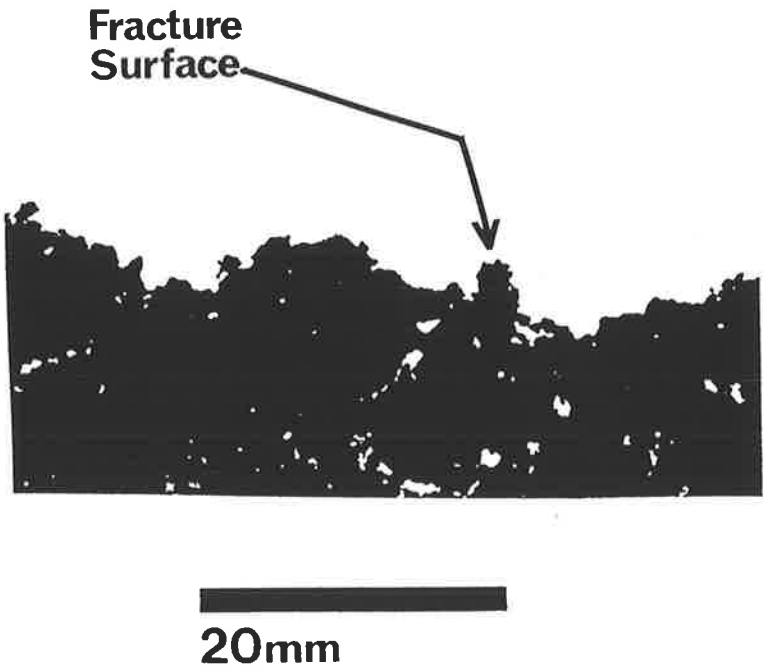

Figure 3-3. Soil fracture surface illustrating the angular nature or abrupt nature of both large and small surface features.

reveals the fundamental wave and the harmonics of only the largest soil features; the variance due to the smaller surface features is swamped by the harmonics from the larger surface features and cannot be resolved by Fourier analysis. Many of the soil samples examined in the present study exhibited fracture surfaces having abrupt, angular soil features. As a result, it was impossible to distinguish the dimensions of the smaller soil features using Fourier analysis, so the technique was not used for soils in this study.

3.4 Standard Deviations and Running Means

An alternative (and simpler though less sophisticated) way to characterise the rugosity of soil fracture surfaces is to calculate the variance, σ^2, of the elevation, **y**, along a transect of say **N** points across the soil fracture surface (Figure **3-4**).

$$\sigma^2 = \left[\frac{1}{N-1} \sum_{i=1}^{N} (y_i - \bar{y})^2 \right] \qquad [3-2]$$

The mean surface elevation, $\bar{y}$, is a constant, however, which makes σ^2 from equation **[3-2]** very sensitive to sample orientation within the **x-y** coordinate system. Consequently, a range of σ^2-values may be obtained for a single sample simply by tilting it at different angles. A more satisfactory result, which overcomes this problem uses local or running mean elevations, $\hat{y}_i$ where

$$\hat{y}_i = \left[\frac{1}{n} \sum_{i=j-a}^{j+a} y_j \right] \qquad \text{for} \quad a < i \leq N-a \qquad [3-3]$$

where $n = 2a + 1$, the number of values used in calculating $\hat{y}_i$,

$a = (n-1)/2$, the number of values used from each side of point, y_j, in calculating $\hat{y}_i$,

N = the total number of values in the data set.

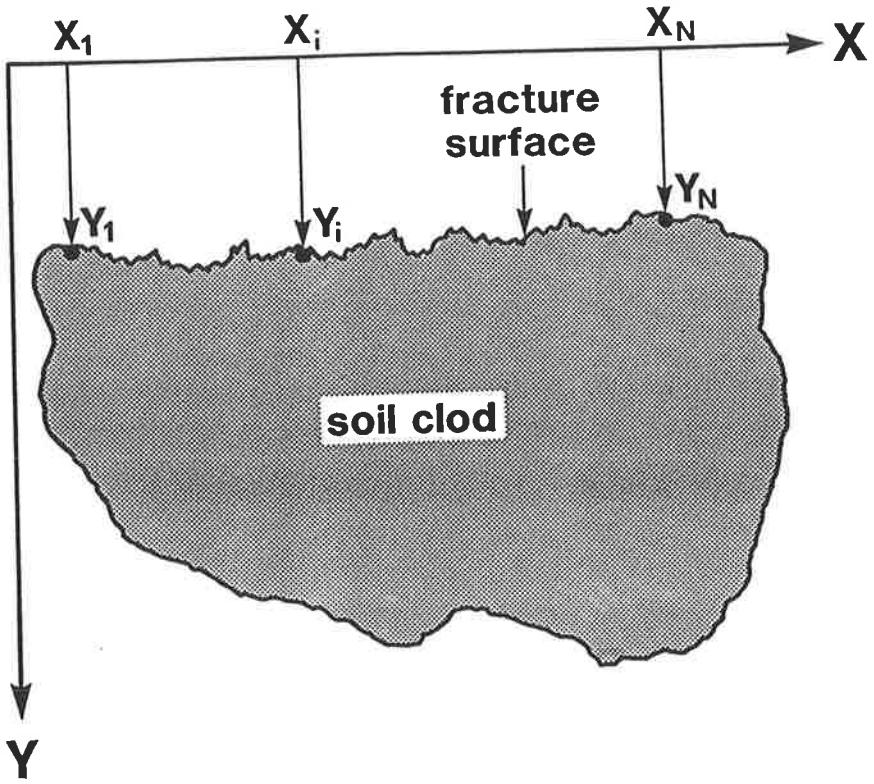

Figure 3-4. Representation of a cross section of a soil fracture surface illustrating the way in which surface elevation, y_i, was measured along a transect from (x_1,y_1) to (x_N,y_N).

(If Δx is the spacing in millimetres between successive measurements in the **x** direction, then the length, in millimetres, of the running mean, **M**, is equal to $2a\Delta x$). Use of running mean elevations, $\hat{y}_i$, in conjunction with the original elevations, y_i, to calculate the variance, σ^2, effectively eliminates errors which would otherwise arise from any tilting of the sample. In addition, it filters or attenuates the variance associated with large-scale features on the fracture surface (i.e. long wavelength features with $\lambda > M$). Note that the symbol λ is commonly used in reference to the dimensions of structural features (Miller and Miller, 1956), particularly in studies on the crystal structure of silicate minerals (Mitchell, 1976). The attenuation of variance caused by the use of *differences* from running mean values is outlined in Appendix 1. Some minor loss of accuracy in estimating the variance associated with smaller-scale features also occurs, and this is caused partly by the attenuation function involved, and partly by the reduction in the length of the data set by n points. The length of the running mean used in this study was 4 mm (corresponding to $n=41$ values of y_i) and the choice of $M=4$ mm is outlined in Appendix 1. The variance is now calculated on the differences between the surface elevation measurements, y_i, and their corresponding running mean values, $\hat{y}_i$:

$$\sigma_R^2 = \left[\frac{1}{N-n-1} \sum_{i=a}^{N-a} \left((y_i - \hat{y}_i) - (y_i - \hat{y}_i) \right)^2 \right] \qquad [3-4]$$

where the subscript **R** indicates that a running mean has been used. The standard deviation, σ_R, is used as a measure of the rugosity of the fracture surface. Large values of σ_R come from bumpy, irregular surfaces, whereas smaller values of σ_R come from smoother surfaces. More sophisticated analyses are possible (to be discussed in **SECTION 7**) but the simplicity of the technique outlined above for quantifying soil fracture surface rugosity carries considerable appeal.

3.5 Fracture Surface Rugosity and Tensile Strength in Relation to Air-filled Cracks

3.5.1 Theory for Fracture Surface Rugosity, σ_R

The idea suggested by Snyder and Miller (1985) that initiation of tensile failure occurs at sites of drained or unsaturated pores, has important implications for the tensile strength and the rugosity of soil fracture surfaces. If, for example, air-filled pores are considered to be the weakest flaws in the soil, then they will be relatively far apart from each other in wet soils. It has been argued in the hypothesis outlined in **SECTION 3.2** that under this condition, there would probably result a relatively jagged or rugose fracture surface. In drier soils, where air-filled pores (weakest flaws) are much closer together, smoother fracture surfaces should therefore be created under tensile stress. The validity of this idea depends on there being some relationship between the fracture surface rugosity and the distance between air-filled pores.

The nature of the relationship between fracture surface rugosity, σ_R, and the distance between air-filled cracks or pores may be assessed by modelling the soil as a porous, non-shrinking (constant volume) cubic block (dimensions L^3) consisting of smaller porous cubic blocks (dimensions l^3) in some hierarchical fashion (Figure **3-5**). In this model each block in the structural hierarchy is connected to other blocks of the same structural order by a bridge of some cementitious material of constant composition (eg. clay, O.M., or some mixture of both). The cementitious bridges between blocks occupy some proportion, **P**, of the volume of each crack. The value of **P** lies in the range $0 < P < 1$, and may or may not be variable at different size scales, depending on the soil friability. If the soil is very friable (cf. **SECTION 2.4.2**) the proportion of the crack-volume, **P**, occupied by cementitious bridges would be greater for smaller blocks than for larger blocks. If the soil is non-friable, **P** would be constant for all sizes of blocks. (This assumes that the tensile strength of cementitious bonds at various size scales is only a function of the volume of cement, which is true as long as the cement-composition is relatively constant). As the soil

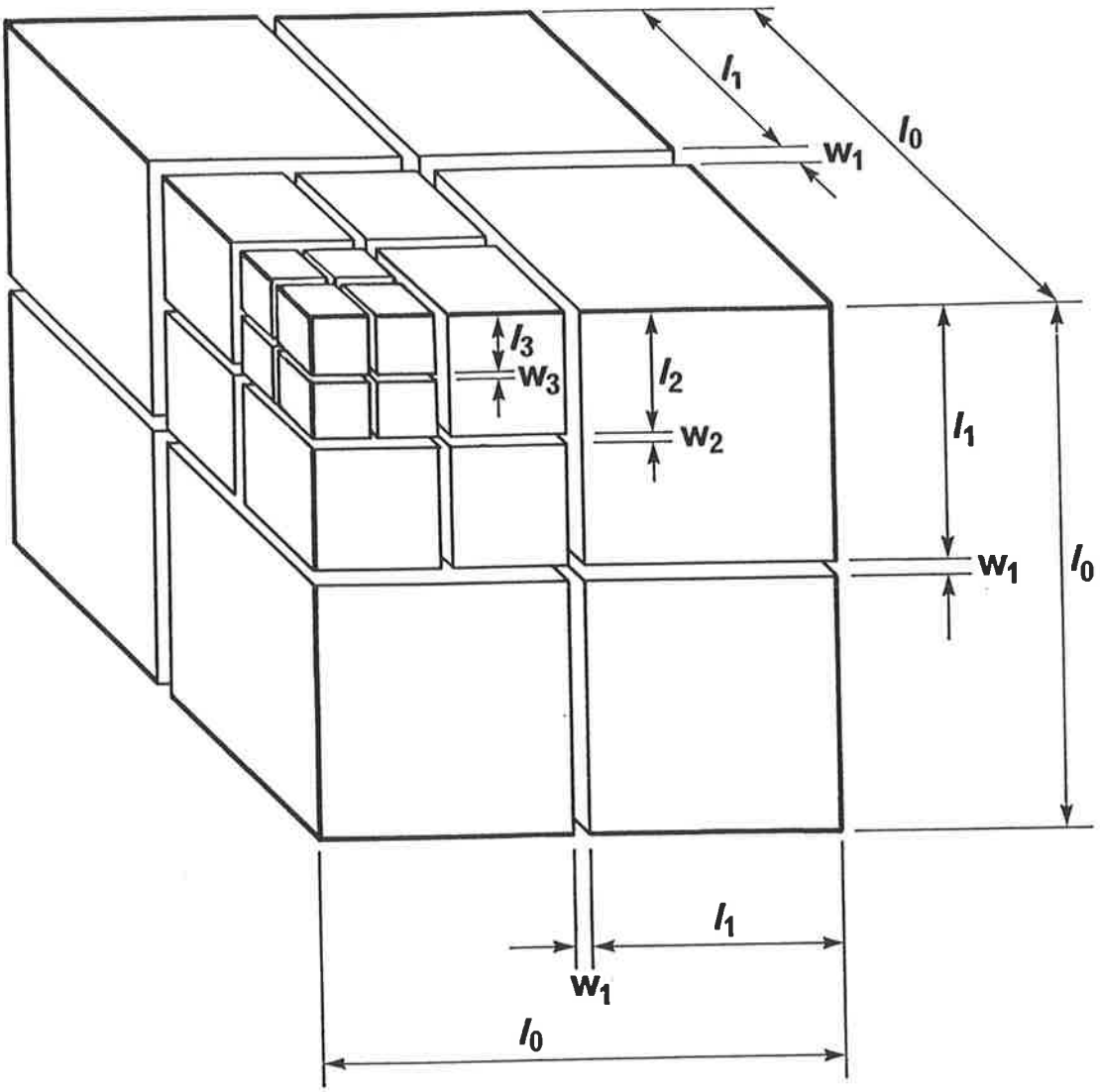

Figure 3-5. Cubic soil unit of macroscopic length, l_o, showing orthogonal, face-centred, continuous cracks of width, w_i, dividing the soil unit into eight cubes of length, l_i, where i = 1,2,3, representing progressively smaller levels of scale.

block (of bulk volume, $V_B = L^3$) gradually drains under suction from saturation, an unknown number of cracks, n_w, having width, w, will empty on each face of the block.

The unknown number of air-filled cracks, and the spacing between them may be estimated from the following model. Consider the drainage of the soil cube from a state i (having volumetric water content θ_i, corresponding to suction, h_i, and crack width, w_i) to a drier state, $i+1$ (having θ_{i+1}, h_{i+1}, w_{i+1}) The simplest case during drainage occurs where a single, face-centred crack of width, w_i, drains along each of three orthogonal axes of the cube (i.e. $n_{wi}=1$). Let these three cracks be continuous through to opposites sides of the cube so that the block is divided into eight smaller cubes each having volume $l_i^3 = \{(l_{i-1} - n_{w\,i} w_i)/(n_{w\,i}+1)\}^3$. (For drainage of the first cracks, $l_{i-1} = l_0 = L$, which is the length of the original saturated soil cube). The air-filled volume for each of the cracks between the eight smaller cubes is (ignoring for now the volume of saturated soil material bridging the crack and preventing it from collapsing when it drains):

$$V_{ci} = w_i l_i^2 \qquad [3-5]$$

and the number of these cracks in the whole soil block, N_{wi}, is

$$N_{w\,i} = 3n_{w\,i}(n_{w\,i}+1)^2 \qquad [3-6]$$

Considering now the volume of the saturated soil material bridging each crack, the width of soil bridge is determined by the crack-width, w_i, and it is assumed here, for simplicity, that the length and breadth of the soil bridge are both equal to some length, x_i (refer to Figure 3-6). So the proportion, P_i, of the crack volume, V_{ci}, that is occupied by soil bridges is:

$$P_i = \frac{V_{si}}{V_{ci}} = \frac{w_i x^2}{w_i l_i^2} = \frac{x_i^2}{l_i^2} \qquad [3-7]$$

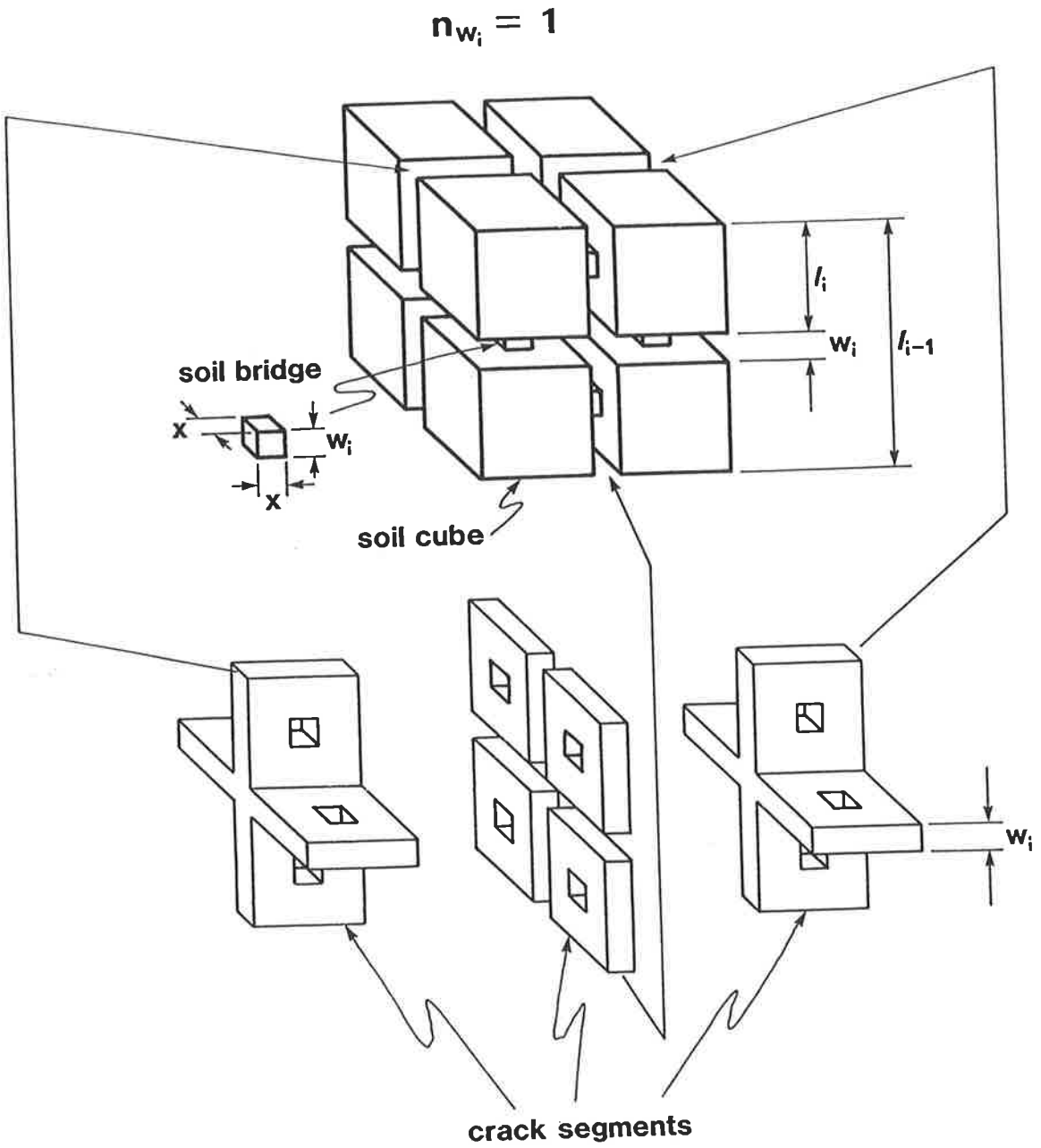

Figure 3-6. Soil cube of length, l_{i-1}, cracked once ($n_{wi} = 1$) in each of three orthogonal directions creating eight cubes (length = l_i) and illustrating the volumes of the crack segments (width, w_i, and the volumes of the soil bridges ($X \times X \times w_i$) across the cracks.

where V_{sl} is the volume of the soil bridge. Hence the proportion of a crack that is truly empty is $(1-P_l)$, and so the volume of all cracks, V_{Tl}, of width, w_l, within the whole soil block is the product of the volume of one crack segment, V_{cl}, times the fraction of the crack that is truly void, $(1-P_l)$ times the total number of crack-segments in the whole block:

$$V_{Tl} = w_l l_l^2 (1-P_l) \; N_{wl} \qquad [3-8]$$

So in the case of one crack on each face draining in each of the three orthogonal directions, $V_{Tl} = 12 w_l l_l^2 (1-P_l)$, and in the case of two cracks, it can be seen from Figure 3-7 and equation [3-8] that $V_{Tl} = 54 w_l l_l^2 (1-P_l)$. Likewise, the volume of cracks, V_{Tl}, for any number of cracks per face, n_{wl}, can be calculated, and some of these volumes are shown in Table 3-1. For large numbers of cracks (eg. $n_{wl} > 50$) the value of $n_{wl}+1$ approaches n_{wl}, so that equation [3-8] may be approximated as

$$V_{Tl} = w_l l_l^2 (1-P_l) \; 3 n_{wl}^3 \qquad [3-9]$$

The total volume of cracks, V_{Tl}, of width w_l, relative to the bulk volume of the original soil cube, V_B, is described by the relation:

$$\frac{V_{Tl}}{V_B} = \frac{w_l l_l^2 \; (1-P_l) \; N_{wl}}{L^3} \qquad [3-10]$$

Measurement of $\frac{V_{Tl}}{V_B}$ can be determined experimentally from a soil-water desorption curve because it relates directly to changes in the volumetric water content. That is,

$$\frac{V_{Tl}}{V_B} = \Delta\theta_l \qquad [3-11]$$

where θ_l is the volumetric water content, and $\Delta\theta_l$ is $(\theta_l - \theta_{l+1})$, the change in the volumetric water content during desorption from a wetter state, i, to a drier state, i+1. Values of θ_l come from the desorption curve:

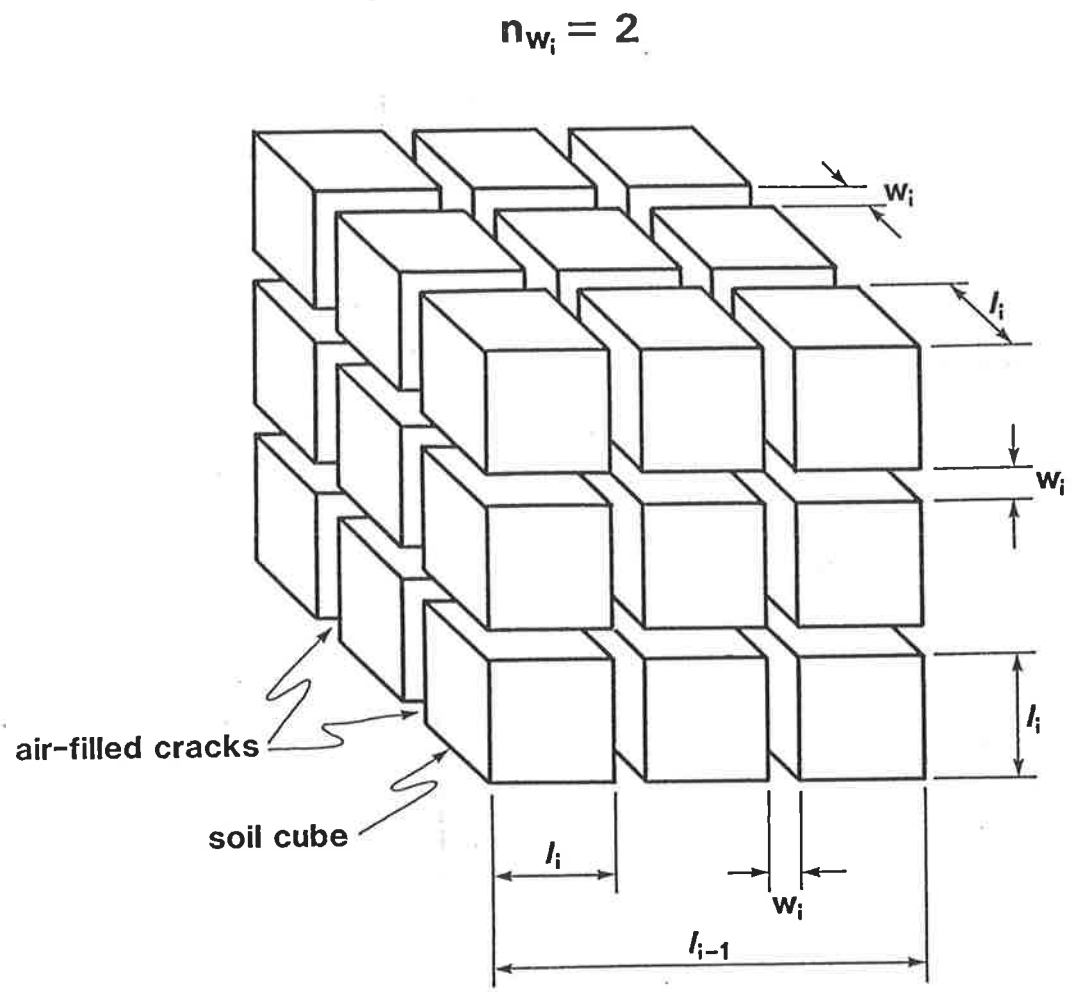

Figure 3-7. Cube of soil (length = l_{i-1}) cracked twice (n_{wi} =2) in each of three orthogonal directions, creating $(n_{wi} + 1)^3$ = 27 smaller cubes of length l_i, and crack width, w_i.

drainage state i	n_{wi}	$3n_{wi}(n_{wi}+1)^2$	V_{Ti}	
1	1	12	$12w_i^2$	(1-P)
2	2	54	54 "	
3	3	144	144 "	
4	5	540	540 "	
5	10	3.63×10^3	3.63×10^3 "	
6	25	5.07×10^4	5.07×10^4 "	
7	50	3.75×10^5	3.75×10^5 "	
8	100	3.06×10^6	3.06×10^6 "	
9	1000	3.01×10^9	3.01×10^9 "	

Table 3-1. Number of cracks, n_{wi}, of width, w_i, on orthogonal cube faces, number of cracks in whole soil cube, and total volume, V_{Ti}, of cracks having width, w_i, in whole soil cube at drainage state i.

$$\theta_i = F(h_i) \qquad [3-12]$$

where h_i is the soil water suction. Values of crack-width, w_i, may be calculated for any suction, h_i, using the modified Kelvin equation applicable to flat parallel plates, as used by Innes (1957), Aylmore and Quirk (1967) and Greenland (1979):

$$w_i = \frac{2\sigma}{\rho g h_i} \qquad [3-13]$$

where the surface tension of water, $\sigma = 7.342 \times 10^{-3}$ kgm^{-1}, the density of water at 20° C, $\rho = 1000$ kgm^{-3}, and the gravitational acceleration, $g = 9.8$ ms^{-2}.

Equating [3-11] to [3-10] and solving for the number of cracks per face, n_{wi}, of width, w_i, gives the relation:

$$n_{wi} = \left(\frac{\Delta\theta_i \, (l_{i-1})^3}{3 \, w_i \, l_i^2 \, (1 - P_i)} \right)^{1/3} \qquad [3-14]$$

Equation [3-14], however, cannot be solved in its present form because l_i is also a function of n_{wi}, viz:

$$l_i = \frac{l_{i-1} - n_{wi} \, w_i}{n_{wi} + 1} \qquad [3-15]$$

Substitution of equation [3-15] in equation [3-14] gives

$$\left(\frac{l_{i-1} - n_{wi} \, w_i}{n_{wi} + 1} \right)^2 n_{wi}^3 = \frac{\Delta\theta_i \, (l_{i-1})^3}{3 \, w_i \, (1 - P_i)} \qquad [3-16]$$

In most cases $w_i << l_{i-1}$, and because we are using values of $n_{wi} < 10$, we can say that $n_{wi} w_i$, in equation [3-16] is negligible, and can therefore be approximated by:

$$\left(\frac{l_{i-1}}{n_{wi} + 1} \right)^2 n_{wi}^3 = \frac{\Delta\theta_i \, (l_{i-1})^3}{3 \, w_i \, (1 - P_i)} \qquad [3-17]$$

Using values of l_{i-1}, $\Delta\theta_i$, w_i, and P_i, equation [3-17] may be solved numerically for n_{wi} as follows:

$$0 = \left(\left(\frac{l_{i-1}}{n_{wi}+1}\right)^2 n_{wi}^3 \left(\frac{3\, w_i\,(1-P_i)}{\Delta\theta_i\,(l_{i-1})^3}\right)\right) - 1 \qquad [3-18]$$

As the soil drains, progressively smaller and smaller cracks are exposed. Substitution of calculated values of n_{wi} from equation [3-18] into equation [3-15] enables the calculation of l_i, which is the average distance between cracks of the same width, w_i, or the distance between the smallest air-filled pores. If this idea is valid, the magnitude of l_i should be somehow related to the fracture surface rugosity, σ_R, at least for soils where air-filled pores are the weakest flaws.

3.5.2 Theory for Tensile Strength, TS

From the work of Snyder and Miller (1985), the tensile strength, TS, of unsaturated, uncemented, cracked soils (or flawed, granular materials) may be predicted from the relation:

$$-(TS-u_a) = (u_a-u_w)\,\frac{\chi}{2} \qquad [3-19]$$

or

$$TS = \frac{\chi\, u_w}{2} + u_a\left(1 - \frac{\chi}{2}\right) \qquad [3-20]$$

where u_w is the gauge pressure of the pore water, u_a is the gauge pressure of the pore air relative to atmospheric pressure, and χ is a dimensionless parameter varying between zero and unity, and described by equation [2-51] after Snyder and Miller (1985) and Aitchison (1961):

$$\chi = s + \frac{0.3}{(u_a - u_w)} \int_{i=s}^{1.0} (u_a-u_w)_i \, d\, s_i \qquad [3-21]$$

where s_i = the degree of pore saturation (see equation [2-45]), and where $(u_a - u_w)$ is the pore water pressure deficiency at any point i between i=s and complete saturation (i=1.0).

The pore water pressure deficiency $(u_a - u_w)$, when expressed as a pressure potential, Ψ, is:

$$\Psi = -\rho gh = -(u_a - u_w) \qquad [3-22]$$

So by substitution into equation [3-21], we may write

$$\chi = s + \frac{0.3}{(-\Psi)} \int_s^{1.0} (-\Psi)\, ds \qquad [3-23]$$

To evaluate the integral in equation [3-23], consider the general relation between Ψ and θ, viz:

$$(-\Psi) = f(\theta), \text{ or the inverse function, } \theta = F(-\Psi)$$

and $$[3-24]$$

$$(-\Psi) = g(s), \text{ or the inverse function, } s = G(-\Psi)$$

Many forms of equation [3-24] have been proposed to describe the functional relationship between Ψ and θ (or s), all of which are empirically derived, and useful over only relatively narrow ranges (Hillel, 1980). The form of the equation used in this study to describe the relation between the potential, Ψ, and the water content θ (for the range of $-\Psi$=0 to 50 kPa) was

$$f(\theta) = \exp(a + b\theta)$$

or $$[3-25]$$

$$g(s) = \exp(a + ns)$$

where a and b are adjustable parameters, n=bf, θ is the volumetric water content, and s is the degree of saturation. By substituting equation [3-25] into equation [3-23], the solution for χ is found to be:

$$\chi = s + \frac{0.3}{\exp(a+ns)} \int_{s}^{1.0} \exp(a+ns)\,ds \qquad [3\text{-}26]$$

or

$$\chi = s + \frac{0.3}{n \exp(ns)} \left(\exp(ns)_{s}^{1}\right) \qquad [3\text{-}27]$$

To obtain an estimation of the tensile strength of the soil, the value of χ from equation [3-27] is substituted into equation [3-20]. In situations where the gauge pressure of the pore air, u_a, is equal to zero, equation [3-20] is considerably simplified, and the tensile strength of the soil becomes:

$$TS = \frac{\chi}{2} u_w \ . \qquad [3\text{-}28]$$

3.5.3 Experimental Relation between *I* and σ_R and between Predicted- and Measured-Tensile Strengths, TS.

3.5.3.1. Materials and Methods

The relation between *I* and σ_R was investigated using a soil water-release curve determined from soil clods on which tensile strength, **TS**, was also measured. A large number of fist-size clods from within the top 10 cm was dug from a small area (2m x 2m) in Field-W-10 at the Waite Agricultural Research Institute. The soil was an Urrbrae Red-brown Earth (Soil A-2 as described in Litchfield, 1951), containing 17% clay, the mineralogy of which was dominated by illite and kaolinite (Chittleborough and Oades, 1980; Williams, 1981). Field W-10 was previously used for approximately ten years of cereal crop management, and had a soil organic carbon content of 1.32%.

Clods were reduced in volume from fist-size to approximately 200 cm^3 by trimming with a pallet knife. They were then gradually wetted to near saturation in the laboratory by applying de-ionized water using a spray atomizer and covering the samples for several days. The wet clods were then set on porous ceramic plates where five controlled water suctions (0.5, 1.0, 5.0, 10.0, and 50.0 kPa) were used to

establish a range of soil water contents over a period of several weeks. Contact between the samples and the ceramic plates was made using a thin layer of moist soil. Previous experience showed that approximately ten days was necessary for equilibrium water contents to be attained. At equilibrium, clods were broken by hand into 3 to 4 pieces, and then measurements of tensile strength, **TS**, (kPa), penetrometer resistance, Q_p, (kPa), soil water content, **w**, (kg kg^{-1}), bulk density, ρ_b, (kg m^{-3}) and fracture surface rugosity, σ_R, (mm) were conducted on separate pieces from single clods.

Tensile strength measurements were made using the indirect tension test (Ingles and Frydman, 1963; Frydman, 1964; Dexter, 1988b) which fractures clods between flat, parallel plates. The tensile strength, **TS**, was calculated (after Dexter, 1975, and Dexter and Kroesbergen, 1985) as:

$$TS = \frac{0.576\ F'}{d^2} \qquad [3\text{-}29]$$

where F' is the polar force measured at failure (i.e. as soon as a central crack occurs, and **d** is the geometric mean diameter, **d**, of the soil clod calculated (from the diameters d_1, d_2, d_3 on three orthogonal axes) as follows:

$$d = (d_1\ d_2\ d_3)^{1/3} \qquad [3\text{-}30]$$

For the results reported in this thesis, errors due to flattening of the soil samples at the contact points were negligible. Measured values of tensile strength were compared to those predicted from equation **[3-28]** to investigate the contribution of soil water to the tensile strength.

Penetrometer force was measured once on each clod with a motor-driven (3mm min^{-1}) steel probe, having cone diameter 1mm and total cone angle = 60°. The shaft of the probe was relieved for 7mm behind the tip. Each clod to be probed was placed on the pan of a top-loading electronic digital balance (Mettler type PC-4400) and the force exerted by the probe was recorded by using the balance-reading at a penetration depth of 5mm. This depth was chosen on the basis of Dexter and Tanner's (1973) finding that the penetration force for cones reaches a relatively constant maximum at depths greater than four times the cone diameter. Penetrometer resistance, Q_p, was calculated as:

$$Q_p = \frac{F}{\pi r^2} \quad ,kPa \qquad [3\text{-}31]$$

where **F=Ma** in N, **M**= electronic balance reading in kg, **a**= gravitational acceleration constant (9.806 ms^{-2}), and **r**= cone radius in m.

Water contents (mass basis) were determined at the time of indirect tensile fracture and at the time of penetrometer probing. Bulk densities were determined on air-dry clods using the clod-paraffin method of Blake (1965).

Two fracture surfaces were selected from each main clod by fracturing it (1) in the hands, by direct tension, as well as (2) using the indirect tension test (see Dexter, 1975). One half of each fractured sample was arbitrarily chosen for analysis of fracture surface rugosity, σ_R. The selected half of the fractured soil sample was fitted into a plastic vial (inside diameter = 3.0mm) such that the fracture surface stood vertically. The vial was filled with a white epoxy compound (Ciba-geigy Araldite, in the ratio 5:1:1 resin-LC-191 : white pigment-DW0131-W : hardener-HY951), which hardened within 24 hours. The epoxy compound provided an effective white contrast against the darker coloured soil, a necessary feature to produce a precise computer image. The vials were then bisected horizontally using a diamond saw to produce a transect, or profile of the fracture surface, across an arbitrarily selected plane that was perpendicular to the fractured surface (see Plate **3-1**). The extent to which this single transect was 'representative' of the soil surface depended on the assumption that the soil contained randomly (or isotropically) distributed flaws. This was considered to be a reasonable assumption for the soils used in this study.

The profile exposed in each cross section was examined with a video camera (National WV-140N/A) equipped with a 25mm focal length lens. The video picture was digitized by an Apple II^+ microcomputer that was fitted with a Video Digitising Card (Digisector DS-65). The vertical distance between the camera and all the soil profiles was held constant at 130mm to ensure identically-scaled images. A scanning procedure was conducted by the computer, first along a standard 20mm linear scale (to calibrate the system) and then along a fixed length of 23mm (comprising N=236 digitised points) across the centre of each soil profile.

Plate 3-1. Preparation of soil clods for fracture surface analysis: (a) direct tensile fracture in hands. (b) indirect tensile fracture of clod between parallel plates. (c) pouring of white epoxy resin around one half of fractured clod. (d) cross-sectional transect of clod embedded in the hardened epoxy resin. (e) video camera (on right) projects image of soil cross-sections onto a television screen (centre) and the image is then digitixed by the computer to produce an image for rugosity analysis (left).

a

b

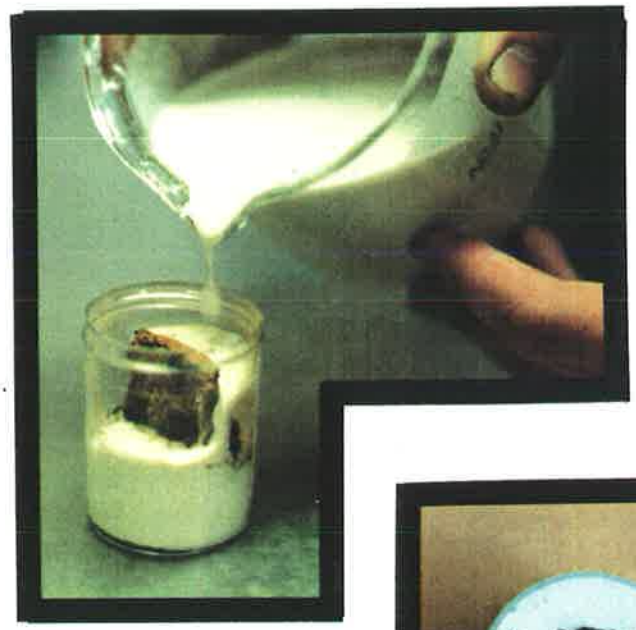

c

d

Plate 3-1.

e

The scanning procedure involved a pixel-by-pixel examination of the video-image of the cross-sectioned soil surface, from a fixed **y**-position on the video screen above the image (where the background colour was white) down toward the image until the 'moving-pixel' encountered a contrasting colour at the soil surface. The **x** and **y** coordinates at the soil surface were recorded at the point where the colour-change occurred, and then the moving-pixel shifted across the image by **x**=1 pixel and the scanning procedure was re-initiated from the fixed **y**-position above the image on the video screen (cf. Figure **3-4**). This procedure was carried out for **N**=236 pixels at fixed intervals of $\Delta x = 9.75 \times 10^{-2}$ mm. The resolution in the y direction, Δy, was equal to Δx. The 236 **x-y** pairs were stored for future analyses as an array for each sample that was scanned.

Values of fracture surface rugosity, σ_R, were then computed on the **y**-values of each profile using equations **[3-3]** and **[3-4]**. The inherent error, or sensitivity of the scanning and digitising procedure was assessed by measuring values of σ_R^2 for a straight line held at different angles. The value of σ_R^2 expected for a perfectly smooth, straight and horizontal line is zero if the scanning and digitising equipment had infinite resolution. It was found, however, that a straight line had a small, but measurable value of $\sigma_R^2 = 0.00216$ mm, which meant that each measurement of σ_R on soil surfaces would be over-estimated. We therefore applied the following correction to each measured value of σ_R :

$$\sigma_{R\,(correct)} = (\sigma_{R\,(measured)}^2 - \sigma_{R\,(line)}^2)^{1/2} \qquad [3-32]$$

All values of corrected-fracture surface rugosity in this study will be referred to by the symbol σ_R.

3.5.3.2 Results and Discussion

3.5.3.2.1 Relation Between l and σ_R

Listed in Table **3-2** for each of five water suctions, **h**, are the average gravimetric water contents, $\bar{w}$, measured for each clod from Field W-10, as well as the bulk densities, ρ_b, (determined on relatively large pieces for each clod) and the volumetric water contents, θ, (calculated on a clod-by-clod basis using the bulk densities). The gravimetric water contents, $\bar{w}$, in Table **3-2** came from two measurements on each clod. One water content was from the piece fractured by indirect tension while the other water content was from the piece used for penetrometer resistance. Both values of water content are reported in Appendix **2**, Table **A2-1**, but because the water contents were so close for the two pieces of each clod, only the averages are reported here in Table **3-2**.

Estimation of the average distance between cracks (or average length of uncracked soil), l_i, according to the theory outlined in **SECTION 3.5.1**, involves the calculation of volumetric water contents, θ', from equation **[3-12]**. To do this, the five levels of suction, **h** and their corresponding measured average values of volumetric water content listed in Table **3-2** were used to calculate the equation for the desorption curve:

$$\theta' = 0.400 - 0.044 \log_{10} h \qquad (R=0.972; \quad n=5) \qquad [3-33]$$

where **h** is expressed in hPa (1 hPa $\simeq$ 1 cm water). Five values of θ', calculated from equation **[3-33]** for suctions 5, 10, 50, 100, 500 hPa, are listed under the measured average values, $\bar{\theta}$ in the right-hand column of Table **3-2**.

From equation **[3-33]** the volumetric water content, θ', may be used to compute the number of cracks, n_{wi}, of various sizes, w_i, and hence the average distance, l_i, between these cracks. A range of fifteen (arbitrarily-selected) **h**-values was initially substituted into equation **[3-33]**, such that as the soil drained from state **i** to state **i+1**, the ratio $\frac{h_{i+1}}{h_i}$ was ideally less than a factor of three. The reason

Table 3-2. Average gravimetric water contents (clod-by-clod basis) of soil clods taken from Field W-10 (Waite Agricultural Research Institute) and equilibrated at 5, 10, 50, 100, and 500 hPa water suctions; bulk densities (clod-by-clod basis; except for 5 hPa samples for which the average value of all other clods was assigned); volumetric water contents, θ and θ' (θ calculated using bulk densities, assuming a particle density of 2650 kgm^{-3}) and θ' predicted form equation [3-33]), and average volumetric water contents, $\bar{\theta}$.

Table 3-2

Water Suction h, (hPa)	Clod #	Average Water Content $\bar{w}$ ($kgkg^{-1}$)	Bulk Density (kgm^{-3})	θ (m^3m^{-3})	$\bar{\theta}$ ± s.e. & n and (θ')
5	1	0.244	1540	0.376	0.378
"	2	0.256	"	0.394	± 0.009
"	3	0.282	"	0.434	n=8
"	4	0.238	"	0.367	
"	5	0.234	"	0.360	(θ' = 0.370)
"	6	0.231	"	0.356	
"	7	0.233	"	0.359	
"	8	0.244	"	0.376	
10	1	0.230	1500	0.345	0.346
"	2	0.213	1570	0.334	± 0.008
"	3	0.213	1540	0.328	n=8
"	4	0.212	1480	0.314	
"	5	0.233	1570	0.366	(θ' = 0.356)
"	6	0.224	1540	0.345	
"	7	0.227	1560	0.354	
"	8	0.242	1580	0.382	
50	1	0.202	1550	0.313	0.332
"	2	0.209	1480	0.309	± 0.010
"	3	0.205	1550	0.318	n=9
"	4	0.248	1550	0.384	
"	5	0.190	1540	0.293	(θ' = 0.326)
"	6	0.192	1620	0.311	
"	7	0.231	1510	0.349	
"	8	0.226	1550	0.350	
"	9	0.227	1580	0.359	
100	1	0.186	1480	0.275	0.305
"	2	0.204	1540	0.314	±0.006
"	3	0.189	1510	0.285	n=9
"	4	0.210	1540	0.323	
"	5	0.214	1540	0.330	(θ' = 0.312)
"	6	0.217	1470	0.319	
"	7	0.206	1480	0.305	
"	8	0.200	1490	0.298	
"	9	0.200	1490	0.298	
500	1	0.178	1570	0.279	0.285
"	2	0.186	1540	0.286	± 0.005
"	3	0.188	1600	0.301	n=8
"	4	0.188	1560	0.293	
"	5	0.163	1550	0.253	(θ' = 0.282)
"	6	0.192	1530	0.294	
"	7	0.179	1560	0.279	
"	8	0.189	1560	0.295	

for trying to maintain relatively small steps in suction, **h**, was to minimize the error of attributing the volume of pores drained ($\Delta\theta_i' = \theta_i' - \theta_{i+1}'$) all to smaller pores of width w_{i+1}. The problem was further minimized by matching values of $\Delta\theta_i'$ with 'average' pore widths, $\bar{w}_i$, (from equation **[3-13]**) using average suctions, $\bar{h}_i$, defined by:

$$\bar{h}_i = \frac{h_i + h_{i+1}}{2} . \qquad \textbf{[3-34]}$$

In calculating the number of cracks, n_{wi}, from equation **[3-18]**, an assumption was needed regarding the proportion of cracks, **P**, occupied by soil bridges at each size scale. If **P** were constant, the soil friability, **k** (cf. equation **[2-53]**), would be zero, and (although no measurement of soil friability was made) the soil was considered to have some amount of friability, so it was expected that P would increase gradually for smaller and smaller soil cubes, as the soil drained. Even so, the relationship between **k** and **P** is unknown (and only of conceptual interest for this model) so an arbitrary scale of increasing **P**-values from 0.20 to 0.85 was assigned to the fifteen progressively decreasing crack sizes. Table **3-3a** lists the fifteen initial drainage states, **i**, with selected suctions, h_i, volumetric water contents, θ_i', average crack-widths, $\bar{w}_i$, (from average suction, $\bar{h}_i$), and P_i-values, chosen for use in equation **[3-18]**.

The fifteen selected steps between drainage states were found to be too small, because in eight of the fifteen steps, there wasn't sufficient water drained to leave pores of appropriate width, $\bar{w}_i$, to form a single crack. Whenever this occurred, (i.e. whenever equation **[3-18]** predicted there to be **<** 1 crack) drainage states were combined, and values of average suction, $\bar{h}_i$, average crack width, $\bar{w}_i$, and $\Delta\theta_i'$ were calculated again. This procedure was repeated until at least one crack ($n_{wi} = 1$) was predicted to drain, and then another drainage state for suctions, **h**, ranging from 1 to 500 hPa was tested. The number of cracks, n_{wi}, crack-segments ($n_{wi} + 1$), and the distance between cracks, l_i, of size $\bar{w}_i$ are listed in Table **3-3b**, with corresponding

Table 3-3. **(a)** List of initial inputs to the numerical model for calculating numbers of cracks: fifteen drainage states, **i**, with selected suctions, h_i, corresponding θ'-values, average crack widths, $\bar{w}_i$, and soil bridge portions, P_i. **(b)**Reduced final inputs to the numerical model with numbers of cracks of width, $\bar{w}_i$, and numbers of soil segments per cube-face, and the average distance between cracks on each cube face.

Table **3-3a: Initial Inputs to model**

Drainage State i	Selected Suction h_i (hPa)	Average Suction $\bar{h}_i$ (hPa)*	Vol. Water Content θ_i' **	$\Delta\theta_i'$ @	Aver. Crack Width $\bar{w}_i$ (mm) @@	Soil bridge Portion P_i
1	1	- -	0.400	- -	- -	- -
2	3	1.5	0.379	2.10×10^{-2}	9.80×10^{-1}	0.20
3	5	4	0.370	9.00×10^{-3}	3.67×10^{-1}	0.25
4	10	7.5	0.356	1.36×10^{-2}	1.96×10^{-1}	0.30
5	15	12.5	0.349	7.31×10^{-3}	1.18×10^{-1}	0.35
6	20	17.5	0.343	5.49×10^{-3}	8.40×10^{-2}	0.40
7	30	25	0.335	7.74×10^{-3}	5.88×10^{-2}	0.45
8	50	40	0.326	9.76×10^{-3}	3.67×10^{-2}	0.50
9	75	62.5	0.318	7.74×10^{-3}	2.35×10^{-2}	0.55
10	100	87.5	0.312	5.49×10^{-3}	1.68×10^{-2}	0.60
11	150	125	0.305	7.74×10^{-3}	1.18×10^{-2}	0.65
12	200	175	0.299	5.49×10^{-3}	8.40×10^{-3}	0.70
13	300	250	0.291	7.74×10^{-3}	5.88×10^{-3}	0.75
14	400	350	0.286	5.49×10^{-3}	4.20×10^{-4}	0.80
15	500	450	0.282	4.26×10^{-3}	3.27×10^{-3}	0.85

* $\bar{h}$ is calculated from equation **[3-34]**.

** θ_i' is calculated form equation **[3-33]** using values of h_i.

@ $\Delta\theta_i' = (\theta_{i-1}' - \theta_i')$.

@@ $\bar{w}_i$ is calculated from equation **[3-13]** using $\bar{h}_i$

Table **3-3b: Final inputs to model, with results**

i	h_i (hPa)	$\bar{h}_i$ (hPa)	θ_i' (m^3m^{-3})	$\Delta\theta_i'$ (m^3m^{-3})	$\bar{w}_i$ (mm)	P_i	n_{wi} *	$n_{wi}+1$ **	l_i # (mm)
1	0	- -	0.400$	- -	- -	- -	0	1	50.00
2	3	1.5	0.379	0.021	9.80×10^{-1}	0.20	3	4	11.77
3-4	10	6.5	0.356	0.023	2.26×10^{-1}	0.30	1	2	5.77
5-6	20	15.0	0.343	0.013	9.80×10^{-2}	0.40	1	2	2.84
7-9	75	47.5	0.318	0.025	3.09×10^{-2}	0.55	1	2	1.40
10-12	200	137.5	0.299	0.019	1.07×10^{-2}	0.70	1	2	0.696
13-15	500	350.0	0.282	0.017	4.20×10^{-3}	0.85	1	2	0.346

* n_{wi} is calculated from equation **[3-18]**

** $n_{wi}+1$ represents the number of soil segments per cube-face created by n_{wi} cracks.

$ The value of $\theta_i' = 0.400$ at $h_i = 0$ actually corresponds to a suction of h=1, because h cannot be zero in equation **[3-33]**. It is, however, close enough to the calculated value of total porosity, f, from average bulk density measurements, f = (1-1540/2650) = 0.419.

\# l_i is calculated from equation **[3-15]**

values of h_i, $\bar{h}_i$, θ_i', $\Delta\theta_i'$, $\bar{w}_i$, and P_i. The value of l_i at $h_i = 0$ is the original length of the soil cube, 50.00mm, which is typical of the size of the natural soil clods used in this study.

There is an exponential increase in the distance between air-filled pores, l, with increasing volumetric water content, θ' (Figure **3-8**), which is described by the regression equation:

$$l' = 4.28 \times 10^{-7} \exp(39.81\theta') \qquad (R = 0.992, n=7) \qquad [3\text{-}35]$$

where l' is the value of l predicted from the regression equation. This corresponds to a negative, log-log relationship between l and the suction, h (Figure **3-9**), described by the regression equation:.

$$\log_{10} l' = 1.404 - 0.685 \log_{10} h \qquad (R = 0.998, n=6) \qquad [3\text{-}36]$$

The values of l from the model of soil cubes may be compared with the fracture surface rugosity, σ_R, data listed in Table **3-4**. The σ_R-data came from the same clods for which water content data are reported in Table **3-2**, and Appendix-Table **A2-1**. Several values of σ_R from samples fractured under indirect tension were not determined because after crushing, the remaining pieces were too small to obtain a suitable fracture surface.

An analysis was done to determine whether the σ_R-values from the direct- and indirect-tension techniques were significantly different from each other. The mean value of σ_R for the direct-tension method was 0.316 mm ($s^2 = 5.03 \times 10^{-3} mm^2$; n=41 samples) and the mean value of σ_R for the indirect-tension method was 0.343 mm ($s^2 = 1.08 \times 10^{-2} mm^2$; n=33 samples). A pooled variance ($s^2_p = 7.58 \times 10^{-3} mm^2$) and pooled standard error ($s.e._p = 2.09 \times 10^{-2}$ mm; 72 df) were calculated, from which a t-test revealed that there was no significant difference between the two mean values of σ_R.

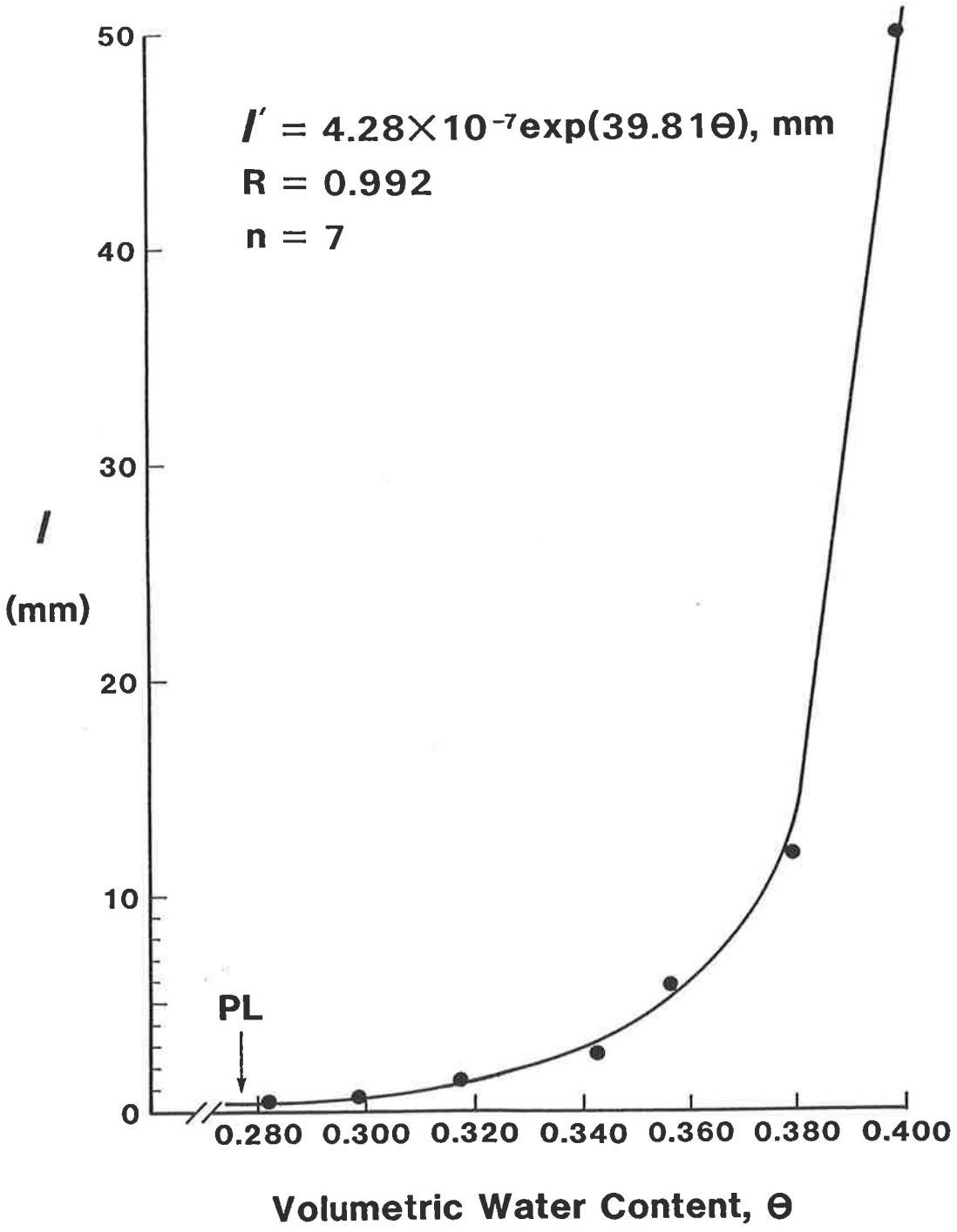

Figure 3-8. Effect of volumetric water content, θ, on the calculated distance, *l*, mm, between air-filled pores using the model of soil cubes, and desorption data from natural soil clods.

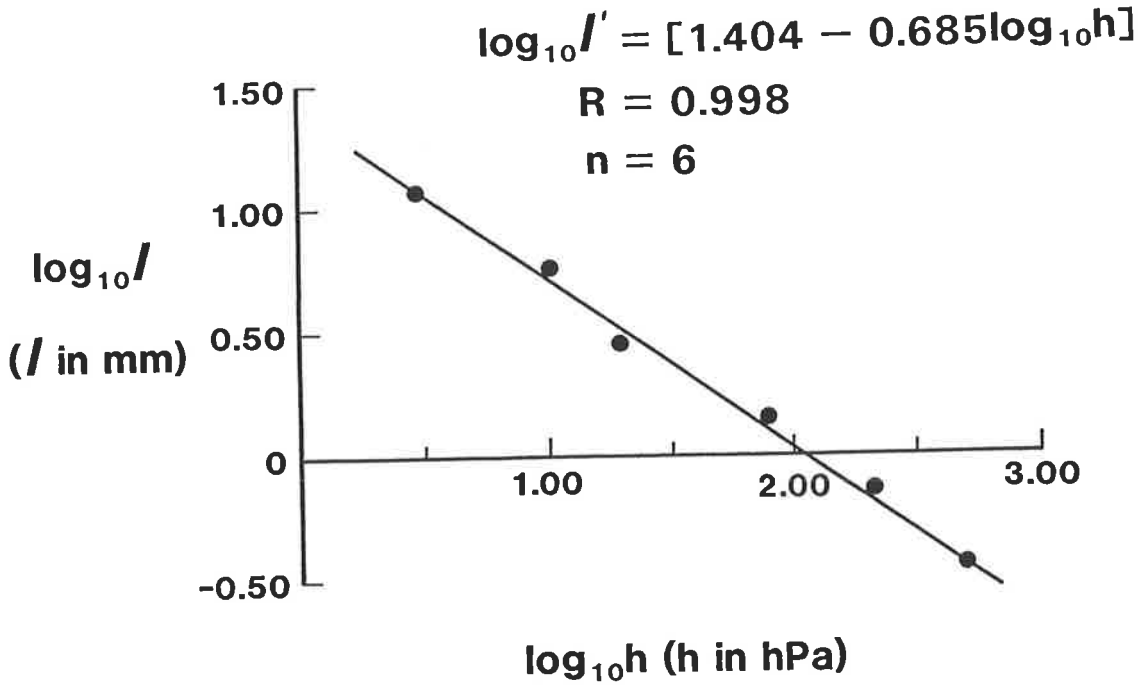

Figure 3-9. Log-log relationship between the applied soil water suction, **h**, and the distance between air-filled pores, *l*, using the model of soil cubes and desorption data from natural soil clods.

Table 3-4. Individual fracture surface rugosity data for fire water suctions, (clod-by-clod basis) using direct and indirect tension fracturing techniques; average values of σ_R (both techniques; clod-by-clod basis) and average σ_R by suction.

Table 3-4

h (hPa)	Clod #	σ_R (mm) direct tension	σ_R (mm) indirect tension	Average σ_R (by clod) (mm)	Average σ_R (mm) (by suction, h) ± s.e. & n
5	1	0.346	- -	0.346	0.348
"	2	0.316	- -	0.316	±0.011
"	3	0.365	- -	0.365	n=8
"	4	0.278	0.345	0.312	
"	5	0.345	- -	0.345	
"	6	0.317	0.331	0.324	
"	7	0.395	- -	0.395	
"	8	0.257	0.508	0.383	
10	1	0.259	- -	0.259	0.351
"	2	0.347	0.515	0.431	± 0.032
"	3	0.232	0.298	0.265	n=8
"	4	0.478	0.357	0.418	
"	5	0.279	0.373	0.326	
"	6	0.229	0.335	0.282	
"	7	0.401	0.619	0.510	
"	8	0.406	0.226	0.316	
50	1	0.209	0.250	0.230	0.331
"	2	0.223	0.391	0.307	± 0.028
"	3	0.377	0.193	0.285	n=9
"	4	0.354	0.419	0.387	
"	5	0.311	0.495	0.403	
"	6	0.225	0.242	0.234	
"	7	0.405	0.527	0.466	
"	8	0.265	0.281	0.273	
"	9	0.317	0.465	0.391	
100	1	0.266	0.279	0.273	0.320
"	2	0.271	- -	0.271	± 0.022
"	3	0.257	0.279	0.268	n=9
"	4	0.488	0.351	0.420	
"	5	0.331	0.275	0.303	
"	6	0.443	- -	0.443	
"	7	0.264	0.404	0.334	
"	8	- -	0.268	0.268	
"	9	0.289	0.306	0.298	
500	1	0.338	0.240	0.289	0.291
"	2	0.315	0.348	0.332	±0.015
"	3	0.303	0.190	0.247	n=8
"	4	0.252	- -	0.252	
"	5	0.237	0.266	0.252	
"	6	0.255	0.291	0.273	
"	7	0.404	0.296	0.350	
"	8	0.300	0.371	0.336	

This result enabled the grouping of the σ_R-values from both techniques to produce an average σ_R-value for each of the five suctions listed in Table **3-4**.

A plot of σ_R versus the volumetric water content (using the five values of θ' in Table **3-2**) is shown in Figure **3-10**, and is described by the regression equation:

$$\sigma_R' = 0.107 + 0.673\,\theta' \quad ,mm \quad (R= 0.971, n=5) \qquad [3-37]$$

where σ_R' is the value of σ_R predicted from the regression equation. The positive linear slope-coefficient in equation **[3-37]** indicates as the soil becomes progressively wetter that tensile fracture surfaces become increasingly jagged or rugose. This result is consistent with the idea that tensile fracture occurs by the propagation of air-filled cracks (which get further and further apart in wetter soils).

The experimental results shown in Figure **3-10** differ from those predicted for I and should be compared with the exponential relationship between I and θ' that is shown in Figure **3-8**, described in equation **[3-35]**. It can be seen that the fracture surface rugosity, σ_R, increases with increasing θ' (just as does I), but the difference is that the σ_R-θ' relationship is linear, rather than exponential in nature. The fracture surface rugosity, σ_R, is also plotted as a function of the logarithm of the soil water suction, **h**, in Figure **3-11**, and is described by the regression equation:

$$\sigma_R' = 0.376 - 0.0296 \log_{10} h \quad ,mm \quad (R= 0.970, n=5) \qquad [3-38]$$

Equation **[3-38]** may be compared to the log-log relationship between I' and **h** in Figure **3-9**, which is described in equation **[3-36]**.. Again, the main difference is that I' changes exponentially while σ_R' changes only linearly.

An additional comparison of σ_R and I can be made by correlating their predicted values from equations **[3-38]** and **[3-36]** (σ_R' and I') at the same suctions (5, 10, 50, 100 and 500 hPa). Values of **h**, θ', I', σ_R' and $\sigma_{R(measured)}$ are listed in Table **3-5** and plotted in Figure **3-12**. Both the measured values of σ_R and the predicted

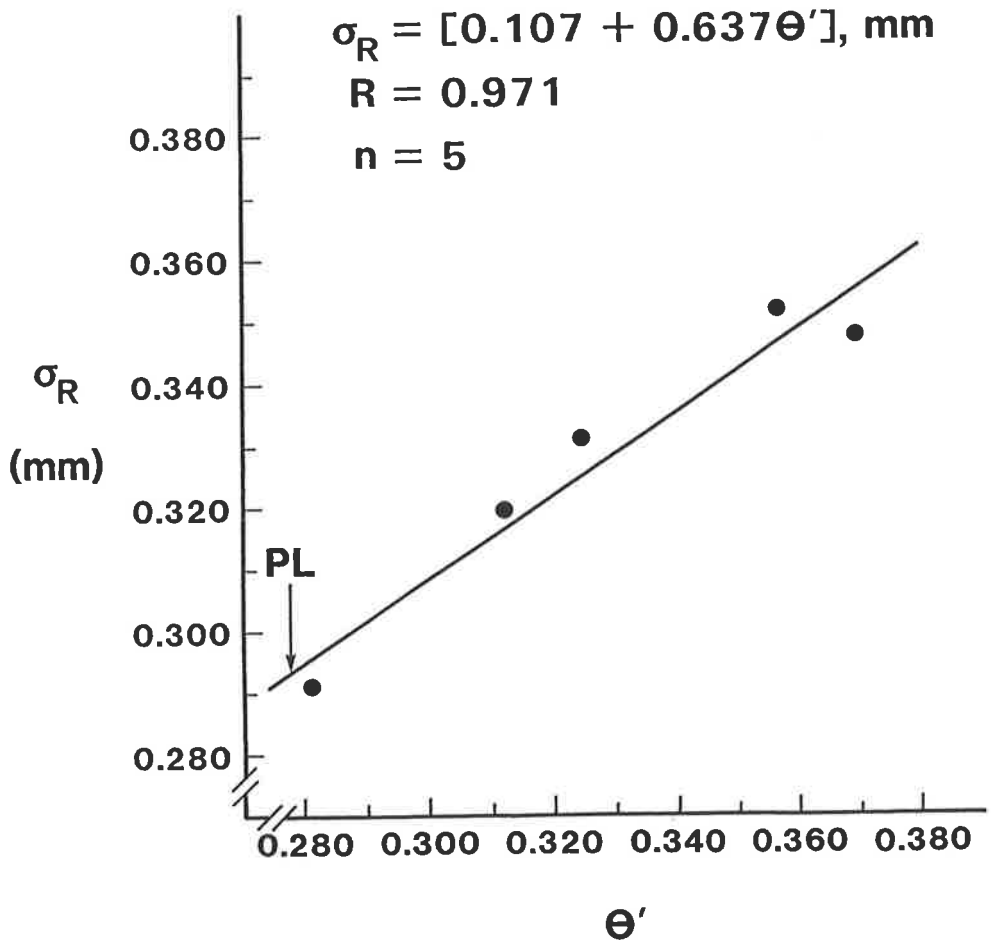

Figure 3-10. Effect of volumetric water content, θ', estimated from equation [3-33]) on fracture surface rugosity, σ_R, measured on natural soil clods.

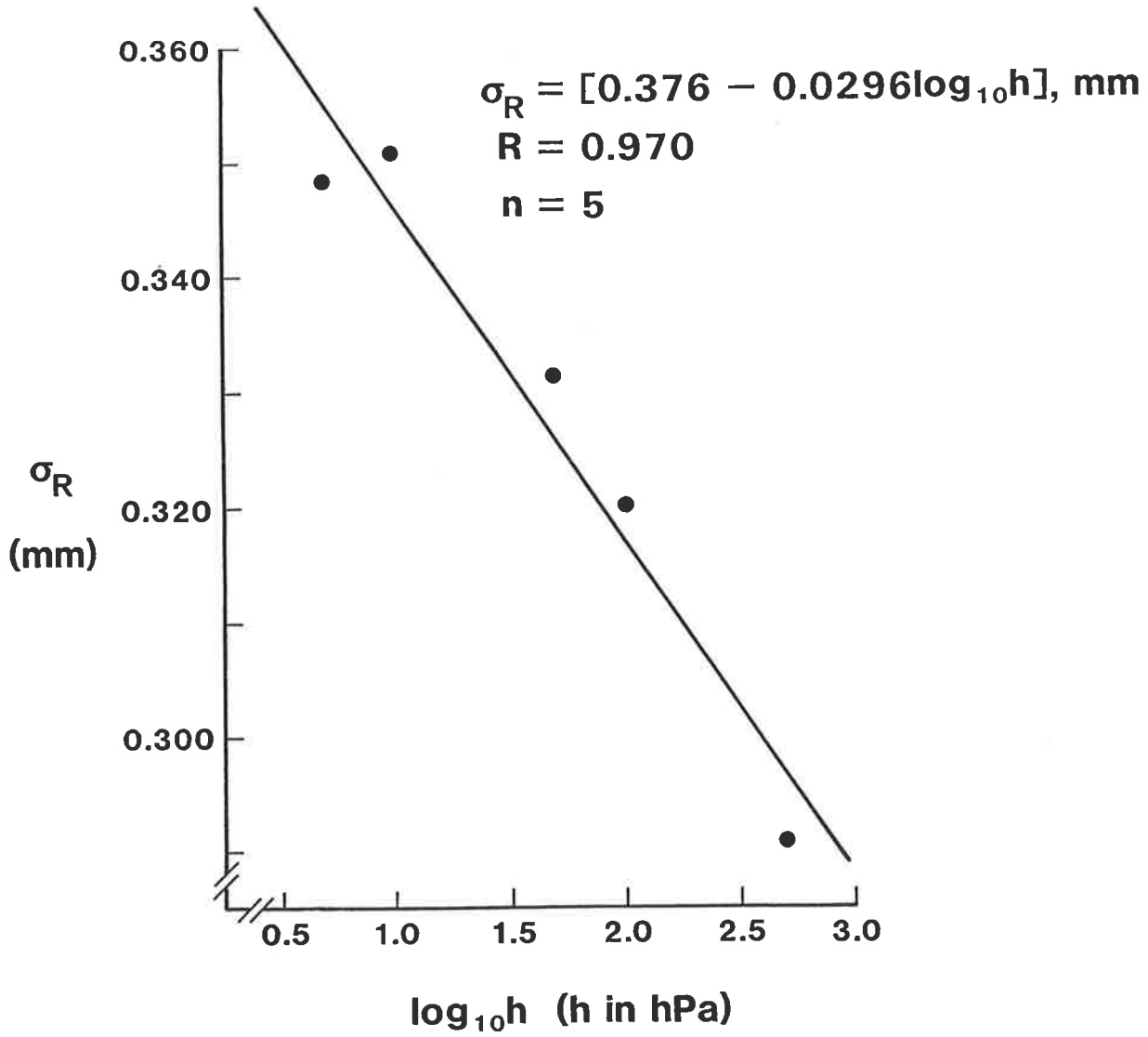

Figure 3-11. Log-linear relationship between the applied soil water suction, h, and the fracture surface rugosity of natural soil clods.

Table 3-5

h (hPa)	θ' (m^3m^{-3})$	l' (mm)$	σ_R' (mm)$	$\sigma_R \pm$ s.e. (mm)*	$\sigma \pm$ s.e. (mm)**
5	0.370	8.42	0.355	0.348 ± 0.011	1.030 ± 0.037
10	0.356	5.24	0.347	0.351 ± 0.032	0.923 ± 0.041
50	0.326	1.74	0.326	0.331 ± 0.028	0.794 ± 0.069
100	0.312	1.08	0.317	0.320 ± 0.022	0.985 ± 0.093
500	0.282	0.359	0.296	0.291 ± 0.015	0.872 ± 0.018

$ The values of θ', l', and σ_R' are predicted from equations **[3-33]**, **[3-36]**, and **[3-38]**, respectively.

* The values of σ_R were the five measured average values for each suction, listed in Table **3-4.**

** The values of σ were calculated on a clod-by-clod basis without using a running mean and are therefore more variable. The average values were calculated in the same way that the σ_R - values were calculated.

Table **3-5.** Comparison of the average distance between air-filled cracks from the model of soil cubes, with estimated and measured values of fracture surface rugosity, σ_R, as well as corresponding values of fracture surface rugosity, σ, calculated without the use of a running mean. Comparisons are made at the five suctions used in the experiments.

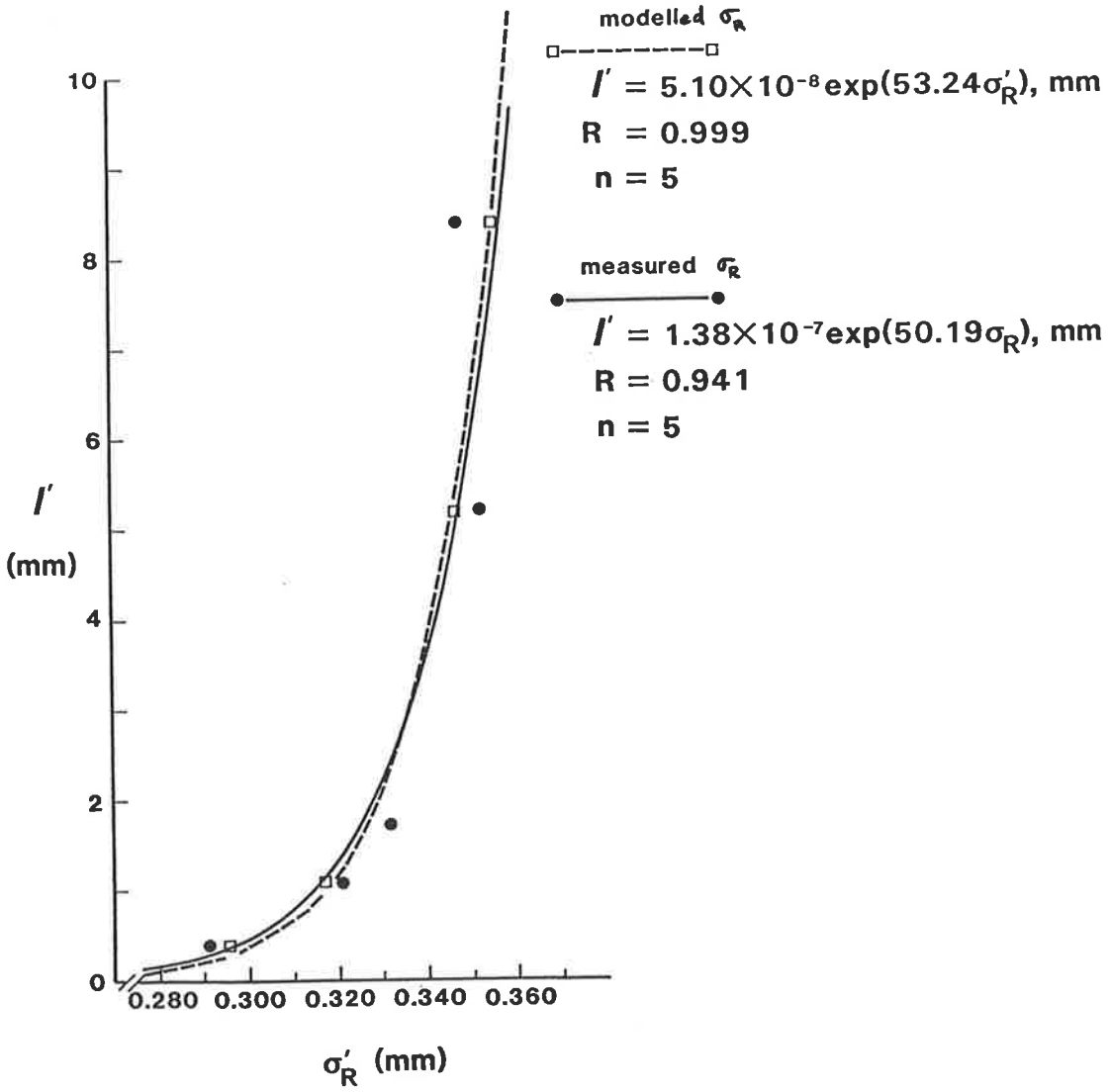

Figure 3-12. Correlation of modelled as well as measured values of fracture surface rugosity from natural soil clods with the calculated distance between air-filled cracks, l, from the model of soil cubes.

values, σ_R', are strongly correlated exponentially with the distance between air-filled cracks, l', predicted at the same suctions from equation **[3-36]**. The exponential correlation between σ_R' and l' is explained by the nature of the model of soil cubes. The model requires at each level of drainage, **i**, that there will always be $(2)^{3i}$ cubes created. The distance between the cracks in the cube, l', is therefore forced to decrease very rapidly as the soil drains, and this fact is clearly illustrated in Figure **3-8**. The cubic model, as outlined in this thesis may be somewhat unrealistic for natural soils, however, it successfully demonstrates that the distance between air-filled pores decreases during drainage. Furthermore, it is a relatively straightforward model and easy to use, as shown by the recent work of Hallaire (1988) who used a cubic model to study the cracking and shrinking of heavy clay soils.

The values of σ_R' and l' also differ (i.e. they are not linearly related) for two other reasons. The first reason, which explains part of the differences, is related to the use of running means in the calculation of σ_R. It was essential to use running means in this study to filter out any long-wavelength data caused by tilting of the samples under the video camera. Tilting from the horizontal under the video camera (which is impossible to detect) would introduce a large amount of structurally unrelated variance. At the same time, however, all features larger than the running mean (4 mm in this case) were also filtered out (cf. Appendix **1**), and so the upper limit to any values of σ_R would be 4 mm. Presented in Table **3-5** are five average values of σ (calculated without running means) for the exact same data as for the σ_R-values. The values of σ are all approximately three times larger than the corresponding values of σ_R. The largest value of σ is only 1.030 mm, which is still smaller than most of the l-values listed in Table **3-5**. The use of running means therefore does not account for the main difference between values of σ_R and l.

The main reason explaining the differences between l and σ_R is related to the nature of the model of soil cubes used in this study. The model (cf. equations **[3-15]** & **[3-18]**) was only tested in this study using stepped, average values of crack-width, $\bar{w}_i$, and soil-bridge proportion, **P**, as given in Table **3.3**. In real soils, however,

these single-values would be inappropriate due to the natural structural heterogeneity present in undisturbed soil clods, and would need to be replaced by distribution functions. These distribution functions would reflect the fact that between any two suctions, a range of effective crack widths will drain, and that these would also be influenced by a range of soil-bridge proportions in every crack. Inclusion of such distribution functions would result in a broader range of crack sizes being predicted by the model of soil cubes, which would therefore reduce the tendency of any one crack size to increase exponentially in number.

3.5.3.2.2 Relation Between Predicted- & Measured-Tensile Strengths

Predictions of tensile strength of the clods from Field W-10 were made using equation **[3-28]** as follows. The five values of average volumetric water content, θ, listed in Table **3-2** for the five suctions, **h**, were used to calculate the degree of pore saturation, **s**, at each suction according to equation **[2-45]**. An average value of total porosity, **f**= 0.419, was calculated for this purpose, using the average bulk density, ρ_b, of all the clods collected (ρ_b = 1540 kgm^{-3}), and average particle density of ρ_s=2650 kgm^{-3}. The suctions listed in Table **3-2** were converted to pressure potentials (Ψ, kPa), using equation **[3-22]** and the following relations were calculated in the form outlined for equation **[3-25]** to describe the relationships between Ψ and θ, and Ψ and **s** respectively:

$$f(\theta) = (-\Psi) = \exp(17.73 - 49.50\theta) \quad (R=0.973, n=5) \quad [3-39]$$

and

$$g(s) = (-\Psi) = \exp(17.73 - 20.75s) \quad (R=0.973, n=5) \quad [3-40]$$

The values of χ needed for predicting the tensile strength of the soils were calculated from equation **[3-27]**, and the results along with the predicted- and measured-values of tensile strength are listed in Table **3-6**, and plotted in Figures **3-13a** and

Table 3-6

h (hPa)	Ψ (kPa)	$\bar{\theta}$ (m^3m^{-3})	s	χ^*	$TS_{(pred.)}$ (kPa)	Average $TS_{(meas.)} \pm$ s.e. (kPa)
5	-0.5	0.378	0.902	0.915	0.229	2.53 ± 0.41
10	-1.0	0.346	0.826	0.840	0.420	3.50 ± 0.31
50	-5.0	0.332	0.792	0.806	2.015	5.17 ± 0.57
100	-10.0	0.305	0.728	0.742	3.710	6.09 ± 0.90
500	-50.0	0.285	0.680	0.694	17.350	6.94 ± 0.31

* the constants used for calculating χ in equation **[3-27]** were a=17.73 and **n**=-20.75, taken from equation [3-40]; cf. [3-25].

Table **3-6.** Average volumetric water contents, $\bar{\theta}$, (measured at five water suction, **h**, converted to matric potentials, Ψ); degrees of pore saturation, **s**, and corresponding values of χ, used for predicting the tensile strength, $TS_{(pred)}$; and average measured tensile strengths of natural soil clods.

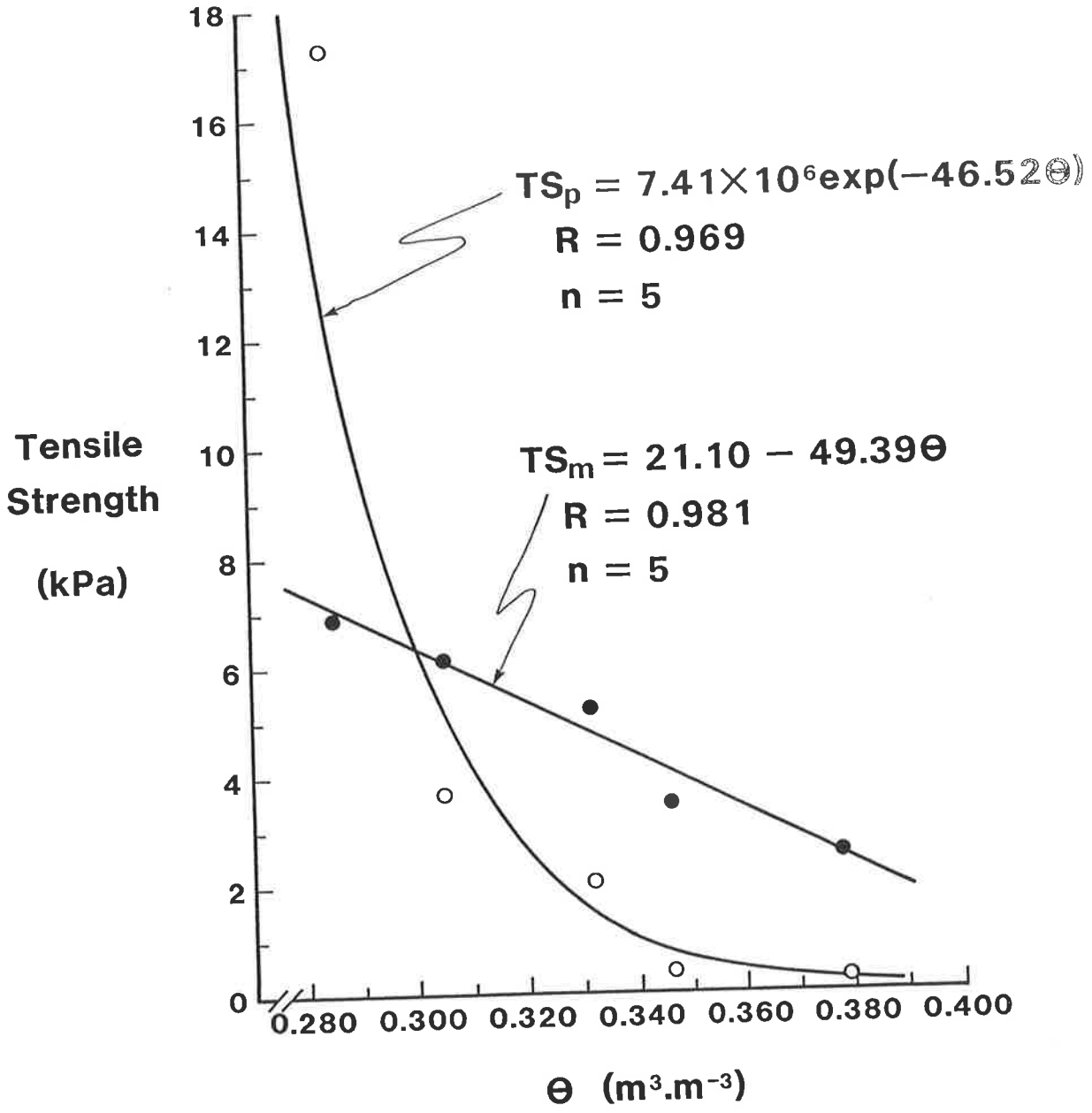

Figure 3-13a. Predicted and measured tensile strengths, TS_p, TS_m, as functions of the volumetric water content, θ, of natural soil clods.

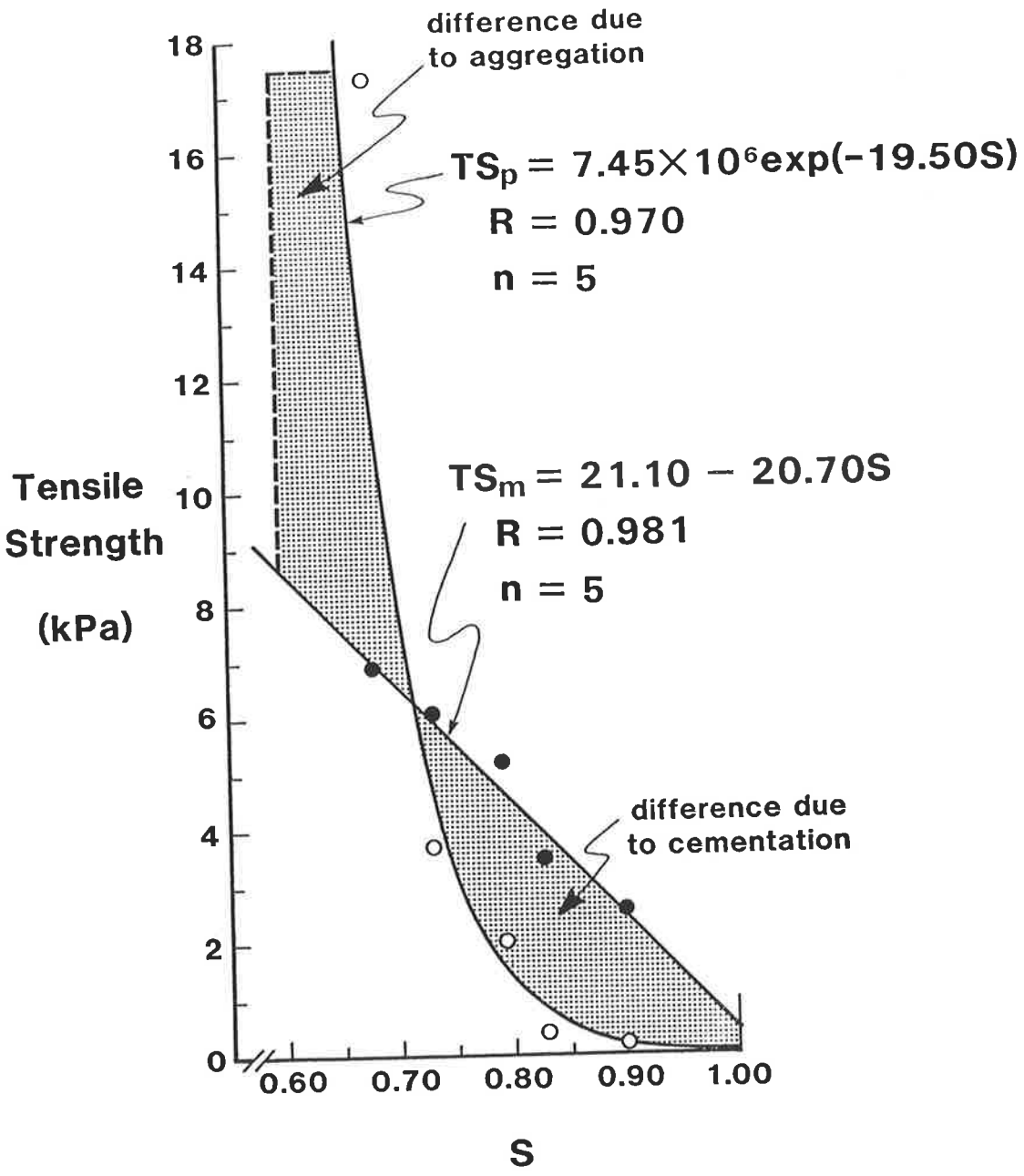

Figure 3-13b. Predicted and measured tensile strengths, TS_p, TS_m, as functions of the degree of pore saturation, **s**, of natural soil clods. The shaded area to the right of **s** = 0.70 represents the higher tensile strength of natural soil clods (relative to the model) due to age hardening and cementation; the shaded area to the left of **s** = 0.70 represents the lower tensile strengths of natural soil clods (relative to the model) due to aggregation which reduces the inter-aggregate water active in tensile cohesion.

Figure **3-13b**. The predicted and measured tensile strengths are described as functions of the volumetric water content, θ, in the regression equations:

$$TS_{pred} = 7.43 \times 10^{6} \exp[-46.52\theta] \quad (R=0.970, n=5) \quad [3-41]$$

and

$$TS_{meas} = 21.10 - 49.39\theta \quad (R=0.981, n=5) \quad [3-42]$$

The tensile strengths are also described as functions of the degree of pore saturation, **s**, in the regression equations:

$$TS_{pred} = 7.43 \times 10^{6} \exp[-19.50s] \quad (R=0.970, n=5) \quad [3-43]$$

and

$$TS_{meas} = 21.10 - 20.70s \quad (R=0.981, n=5) \quad [3-44]$$

Both the predicted and the measured tensile strengths decrease with increasing water content, as is usually observed (see for example, Dexter, 1988b). Furthermore, the tensile strength is, in most cases, at least an order of magnitude lower than the penetrometer resistance, Q_p, measured on the same clods (shown on a clod-by-clod basis in Figure **3-14** as a function of the volumetric water content, θ ; see also **Appendix 2,** Table **A2-2**).

The modelled-tensile strengths according to the theory of Snyder and Miller (1985) are clearly quite different from the measured tensile strengths in this experiment as shown in Figures **3-13a & 3-13b**. The Snyder and Miller model underestimates the measured-tensile strength when the soil is relatively wet (i.e. $s > 0.70$), and it predicts that the soil will have negligible tensile strength at saturation ($s=1.0$ in Figure **3-13b**) which is not always the case. The measured tensile strengths, on the other hand, decrease linearly toward saturation, and the linear regression equation predicts that there will be at least some measurable tensile strength at saturation (**TS**= 0.41 kPa at $s=1.0$ in Figure **3-13b**). This is consistent

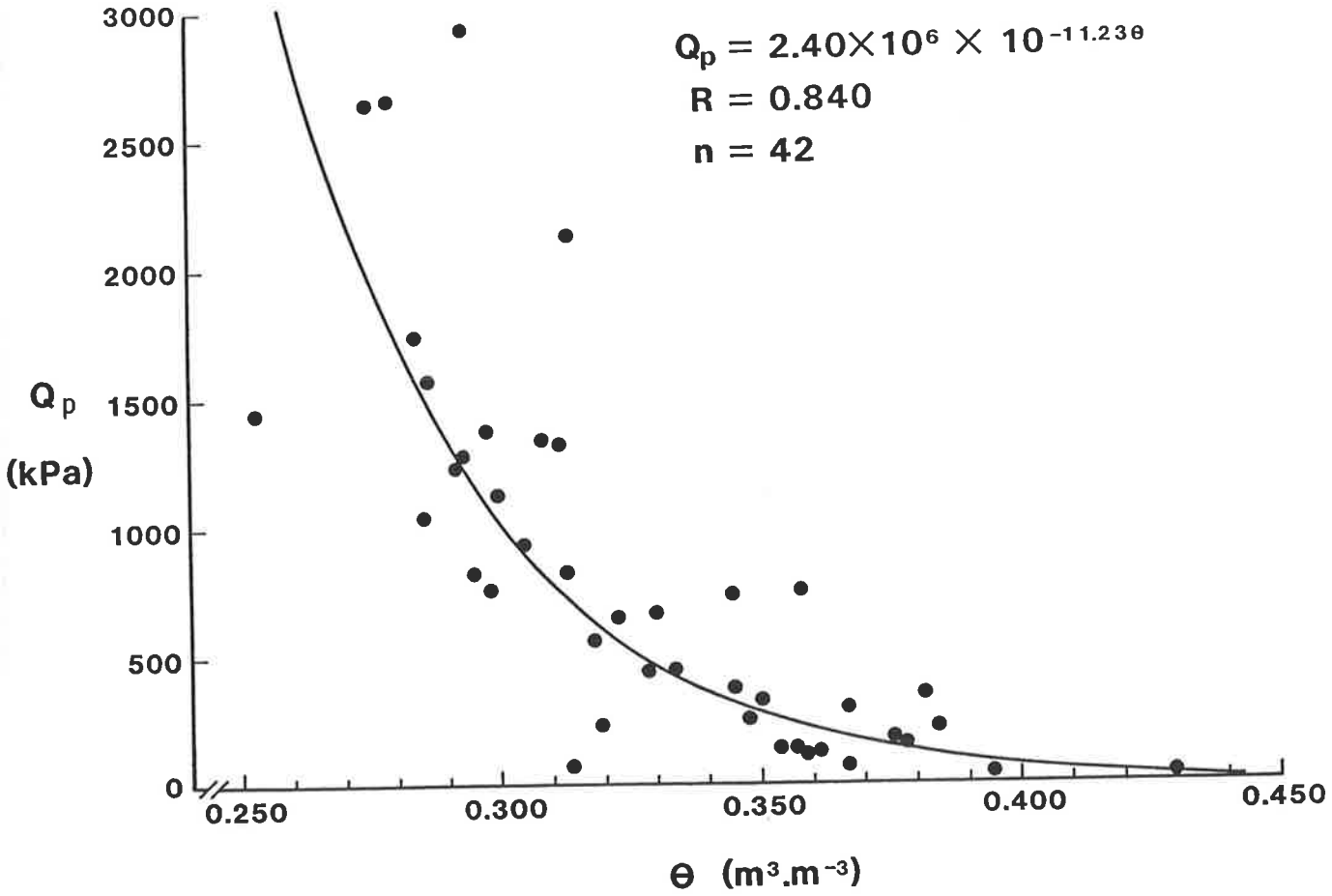

Figure 3-14. Penetrometer resistance (clod-by-clod basis) as a function of the volumetric water content, θ, of the same natural soil clods used for all other measurements in SECTION 3.

with the fact that the tensile strength of natural soil aggregates is often greater than zero at saturation (Braunack and Dexter, 1978).

The predictions of tensile strength for **s** > 0.7 (Figure **3- 13b**) based on the Snyder and Miller model are also too low for another reason. The theory was developed by Snyder and Miller for recently disturbed soils, which exhibited no cementation and age hardening. The model estimates the contribution of only water menisci to the tensile strength, and would therefore be expected to predict somewhat lower strengths than for age hardened soils where cementation has been able to occur. The natural soil clods used in this study, however, had been through at least one full year of wetting, drying, and age hardening prior to analysis, and consequently, the measured strengths are as much as ten times higher than the predicted ones.

Below **s**= 0.70, predictions from the Snyder and Miller model overestimate the measured tensile strength. Equation **[3- 28]** (cf. Figures **13a & 13b**) predicts that the tensile strength of air dry soil clods (i.e. θ =0.05; **s**= 0.12) is even higher than limestone (c.f. Table **2- 1**), which is clearly incorrect. The model overestimates the measured tensile strength below **s**=0.70 presumably because the water in the natural (well-aggregated) soil clods is not contributing as much to the cohesion as would be predicted by the degree of pore saturation, **s**. As indicated by Kemper and Rosenau (1984) and Snyder and Miller (1985), only inter-aggregate water contributes to cohesion due to capillary menisci (Snyder and Miller, 1985), and yet a great deal of the water in well-aggregated soils, such as the clods of this study, is associated with intra-aggregate pores.

On the other hand, the linear regression equations for the measured tensile strengths in Figures **13a & 13b** also have limitations, because they predict that the maximum tensile strength of oven dry clods (i.e. θ =0; **s**= 0) is only 21 kPa. This value is somewhat low in comparison to similar soils listed in Table **2- 1**, and described later in this study, and therefore use of the regression equations should be restricted to the range of measured water contents (i.e. θ = 0.280 to 0.380) in this study.

The measurements on natural soil clods in this study indicate that water plays a major role in determining the tensile strength, but that it is not the only determinant. The fact that the samples were 'natural' or 'undisturbed' (and therefore age hardened) appears to be very important, particularly when the soil is relatively wet (**s** > 0.70). The strength of cementitious bonds under these circumstances increases the tensile strength considerably over that predicted from the model of Snyder and Miller for recently moulded, non-cemented soils. The well-aggregated state of the soil clods presumably increased the intra-aggregate water content relative to the inter-aggregate water, and this reduced the proportion of water acting as menisci between soil aggregates. Consequently the (effective) degree of pore saturation was overestimated considerably by Snyder and Miller's model, and therefore so was the tensile strength.

3.6 General Discussion, Summary and Conclusions

The tensile strength of natural soil clods is influenced by both the degree of pore saturation, **s**, as well as by the extent of cementitious bond formation (especially in relatively wet soil: **s** >0.70) and also by the state of soil aggregation (when **s** >0.70) . Predictions of tensile strength based on the model of Snyder and Miller should be restricted to recently moulded soils where neither cementation nor aggregation modify the role of water menisci in response to tensile stresses. Considerable work needs to be done to incorporate the state of aggregation and age hardening into a model to predict the tensile strength of unsaturated, natural soils.

The fact that the tensile strength is influenced by other factors in addition to the water content has important implications for the prediction of fracture surface rugosity, σ_R. It was hypothesized in **SECTION 3.2** and **3.5.1** that if air-filled pores were sites of crack initiation under tensile stress, as suggested by Snyder and Miller (1985), then there should be a good correlation between σ_R and the distance between air-filled pores. A model of soil cubes was used to predict the distance between air-filled cracks, l , as the soil drained from saturation. The results indicate that although

σ_R changes in the same direction as l when the water content changes, they are by no means equal (σ_R is a linear function of θ, whereas l is exponentially related to θ). The model used in this thesis is a greatly simplified one, for the purposes of the special calculations outlined above. Future work on this model, however, might investigate the magnitude of **P** in order to reduce the arbitrary nature of assigning the **P**-values. Alternatively, attention could be given to developing more sophisticated models (c.f. Hadas, 1987) which might include mixtures of interconnected unit cells of different hierarchical states or levels, rather than restricting the distance between cracks to single-stepped categories.

The model outlined in this study shows that the estimated distance between air-filled cracks, l, is much larger than the measured values of σ_R (Table **3- 5**). The large difference between σ_R and l is accounted for mainly by the nature of the cubic model whose cracks are forced to drain in a geometric manner, which is somewhat unrealistic for soils. There is considerable room for improvement of the model, which needs to be tested on a wider range of soils than used in this study. Furthermore, the cubic model for l is based entirely on the drainage of water from cracks and takes no account of other factors which influence the distance between weakest flaws (eg. cementitious bonds). In very wet soils, for example, the distance between air-filled pores is relatively large (several mm) and these pores are usually isolated from each other, even in well- aggregated soils. While the air-filled pores may be the weakest flaws in the soil, (and therefore control the overall direction of the fracture pathway) the distribution and strength of cementitious bonds between air-filled pores will also influence the way in which cracks propagate to connect the air-filled pores. Cementitious bonds between air-filled pores may cause a more uniform distribution of weak (and strong) points in the soil matrix. This would have the effect, during tensile failure, of generating cracks which could by-pass (short circuit) the air-filled pores. The magnitude of σ_R therefore reflects not only the distance between air-filled pores, but also the distance between cementitious bonds that exist between the air-filled pores.

SECTION 4. EFFECT OF CALCIUM ON FRACTURE SURFACE RUGOSITY

4.1 Introduction

It was postulated in **SECTION 3** that when tensile stresses are applied to unsaturated, natural soil clods, they fracture in a manner depending on the distance between weakest flaws in the soil matrix. If one examines the topography of new soil surfaces created by fracturing soil in tension, the average distance between weakest flaws can be deduced from a measurement of the fracture surface rugosity, σ_R. The fracture surface rugosity, σ_R, was shown to reflect the distance between air-filled pores, and that it increases with increasing water content. It was also suggested, however, that cementitious bonding in undisturbed soils can exert an influence on the tensile fracture pathway, and reduces the measure of σ_R below estimates predicted based solely on the distance between air-filled pores.

The degree to which cementitious bonding influences the distance between weakest flaws is probably dependent upon numerous factors such as the uniformity of the soil material, clay content, clay mineralogy, exchangeable cations and organic carbon content of the soil (Sleeman, 1963). Calcium from calcium carbonate or gypsum, for example strongly influences the exchangeable cations in the soil and is particularly well known for improving the soil structure (eg. soil friability - see Shanmuganathan and Oades, 1983b) and hence workability of the soil (Loveday et al, 1970; see **SECTION 2.4.5.2**).

It is hypothesized that changes to the soil structure that are induced by calcium are the result of the influence of calcium on the distance between weakest flaws in the soil. On this basis, the method of fracture surface rugosity, which is outlined in **SECTION 3** is ideally suited for the testing of the hypothesis. The studies outlined in this **SECTION** were designed to accomplish this testing.

4.2 Materials and Methods

A gypsum and calcium carbonate trial was established in 1980 on a sandy loam Natrixeralf for a separate study (reported in Shanmuganathan and Oades, 1983b) at the Charlick Experiment Station, Strathalbyn, South Australia. The soil was in a degraded condition. Different amounts of gypsum ($CaSO_4 \cdot 2H_2O$) and calcium carbonate ($CaCO_3$) ranging in increments of 2 t ha^{-1} from 0 to 20 t ha^{-1} were applied and worked into the soil on unreplicated plots (8m x 50m) and then sown to pasture. No further additions of gypsum and calcium carbonate have been made and the soil has not been tilled since 1980. The annual rainfall recorded during the two years that samples were collected for this study was 500.4 mm in 1986 and 479.4 mm in 1987. The annual rainfall in 1985 was 500 mm, prior to which no meteorological data exist (University of Adelaide, 1988). Table **4-0** lists particle size distributions and specific surface areas for the plots examined in 1987.

The plots were sampled in May 1986 prior to the main winter rains, and then again in June 1987. Samples collected in 1986 were taken from the gypsum- and the $CaCO_3$-treated plots having application rates of 0, 2, 4, 10, 14 & 20 t ha^{-1}. All samples in 1986 were analysed at the water contents as they were found in the field. In 1987, however, samples were collected from only the $CaCO_3$-treated plots having application rates 0, 4, 10, 14 & 20 t ha^{-1}, and then they were brought into the laboratory where a range of water contents was imposed prior to analyses. The 1986 and 1987 experiments for samples from the gypsum- and $CaCO_3$-treated plots will be outlined separately.

4.2.1 1986 Experiments

In 1986, twenty soil clods were collected from positions evenly spaced in a zigzag fashion along the full length of the plots. To obtain each clod, the top few centimetres of sod were cut away with a shovel and then a large clod was dug out. A smaller, fist-size clod was then isolated from within the larger one by carefully scraping soil away with a pallet knife until the sample was sufficiently small to hold in the hands. The clod was immediately fractured in half by applying as nearly as possible a direct tensile stress using the hands. One half was fitted into a plastic vial for analysis of the fracture surface rugosity, σ_R, (cf. **SECTIONs 3.4 & 3.5.3.1**) while

Table 4-0

Application Rate ($CaCO_3$) (t ha^{-1})	% < 2μm	% 2-53μm	% >53μm	B.E.T. Surface Area (m^2 g^{-1})
0	13.1%	18.3%	68.6%	16.5
4	35.5	13.2	51.3	26.1
10	24.2	15.1	60.7	26.3
14	21.1	13.2	65.7	26.4
20	24.2	14.1	61.7	16.4

Table 4-0: Particle size distributions (determined by hydrometer method, and checked gravimetrically), and surface areas (determined by the method of Brunauer et. al. 1938) for plots to which 0, 4, 10, 14, 20 t ha^{-1} $CaCO_3$ were applied.

the other half was stored in a sealed container with other clods from the same plot to obtain overall or gross estimates of soil water content and soil organic carbon content for each plot.

4.2.2 1987 Experiments

In 1987, a larger size and number of samples than in 1986 were collected to allow a series of other measurements, such as dispersible clay content, bulk density, plastic limit, tensile strength, penetrometer resistance and organic carbon content (again) to be made on the same samples used for determination of fracture surface rugosity, σ_R. Twenty-five large clods were collected from each of the five $CaCO_3$-treated plots, then carefully packed in moist, loose soil in polythene bags, and returned to the lab. Clods were then trimmed to fist-size, wetted slowly to near-saturation over a period days and placed on porous ceramic plates for two weeks at one of five different water suctions (0.5, 1.0, 5.0, 10.0 or 50.0 kPa) as described in **SECTION 3.5.3.1**.

When water contents were established, clods were removed from the ceramic plates and broken carefully by hand into 3-4 pieces. One piece of the clod was used to determine penetrometer resistance and bulk density. Penetrometer force was measured twice on each piece with the motor-driven steel probe used in **SECTION 3**. Bulk densities were determined, also as described in **SECTION 3**. Another piece of the clod was fractured by direct tension and used exclusively for analysis of fracture surface rugosity, σ_R. It was placed directly into a plastic vial and allowed to air dry several days before pouring the white epoxy compound around it as described in **SECTION 3**. A third piece was trimmed with a pallet knife into a relatively round shape, its weight (for water content) and its geometric mean diameter determined by taking measurements across the three principle axes. It was then fractured using indirect tension between parallel plates (Dexter and Kroesbergen, 1985) to determine its tensile strength. Soil from each piece of the clod was air-dried and kept for the determination of dispersible clay content using the method of Shanmuganathan and Oades (1983b).

4.3 Results and Discussion

4.3.1 Results: 1986 Experiments

Table 4-1 presents estimates of soil organic carbon content, and water content (gravimetric basis, on single bulk samples of disturbed soil) as well as mean values of fracture surface rugosity, σ_R, in relation to the amount of calcium supplied by each amount of applied gypsum and $CaCO_3$. Standard errors for the individual water contents and organic carbon contents in Table 4-1 are not presented because the data were obtained on single replicates from bulk samples. In any case, no significant effects (linear or otherwise) of applied-calcium on the estimates of either soil organic carbon content or field water content from bulk samples were found. The constancy of both water and organic carbon contents across all plots enabled a straightforward statistical analysis to be performed on the effects of calcium. The experimental design (single replicate plots with graded steps in the amount of applied-calcium) made simple linear regression the most suitable means to analyse the results. Mean values of fracture surface rugosity, σ_R, are presented in Figure 4-1 as a linear function of the amount of applied calcium for both gypsum and $CaCO_3$ sources. The effect of calcium added (**Ca**, t ha^{-1}) on σ_R, is described in the regression equation:

$$\sigma_R = \underset{(\pm\ 0.0092)}{0.335} \underset{(\pm\ 0.0026)}{-0.0153\ Ca}, \quad m\ m \quad (R = 0.88, n=12) \quad [4-1]$$

The numbers bracketed under the coefficients in equation [4-1], and in subsequent equations, are standard errors of the coefficients. In equation [4-1], both coefficients are significant at $P < 0.001$.

4.3.2 Results: 1987 Experiments

Consistent with the 1986 results, no significant effect of the amount of calcium applied on the soil organic carbon content was found. In addition, the bulk density of the soil clods, the plastic limit (Stakman and Bishay, 1976; Smith et al., 1985) and

Table 4-1

Compound Added	Application Rate ($t\ ha^{-1}$)	Calcium applied ($t\ ha^{-1}$)	OC (%)	w ($kg\ kg^{-1}$)	Mean* $\sigma_R \pm$ (s.e.) (mm)
Gypsum	0	0	1.09	0.121	0.337 ± (0.018)
	2	0.47	0.99	0.116	0.341 ± (0.027)
	4	0.93	0.93	0.136	0.317 ± (0.049)
	10	2.33	0.88	0.136	0.305 ± (0.032)
	14	3.26	0.95	0.136	0.277 ± (0.023)
	20	4.65	0.92	0.124	0.265 ± (0.024)
$CaCO_3$	0	0	0.92	0.114	0.376 ± (0.026)
	2	0.80	1.02	0.116	0.305 ± (0.026)
	4	1.60	0.81	0.080	0.267 ± (0.019)
	10	4.00	0.87	0.140	0.276 ± (0.014)
	14	5.60	0.95	0.145	0.238 ± (0.014)
	20	8.00	0.87	0.131	0.230 ± (0.014)
	Means	0.93	0.125		--
	(±s.e.)	(± 0.022)	(± 0.051)		--
	n	12	12		--

Table 4-1: Soil organic carbon contents, %OC, field water contents, w, and mean fracture surface rugosity, σ_R, of n=20 natural soil clods measure in 1986, in relation to the amount of calcium applied to the soil in 1980.

*Values of σ_R were determined using a running mean length of M=4 mm.

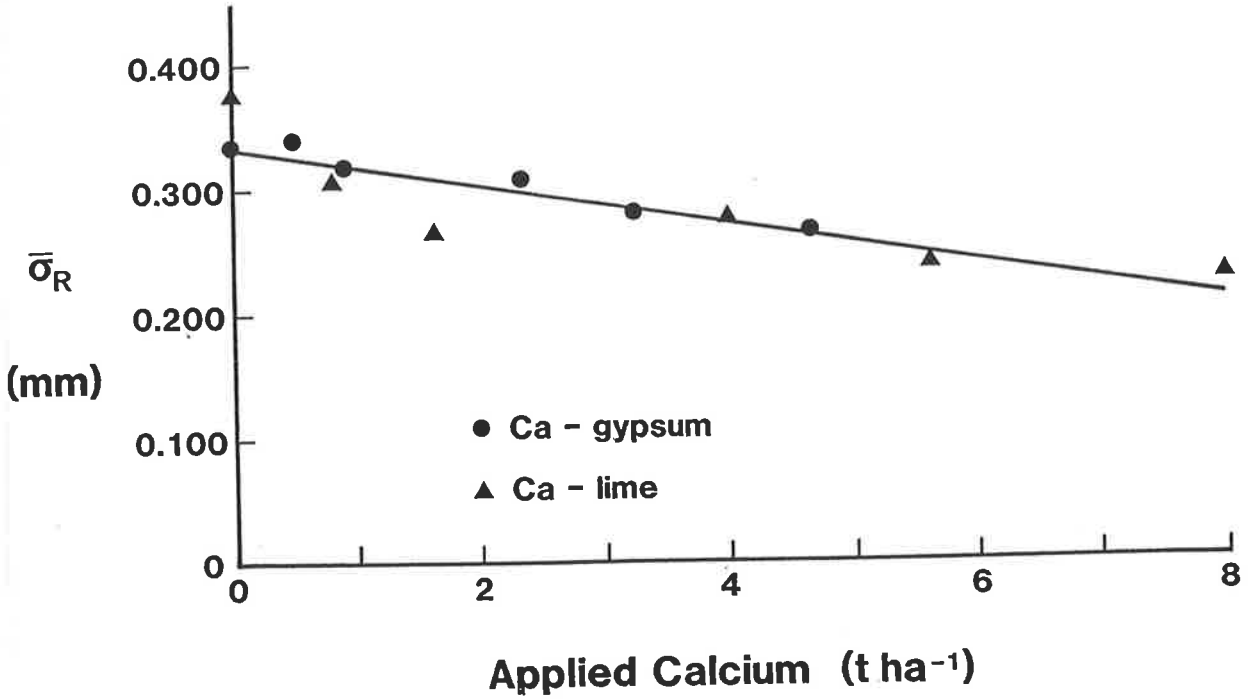

Figure 4-1. Mean fracture surface rugosity, σ_R, of natural soil clods measured in 1986, as a function of the level of calcium, Ca, applied to the soil in 1980.

the dispersible clay content of the soil were not significantly affected by the amount of applied calcium (Table 4-2).

By contrast to the 1986 results, however, the amount of applied calcium was found to influence the mean water content of the soil clods at the smaller suctions (suctions smaller than 5.0 kPa in Figure 4-2 and Table 4-3). The effect of calcium is not detectable at suctions ≥ 10 kPa, so it has acted mainly to increase the porosity in pores >60 μm (effective cylindrical pore diameter), rather than the total porosity.

Due to the influence of calcium on soil water content, and the influence of soil water content on tensile strength and penetrometer resistance (cf. Figures 3-13 & 3-14) it was necessary to employ multiple linear regressions to isolate the effect of calcium alone on soil strength. Regressions of mean values of tensile strength, TS, and penetrometer resistance, Q_p, on both the amount of applied calcium and the corresponding mean water contents of the soil clods (Table 4-3) were performed. The results are summarized in the regression equations:

$$TS = 9.50 \underset{(\pm 1.43)}{} - 0.016\,Ca \underset{(\pm 0.12)}{} - 18.31\,w \underset{(\pm 9.03)}{},\ kPa \quad (R = 0.51,\ n=24) \qquad [4\text{-}2]$$

and

$$Q_p = 5459 + 27Ca - 25229\,w,\ kPa \quad (R = 0.89,\ n=24) \qquad [4\text{-}3]$$
$$(\pm 442)\ (\pm 36)\ (\pm 2788)$$

The w-coefficients in equations [4-2] and [4-3] are significantly different from zero at $0.05 < P < 0.10$ and $P < 0.001$ respectively. The calcium coefficients, however, were found to be not significant at P = 0.10 in both equations [4-2] and [4-3], thus indicating that the soil water content had the greatest influence on soil strength.

The dominating influence of water content (over that of calcium) on tensile strength and penetrometer resistance was also reflected in the fracture surface rugosity data. To illustrate this influence, the vertical axis of the σ_R versus w function has been superimposed for convenience over the vertical axis of the σ_R versus

Table 4-2

$CaCO_3$ Application Rate ($t\ ha^{-1}$)	Calcium applied ($t\ ha^{-1}$)	Mean % OC*	Mean % D.C.* (of whole soil)	Mean ρ_b ($kg\ m^{-3}$)	Mean PL* (± s.e., n) ($kg\ kg^{-1}$)
0	0	1.12 (0.02)	11.61 (± 0.55)	1640 (± 10)	0.116 (±0.004, 14)
4	1.60	1.06 (0.03)	15.75 (± 0.49)	1680 (± 10)	0.129 (±0.001, 9)
10	4.00	1.12 (0.03)	15.19 (± 0.78)	1680 (± 10)	0.123 (±0.007, 9)
14	5.60	1.01 (0.02)	14.64 (± 0.53)	1640 (± 20)	0.135 (±0.002, 9)
20	8.00	1.05 (0.02)	12.20 (± 0.29)	1640 (± 10)	0.126 (±0.003, 9)
	Mean	1.07	13.88	1650	0.126
	(±s.e.)	(± 0.021)	(± 0.830)	(± 0.011)	(± 0.003)
	n	5	5	5	5

* **%OC** is the mean organic carbon content of the soil; **%DC** is the mean dispersible clay content of the soil; ρ_b is the mean bulk density of the soil clods.

Table 4-2: Mean soil organic carbon contents, **%OC**, and mean dispersible clay contents, **%DC**, and mean bulk densities, ρ_b, of **n**=25 clods as well as mean plastic limit of soil measured in 1987, in relation to the amount of calcium applied to the soil in 1980.

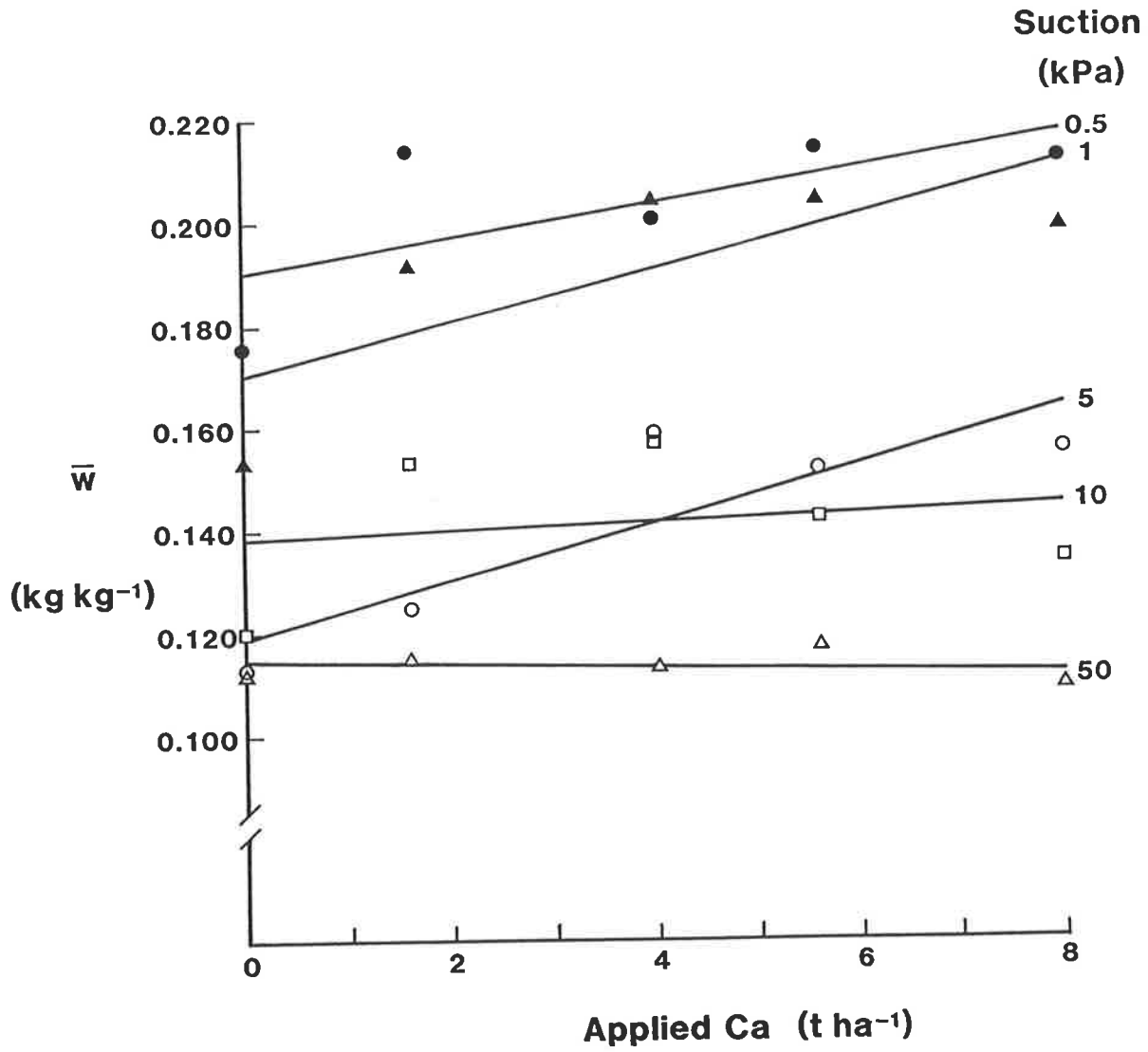

Figure 4-2. Mean gravimetric soil water content, **w**, of natural soil clods at five different water suctions (● = 0.5 kPa, ▲ = 1 kPa, ○ = 5 kPa, □ = 10 kPa, △ = 50 kPa) measured in 1987 as a function of the level of calcium, **Ca**, applied to the soil in 1980 (cf. Table 4-3).

Table 4-3

Water Suction	Calcium Applied ($t\ ha^{-1}$)				
	0	1.6	4.0	5.6	8.0
(kPa)	($kg\ kg^{-1}$)	($kg\ kg^{-1}$)	($kg\ kg^{-1}$)	($kg\ kg^{-1}$)	($kg\ kg^{-1}$)
0.5	0.176†	0.214	0.201	0.214	0.212
1.0	0.153†	0.191*	0.204	0.204	0.199
5.0	0.113	0.125	0.159	0.152	0.155
10.0	0.120	0.153	0.157	0.142	0.134
50.0	0.112	0.115	0.113	0.117	0.109

* average value of water content for 4 rather than 5 clods

† average value of water content for 3 rather than 5 clods

Table 4-3: Mean gravimetric soil water contents, w, at different water suctions measured in 1987 for natural soil clods from plots having different amounts of calcium applied in 1980. (Mean values of w are for 5 clods, except where indicated).

Ca function (Figure **4-3**). Data for the σ_R versus **w** function are averaged across all five water suctions. (Interpolations across the superimposed axes are not valid).

The negative slope coefficient for the σ_R versus **Ca** function (although not significant at P = 0.05) is consistent with the results of 1986 (which were highly significant; Figure **4-1**) despite the fact that the water content was altered in 1987, whereas in 1986, it was relatively constant (Table **4-1**). Clearly, however, the soil water content has an opposite, and stronger effect (significant at $0.05 < P < 0.10$) on σ_R than does the calcium in Figure **4-3**). This dominating influence of soil water content on σ_R probably concealed or at least reduced the effects of calcium on σ_R. A multiple linear regression of σ_R on both **w** and **Ca** was therefore performed on the 25 mean values of **w** and σ_R (from Tables **4-3** & **4-4**). From this analysis, the contribution to σ_R made by both **Ca** and **w** is described in the linear equation:

$$\sigma_R = \underset{(0.024)}{0.209} \quad \underset{(1.96 \times 10^{-3})}{-4.22 \times 10^{-3} Ca} \quad \underset{(0.151)}{+0.431 w}, \quad \text{mm} \quad (R = 0.57, n = 25) \quad [4\text{-}4]$$

The negative **Ca**-coefficient is significant at $0.02 < P < 0.05$ and the positive w-coefficient at $P < 0.01$. Clearly, both factors have highly significant and opposite effects on σ_R, best isolated using multiple linear regression.

As a result of the relation between the amount of applied calcium and the soil water content (Figure **4-2**), however, the 'smoothing' effect of calcium on fracture surface rugosity, σ_R, is probably underestimated. That is, the magnitude of the negative slope coefficients for the σ_R versus **Ca** regressions in Figures **4-1** & **4-3** is probably too small. This is because the applied calcium increases the soil water content at low suctions (Figure **4-2**) which causes the distance between the smallest air-filled pores to increase, and as seen from the results from **SECTION 3**, (cf. Figure **3-10**), this increases the fracture surface rugosity, σ_R. The calcium effect must therefore be very strong to not be entirely concealed by the opposing water content effect.

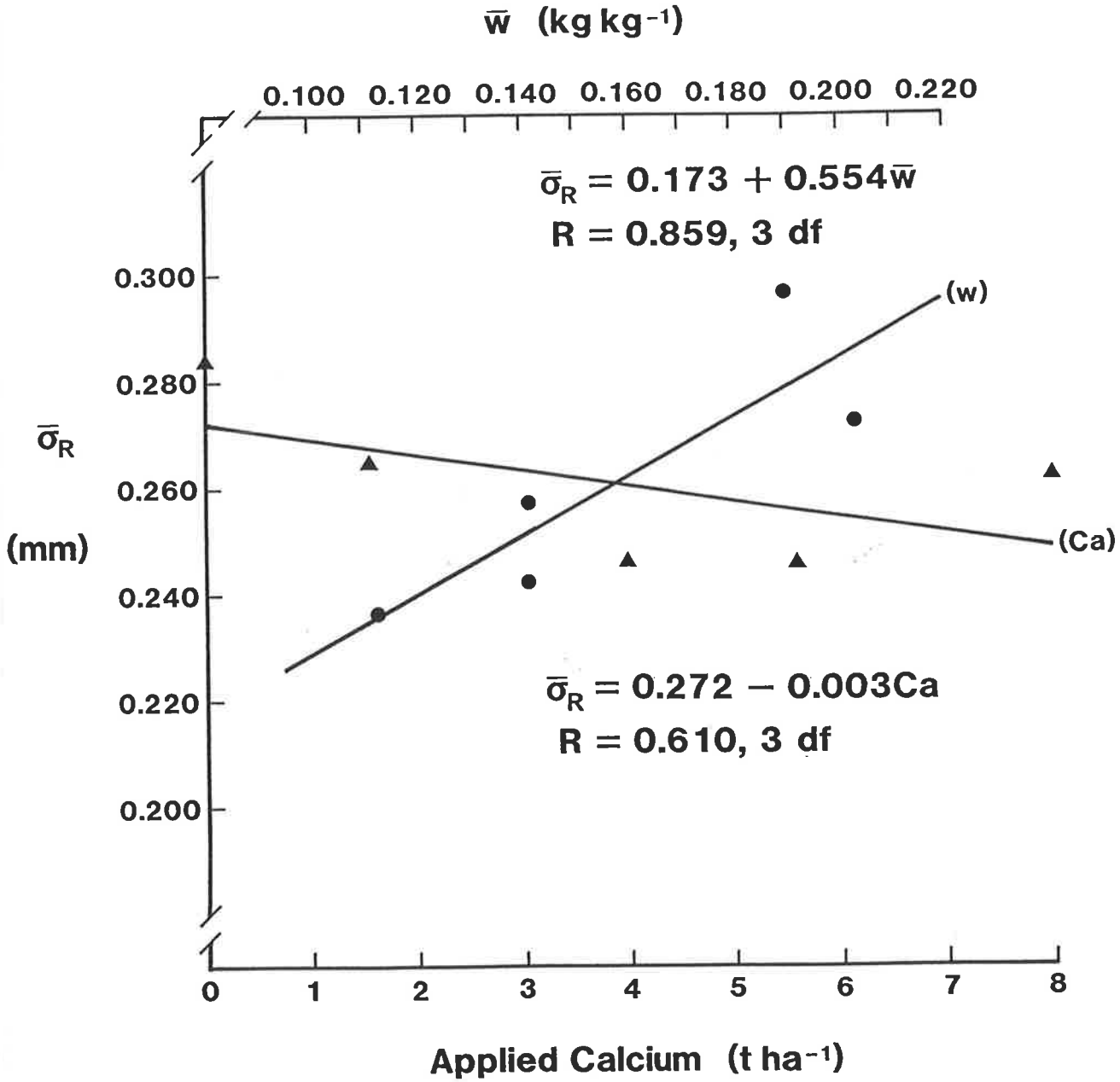

Figure 4-3. Mean fracture surface rugosity, σ_R, of natural soil clods measured in 1987, as functions of the mean gravimetric water content at the time of fracture, w, and the amount of calcium, Ca, applied to the soil in 1980.

Table 4-4

Water Suction	Calcium Applied (t ha^{-1}) 0.0	1.6	4.0	5.6	8.0
	σ_R	σ_R	σ_R	σ_R	σ_R
(kPa)	(mm)	(mm)	(mm)	(mm)	(mm)
0.5	0.304	0.278	0.249	0.243	0.285†
1.0	0.309	0.317	0.265	0.293	0.296
5.0	0.263	0.255*	0.277	0.224	0.268
10.0	0.304	0.236	0.221	0.213	0.234
50.0	0.239	0.237	0.219	0.259	0.228
Mean	0.284	0.265	0.246	0.246	0.262
(± s.e.)	0.014	0.015	0.012	0.014	0.014

* average value of σ_R for 4 rather than 5 clods

† average value of σ_R for 3 rather than 5 clods

Table 4-4: Mean fracture surface rugosity, σ_R, at different water suctions measured in 1987 for natural soil clods from plots having different amounts of calcium applied in 1980. (Mean values of σ_R are for 5 clods, except where indicated).

4.4 General Discussion

It may not be immediately obvious why higher amounts of applied calcium should reduce the rugosity of soil fracture surfaces as illustrated by the data of both 1986 and 1987. In the first place, the calcium amendments were applied to the soil six years prior to the first sampling in 1986. Usually, the applied calcium, especially from gypsum, would be expected to dissolve and leach fairly rapidly. Under irrigated and tilled conditions, gypsum has been shown to leach within approximately three years, after which its beneficial effects on hydraulic conductivity usually decline considerably (Loveday, 1976). Periodic additions of gypsum are recommended to maintain its effects on the pore size distribution beyond this period (Chartres et al., 1985). In the present study, however, no irrigation was used, so leaching of calcium, especially from $CaCO_3$ (which is less soluble than gypsum) would have been slower than under irrigated conditions. Furthermore, the plots received no tillage after establishment in 1980. Hence the potential existed in this experiment for longer-lasting effects.

In the second place, contrary to expectations (Rengasamy, 1983) the effects of calcium were not detected in this study through measurement of the dispersible clay content of the soil. An explanation may lie in the fact that dispersible clay determinations were made on disturbed soil samples, whereas rugosity measurements were made on undisturbed, natural clods. If all the added calcium were leached by the time sampling was started in 1986, then no differences could be expected to show up from measurements of physical properties made on disturbed samples. If, on the other hand, the improved structure that was induced by calcium sometime shortly after application in 1980 were left undisturbed (i.e. no tillage) improved structure might still be left. The lack of tillage after the establishment of pasture on the experimental site in 1980 may have enabled the structure created after the incorporation of calcium to be stabilized through age hardening (Utomo and Dexter, 1981a) and cementation processes under pasture management. Had the soil been tilled each year since 1980,

the 'blue print' might have been lost, and rugosity measurements might have revealed no differences, just as with the dispersible clay results (Table **4- 2**).

Regardless of why a measurable effect lasted for so long on these plots, the question still remains as to why higher amounts of applied calcium resulted in smoother soil fracture surfaces. To some extent, the effect of calcium on σ_R may be comparable, or similar to the effect suggested in **SECTION 3** (Figures **3- 13a** & **3- 13b**) to be due to cementitious bonding between particles in relatively wet soil, after age hardening in the field. Equations **4- 2** and **4- 3** suggest that calcium was probably not a cement, as such, because it had no significant effect on the tensile strength and penetrometer resistance of the soil. But calcium may have been responsible for stabilizing cementitious material (eg. clay and organic matter) between soil particles shortly after its application in 1980. The soil was undisturbed since 1980, and age hardening processes in the field might gradually have stabilized the cementitious material even after the calcium had been leached away. Therefore direct effects of calcium on soil strength (as for the dispersible clay) would not be expected in 1987, even though a 'blueprint' of the undisturbed structure would still be detected from measurements of fracture surface rugosity.

The most likely explanation, however, as to why higher applications of calcium resulted in smoother soil fracture surfaces lies in the differences in size scales between the features detected by the scanning procedure ($\geq$ 0.1 mm), and the sizes of the particles that are stabilized by calcium ($<$ 0.1 mm). Flocculation of dispersible clay into stable domains and microaggregates occurs in the vicinity of calcium ($CaCO_3$ or gypsum) particles. This process, which results in a closer packing of clay particles and the concomitant expulsion of water from among them (syneresis), leaves gaps (water-filled pores) in a manner similar to that described by Peterson (1947). Upon drying, these gaps or zones of weakness become air-filled pores and hence potential sites for crack propagation when tensile stresses are applied. Because these gaps are so small, close together and interconnected, the rugosity of any fracture surface running between them would be small when measured on the 0.1 mm scale used here.

By contrast, a soil to which no $CaCO_3$ has been added would contain more widely-spaced zones of relative weakness, thus containing fewer sites for crack propagation under an applied stress. Failure by the concatenation of widely spaced zones of weakness creates a more jagged fracture surface on the 0.1 mm scale used here (cf. **SECTION 3**)

The different types of fracture surfaces which result from the addition of calcium can be visualized by examining the thin sections of soil clods shown in Plate 1 of Loveday and Scotter (1966), (shown here in Figure **4- 4**). Loveday and Scotter present much smaller samples than those used in the present study, but the thin sections in Figure **4- 4** are shown at approximately the same scale as used in the present study. The greater interconnection between voids in the calcium-treated soil reduces the distance that a propagating crack would need to deviate from a straight-line path across the clod. Hence a straighter trajectory can be envisaged connecting pores in the calcium-treated soil than in the control soil. At the same time, however, if the pore walls in Loveday and Scotter's Plate are examined closely (at higher magnification) it can be seen that they follow a rather circuitous pathway, much more so than in the control sample. On this basis it is proposed that if it were possible to measure surface micro-topography to a resolution of say 10 μm, then the rugosity of the very same fracture surfaces would reveal a reverse picture (i.e. an increase in rugosity with calcium application).

This sort of observation is compatible with the observation of Ingles (1962a) that

> "considerable variation of rugosity is found at all levels, ... from the atomic scale (lattice defects-'holes' - isomorphous replacements, etc.) through the molecular scale (dislocations, packing errors) through the microscale disorientations, to the macroscale pittings, striations and serrations".

The scale at which fracture surface rugosity is determined is therefore very important. The dependence on scale of measurement of rugosity is probably similar to the dependence on scale of measurement of the length of a rugged coastline (see Mandelbrot, 1977). For this reason, the scale and resolution of rugosity measurement (0.1 mm) has been kept constant for all samples in this **SECTION** as well as in other **SECTION**s of this thesis.

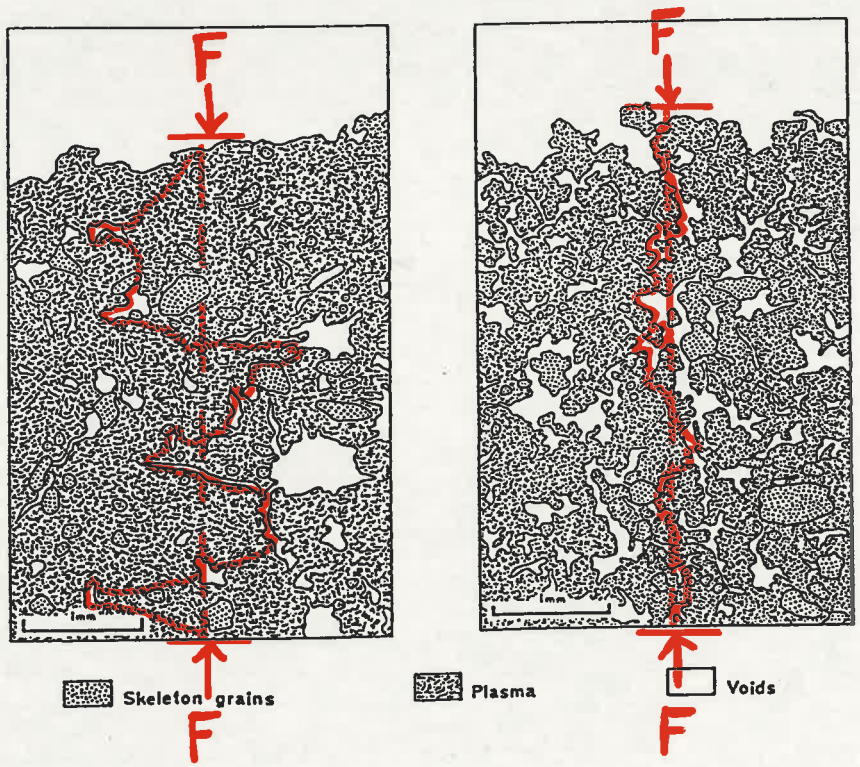

Figure 4-4. Mean fracture surface rugosity, σ_R, of natural soil clods from Plate 1 of Loveday and Scotter (1966) (reproduced by permission of the Australian Journal of Soil Research). Left-hand thin section comes from soil to which normal irrigation water was added, while right-hand thin section comes from soil to which calcium was added to the irrigation water. The acetate-overlay illustrates the smoother potential trajectory for a tensile failure surface to follow at a scale of 0.1mm.

4.5 Conclusions

It was proposed that differences in soil structure induced by calcium should be related to the distance between weakest flaws in the soil, and that this idea could be tested using the technique of fracture surface rugosity, σ_R. Fracture surface rugosity, as measured on a scale of approximately 0.1 mm, appears from the results of this study to be sensitive to at least two properties important to the structure and workability of the soil, viz: the soil water content, **w**, and the amount of applied-calcium, **Ca**.

Of the two soil properties used in this study, the soil water content was the most significant variable affecting the way in which soil fractured in tension. The wetter the soil, the greater the distance between air-filled pores (weakest flaws) and this increased the fracture surface rugosity (cf. Equation **4- 4**).

By contrast, the application of calcium to the soil reduced the distance between weakest flaws and hence produced smoother fracture surfaces (cf. Figures **4- 1 & 4- 3**, and Equation **4- 4**). This effect was detectable despite the interaction at small suctions between calcium and soil water content (cf. Figure **4- 2**) which, by increasing the macroporosity (pores **>** 60 μm diameter), tended to increase the distance between air-filled pores (which tended to increase, rather than decrease σ_R). It is suggested that the most likely explanation for the apparent 'smoothing' effect of calcium on soil fracture surfaces is the differences in size scales between the features detected by the scanning procedure ($\geq$ 0.1mm) and the sizes of the particles that are stabilized by calcium (**<<** 0.1 mm).

SECTION 5. EFFECT OF ORGANIC CARBON CONTENT ON FRACTURE SURFACE RUGOSITY

5.1 Introduction

Fracture under tensile stress (eg. during tillage) is controlled by the distance between weakest flaws in the soil (Braunack, et al. 1979) and it has been shown in **SECTIONs 3** and **4** that various soil properties influence this distance, which can be estimated using the method of fracture surface rugosity, σ_R. For example, at constant organic carbon content, the soil water content may be the most significant factor controlling the distance between weakest flaws (smallest air-filled pores) in the soil. These flaws are more widely dispersed in wet soil and much closer together in drier soil. It is partly on this basis that at a critical water content, **w** (usually equal to or just below the lower plastic limit, **PL**) the spacing between the weakest flaws in the soil is probably optimized in such a way that maximum soil fragmentation takes place during tillage (Ojeniyi and Dexter, 1979; Utomo and Dexter, 1981b). At other water contents, tillage produces less fragmentation of the soil and therefore leaves relatively large clods (Dexter, 1979).

Soils having different organic carbon contents, on the other hand, exhibit different plastic behaviour (Mitchell, 1976), due in part to the differences in water retention, but also due to the differences in strength caused by the preferential accumulation of polysaccharides in macropores (Foster, 1981; Oades, 1986). It is proposed in this **SECTION** that the differences in plasticity and strength commonly caused by soil organic carbon can influence the distance between weakest flaws in the soil, and that the differences should therefore be reflected in measurements of fracture surface rugosity, σ_R. The following experiments outline the manner by which this proposal was tested, using both natural soil clods as well as moulded soil disks.

5.2 General Outline of Experiments

A 'Permanent Rotation Experiment' was established in 1924 on a Red Brown Earth (Rhodoxeralf) at the Waite Agricultural Research Institute. The Experiment includes combinations of wheat, pasture and fallow in various rotations on unreplicated plots (90.53m x 6.71m). The soil from each of five rotations (Table 5-1) provided a significant range of organic carbon content values for this study. Each component of the five rotations is represented on one plot in any year, so the number of samples, **n**, for any measurement is a multiple of the number of components in the rotation, because all plots (ten in total) were sampled.

Four separate experiments were conducted on the soil from the Rotation Plots in order to quantify the effect of soil organic carbon on fracture surface rugosity, σ_R. The first experiment (see **SECTION 5.3**) attempted to isolate the influence of organic carbon on soil strength and fracture surface rugosity by looking at its effects on the soil water content and total porosity of natural soil clods held at a constant water suction of 10 kPa. The second experiment (see **SECTION 5.4**) was planned to be coupled with the first experiment, and was designed to test whether by destruction of the macroporosity (through moulding) the effects of organic carbon on strength and fracture surface rugosity would be eliminated. The third experiment (see **SECTION 5.5**) investigated the range of water contents over which differences in organic carbon content influence the plastic behaviour of moulded soil, its strength and its fracture surface rugosity. The fourth experiment (see **SECTION 5.6**) used air dry and oven dry natural soil clods, and was designed to isolate the effects of organic carbon on soil strength and fracture surface rugosity, independently from the very prominent effects of soil water content.

5.3 Natural Clods at Constant Suction (10 kPa)

5.3.1 Materials and Methods

Ten or eleven fist-size clods were collected in a zigzag fashion across the length of each of the ten rotation plots. The clods were then slowly wetted to near-saturation

Table 5-1

Rotation Components*	Plot** #	n	%OC ± (s.e.)	PL ($kgkg^{-1}$)
W/P/F	5,6,7	33	1.07 ± (0.01)	0.166
W	17	11	1.29 ± (0.07)	0.182
W/P/P	18,19,20	33	1.95 ± (0.05)	0.205
P	29	11	2.45 ± (0.15)	0.234
W/F	34,35	22	0.97 ± (0.08)	0.168

* W = Wheat, P = Pasture, F = Fallow

** Water desorption data for natural soil clods from each of the ten rotation plots are listed in **Appendix 3.**

Table 5-1. Mean soil sorganic carbon contents, %OC, and mean plastic limits, PL, for different crops in the Permanent Rotation Experiment, Waite Agricultural Research Institute, October, 1987. Standard errors (± s.e.) are bracketed.

in the laboratory for a few days, then placed on porous ceramic plates at a water suction of 10 kPa for two weeks. When constant water contents were established, each clod was broken by hand into 3-4 pieces and then analysed for water content (two estimates; **w**, $kgkg^{-1}$), penetrometer resistance (Q_p, kPa), organic carbon content (**%OC**), bulk density (ρ_b, kgm^{-3}), tensile strength (**TS**, kPa) and fracture surface rugosity (two estimates; σ_R, mm) according to the methods outlined in **SECTION 3.**

5.3.2 Results and Discussion

The large number of raw data for this experiment are listed in **Appendix 4, Table A4-1.** Several interactive effects are apparent from the data and they may be summarized as follows. .Firstly, soil organic-carbon content (**%0C**) was found to have a strong influence on the soil water content (**w**, $kgkg^{-1}$) of the clods at a water suction of 10 kPa:

$$w = \underset{(\pm\ 0.003)}{0.137} + \underset{(\pm\ 0.002)}{0.0311}\ \%OC\ ,\ kgkg^{-1}\quad (R = 0.88,\ n = 106) \qquad [5\text{-}1]$$

The coefficients in equation **[5- 1]** are significant at $P < 0.001$ and indicate that increasing amounts of organic carbon increased the porosity in pores < 30μm effective cylindrical diameter in soils on these plots. The organic carbon content also influences the bulk density of the soil (Jeffrey, 1970; Adams, 1973), the relationship for the clods in this study being:

$$\rho_b = \underset{(\pm 12)}{1680} - \underset{(\pm 8)}{61}\ \%OC\ ,\ kgm^{-3} \qquad (R = 0.62,\ n = 106) \qquad [5\text{-}2]$$

The **OC**-coefficient is significant at $P < 0.001$. The clods with higher carbon content thus had higher water contents and lower bulk densities than the clods with lower carbon contents.

This strong influence of organic carbon on both **w** and ρ_b made the usually-accepted model for relating penetrometer resistance, Q_p, to **w** and ρ_b (Heinonen, 1954) unusable. The accepted model is:

$$Q_p = \exp(a + b\rho_b - cw) \qquad [5-3]$$

where **a**, **b**, **c** are constants, and it predicts an exponential increase in Q_p with increasing ρ_b and decreasing **w**. Where organic carbon is also a variable, however, such as in this experiment, the reverse picture can also be found. In this study, for example, a higher **OC**-content generally increased the penetrometer resistance of natural clods, even though the bulk densities were lower and the water contents were higher than for clods with lower **OC**-content. The well-known relationship between tensile strength and water content (Farrell, et al., 1967) is also confounded by the interaction between **OC** and **w** and ρ_b. To accommodate this interaction, a simple term was computed that includes the three interacting variables, **OC**, **w** and ρ_b. The variables were combined in a single-product term, **X**, that reflects their relations to one another. That is, organic carbon is directly correlated to the water content and inversely correlated to the bulk density, so the interaction term was calculated as:

$$X = \frac{\rho_b}{OC\ w} \qquad [5-4]$$

With ρ_b in the numerator and **w** in the denominator of equation **[5-4]**, the interaction term, **X**, also reflects the direct and inverse correlations, respectively, with soil strength. The use of **X** in the analyses of the mean penetrometer and tensile strength data from the ten rotation plots gave the relations:

$$Q_p = \exp(\underset{(\pm 2.53)}{6.52} - \underset{(\pm 14.8)}{2.08w} + \underset{(\pm\ 0.68)}{2.17\ \%OC} + \underset{(\pm\ 0.096)}{0.228X}),\ kPa \quad (R = 0.83,\ n = 10) \qquad [5-5]$$

and

$$TS = (44.53 - 195.0w + 3.81\ \%OC - 1.05\ X),\ kPa \quad (R = 0.95,\ n = 10) \qquad [5\text{-}6]$$
$$(\pm 8.80)\ \ (\pm 51.3)\ \ (\pm 2.34)\ \ \ (\pm 0.33)$$

The **w**-coefficient in equation **[5-5]** and the **%OC**-coefficient in equation **[5-6]** were not significantly different from zero at P = 0.10, but were included to illustrate the trends. The low significance of these terms indicates that the effect of **w** on Q_p and the effect of **%OC** on **TS** are tied up in the interaction term, **X**, which is highly significant in both equations **[5-5]** and **[5-6]**.

Both estimates of fracture surface rugosity, σ_R, (i.e. from direct and indirect tension methods; cf. **Appendix 4, Table A4-1**) were pooled in this experiment, clod by clod, and then averaged to obtain a mean σ_R-value for each of ten rotation plots. (The same pooling procedure was used in **SECTION 3** because the direct and indirect fracture techniques produced σ_R-values which were not significantly different from each other). As no known relationships exist between σ_R and the **(OC-w-**ρ_b**)**-interaction, a multiple linear regression of σ_R on **%OC**, **w** and ρ_b from the ten plots was performed to determine the effects of each factor.

$$\sigma_R = (3.75 - 2.64w + 0.014\ \%OC - 1.89\rho_b),\ mm \quad (R=0.82,\ n=10) \qquad [5\text{-}7]$$
$$(\pm\ 1.15)(\pm\ 2.13)\ \ (\pm\ 0.066)\ \ \ (\pm\ 0.59)$$

Although this equation accounts for a reasonable portion of the variance, only the ρ_b-coefficient was found to be significant at $P < 0.05$. For this reason, the interaction term, $\frac{1}{X}$, was substituted in place of **OC** and **w**, which then gave the relation:

$$\sigma_R = (3.05 - 1.70\ \rho_b - 0.426\ \frac{1}{X}),\ mm \quad (R = 0.80,\ n=10) \qquad [5\text{-}8]$$
$$(\pm\ 0.86)(\pm\ 0.52)\ \ (\pm\ 0.195)$$

All the coefficients in equation **[5-8]** are significantly different from zero at $P < 0.05$. The use of $\frac{1}{X}$, rather than **X**, placed the water content, **w**, into the numerator of the interaction term, and thus better reflected the direct correlation, which has been found

in **SECTIONs 3** and **4** to exist between σ_R and **w**. The fact that the coefficient for $\frac{1}{X}$ is negative (instead of positive, as might be expected from the results of **SECTION 3**) may indicate that the bulk density exerts a stronger effect in the interaction term. It is apparent from these results that the effect of organic carbon on brittle fracture is very difficult to isolate from other factors with which organic carbon interacts.

5.4 Moulded Disks at Constant Suction (50 kPa)

5.4.1 Materials and Methods

Soil from each of the ten plots from the five rotations listed in Table **5-1** was air-dried at 20°C in the lab and passed through a 2mm sieve prior to moulding at a water content of **w**=0.20 $kgkg^{-1}$. The sieved soil was rewetted by mixing it with a calculated amount of de-ionized water and then working it with a small knife for 30-45 minutes. Moulding was meant to remove most discontinuities (macropores) and to destroy soil structural units to sizes between 2 and 50 μm (Emerson and Dettmann, 1959; Emerson, 1968). Ten soil disks for each plot were prepared in plastic rings (inside diameter=26 mm; height=10 mm), then saturated and placed on porous ceramic plates for two-three weeks at a constant water suction of 50 kPa. Hydraulic contact was established by pressing the wet disks (in their plastic rings) onto the ceramic plates that were initially saturated. It was found to be necessary to use 50 kPa (rather than 10 kPa, as in **SECTION 5.3**) because it was found that the moulding process drastically reduced the cohesive strength of disks at only 10 kPa suction and they could not be handled without plastically deforming them. The use of 10 kPa suction would therefore have prevented the desired measurement of tensile strength, and so a greater suction of 50 kPa was used. When equilibrium water contents were established, all disks were fractured using indirect tension (see Plate **5-1**), water contents were determined, and then one half of each disk was arbitrarily selected and prepared for analysis of the fracture surface rugosity, σ_R as follows. One of the two halves of each fractured disk was placed flat with its fracture-face oriented vertically in a small plastic vial filled with white epoxy (as described for natural soil clods in **SECTION 3**). The epoxy hardened for 24 hours, then the vials were bisected in a plane mid-way between the two outer disk faces, using a diamond saw. A schematic representation of

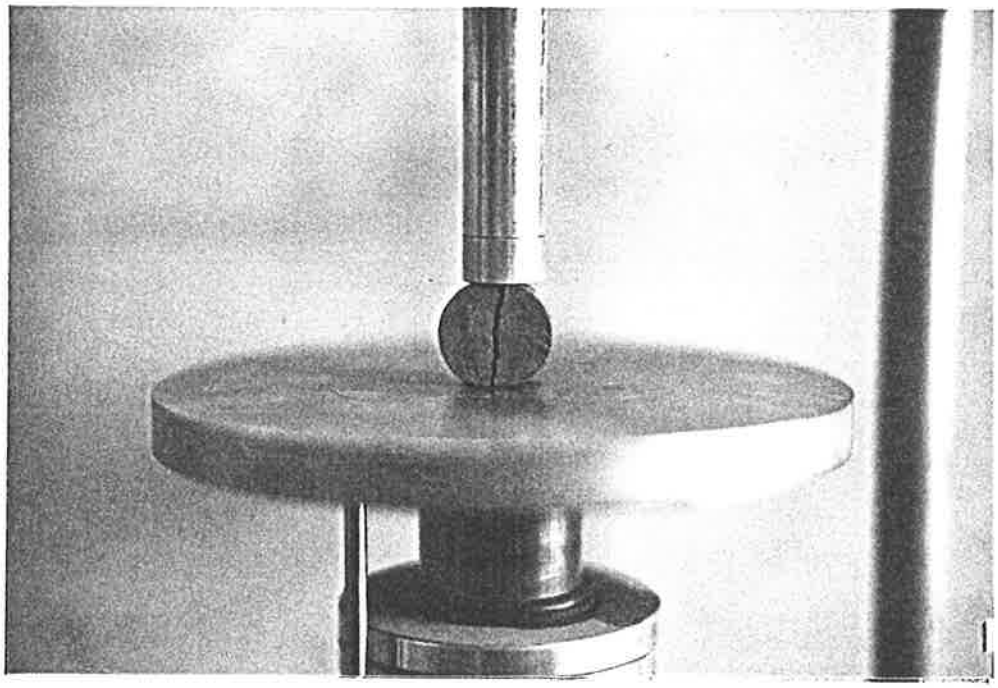

Plate 5-1. Soil disk being fractured by indirect tension between parallel plates.

the sliced profile showing the x and y coordinates of the topography of the disks fracture surface is shown in Figure 5-1.

5.4.2 Results and Discussion

Consistent with the results for natural clods at 10 kPa (SECTION 5.3) the organic carbon content had a major influence on both the water content and bulk density of moulded soil disks from the same rotation plots. Not only does organic carbon control the water content and bulk density, it also modifies the lower plastic limit, PL, of the soil (Odell, et al. 1960). The increase in the mean lower plastic limit due to organic carbon content of the soils from the five rotations listed in Table 5-1 is shown in Figure 5-2 and is significant at $P < 0.001$.

Clearly, an assessment of the effect of organic carbon on the fracture properties of moulded soil must take into account inherent differences in both bulk density and the plastic behaviour of the soil at different water contents. To this end, the lower plastic limit serves as a convenient reference for standardizing the water contents of different soils. Relative water contents may be calculated by using the dimensionless ratio $\frac{w}{PL}$. The practical significance of this ratio comes from the work of Greacen (1960) who has indicated that the strength and plastic behaviour of soils having equal bulk density should be similar for water contents at or near the lower plastic limit, i.e. at $\frac{w}{PL} = 1.0$.

For disks held at a water suction of 50 kPa, the relations between water content and organic carbon, and between bulk density and organic carbon content were described in the respective equations:

$$w = \underset{(\pm\ 0.003)}{0.121} + \underset{(\pm\ 0.002)}{0.0421}\ \%OC),\ kgkg^{-1} \qquad (R=0.99,\ n=10) \qquad [5\text{-}9]$$

and

$$\rho_b = \underset{(\pm\ 30)}{2040} - \underset{(\pm\ 19)}{177}\ \%OC),\ kg\,m^{-3} \qquad (R = 0.96,\ n=10) \qquad [5\text{-}10]$$

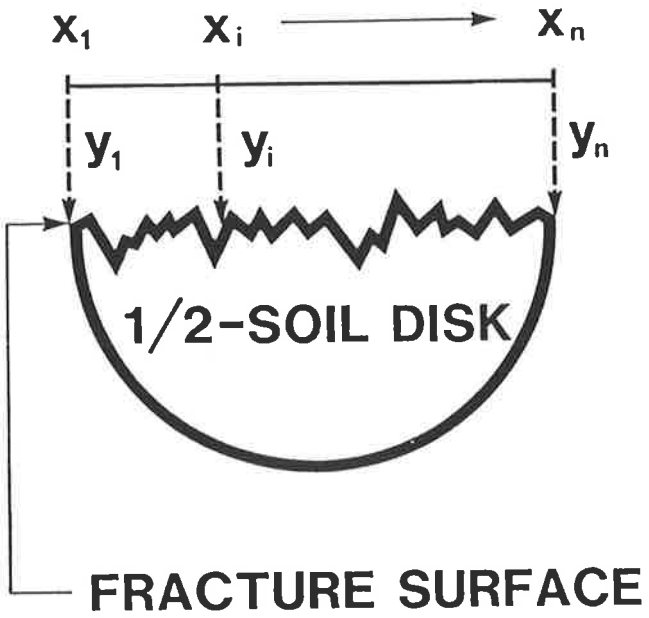

Figure 5-1. Cross-sectional profile of a soil hemi-disk illustrating the scanning procedure used to obtain the Cartesian coordinates (x_i,y_i) of the topography across the transect of the soil fracture surface.

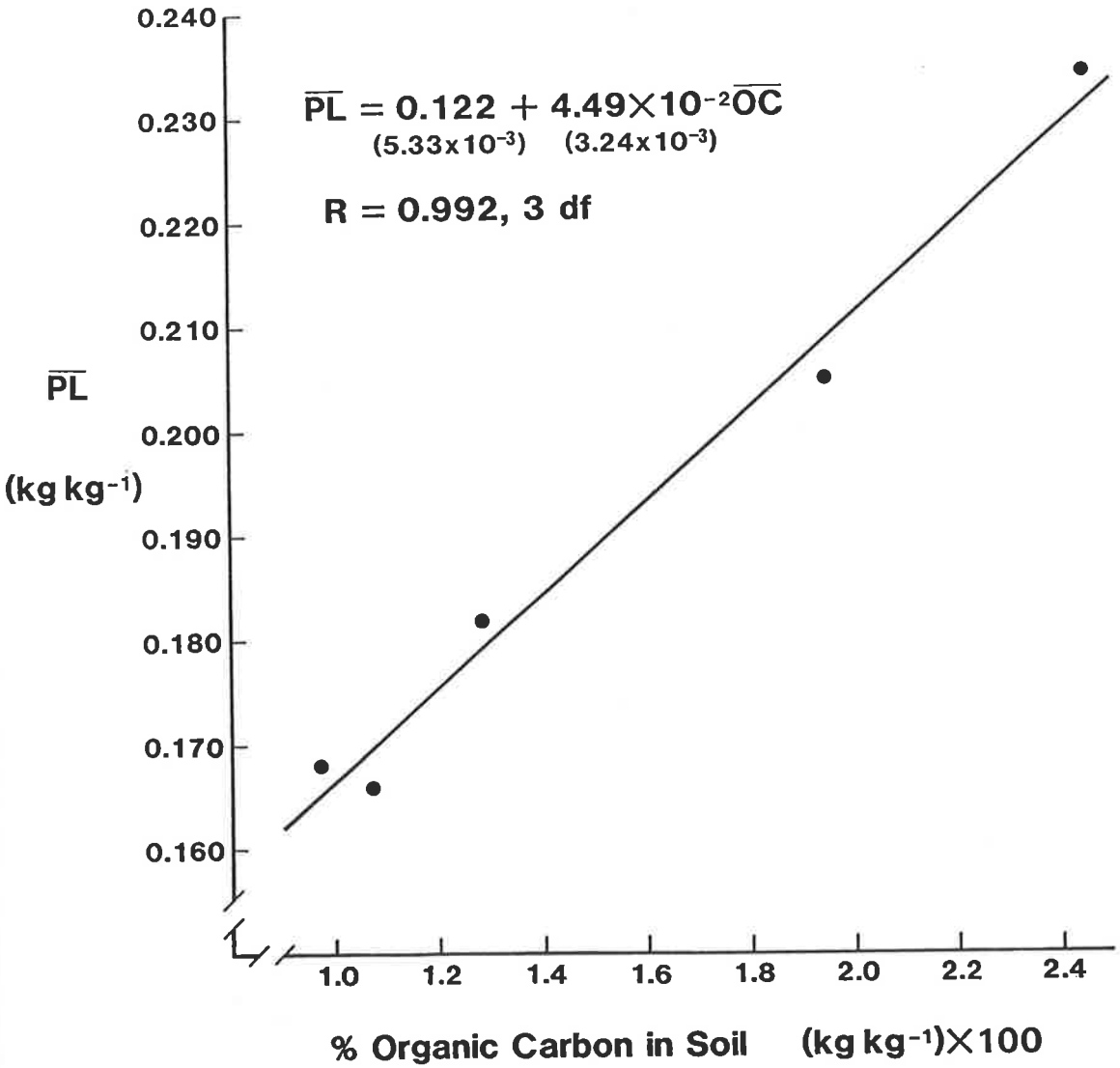

Figure 5-2. Mean lower plastic limit, PL, as a function of the mean soil organic carbon content, %OC, from the Permanent Rotation Experiment, Waite Agricultural Research Institute, Oct., 1987 (cf. Table 5-1).

The **OC**-coefficients in equations **[5- 9]** and **[5- 10]** are both significant at $P < 0.001$. For this reason, the interaction term, **X**, (equation **[5- 4]**) was used to characterize the combined effects of **OC**, **w** and ρ_b on tensile strength, **TS**:

$$TS = \Big(\underset{(\pm\ 55.8)}{-109.0} + \underset{(\pm\ 29.6)}{69.0\rho_b} + \underset{(\pm\ 61.8)}{40.3\frac{w}{PL}} \underset{(\pm\ 0.81)}{-2.21\ X} \Big), \text{ kPa} \quad (R=0.81, n=10) \quad [5-11]$$

The relative water content term, $\frac{w}{PL}$, in equation **[5- 11]** is not significantly different from zero at any reasonable level of probability. The reason for this can be seen in Table **5- 2**, which shows that the $\frac{w}{PL}$ values are all virtually the same, and furthermore they all correspond to values practically equal to their plastic limits $\frac{w}{PL} = 0.99\ (\pm\ 0.005)$.

It was not intended in this experiment that the water suction should correspond so closely with the suction at the plastic limit of these soils, but the results shown in Table **5- 2** are nonetheless quite informative with regard to the fracture surface rugosity data. It can be seen that the mean σ_R-values for each of the ten Rotation Plots are completely indistinguishable from one another and have an overall average value of $\sigma_R = 0.211 \pm 0.004$ mm. (A photograph of all the fracture faces is shown in Plate **5-2** to illustrate the visual similarities despite the noticeable differences in shade (actually colour) between the disks from different plots). This would indicate that there is a common average distance between weakest flaws in moulded soil, which occurs at a water content equal to the lower plastic limit.

Table 5-2

Rotation Plot#	Mean OC (%)	Mean PL ($kgkg^{-1}$)	Mean* w(@50kPa) ($kgkg^{-1}$)	Mean* ρ_b (kgm^{-3})	Mean $\frac{w}{PL}$ (mm)	Mean* $\sigma_R \pm$ (s.e.) (mm)
5	0.97	0.168	0.165	1880	0.98	0.221 ± (0.023)
6	1.07	0.163	0.167	1870	1.02	0.195 ± (0.012)
7	1.18	0.167	0.165	1900	0.99	0.221 ± (0.015)
17	1.29	0.182	0.177	1780	0.97	0.221 ± (0.015)
18	1.80	0.196	0.196	1720	1.00	0.223 ± (0.016)
19	2.01	0.209	0.203	1670	0.97	0.202 ± (0.019)
20	2.04	0.209	0.206	1690	0.99	0.195 ± (0.010)
29	2.45	0.234	0.229	1610	0.98	0.214 ± (0.015)
34	0.98	0.167	0.163	1840	0.98	0.200 ± (0.018)
35	0.97	0.169	0.165	1840	0.98	0.218 ± (0.015)
					Mean = 0.99 ± s.e. = (0.005)	0.211 mm (0.004) mm

* raw data for this Table are listed in **Appendix 4, Table A4-2**, along with tensile strengths on a disk-by-disk basis.

Table 5-2. Physical and chemical properties of soil from the ten Permanent Rotation Plots in relation to the mean fracture surface rugosity, σ_R, of moulded soil disks held at 50 kPa water suction prior to fracture.

Plate 5-2. Fracture faces of soil hemi-disks from ten different Permanent Rotation Plots at the Waite Institute, which were held at a suction of 50 kPa.

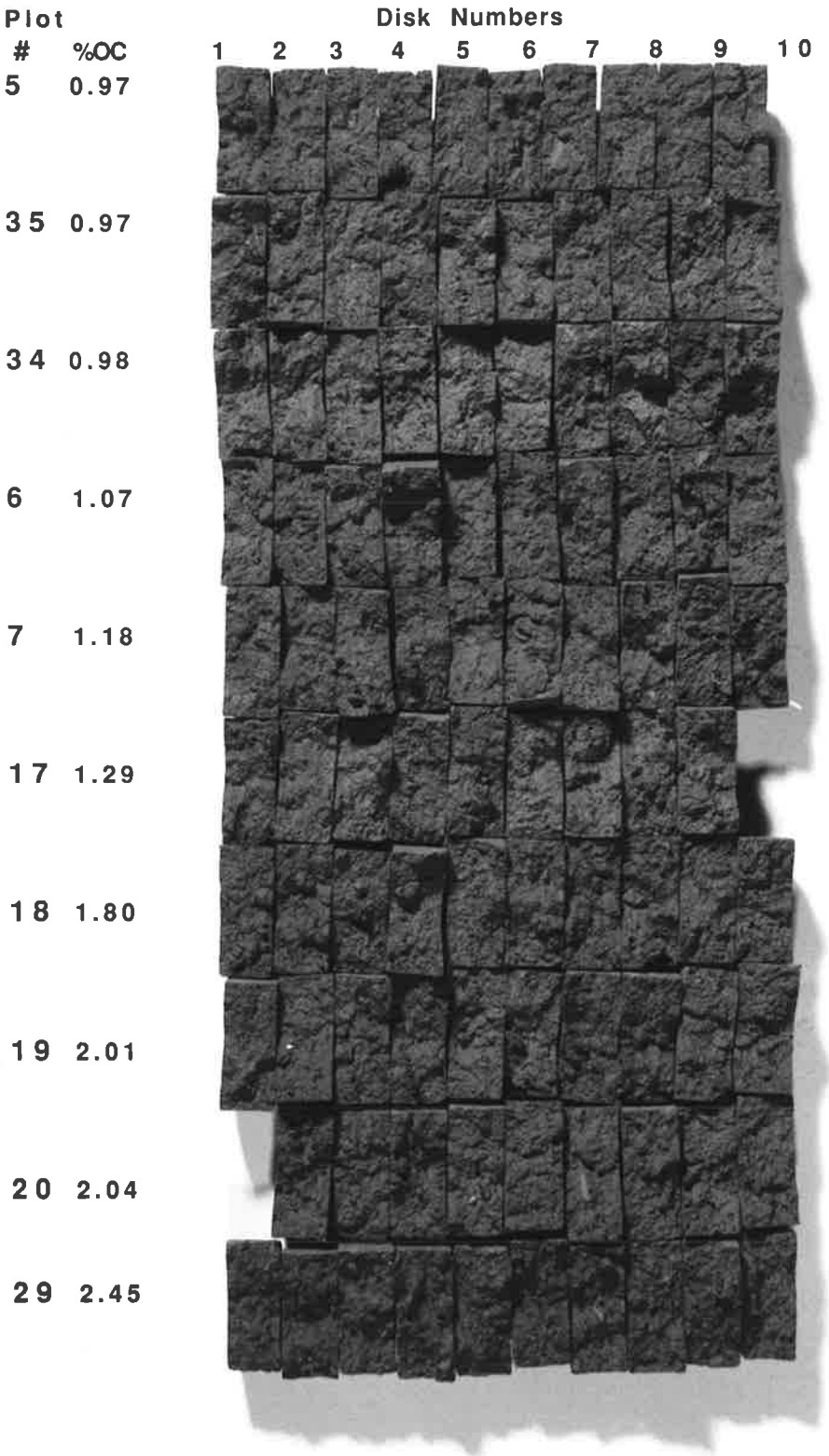
Plot
%OC
Disk Numbers
1 2 3 4 5 6 7 8 9 10
5 0.97
35 0.97
34 0.98
6 1.07
7 1.18
17 1.29
18 1.80
19 2.01
20 2.04
29 2.45

5.5 Moulded Disks at Different Water Suctions

5.5.1 Materials and Methods

Soil was collected from two of the ten plots from the five rotations listed in Table 5-1, both plots having markedly different management practices. One of the plots (#29) was under permanent pasture (P) management, while the other plot (#35) was in a wheat/fallow (W/F) rotation. Soil from each plot was air dried at 20°C in the lab and passed through a 2 mm sieve prior to moulding at a water content, $w=0.20\ kgkg^{-1}$. Seventy soil disks (diameter = 25.5 mm; thickness = 10.0 mm) from each of the two plots were moulded. They were then divided into groups of ten disks, saturated and brought to seven different water contents by either placing them (in the rings) on porous ceramic plates for two-three weeks at one of five different water suctions (0.1, 1.0, 5.0, 10.0, or 50.0 kPa), or by air-drying them at 20°C for seven days (assumed to be 10^7 kPa), or by oven-drying them at 105°C for 2 days (assumed to be 10^8 kPa). Samples were weighed to determine water contents and then penetrometer resistance was measured on all disks (except the air-dry and oven-dry disks) prior to breaking them in half manually (see Plate 5-3). Fracture was accomplished by applying as nearly as possible a direct tensile stress between the fingers. Indirect tension was not possible on the wetter samples, because they lacked sufficient cohesive strength to withstand the compressive stress in a loading frame. The air-dry and oven-dry disks, on the other hand, were too strong to be broken from direct tension by hand, so they were fractured using indirect tension between parallel plates (Dexter & Kroesbergen, 1985). One of the two halves of each disk was arbitrarily selected for measurement of fracture surface rugosity, σ_R, by the methods described previously, while the other half was kept for photography of the fracture faces.

5.5.2 Results and Discussion

Raw data on a disk-by-disk basis are listed in **Appendix 4, Table A4-3**. As found in **SECTIONs 5.3 & 5.4**, the dramatic effect of organic carbon on water content and bulk density of the soil complicates an assessment of the penetrometer and rugosity

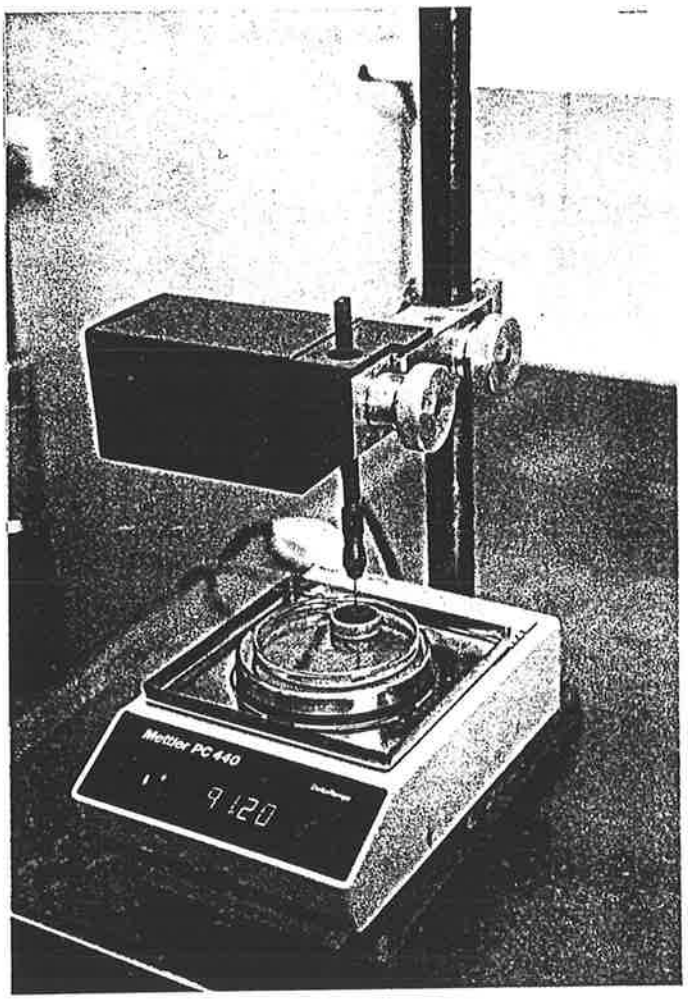

Plate 5-3. Measurement of penetration resistance, Q_p, with a laboratory penetrometer.

data of moulded soil disks. At the same seven water suctions that were used in **SECTION 5.3.2**, the disks from the high-**OC** soil (plot #29) have substantially higher mean water contents, **w** , and lower mean bulk densities, ρ_b, than the disks from the low-**OC** soil (plot #35) as seen in Table **5- 3**. The mean difference in bulk density of disks due to organic carbon, between plot #29 and #35 is **-**170 kgm^{-3} (**s.e.** = 10 kgm^{-3}, **n**=7, significant at P **<** 0.001). The difference in water content between plots #29 and #35, however, was dependent on the water suction, but approached a constant difference at suctions wetter than 5 kPa (Figure **5- 3**) .

As indicated in **SECTION 5.4.2** the strength and plastic behaviour of soils having equal bulk density should be similar for water contents at or near the lower plastic limit (cf. Greacen, 1960), that is, at $\frac{w}{PL} = 1.00$. For two soils having ***different*** densities, however, a plot of strength versus $\frac{w}{PL}$ should show that the line for a soil having the higher bulk density will lie above, yet parallel to, the line for the same soil having a lower bulk density. Greater strength at higher bulk densities (and equal water contents) is due primarily to reduced porosity and a greater number of particle-to-particle contacts (Ingles, 1962c). Mean penetrometer resistance ($\log_{10}Q_p$, kPa) is presented in Figure **5- 4** as a function of the relative water content, $\frac{w}{PL}$, for moulded soil disks from the two rotation plots (#29 and #35) having different organic carbon contents. Comparison of the slopes of the two intersecting lines reveals that they are significantly different from each other at P<0.01.

Disks from plot #29 had significantly lower bulk densities than those from plot #35, and would therefore be expected, with all things equal, to show a line lying parallel to, and below that for plot #35 (hypothetical dashed line in Figure **5- 4**). Plot #29, however, also had a considerably higher organic carbon content than plot #35. It is therefore possible, as shown with arrows in Figure **5- 4**, that the organic carbon caused the strength-line to swing upward to a level above that expected from its lower bulk density. Crossing of the two lines, which occurs at $\frac{w}{PL}$=0.9, is consistent with the

Table 5-3

Water Suction (kPa)	Plot #29-(P) (High-OC) Mean w* ($kgkg^{-1}$)	Mean ρ_b** (kgm^{-3})	Plot #35-(W/F) (Low-OC) Mean w* ($kgkg^{-1}$)	Mean ρ_b** (kgm^{-3})	Differences Δw ($kgkg^{-1}$)	$\Delta \rho_b$ (kgm^{-3})
0.1	0.276	1660	0.201	1850	0.075	-190
1.0	0.265	1650	0.189	1820	0.076	-170
5.0	0.250	1650	0.185	1800	0.075	-150
10.0	0.243	1640	0.176	1840	0.067	-200
50.0	0.186	1650	0.149	1830	0.037	-180
10^7 (AD)	0.017	1610	0.013	1770	0.004	-160
10^8 (OD)	0.000	1610	0.000	1760	0.000	-150

* s.e. for mean **w**-values are all ≤ 0.002 $kgkg^{-1}$, with n = 10 disks.

** s.e. for mean ρ_b-values are all ≤ 10 kgm^{-3}, with n = 10 disks.

Table 5-3. Mean gravimetric water contents, **w**, bulk densities, ρ_b, of moulded soil disks having either high or low soil organic carbon contents, **%OC**.

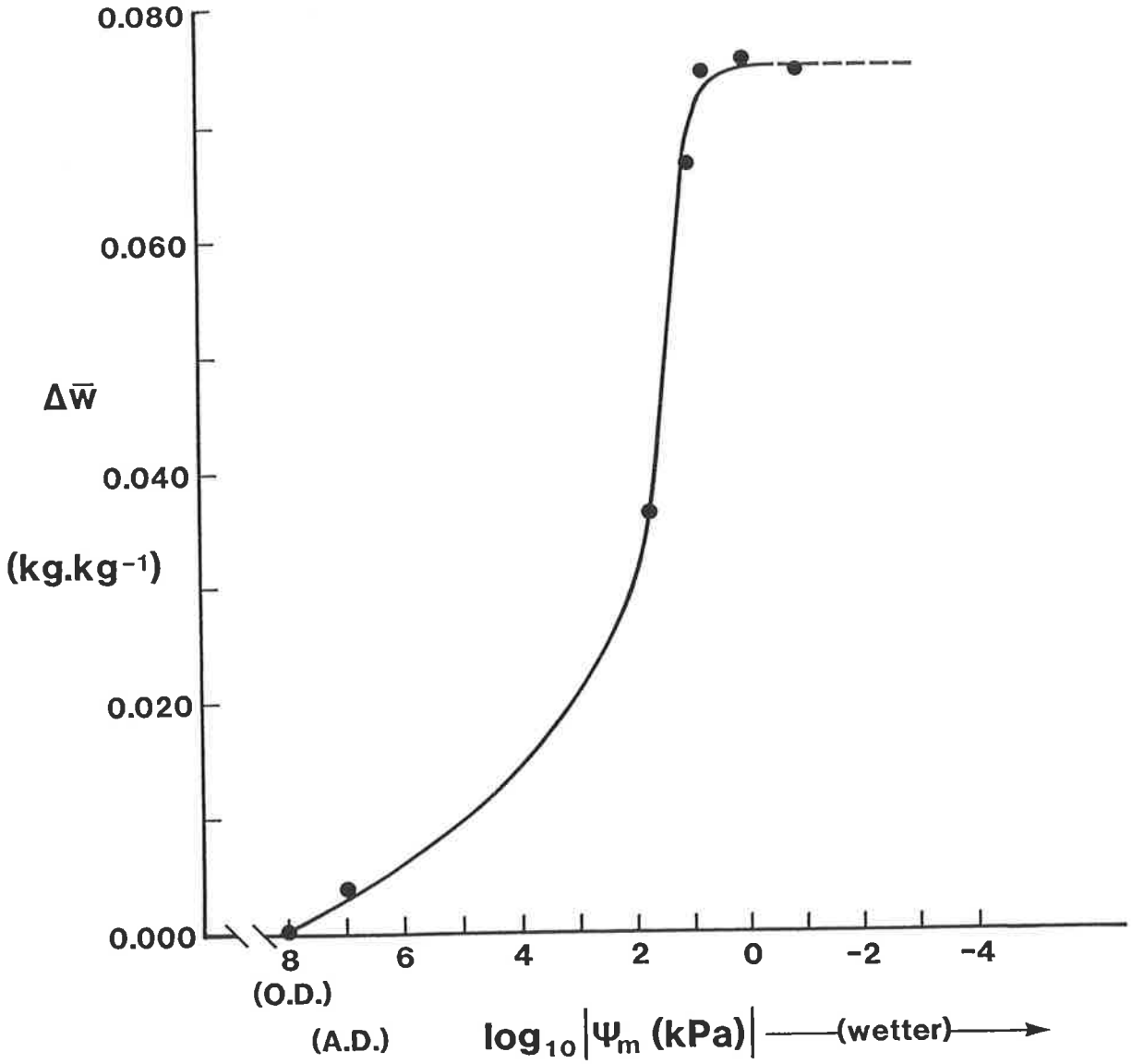

Figure 5-3. Difference in mean gravimetric water content, Δw, between soils of high organic carbon and soil of low organic carbon contents, as a function of the soil water suction ($\log_{10}|\Psi_m$, kPa|).

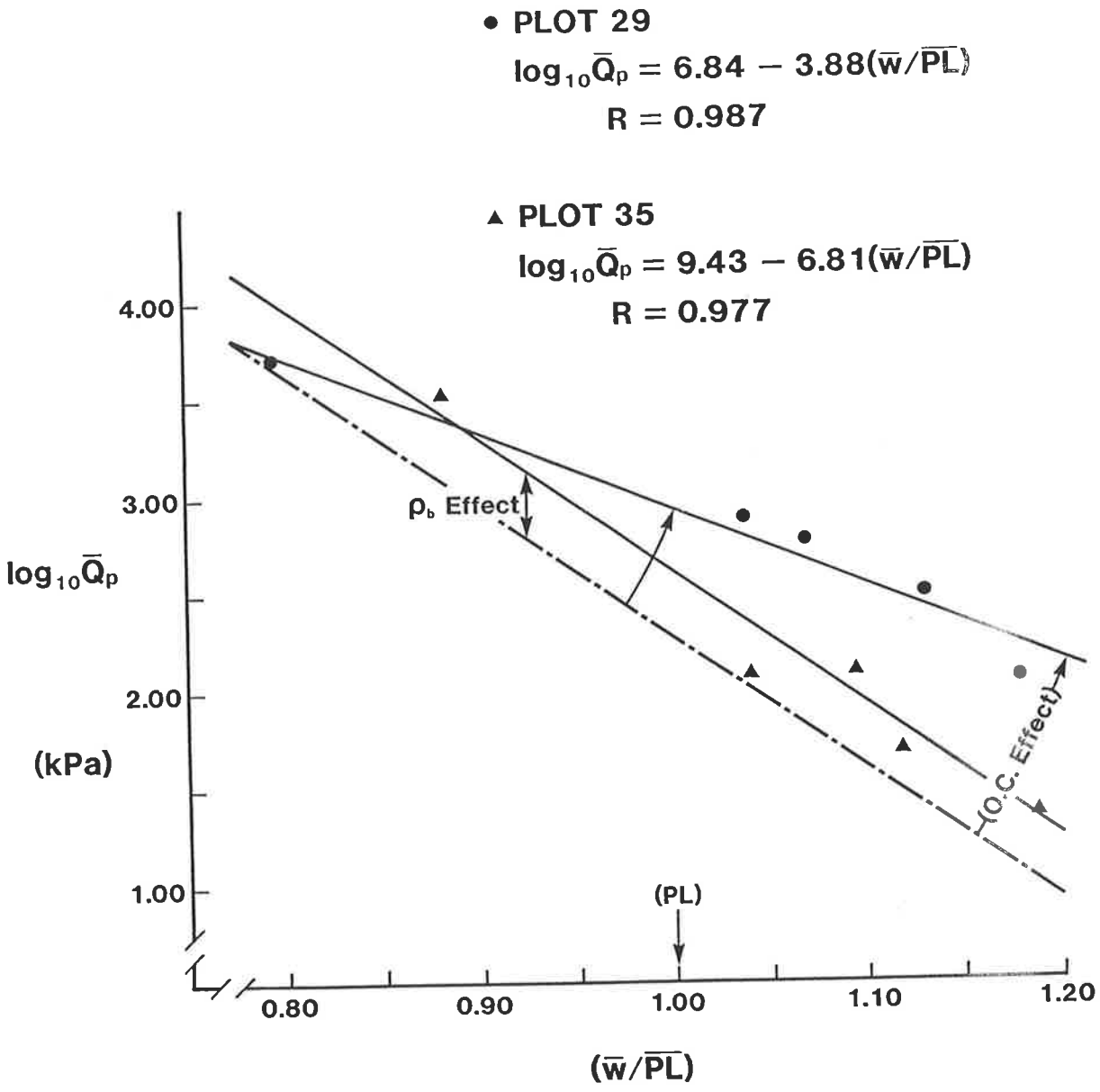

Figure 5-4. Mean penetrometer resistance ($\log_{10}Q_p$, kPa) for moulded soil disks (n=10 disks for each point on the graph) as a function of the relative water contents of the disks at the time of fracture ($\frac{w}{PL}$) , for plot 29 (%OC=2.45%; ρ_b=1650 kgm^{-3}), % for plot 35 (%OC= 0.97%; ρ_b=1830 kgm^{-3}). The dashed line parallel to the plot-35-line is hypothetical.

commonly observed fact that high-**OC** soils are stronger when wet and weaker when dry than low-**OC** soils (Koolen and Kuipers, 1983; Davies, 1985).

Analysis of the rugosity data indicates that even after moulding, there is still a significant positive correlation between σ_R and **w**, similar to that found with natural soil clods in **SECTION 3**. Organic carbon, however, evades a simple analysis because it appears to exert its influence only indirectly on fracture surface rugosity, primarily through its control over the bulk densities, water contents and their consequent effects on the plastic behaviour of the soil. The mean fracture surface rugosity, σ_R for soil disks is shown in Figure **5- 5** as a function of the mean water content for soil disks at the time of their fracture. (Raw data are listed in **Appendix 4, Table A4-3**). The linear equations for the σ_R versus **w** relations for plots #35 and #29 respectively are:

$$\sigma_{R_{35}} = (-0.014 + 1.20\ w),\ \text{mm} \qquad (R = 0.93,\ n=5) \qquad [5\text{-}12]$$
$$(\pm 0.049)\quad (\pm 0.27)$$

and

$$\sigma_{R_{29}} = (0.088 + 0.428\ w),\ \text{mm} \qquad (R = 0.75,\ n=5) \qquad [5\text{-}13]$$
$$(\pm\ 0.054)\ (\pm\ 0.219)$$

Over the range of water contents common to both lines in Figure **5- 5**, the low-**OC** soil (plot #35) generates fracture surfaces that are considerably more rugose than the high-**OC** soil (plot #29). That is, $\sigma_{R_{35}}$ is between 0.035 and 0.055 mm larger than $\sigma_{R_{29}}$ over the range of mean water contents from **w** = 0.180 to 0.200.

For two main reasons, however, the effect on σ_R shown in Figure **5- 5** cannot be attributed directly to the organic carbon content. Firstly, the mean bulk densities of the two plots were quite different, and, secondly, their plastic limits were also significantly different.

With regard to the differences in bulk density, equations **[5- 7]** and **[5- 8]** suggest that σ_R-values, at least for clods, should decrease at higher bulk densities. That is, zones of relative weakness are closer together in denser soils. Dense and compacted soils lack the macropores and other major flaws, which more friable soils, having

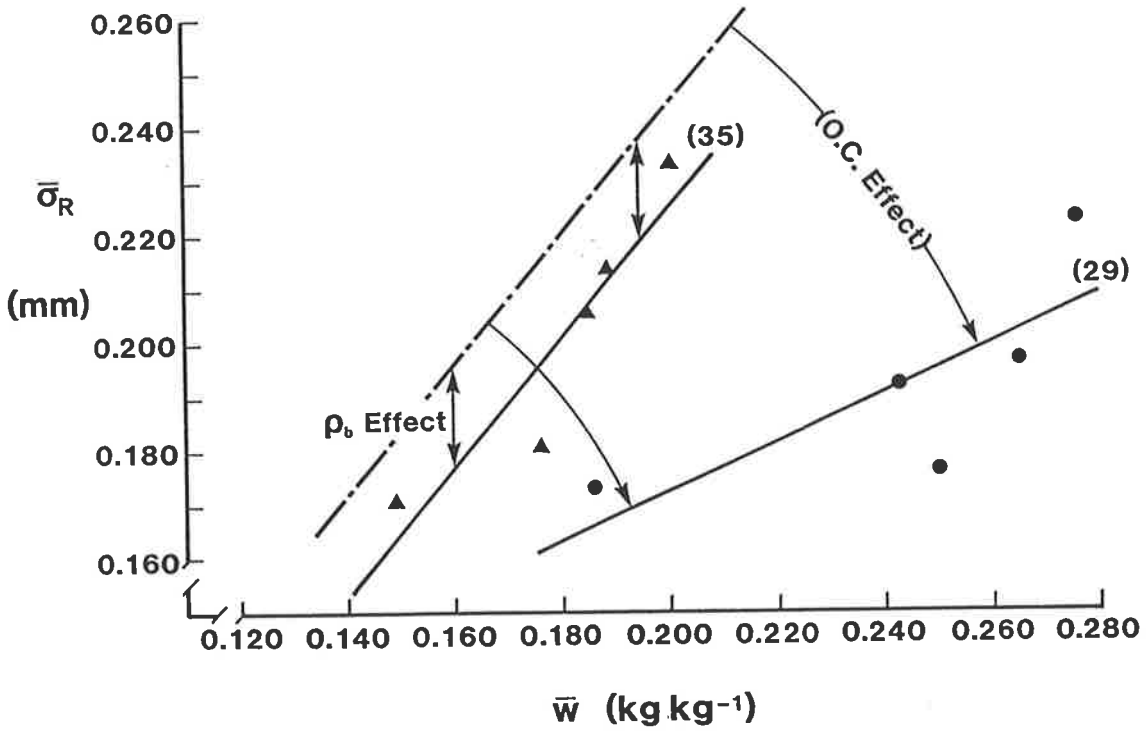

Figure 5-5. Mean fracture surface rugosity, σ_R, of moulded soil disks held at different water suctions, as a function of the mean gravimetric water content at the time of fracture, w.

lower bulk density contain. While the tensile strength of high-ρ_b soils is greater, (see results for oven-dry, air-dry, and 50kPa in **Appendix 4, Table A4-3**) the pores which connect to form the fracture pathways are smaller and more uniformly distributed. As ρ_b increases due to compaction and shear, the remaining pores become smaller and smaller, until in the limit, only pores between primary particles exist, all of which are very close together. Hence the fracture faces of very dense soils should be almost as smooth as the structural arrangement of primary particles.

Considering the issue of bulk density alone, the σ_R-line in Figure **5- 5** for plot #29 (low-ρ_b) should therefore have fallen above, and possibly parallel to the σ_R-line for plot #35, as indicated with the dashed hypothetical line in Figure **5- 5**. The reason for the shift of the hypothetical dashed line to its position determined by the data of plot #29 in Figure **5- 5**, is not yet understood. One may speculate, however, that at constant bulk density, a soil matrix containing its weakest pores in a certain size range will be uniformly strengthened by higher levels of **OC**, as suggested by Quirk and Panabokke (1962) and by Williams et al (1968). Polysaccharides, which are an important group of compounds responsible for stabilizing aggregates, tend to be preferentially located in coarser pores (Foster, 1981). They are located in the coarser pores because the biota that produce the compounds proliferate best in an aerobic environment (Sequi, 1978; Oades, 1986). The increase in strength of the soil between these pores due to the polysaccharides, prevents them from being the weakest pores any longer (Williams et al, 1968), and so pores of a smaller size range, closer together, become the weakest points in the matrix. This implies that while large pores exist in high-**OC** soils, they may be effectively prevented from acting as weak points by a 'short-circuiting' effect of smaller pores, which are closer together.

With regard to the differences in the plastic limits between the two soils (PL_{35} = 0.169, PL_{29} = 0.234), it may be significant that the two soils have exactly the same σ_R-value (σ_R = 0.188 mm) where their respective plastic limits cross the σ_R versus **w** lines of Figure **5- 5**, as illustrated in Figure **5- 6a**. Using relative water contents, $\frac{w}{PL}$, to normalize the effect of **OC** on **w**, it is seen in Figure **5- 6b** that the σ_R versus $\frac{w}{PL}$

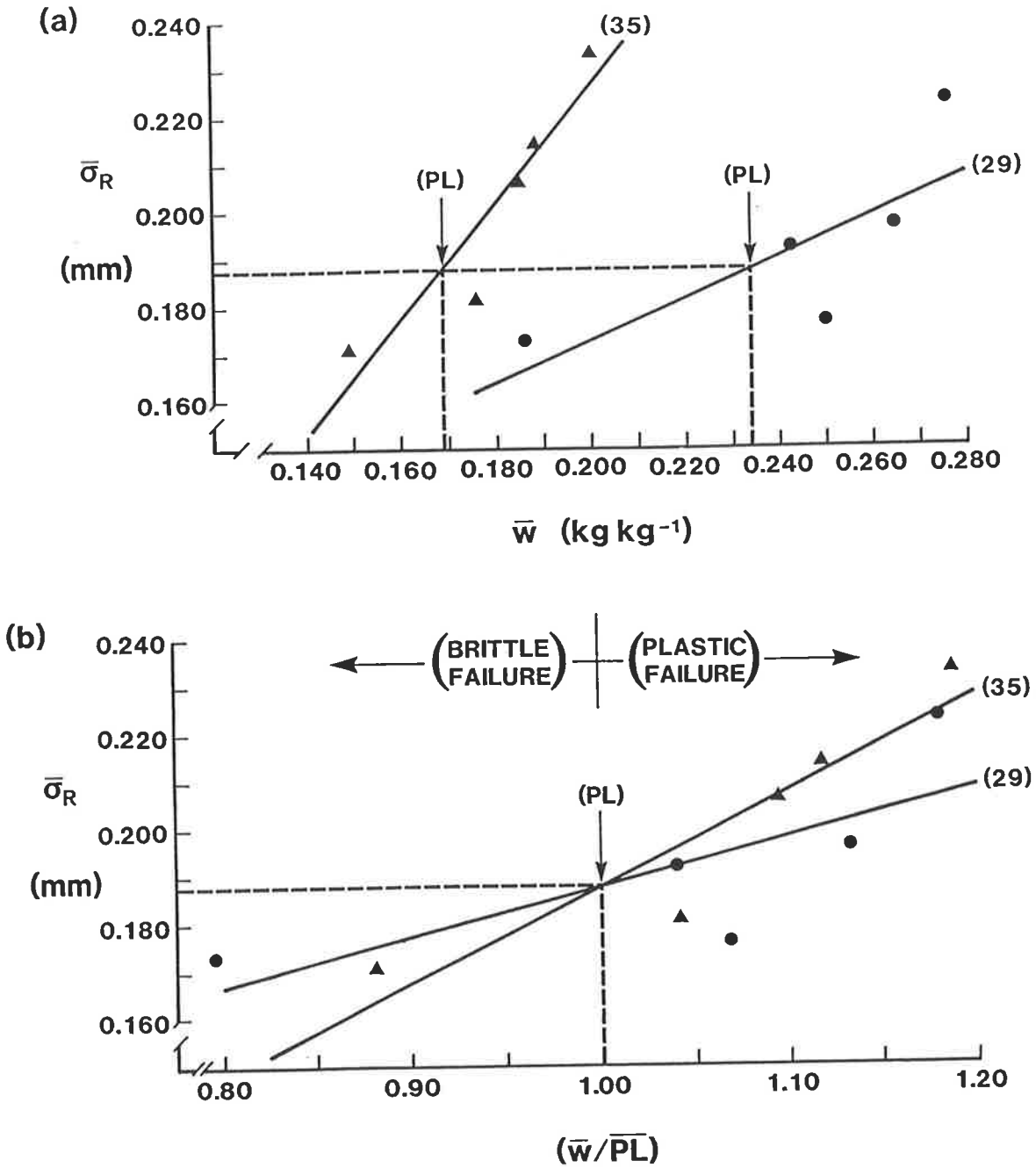

Figure 5-6. Mean fracture surface rugosity, σ_R, of moulded soil disks held at different water suctions, as a function of (a) mean gravimetric water content, w, and (b) relative water content, $\frac{w}{PL}$, with reference to the lower plastic limits of plots 29 (high %OC) and plot 35 (low %OC).

lines intersect at exactly $\frac{w}{PL} = 1.00$. The normalized functions of σ_R versus $\frac{w}{PL}$ for plots #35 and #29 have respective equations:

$$\sigma_{R_{35}} = (-0.014 + 0.202\,\frac{w}{PL}),\ mm \qquad (R = 0.93,\ n=5) \qquad [5\text{-}14]$$
$$(\pm\ 0.049)\ \ (\pm\ 0.046)$$

and

$$\sigma_{R_{29}} = (0.088 + 0.100\,\frac{w}{PL}),\ mm \qquad (R = 0.75,\ n=5) \qquad [5\text{-}15]$$
$$(\pm\ 0.054)\ \ (\pm\ 0.051)$$

The coefficients of $\frac{w}{PL}$ in equations **[5-14]** and **[5-15]** have respective significance levels $0.02 < P < 0.05$ and $0.10 < P < 0.20$. As the negative intercept of equation **[5-14]** suggests, these linear equations are probably valid only in the relative water content range $0.80 \leq \frac{w}{PL} \leq 1.20$, below which the σ_R-values level off to some positive intercept. That is, the fracture of oven-dry soil will not produce perfectly smooth surfaces.

The slopes of equations **[5-14]** and **[5-15]** are not quite significantly different from each other at P=0.05, but despite this fact, the intersection of the two lines at the value of $\frac{w}{PL}$=1.00 is instructive, because it provides a clue about the role of **OC** during fracture of soils at water contents surrounding the plastic limit. In the range of brittle fracture ($\frac{w}{PL} < 1.0$), the higher content of **OC** (plot #29) generates more rugose fracture surfaces (higher σ_R-values) relative to the lower content of **OC** (plot #35) for soil that is drier than the plastic limit. The difference in σ_R due to **OC** (in the brittle-fracture range, $\frac{w}{PL} < 1.0$) persists for water contents down to the air dry state. For the air-dry relative water content, $\frac{w}{PL} = 0.075$, the σ_R-value for plot #29 was 0.141 ($\pm$ 0.011)mm, whereas that for plot #35 was only 0.131 ($\pm$ 0.010)mm (<u>not</u> shown in Figure **5-6**). In the range of semi-plastic fracture, $1.0 < \frac{w}{PL} < 1.2$, the higher content of **OC** generates relatively smoother fracture surfaces (lower σ_R-values) in soil wetter than the plastic limit in comparison to the lower content of **OC** (Plot #35).

It is recognized from Figure **5-6** that most of the data points lie above the plastic limit (i.e. $\frac{w}{PL} > 1.0$), which suggests when the soil disks were broken by direct tension

in the hands, that fracture might not have been brittle. On the other hand, the soils were left on the ceramic plates for long enough to age harden at constant temperature and water content (cf. **SECTION 7**), and so they were sufficiently strong to be held in the hands to break them. Only at the very wettest suction, 0.1 kPa, did the disks deform when fractured, and only the disks from the low-**OC** soil exhibited plastic flow after fracture (See Plates **5-4a** and **5-4b**). So the moulded soil (after age hardening) exhibited brittle behaviour in the zone labelled 'PLASTIC FAILURE' in Figure **5-6b**. Brittle behaviour is not uncommon for age hardened soils at water contents of $\frac{w}{PL} > 1.0$.

5.6 Air- and Oven-Dry Natural Clods Experiment

5.6.1 Materials and Methods

A number (ranging from 8 to 17) of fist-size clods from the 10 rotation plots were trimmed with a pallet knife into relatively round shapes and then either air dried in the lab for seven days at 20°C or else oven dried for two days at 105°C. The geometric mean diameter of each clod was calculated from measurements of the three principal axes and then each clod was fractured using indirect tension to determine its tensile strength. The water content was measured (for air dry samples) and one half of each broken clod was arbitrarily selected and prepared for fracture surface rugosity analysis.

5.6.2 Results and Discussion

With no water present (oven dry), the interactive effects of **w** and **OC** are non-existent, leaving only **OC** and ρ_b as significant variables. Raw data for this experiment are listed in **Appendix 4, Table A4-4**. Analysis of the data according to the rotation groups listed in Table **5-1**, indicates that the mean tensile strength of oven-dry clods was reduced by increasing levels of organic carbon, and increased by higher bulk densities.

$$TS_{OD} = (97.8 - 12.5\ \%OC),\ kPa \qquad (R= 0.82,\ n=5) \qquad [5-16]$$
$$(\pm\ 8.3)\ \ (\pm\ 5.0)$$

and

Plate 5-4a. Fracture faces of soil hemi-disks from Plot #35 (low %OC), which were held at seven different suctions prior to fracture.

PLOT #35: OC = 0.97%

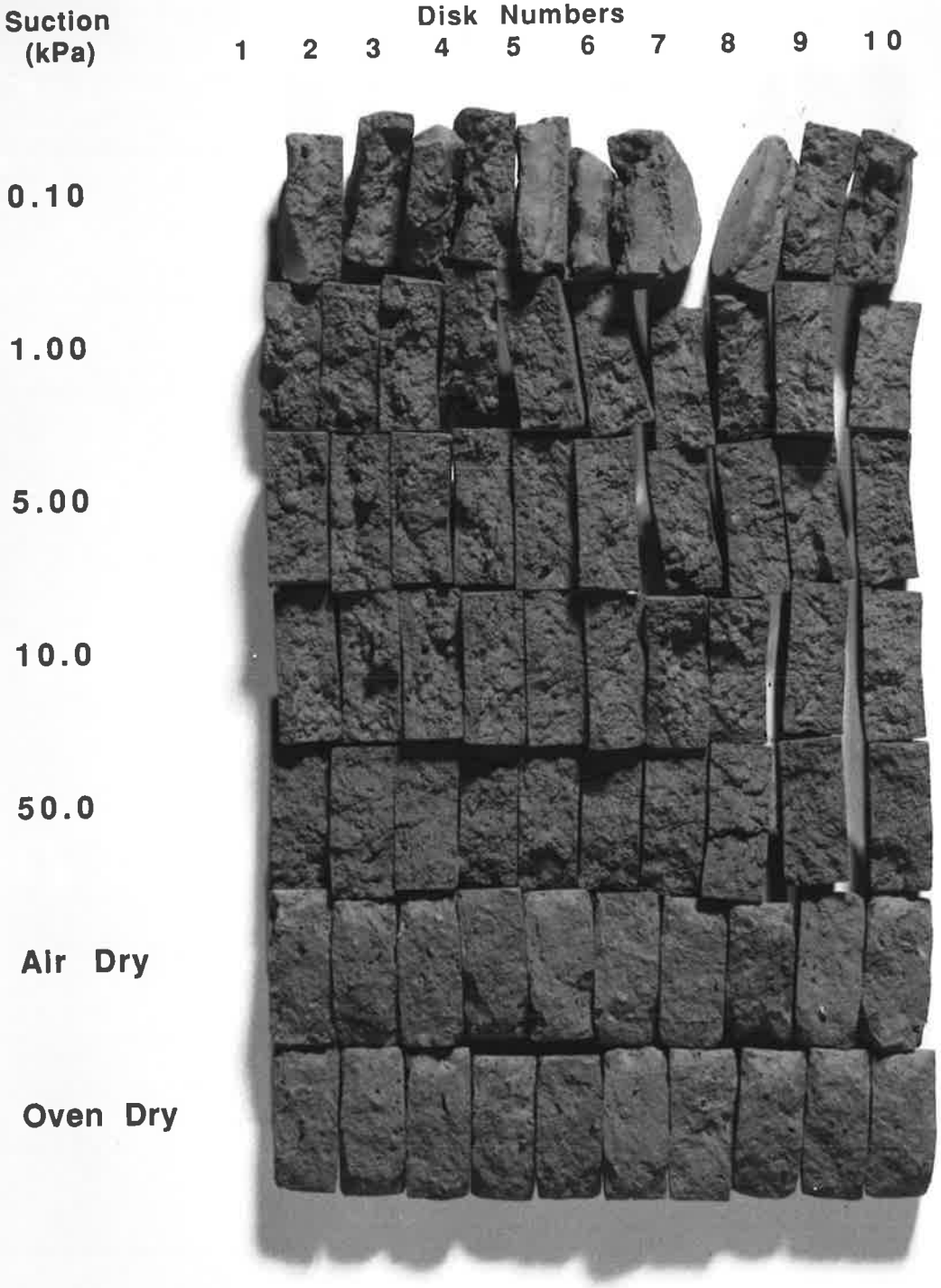

Plate 5-4b. Fracture faces of soil hemi-disks from Plot #29 (high %OC), which were held at seven different suctions prior to fracture.

PLOT #29: OC = 2.45%

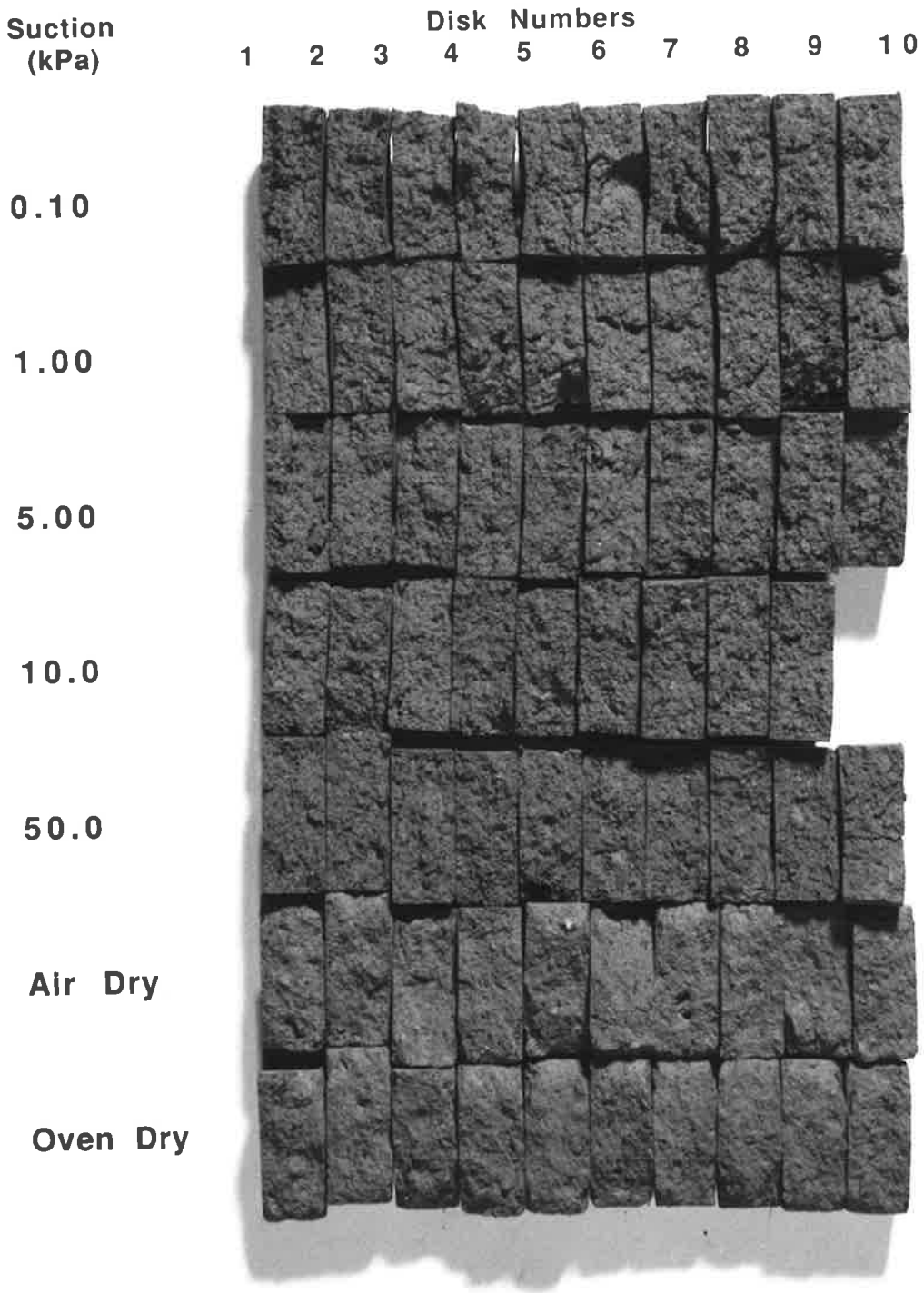

$$TS_{OD} = (-303 + 240\,\rho_b),\ kPa \qquad (R = 0.88,\ n=5) \qquad [5\text{-}17]$$
$$(\pm\ 120)\ (\pm\ 75)$$

Due to the high variability in these oven-dry results, only relations grouped by the five rotations listed in Table 5-1 were significant. Grouping in this way, however, decreased the degrees of freedom in regression too low, so only simple linear regressions were performed, as in equations [5-16] and [5-17]. Hence although an interaction usually exists between organic carbon and bulk density, it has been purposely excluded in equations [5-16] and [5-17]. The coefficients for OC and ρ_b are significant at $0.05 < P < 0.10$ and $0.02 < P < 0.05$ respectively.

The rugosity data showed an opposite trend to that of tensile strength, namely that increasing levels of OC increased the σ_R-values, and higher ρ_b reduced the σ_R-values.

$$\sigma_{R_{OD}} = (0.171 + 0.0243\ \%OC),\ mm \qquad (R = 0.94,\ n=5) \qquad [5\text{-}18]$$
$$(\pm\ 0.009)\ (\pm\ 0.0052)$$

and

$$\sigma_{R_{OD}} = (0.943 - 0.462\rho_b),\ mm, \qquad (R = 0.88,\ n=5) \qquad [5\text{-}19]$$
$$(\pm\ 0.041)\ (\pm\ 0.026)$$

The coefficients of %OC and ρ_b were significant at $0.01 < P < 0.02$ and $P < 0.001$ respectively.

Results for the air-dry clods were similar, but appeared to be affected by the presence of water. While still directly proportional to the organic carbon contents, the water contents of the air-dry clods from the 10 rotation plots all fell within a very narrow range (1.0 - 1.8%). Hence, although the range in w due to organic carbon was insufficient to directly affect the tensile strength of the soil clods, the effect of water content was still present by way of the interaction, X, with OC and ρ_b. The mean tensile strength of air-dry clods, TS_{AD}, kPa, from each of the ten rotation plots as a function of the mean organic carbon content, OC, and its interaction X is described by the linear relation:

$$TS_{AD} = (200 - 51\ \%OC - 0.59X),\ kPa \qquad (R = 0.67,\ n=9) \qquad [5-20]$$
$$(\pm\ 55)\quad (\pm\ 21)\quad (\pm\ 0.25)$$

The coefficients in equation [5-20] are each significant at $0.05 < P < 0.10$.

The effect of mean water content, **w**, on the mean fracture surface rugosity of the air-dry clods, $\sigma_{R_{AD}}$, was similarly negligible on its own, yet significantly tied to the interaction with organic carbon and bulk density, $\frac{1}{X}$, as seen in the linear equation.

$$\sigma_{R_{AD}} = (0.390 - 0.168\ \%OC + 14.6\ \frac{1}{X} - 9.6\ w),\ mm \qquad (R=0.68,\ n=5) \qquad [5-21]$$
$$(\pm\ 0.106)\quad (\pm\ 0.076)\quad (\pm\ 7.3)\quad (\pm\ 7.3)$$

The coefficients of **%OC** and $\frac{1}{X}$ are significant at $0.05 < P < 0.10$, whereas the **w** - coefficient is not significant, even at P = 0.20. No explanation is offered here as to why the **OC**-coefficient is negative rather than positive in sign as expected for fracture at water contents below the lower plastic limit.

5.7 General Discussion of Interactions

One of the purposes of conducting these fracture studies on both natural clods and moulded soil disks was to assess the role of macropores as distinct from that of organic carbon on soil fracturing. It was found, however, that the interactions of **OC** with **w** and ρ_b make this assessment very difficult whenever water is present, and especially at water contents surrounding the plastic limits. It may still be possible from the existing data, nonetheless, to separate the individual roles of macropores versus organic carbon. Using comparable results for oven-dry and air-dry soil clods and moulded disks (Table 5-4), it can be seen that moulding increases the bulk density of the soil, and this is probably responsible for the approximately fourfold increase in tensile strength in both oven-dry and air-dry soils (Williams, et al. 1967). Moulding eliminates the natural planes of weakness and causes a reduction in σ_R. The reduction in σ_R after moulding is consistent with the fact that in higher density soils the pore sizes are usually smaller, more uniformly distributed and therefore closer together.

Table 5-4a (Oven Dry Samples)

Plot # & (%OC)	--- Natural Soil Clods --- w ($kgkg^{-1}$)	ρ_b ($kg\ m^{-3}$)	TS (kPa)	σ_R (mm)	--- Moulded Soil Disks --- w ($kgkg^{-1}$)	ρ_b ($kg\ m^{-3}$)	TS (kPa)	σ_R (mm)
29 (2.45%)	0	1540 (± 20, 11)	69.55 (±6.50, 15)	0.231 (±0.019, 11)	0	1610 (± 3, 10)	324.44 (±8.13, 10)	0.123 (± 0.008, 10)
35 (0.97%)	0	1640 (± 20, 10)	116.48 (± 11.10, 16)	0.179 (± 0.010, 12)	0	1760 (± 10, 10)	387.18 (± 10.87, 10)	0.145 (± 0.010, 10)
Mean	0	1590	93.02	0.205	0	1690	355.81	0.134

Table 5-4b (Air-Dry Samples)

Plot # & (%OC)	--- Natural Soil Clods --- w ($kgkg^{-1}$)	ρ_b ($kg\ m^{-3}$)	TS (kPa)	σ_R (mm)	--- Moulded Soil Disks --- w ($kgkg^{-1}$)	ρ_b ($kg\ m^{-3}$)	TS (kPa)	σ_R (mm)
29 (2.45%)	0.018 (±0.001, 15)	1540 (± 20, 11)	61.69 (±6.17, 15)	0.244 (±0.021, 12)	0.017 (± 0.002, 10)	1610 (± 10, 10)	252.77 (±7.70, 10)	0.141 (± 0.010, 10)
35 (0.97%)	0.014 (±0.001, 16)	1640 (± 20, 10)	98.85 (± 10.81, 16)	0.216 (± 0.020, 10)	0.013 (± 0.002, 10)	1770 (± 10, 10)	293.56 (± 8.10, 10)	0.131 (± 0.011, 10)
Mean	0.016	1590	80.27	0.230	0.015	1690	273.17	0.136

Table 5-4. Mean gravimetric water contents, **w**, bulk densities, ρ_b, tensile strengths, **TS**, and fracture surface rugosity, σ_R, of natural soil clods and moulded soil disks having either high or low organic carbon contents, **%OC** for (a) Oven-Dry samples and (b) Air-Dry samples.

Increased organic carbon content appears to increase the fracture surface rugosity in all cases except in the oven-dried, moulded disks (which had considerably higher tensile strengths; Table **5-4a**). It is possible that as the high-organic-matter disks dried in the oven at 105°C, the organic matter acted as a glue or cement holding the particles together. This cementing process may be responsible for the smoother fracture surfaces, just as would any process which reduces the distance between weakest flaws. It is therefore concluded that higher organic carbon levels increase the rugosity of soil surfaces generated by fracture at water contents below the plastic limit.

Clearly the effect of organic carbon on the dispersion of flaw strengths in the soil is inseparably tied to the soil water content. High-**OC** soils have a greater macro-porosity relative to low-**OC** soils. At high water contents there are more air-filled (drained) pores in the high-**OC** soil, and so zones of weakness are relatively closer together than in the low-**OC** soil. That is, the concentration of weakest flaws is greater for the high-**OC** soil, which therefore produces smoother fracture surfaces under tensile stress. This explains why the σ_R versus $\frac{w}{PL}$ line in Figure **5-6b** for plot #29 (high **OC**) lies below that for plot #35 (low **OC**) at $\frac{w}{PL} > 1.00$.

A higher concentration of weakest flaws (such as for plot #29 over the range $\frac{w}{PL} > 1.00$) does not necessarily imply that the soil strength is lower than in a soil with a lower concentration of weakest flaws (plot #35 at $\frac{w}{PL} > 1.00$). That would only be so in the special case where the weakest flaws in both soils were of the same strength. In the present study, organic carbon probably coats the larger pores (Carr and Greenland, 1972) giving them greater relative strength while wet than in the low-OC soil (Figure **5-4**).

As the soil becomes relatively dry (e.g. $\frac{w}{PL} <<< 1.00$), the dispersion of flaw strengths probably changes as a result of the content of organic carbon in the soil. The low-**OC** soil has a higher bulk density, consisting mainly of micro-pores (cf. Appendix **3**; Figures **A3-1** and **A3-2**), all relatively close together by comparison to the high-**OC** soil. Fracture by the concatenation of these micropores should therefore produce

smoother fracture surfaces than in the high-**OC** soil. Furthermore, with less organic carbon in the soil, there is greater inorganic cementation upon drying, and therefore higher strength due to increased particle-to-particle contact (Kemper et al., 1987). Hence organic carbon tends to reduce the strength of soils at water contents below the plastic limit, while at the same time increasing the rugosity of fracture surfaces.

The σ_R results for $\frac{w}{PL} < 1.00$ quantify the visual observations made many years ago by Chapman (1927) who described in detail the fracture characteristics of air-dried clods from low-**OC** and high-**OC** soils:

> "All crumbs of the low-**OC** plot bore sharp edges and were inclined to break in two directions or when deviating from this, break with a chonchoidal fracture. These crumbs appear more like minerals or other substances of nearly constant chemical composition throughout their mass. In the case of the high-**OC** plot the crumbs were rounded and irregular, far more granular in structure than the low-**OC** plot."

5.8 Overall Conclusions from Organic Carbon Content Experiments

The four groups of experiments conducted in this study all confirm that the organic carbon content of the soil has a very strong influence on the bulk density and the soil water content, with the consequence that whenever the organic carbon content of the soil is not constant, the soil strength and fracture surface rugosity, σ_R, cannot be assessed as a single function of the bulk density and the soil water content. Instead, an additional interaction term needs to be included that reflects the correlation among organic carbon, bulk density and the soil water content. Progress in separating the effects of organic carbon from those of density might be made by repeating the disk-experiments after disks have been compacted to different porosities in a consolidometer.

As shown in Figure **5- 2**, the plastic behaviour of the soil is also strongly influenced by the organic carbon content. For this reason, the lower plastic limit should be used to standardise the water contents of soils having different amounts of organic carbon. The relative water content, $\frac{w}{PL}$, serves as a convenient reference scale for assessing the effects of organic carbon on soil strength and fracture surface rugosity.

Water contents surrounding the lower plastic limit of the soil play a very important role. For example, if soils having very different organic carbon contents and bulk densities are fractured at their respective (different) plastic limits, ($\frac{w}{PL}$=1.00) then they can produce similar values of soil strength (Figure 5-4) and exactly the same values of fracture surface rugosity (Figure 5-6). Different trends, however, develop for relative water contents above and below $\frac{w}{PL}$=1.00. For example, in this study, at constant water content, a higher organic carbon content tends to reduce the soil strength (relative to lower OC content) at water contents that are below the plastic limit (actually $\frac{w}{PL}$< 0.90, Figure 5-4), whereas the reverse situation occurs above the plastic limit.

The results of this study, and of the studies in SECTIONs 3 & 4 suggest that differences in soil strength caused by different soil management practices (e.g. calcium additions, crop rotations, etc.) can be explained on the basis of the different dispersions of flaw strengths they create. The technique of fracture surface rugosity, σ_R, outlined in this study is potentially quite suitable for evaluating different soil management practices. The technique should, however, take into consideration the dominating influence of the soil water content on soil fracture. For example, the fracture behaviour of different soils is very similar at the lower plastic limit ($\frac{w}{PL}$=1.00), so evaluations should be made at water contents well-below the lower plastic limit of each soil.

SECTION 6. MELLOWING OF MOULDED SOILS THROUGH RAPID WETTING

6.1 Introduction

It is possible to improve the structure of many soils through good soil management and use of crop rotations (Tisdall and Oades, 1980b). While this may be true for many soils, it is not the case for every soil. For example, it was shown by Stone, et al. (1985) on a poorly-structured, heavy-textured soil in southern Canada that even after twenty-five years of crop rotation with fertilizer applications, no changes is structure had occurred and no differences could be found in any measurements of soil structure (eg. wet aggregate stability, bulk density, air-filled porosity at 4 kPa suction, turbidity index (Davidson and Evans, 1960) and instability index (Allen, 1984)). Crop rotations on soils which might be improved by them is also not always feasible, and so other ways to improve the structural condition of degenerated soils need to be considered.

It is known, for example, that improvement of soil structure sometimes occurs naturally in heavy clay subsoils when significant drying and shrinking takes place (McGowan, et al. 1983). Rapid wetting, on the other hand, is also an important process for causing soil cracks. It is known to be responsible for both the slaking of soil aggregates (eg. Panabokke and Quirk, 1957) as well as the mellowing of moulded soil (Dexter, 1983; McKenzie and Dexter, 1985).

As indicated in **SECTION 2**, mellowing of soils (which is considered by McKenzie and Dexter (1985) to be partial slaking) occurs when microcracks pervade the soil during rapid wetting, but only when the soil is initially very dry. Wetter soils have already experienced sufficient crystalline swelling, and will therefore experience minimal disruption upon further wetting. Limited knowledge is available on how dry soils must become, or how rapidly they must be re-wetted before significant microcracking will occur. Furthermore, most studies on rapid wetting have looked at the stability of only natural aggregates, and so their results

apply mainly to newly prepared seedbeds. With the exceptions of Telfair, et al. (1957) and Nagahori and Sato (1970), little attention has been paid to the use of water in generating structure in compacted and moulded or puddled soils.

Two main mechanisms are responsible for the mellowing of soils during rapid wetting, viz: (1) air entrapment and (2) differential swelling. As indicated in **SECTION 2**, however, these two mechanisms have been widely studied, and yet a consensus on the relative significance of each in causing aggregate disruption does not exist. The reason for this is that both mechanisms occur at the same time during wetting (Bonneau and Levy, 1982), and Bolt and Koenigs (1972) have suggested that "an aggregate destroyed by air explosion will slake and thus become better accessible for the swelling action of water on the fractured elements." This suggestion of Bolt and Koenigs is of fundamental importance in understanding the soil mellowing process. Yet it has never been tested in reference to the tensile strength and mellowing of soils, especially of moulded, or structurally degenerated soils.

Two studies on the rapid wetting of moulded soils were designed to address the problems outlined above. The first study (see **SECTION 6.2**) was designed to investigate the extent of drying necessary to make moulded soil susceptible to the effects of rapid wetting, and further to determine how rapidly it must be wetted in order to cause mellowing. In this first study, the degree to which the rapid wetting process changed the distance between weakest flaws was also investigated.

The second study (see **SECTION 6.3**) had the objective of quantifying the effects of air entrapment as distinct from those of differential swelling on the tensile strength of moulded soils, and to determine the extent to which the nature of the two processes are augmentative, or 'synergistic', as suggested by Bolt and Koenigs (1972).

6.2 Experiments on Limits of Drying, and Rates of Wetting in the Mellowing Process

6.2.1 Materials and Methods

Two agricultural topsoils in South Australia were used for this study: (1) Urrbrae Red-brown Earth (type A-2 in Litchfield, 1951), and (2) Wiesenboden hydromorphic Black Earth (collected from beside profile #15-A in Stace, et al., 1972). Physical and chemical properties for the two soils are listed in Table **6-1**. The soils were air dried at 20°C for approximately one week, then oven dried at 105°C for 24 hours. They were then passed through a 3mm square sieve and later milled for 15-20 seconds using an N.V. Tema mill (Labor-Scheibenschwingmuhle type T100) to destroy macroaggregation and sand grains. Volume shrinkage was then determined as a measure of their shrink/swell potential by first moulding them at their lower plastic limits, pressing them into cylindrical brass moulds with a palette, and then drying them slowly at 20°C for 5 days, then oven drying them at 105°C for 24 hours. The Urrbrae soil and Wiesenboden shrunk in volume by 6% and 18% respectively.

The experiments described here make use of controlled initial water potentials, Ψ_i, and wetting potentials, Ψ_m, in order to control the initial water contents and wetting rates. Initially-wet, rather than oven-dry or air-dry soils, were used in this study to ensure that the slow drying processes, which occur in compacted and puddled field soils were imitated. Drying to specified water potentials was accomplished using either porous ceramic pressure plates, or saturated salt solutions.

Each of the two soils was mixed with sufficient de-ionized water to make a workable paste. A gravimetric water content of **w**= 0.20 was suitable for the Urrbrae soil, and **w**= 0.40 was suitable for the Wiesenboden. The soil paste was moulded into plastic rings (inside diameter = 26 mm; height = 10 mm) as used by McKenzie and Dexter (1985) and a palette was used to make the outside faces smooth and flat. Disks were left to begin drying in the rings on their edge for an hour

Table 6.-1

Soil	%Sand (>53 μm)	%Silt (2-53μm)	%Clay (<2 μm)	Surface Area (m^2 g^{-1})	PL (kg kg^{-1})	LL (kg kg^{-1})	%OC
Urrbrae	20	63	17*	11	0.194	0.226	1.13
Wiesenboden	24	38	38**	64	0.300	0.479	3.28

* clay fraction mainly illite and kaolinite.
**clay fraction mainly illite with some smectite.

Table 6-1. Physical and chemical properties for the Urrbrae soil (from Field W-10) and the Wiesenboden (beside C.S.I.R.O.) Waite Agricultural Research Institute.

allowing them to shrink slightly so that they could be easily removed from the plastic rings.

Disks that were to be equilibrated at water potentials wetter than -1.5 MPa were placed lying face-down on porous ceramic pressure plates for 14 days. For water suctions drier than -1.5 MPa, disks were placed face-down on damp filter paper, on a galvanised-metal tray placed over a saturated salt solution in a large desiccator (Table **6- 2**). Temperature fluctuations were reduced by surrounding each desiccator with polystyrene beads in a large box. Each desiccator held 20 disks of each soil, approximately half of which were assigned randomly to the standard control treatment (no re-wetting), the other half of which were assigned to the re-wetting treatment.

Each box containing a desiccator was stored at 20° ±1°C for intervals of up to 20 weeks. A wide range of water **absorption** equilibrium times is reported in the literature for dry aggregates under vacuum (Quirk, 1950; Panabokke and Quirk, 1957; R.S. Murray, pers. comm.). It was considered important, however, in this study to estimate the length of time required to reach equilibrium water contents by **desorbing** wet moulded soil at atmospheric pressure, because this more closely simulates the field condition. To this end, a sufficient number of desiccators was used to allow one box containing each salt solution to be opened for re-wetting experiments at intervals of 1, 4, 8, 10, 11, 12 and 20 weeks.

Some technical problems were encountered. During the first 10 weeks of this experiment, condensation of water on the desiccator lids and trays occurred periodically. It is likely that the relative humidities in the desiccators increased to 100% whenever the rate of vapour transport from the soil exceeded the capacity of the saturated salt solutions to absorb the water vapour. It was necessary under these circumstances to open the desiccators and stir the salt solutions to break the water film and to mix the water in. While the solutions were being stirred, selected soil disks were weighed to determine their weight-loss from week to week. It was found that water contents of the disks decreased rapidly for 10 weeks. Only small changes in weight were detected thereafter to 12 weeks and no weight

Table 6-2

Saturated Salt Solution	Relative Humidity at 20°C	Equilibrium Matric Potential (MPa)
KNO_3	0.935	-9.0
NaCl	0.756	-37.9
$MgCl_2$	0.331	-149.2

Table 6-2. Saturated salt solutions used to control the relative humidities and equilibrium soil matric potentials.

loss occurred between 12 and 20 weeks. It was therefore assumed that equilibrium water contents were reached within 12 weeks.

Each soil disk was weighed to determine its initial water content as it was taken from the desiccator prior to the re-wetting experiments. The water contents for samples taken from desiccators prior to 12 weeks were used to interpolate the matric potentials of the soil from desorption curves for the two soils (Figure **6- 1**).

Each soil disk was marked with a dot at the edge of one of its two faces. The dot determined, arbitrarily, the axis along which the disk would subsequently be wetted (Figure **6- 2**) and later crushed after drying to determine its tensile strength using the indirect tension test. For these experiments, groups of approximately 10 disks were wetted simultaneously on coarse sintered-glass funnels (porosity #2) using water at a water potential of -10.0 ± 0.5 hPa. The funnels were de-aired first, to prevent inconsistent wetting behaviour, by immersing them in de-aired water under reduced pressure. Some additional experiments were conducted using oven-dried soil disks and altering the wetting rates by controlling the final water potentials (**h**= 0, -5 or -10 hPa). It was expected that by using the different initial and final water potentials described above, a wide range of wetting rates could be achieved.

The mass of water taken up by the disks as they wetted from bottom to top was measured for 24 hours. The wetting rates (kg kg^{-1} s^{-1}, expressed as kg liquid/ kg soil/ second) were estimated by the slope of the water uptake versus time curves at the point when the wetting front reached halfway up the disks. The magnitude of the wetting rate at the disk's centre was chosen over other possible wetting rates because structural changes that occur at the centre of the disk have the greatest influence on the tensile strength when measured using indirect tension (Dexter and Kroesbergen, 1985). That is, the crushing test used to measure the strength of the disk applies a compressive force, **CF**, across the disk, which generates an indirect tensile stress, **T**, concentrated at the centre of the disk and causing it to crack down the middle (Figure **6- 3**). After wetting for 24 h the disks were air-dried at 20°C and later oven dried at 105°C. The oven-dried disks were then fractured using the indirect

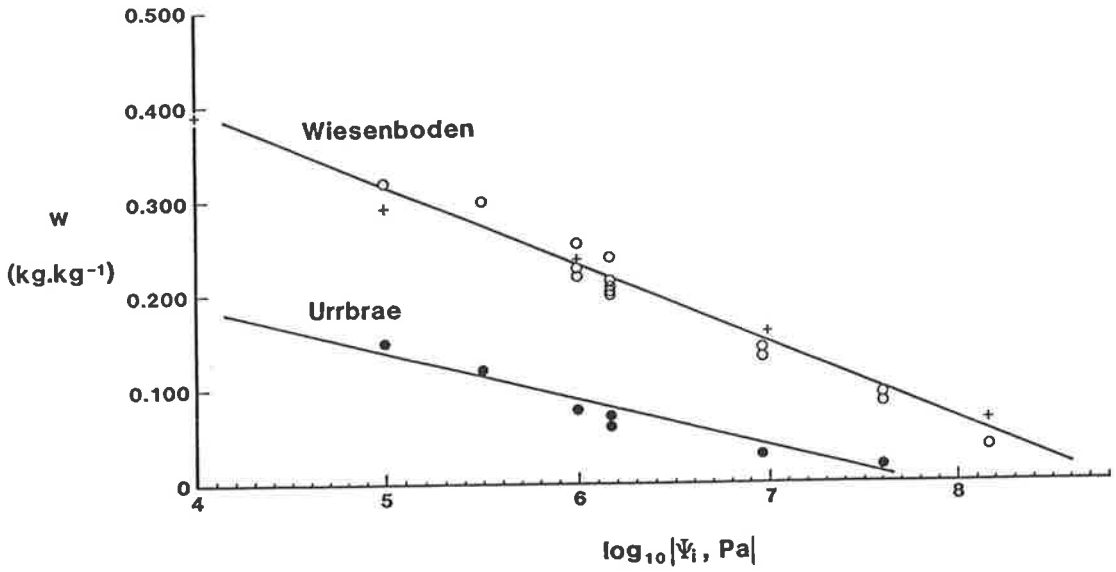

Figure 6-1. Desorption curves established for the Urrbrae soil and Wiesenboden. The circles for both soils were experimentally determined and the upright crosses for the Wiesenboden were interpolated from Panabokke and Quirk (1957).

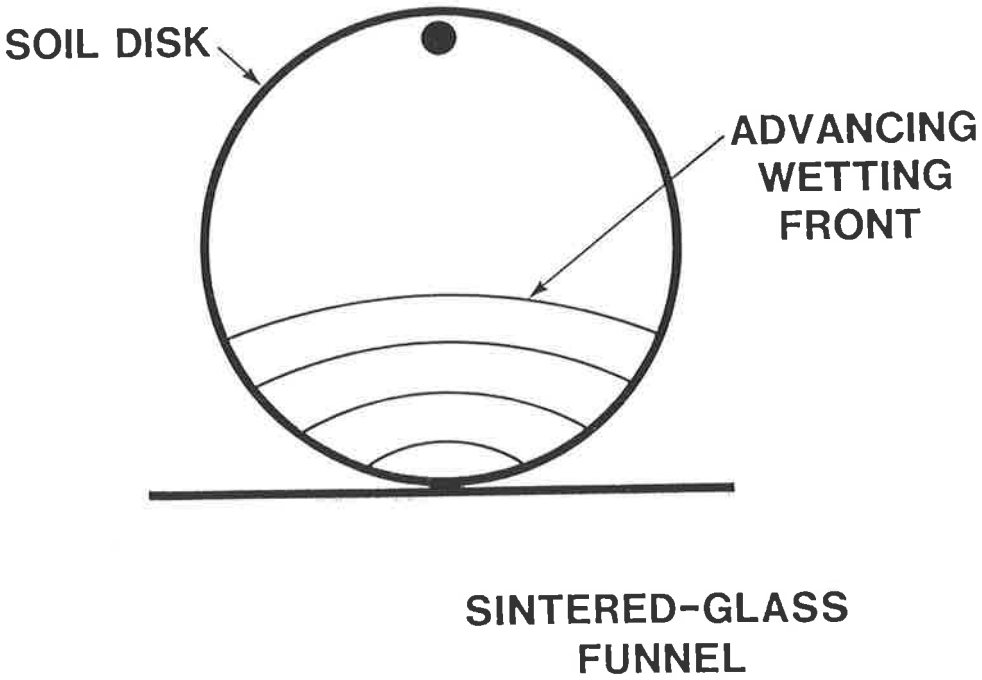

Figure 6-2. Soil disk being wetted on a sintered-glass funnel, showing the dot used to identify the direction of the wetting front across the disk.

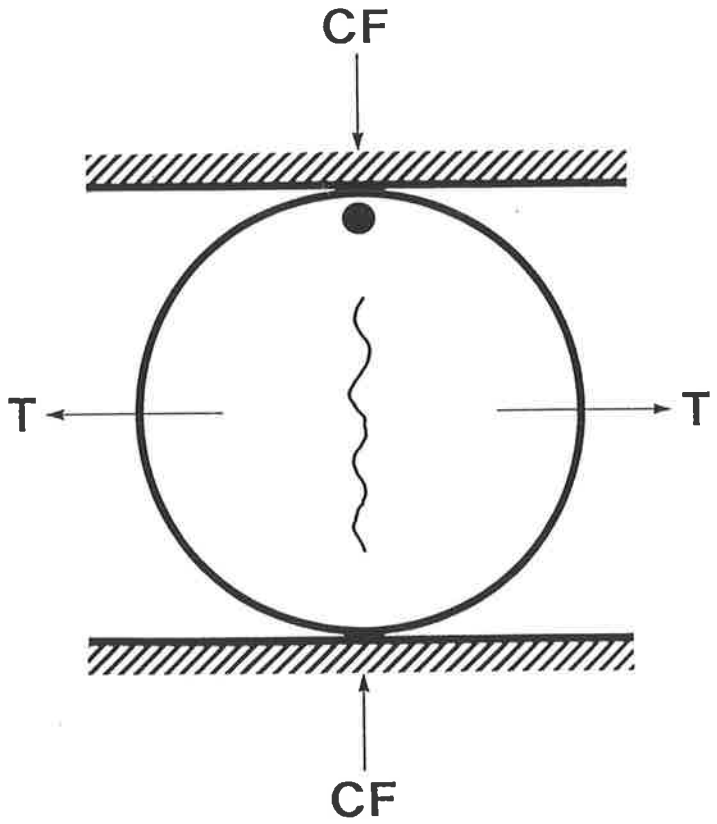

Figure 6-3. Soil disk cracking under the compressive force, **CF**, created in a loading frame. The diagram illustrates the (indirect) tensile forces, T, responsible for causing the disk to fracture.

tension test, outlined in **SECTION 5**. The tensile strength of each disk was determined using the compressive force, **FC**, required to crush the disk according to the relation after Kirkham, et al. (1959):

$$TS = \frac{2FC}{(\pi l d)} \qquad [6\text{-}1]$$

where **l** and **d** are the thickness and diameter, respectively, of the soil disk. The Mellowing Ratio, **MR**, (i.e. ratio of the mean compressive force of the wetted disks to that of the standard, non-wetted disks, after McKenzie and Dexter, 1985) was used as an indicator of the extent of aggregation that was generated by wetting.

Rapid wetting of soil was expected to create a highly variable internal microstructure relative to that of unwetted soil. To test this expectation on the moulded soil disks, the rugosity of the fracture surfaces that were created under tensile stress was determined as described in **SECTION 5** for the moulded soil disks. The dimensionless ratio of mean fracture surface rugosity, σ_R , for wetted disks to that of the standard, non-wetted disks, was calculated and referred to as the 'Relative Rugosity' (**RR**). The **RR**-values indicate the degree of structural change caused by wetting.

6.2.2 Results and Discussion

6.2.2.1 Influence of Initial Soil Water Potential on Wetting Rate

Wetting rates, **WR**, for the Urrbrae and the Wiesenboden are shown in Figures **6-4a** and **6-4b** respectively as a function of the initial soil water potential, Ψ_i, (natural logarithm of absolute values) prior to wetting. For comparison purposes, the wetting potential (i.e. the potential of the water to which the soil disks were exposed) was held constant at -10 hPa for all points in Figures **6-4a** and **6-4b**. The rapid increase in wetting rate at drier initial potentials is described by the regression equations:

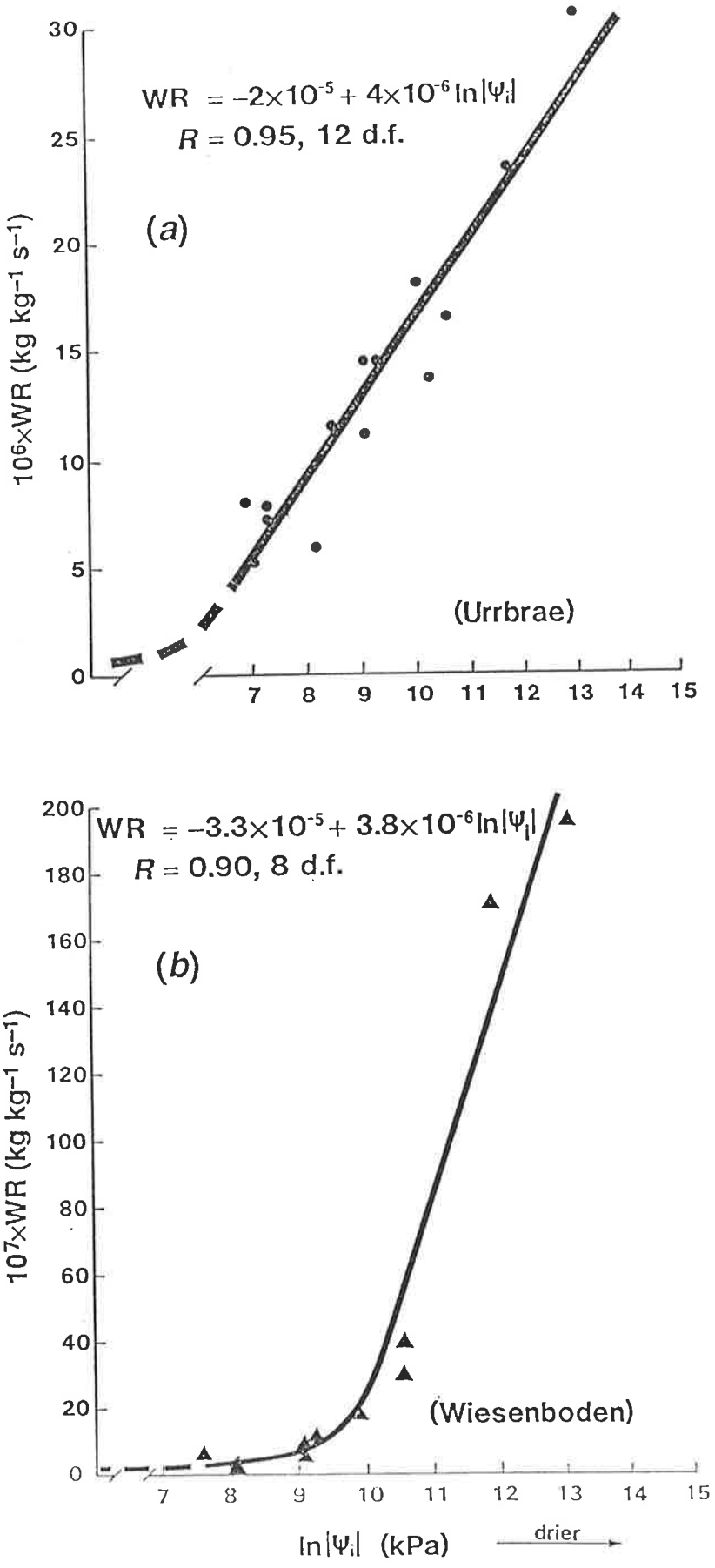

Figure 6-4. Effect of soil water potential prior to wetting, Ψ_i, on the wetting rate, **WR**, for (**a**) Urrbrae soil and (**b**) Wiesenboden.

$$WR = -2.0 \times 10^{-5} + 3.6 \times 10^{-6} \ln|\Psi_i| \quad , kg\,kgs^{-1} \quad (R=0.95, n=14) \quad [6-2]$$

and

$$WR = -3.3 \times 10^{-5} + 3.8 \times 10^{-6} \ln|\Psi_i| \quad , kg\,kgs^{-1} \quad (R=0.90, n=10) \quad [6-3]$$

for the Urrbrae and Wiesenboden respectively. Although the slopes of the equations **[6-2]** and **[6-3]** are similar, the Wiesenboden exhibited a wider range of wetting rates than the Urrbrae soil, and this was primarily due to its higher clay content and shrink/swell potential.

6.2.2.2 Influence of Wetting Rate on Mellowing of Soil

More extreme wetting rates than those shown in Figures **6-4a** and **6-4b** may be achieved for the study of soil mellowing by varying one or both of the initial and final soil water potentials. For the experiments reported here, the fastest rates were found by lowering the initial potential, Ψ_i, to -10^6 kPa (oven dry, 105°C) and by increasing the wetting potential, Ψ_m, to near zero hPa.

The Mellowing Ratio is shown in Figures **6-5a** and **6-5b** as functions of the wetting rate, and described by the regression equations, for the Urrbrae and Wiesenboden respectively:

$$MR = 1.26 - 2.36 \times 10^{4} WR \quad (R = 0.62, n=19) \quad [6-3]$$

and

$$MR = -0.63 - 0.27 \log_{10} WR \quad (R = 0.80, n=21) \quad [6-4]$$

In the case of the Wiesenboden, the wetting rates are reported on a logarithmic scale because the extremes ranged over several orders of magnitude. By contrast, the most extreme wetting rates for the Urrbrae soil fell within a narrower range, and this possibly accounts for the poorer fit of the **MR** versus **WR** relation for this soil.

A Mellowing Ratio, **MR** < 1.00 indicates that soil weakening has occurred during wetting. On the other hand, values of **MR** = 1.00 indicate that wetting has not

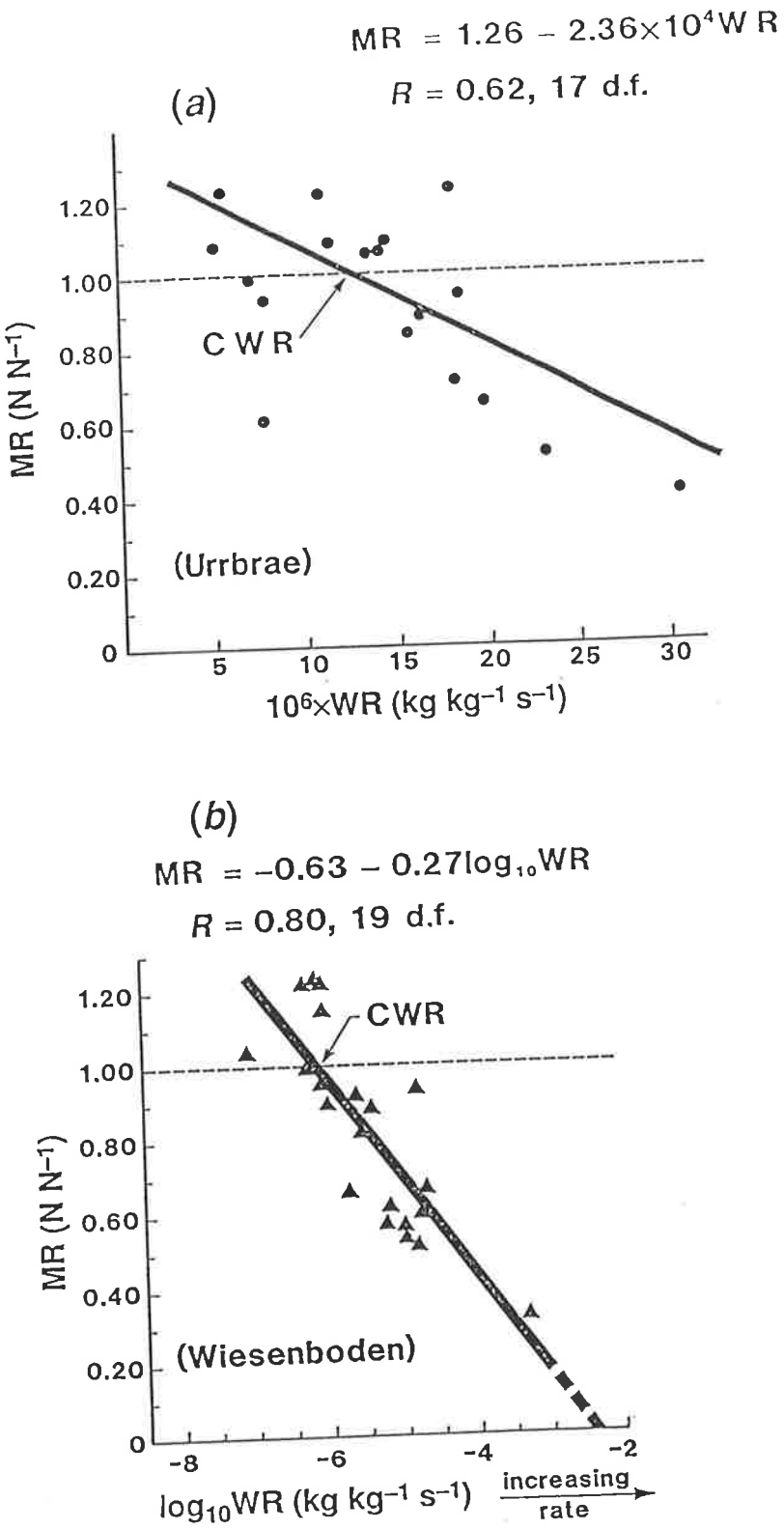

Figure 6-5. Effect of wetting rate, **WR**, on Mellowing Ratio, **MR**, for (**a**) Urrbrae soil and (**b**) Wiesenboden.

occurred rapidly enough for sufficient stress to induce cracks within the soil. Alternatively, values of **MR** > 1.00 could occur. **MR**s greater than 1.0 may result from wetting rates slow enough to allow cementing agents to dissolve, which subsequently re-precipitate upon drying to cause a net increase in soil tensile strength. Thixotropic hardening processes under these conditions may also be responsible. The Mellowing Ratio is shown in these figures to decrease when the wetting rates increase. The horizontal dotted line at **MR** = 1.00 in Figures **6- 5a** and **6- 5b** divides wetting rates that cause mellowing (below the dotted line) from wetting rates sufficiently slow to induce age hardening processes (above dotted line). The wetting rate necessary to induce mellowing (the **C**ritical **W**etting **R**ate, **CWR**) is approximated where the solid line intersects the dotted line at **MR** = 1.00. For the Urrbrae soil, the **CWR** for mellowing is 1.1 x 10^{-5} kg $kg^{-1}s^{-1}$ (Figure **6- 5a**) and for the Wiesenboden, the **CWR** for mellowing is 7.28 x10^{-7} $kgkg^{-1}s^{-1}$ (i.e. in Figure **6- 5b**, the value of $\log_{10}$**WR** = -6.14 ,). An extrapolation to higher wetting rates beyond the data implies that the wetting rate necessary to induce total slaking (i.e. **MR** = 0.00) is approximately 5.3 x10^{-5} $kgkg^{-1}s^{-1}$ for the Urrbrae soil (Figure **6- 5a**) and 4.24 x$10^{-3}$$kgkg^{-1}s^{-1}$ for the Wiesenboden (i.e. the value of $\log_{10}$ **WR** = -2.37, in Figure **6- 5b**) . The **CWR** for mellowing to take place is seen from Figures **6- 5a** and **6- 5b** to be nearly two orders of magnitude smaller for the Wiesenboden than for the Urrbrae soil. In addition, the minimum wetting rate necessary to induce total slaking and dispersion is two orders of magnitude greater for the Wiesenboden than for the Urrbrae soil.

These results have considerable significance for the generation and stability of soil structure under conditions where rainfall normally occurs at low intensities and yet occasionally occurs at extremely high intensities. The Wiesenboden apparently requires a smaller rate of water application (lower **CWR**) to induce mellowing, and would therefore be more likely than the Urrbrae soil to develop an aggregated structure under normal rainfall conditions. Furthermore, the Wiesenboden appears to require a much more intense application of water to cause total slaking (**MR** = 0),

and so it would be more likely than the Urrbrae soil to remain stable during a heavy rainfall event. This is consistent with the fact that the Wiesenboden usually has a stable granular surface structure in the field, whereas the Urrbrae soil, which is only 500 m away is often unstable and slakes to form a surface crust.

The effects of wetting rate on soil mellowing are influenced by the initial soil water content and potential, as well as the wetting potential, all of which interact to control swelling, air entrapment and even age hardening. As an example, some of these interactions are illustrated for the Urrbrae soil in Figure **6- 6**, which shows the Mellowing Ratio as a function of the soil water content (w_i) prior to re-wetting at different wetting potentials (Ψ_m). It can be seen that mellowing can occur even when the initial water content is as high as **w**=0.07, simply by wetting at a matric potential of 0 hPa. The same initial water content has coincidently been reported by (Stengel and Bourlet, 1987) to be associated with cracking during rapid wetting at 0 hPa (free water). At the same time, it can be seen that age hardening can occur during wetting, even if the initial water content is as dry as **w**=0.02, so long as the wetting potential and hence the wetting rate are low enough.

6.2.2.3 Changes in Microstructure of Wetted and Dried Soil

The effects of rapid wetting in the Urrbrae soil can be seen in Plate **6- 1** where sideways profiles of representative half-disks are shown (rapidly wetted at Ψ_m = -5 hPa water, on left-hand side; non wetted control on right-hand side). The disks had been wetted from bottom to top on sintered glass funnels, then dried and fractured using indirect tension. The white lines that pervade the matrix of the half-disk on the left-hand side are cracks that formed during the wetting process. The grey and black areas are the undisturbed soil. A striking visual difference in the vertical fracture surface relief can be seen between the two half-disks.

Plate **6- 2** illustrates fracture surfaces of two Wiesenboden disks placed side by side to compare the disruptive effects of rapid wetting (left-hand side) with the negligible effects of wetting the soil relatively slowly (right-hand side). The

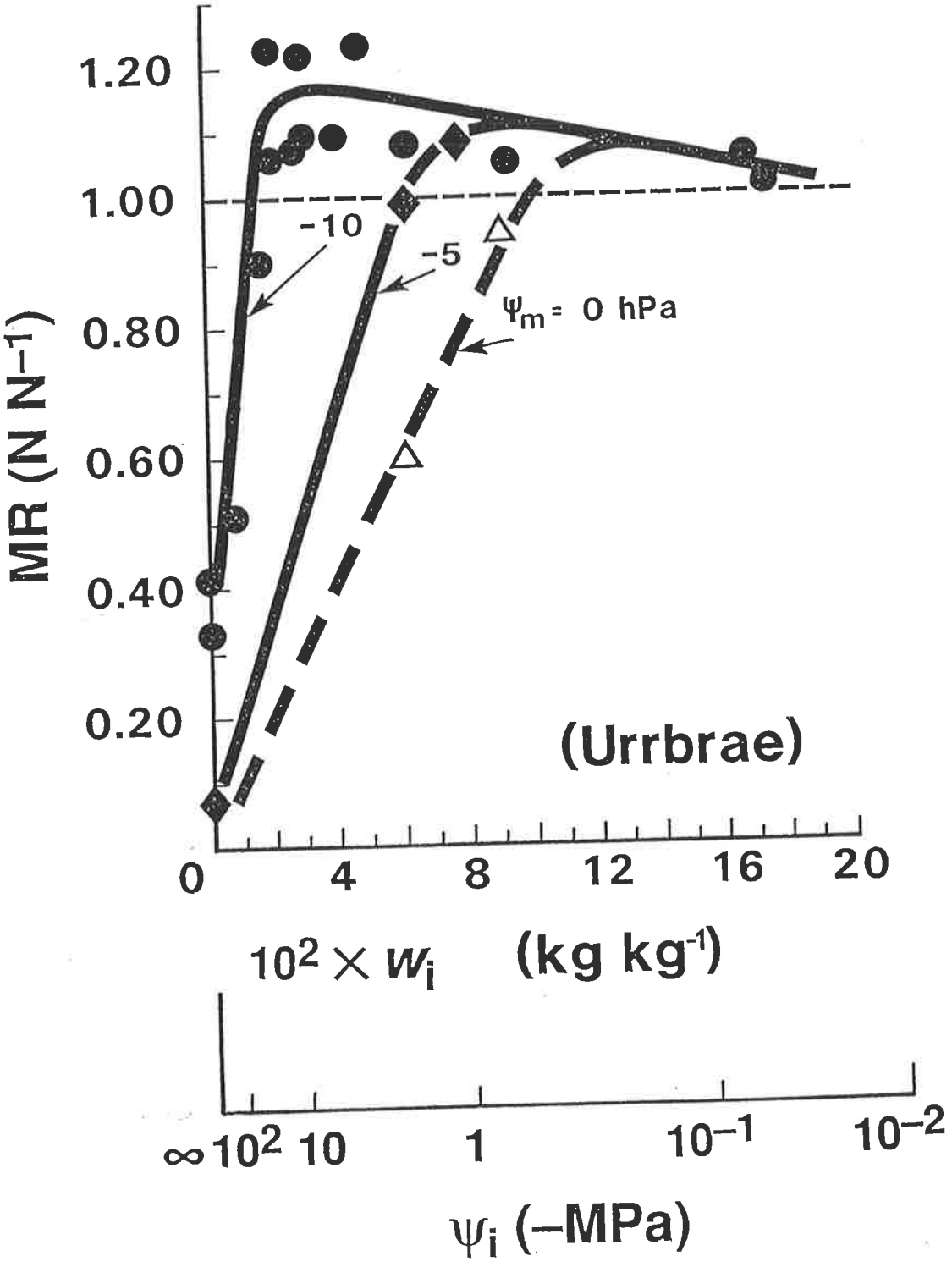

Figure 6-6. Mellowing Ratio, **MR**, as a function of the initial soil water content, w_i, and potential, Ψ_i, prior to wetting by sources of water at three different matric potentials, Ψ_m, for Urrbrae soil disks.

Plate 6-1: Fracture surface profiles of Urrbrae soil hemi-disks, illustrating the effects on the soil fabric due to rapid wetting (left) relative to a non-wetted control (right).

Plate 6-2: Fracture faces of rapidly wetted (left) and slowly wetted (right) Wiesenboden soil hemi-disks. Wetting fronts travelled from bottom to top of each face.

peculiar **V**-shaped pattern shown in the fabric of the disks that were wet rapidly may be associated with the ability of displaced air to escape from the disk faces. On the other hand, Gramberg (1966) has also found a similar **V**-shaped fracture surface in cores of rock, so the pattern could to some extent simply be associated with the method of fracture. No such pattern was found in the Urrbrae soil disks, which suggests that rapid wetting is at least partly responsible for the **V**-shaped pattern. This phenomenon was not analysed in detail.

The fracture surface rugosity (σ_R, mm) is plotted in Figures **6-7a** and **6-7b** as functions of the Mellowing Ratio, and is described by the regression equations for disks of Urrbrae and Wiesenboden, respectively:

$$\sigma_R = 0.38 \exp(-0.97\ MR) \qquad (R=0.88,\ n=25) \qquad [6-5]$$

and

$$\sigma_R = 0.183 \exp(-0.244\ MR) \qquad (R=0.48,\ n=26) \qquad [6-6]$$

A reduction in the tensile strength (i.e. **MR** < 1.00) due to rapid wetting of the soil is accompanied by a more rugose internal microstructure (i.e. higher values of σ_R) in both cases. The slope of the σ_R versus **MR** function for the Wiesenboden is considerably smaller than that for the Urrbrae soil, possibly due to the paucity of points corresponding to values of **MR** less than 0.50 in the Wiesenboden. If the magnitude of σ_R is equated with the extent of microcracking induced by wetting, then this result is not entirely surprising. While on the one hand the Wiesenboden has a greater tendency to mellow (i.e. lower **CWR**) than the Urrbrae soil, it also has greater potential to swell; hence plastic flow can accommodate the associated strain better than the Urrbrae soil, and thus better resist slaking. The same trend can be seen with the Relative Rugosities (**RR**) for the Urrbrae soil (Figure **6-8a**) and for the Wiesenboden (Figure **6-8b**), described by the respective regression equations:

$$RR = 3.12 \exp(-0.98\ MR) \qquad (R = 0.91,\ n=25) \qquad [6-7]$$

and

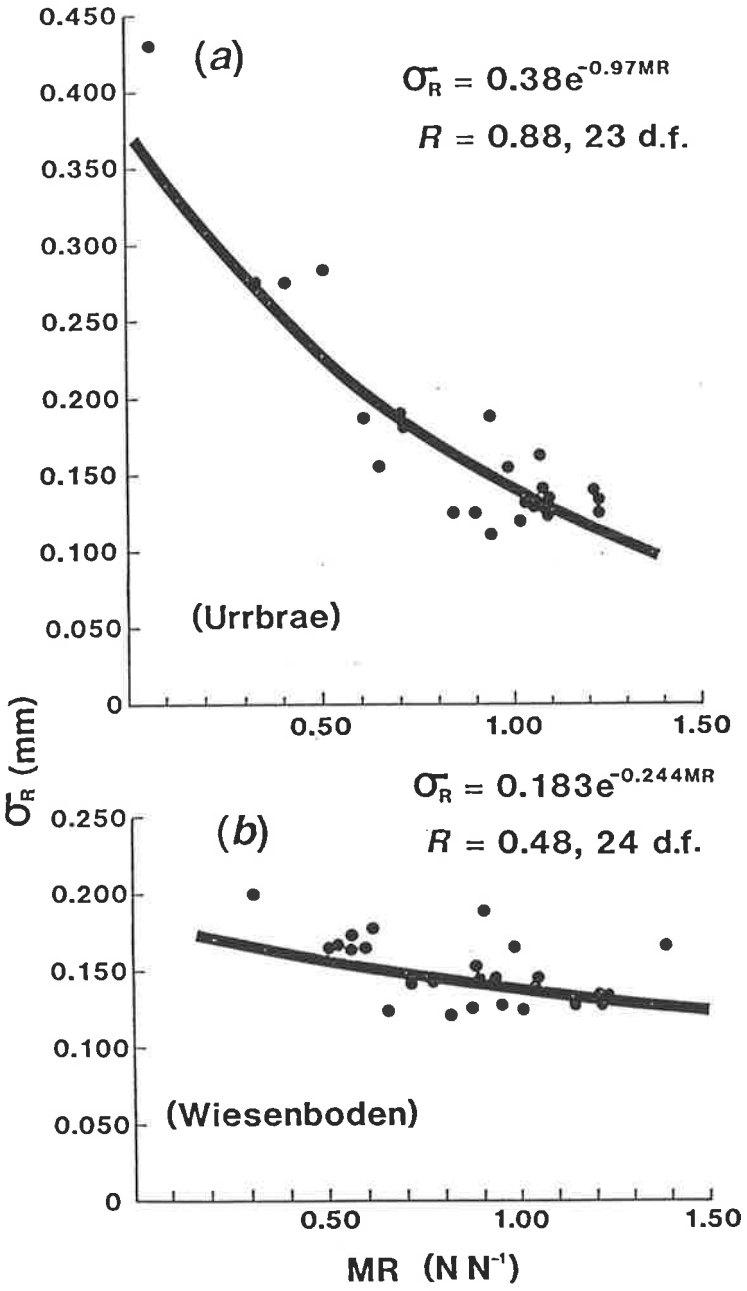

Figure 6-7. Mean fracture surface rugosity, σ_R, of soil disks as a function of their Mellowing Ratio, MR, for (a) Urrbrae soil and (b) Wiesenboden.

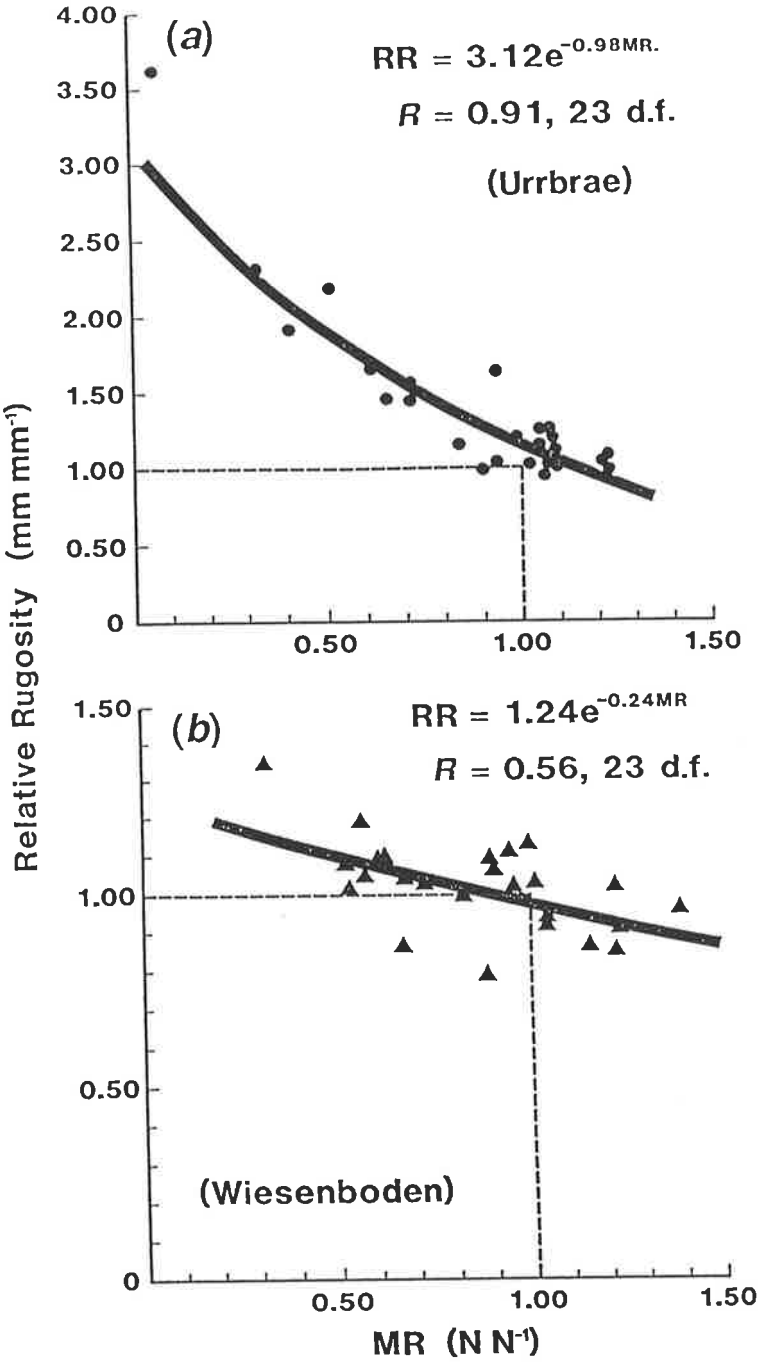

Figure 6-8. Relative rugosity, **RR**, as a function of Mellow Ratio, **MR**, for (**a**) Urrbrae soil disks, and (**b**) Wiesenboden disks.

$$RR = 1.24 \exp(-0.24\ MR) \qquad (R = 0.56,\ n=25) \qquad [6\text{-}8]$$

Values of RR that are dramatically larger than 1.00 indicate that the wetting process has induced substantial structure into the originally homogeneous soil disk. Very few values lie inside the zone boxed by the dotted lines in Figures 6-8a and 6-8b, indicating that structure generation almost always occurs whenever the tensile strength of the soil is reduced during rapid wetting.

6.2.3 Conclusions

Generating micro-cracks is a first step toward developing soil structure that is suitable for tillage in compacted and in puddled soils. Water under certain conditions can play a major role in generating these cracks, even in soils of relatively low clay content, as shown recently by Stengel (1988). The wetting rate seems to be critical. It is important, however, to know the extent to which moulded soils must be dried before the effects of rapid wetting can be utilized. The results of this study suggest two main conclusions regarding the role of water in ameliorating the condition of compacted and puddled soils.

First, the generation of soil structure during rapid wetting appears not to be restricted only to dry soils. A specific maximum matric potential may exist at which mellowing of a compacted soil can still be induced. As an example, for the Urrbrae soil (Figure 6-6) mellowing can occur in moulded soils even when the soil water content is as high as w=0.07 (-1 to -1.5 MPa matric potential). In a practical sense, it may be possible to manage the rate of wetting by measuring the soil matric potential as the soil dries and then by controlling the wetting potential or rate of application of applied water to achieve the extent of mellowing required to make tillage easier. Research is necessary to determine the limiting conditions under which these results can be applied in the field situation.

Secondly, the relief of soil fracture surfaces expresses quantitatively the effects of rapid wetting on the internal fabric of compacted soil. Visual and analytical

evidence from photographs and computer images shows that internal structure generation (i.e. **RR >** 1.0) occurs almost invariably whenever wetting is sufficiently rapid to reduce the tensile strength of the soil (i.e. **MR <** 1.0).

6.3 Air Entrapment versus Differential Swelling Experiments

6.3.1 Materials and Methods

A series of experiments was set up using two different wetting liquids and three different ambient air pressures. A non-polar liquid, cyclohexane (hexahydrobenzene) was used to prevent swelling, and de-ionized water (polar liquid) was used for maximum swelling. Ambient air pressures of 1000, 500 and 250 hPa were used to control the effects of entrapped air.

The same two soils (Urrbrae and Wiesenboden) which were milled and prepared for the study in **SECTION 6.2** were also used here. Each soil was mixed with sufficient deionized water to make a workable paste, as described in **SECTION 6.2** which were then allowed to dry for 24 hours at 20°C before oven drying for 24 hours at 105°C. Each oven dry disk was marked with a dot at the edge of one of its two faces (Dexter, 1983). The dot determined, arbitrarily, the axis across which the disk would subsequently be wetted (Figure **6- 2**) and later crushed after drying to determine its tensile strength. Groups of about 10 disks were wetted simultaneously on coarse sintered-glass funnels (porosity #2) using either de-ionized water at a potential of -10.0 ± 0.5 hPa, or using cyclohexane (density = 780 kg m^{-3} at 20°C) at a potential of -7.0 ± 0.5 hPa. The slightly smaller suction used with cyclohexane was necessary to prevent the bubbling pressure from being exceeded in the porosity #2 funnels. Prior to wetting of the disks, the funnels were de-aired by immersing them in either de-aired water or de-aired cyclohexane under reduced pressure. De-airing the funnels prior to the wetting experiments was done to prevent inconsistent wetting behaviour. The mass taken up by the disks, of either water or cyclohexane was measured for 24 hours, and the wetting rates ($kgkg^{-1}s^{-1}$) were estimated as described in **SECTION 6.2**, using the slope of the liquid-uptake versus time curves

at the point when the wetting front reached half way up the disks as they sat on the sintered-glass funnels. When wetting was completed, the disks were air dried for 24 hours at 20°C, then oven dried for 24 hours at 105°C. The tensile strength of each disk was determined using the indirect tension test in which the compressive force required to crush each disk was measured (Frydman, 1964). The Mellowing Ratio, **MR**, as defined by McKenzie and Dexter (1985) was used to indicate the amount of structure generation caused by the treatments. Mellowing ratios less than unity indicate that soil weakening occurred during wetting.

6.3.2 Results and Discussion

For the experiments conducted in vacuum desiccators, it did not seem to matter whether the ambient air pressure was dropped to 500 hPa or to 250 hPa.. The tensile strength of the disks was not significantly different between the two reduced ambient air pressure treatments, so their results were pooled. The mean tensile strength (actually expressed as compressive forces, **CF**, in N) for the 500 hPa and 250 hPa pressures formed an estimate of the overall effect of reduced ambient air pressure during wetting. Presented in Tables **6- 3a** and **6- 3b**, respectively, for the Urrbrae and Wiesenboden soils, are the analyses of variance for the mean compressive forces resulting from different ambient air pressures.

The various combinations of polar, non-polar fluids, and levels of ambient air pressure enabled the effects of rapid swelling and air entrapment to be quantified separately. Furthermore, a simple independent check on the unwetted control treatment was possible within the experiment, because the treatment of wetting with cyclohexane (non-polar liquid) under conditions of reduced air pressure, should have no effect on the soil structure. The results of the cyclohexane/reduced air pressure treatment would therefore be expected to be the same as those of the unwetted control. As verified in Tables **6- 3a** and **6- 3b**, the mean compressive forces required to crush disks wetted with cyclohexane at ambient air pressures of 500 and 250 hPa are the same as that for the oven dry, unwetted control treatment.

TABLE **6-3a**: ANOVA Table for Urrbrae soil

Treatment	Mean CF* (N)	df	Treatment minus control	Pooled s.e. of difference	Pooled df	2-tail t-test	P-value
Oven dry control (not wetted)	119.94	9	----	----	--	----	------
Cyclohexane 500+250 hPa (no swelling, no entrapped air)	121.06	18	1.12	8.67	28	0.13	P > 0.50
Cyclohexane,1000 hPa (only entrapped air)	116.23	9	-3.71	12.44	18	-0.30	P > 0.50
Water,500+250 hPa (only swelling)	106.92	18	-13.02	8.22	28	-1.58	0.10< P< 0.20
Water,1000 hPa (both swelling and entrapped air)	78.14	9	-41.80	12.91	18	-3.24	0.001< P< 0.01

Table **6-3b** ANOVA Table for Wiesenboden.

Treatment	Mean CF* (N)	df	Treatment minus control	Pooled s.e. of difference	Pooled df	2-tail t-test	P-value
Oven dry control (not wetted)	394.16	9	----	----	--	----	------
Cyclohexane 500+250 hPa (no swelling, no entrapped air)	400.30	18	6.14	18.43	28	0.33	P > 0.50
Cyclohexane,1000 hPa (only entrapped air)	456.89	9	62.73	38.84	18	1.62	0.10< P< 0.20
Water,500+250 hPa (only swelling)	234.52	18	-159.64	14.57	28	10.96	P< 0.001
Water,1000 hPa (both swelling and entrapped air)	209.49	9	-184.67	25.64	18	7.20	P< 0.001

* compressive force, **CF**, (N) for soil wetted with polar and non-polar liquids at atmospheric pressure and at reduced ambient air pressures.

The cyclohexane results for wetting at 1000 hPa air pressure (Tables **6-3a** and **6-3b**) suggest that air entrapment, on its own, does not contribute to structure generation. At the same time, however, this result should be weighed against the fact that cyclohexane does not reduce the internal cohesion of the soil in the manner that even slowly-introduced water can (for example, by dissolving cementing substances, and by slow, uniform swelling). The disks were still hard after wetting with cyclohexane, (cf. Yoder, 1936) so that wetting at high pressures without some amount of swelling, would make the cyclohexane-wet disks less susceptible to the effects of air pressure than the disks wet with water would be.

The results for wetting Urrbrae soil with water under vacuum (Table **6-3a**) indicate that differential swelling, on its own, also does not produce significant structure in the low clay content soil. Only in the Wiesenboden (Table **6-3b**), which has a much higher clay content, does differential swelling appear to play a role. Wetting the Wiesenboden with water under reduced-pressure conditions resulted in approximately a 41% reduction in the compressive force needed to crush the subsequently-dried disks. These data point out that although air entrapment, alone, seems not to be able to generate soil structure, no such general statement can be made about the role of differential swelling. The effects of swelling depend on other soil properties, for example the clay content, and probably the organic matter content

The results of wetting with water using an ambient air pressure of 1000 hPa (i.e. atmospheric pressure),however, indicate that when operating in combination, both air entrapment and differential swelling act together to generate structure in the soil disks. For the Urrbrae soil (Table **6-3a**) the combined effects of air entrapment and differential swelling resulted in approximately a 35% reduction in the compressive force required to crush the soil disks. For the Wiesenboden (Table **6-3b**) a 47% reduction occurred.

Some understanding of why such a synergistic effect exists between air entrapment and differential swelling may lie in how the wetting rate is influenced by the removal of air from the soil. One might normally expect the removal of air to

improve the permeability of the soil (cf. Smith & Browning, 1946). It was noted, however, by Christiansen (1944) that a reduction, rather than an increase, in permeability can occur with reduced ambient air pressures. It was observed in this study as well, without exception, that a reduction in the wetting rates occurred at progressively lower ambient air pressures (Table 6-4a). The fastest wetting rates occurred at 1000 hPa. It is apparent in Christiansen's study, though, that the reduced permeability was associated with structural breakdown of aggregates caused by the evacuation process. In the present study, by contrast, the greatest structural changes occurred in the disks that were wetted at an air pressure of 1000 hPa, not in those wetted under reduced air pressures. In Christiansen's study, which used soil aggregates, slaking may very well have occurred during the evacuation process, possibly because air could not escape fast enough. In the present case, however, where moulded soils were used, it is possible that the air originally present in the dry soil was able to escape during evacuation, so that wetting could have proceeded at rates controlled only by swelling processes. At 1000 hPa air pressure, on the other hand, the induction of cracks by the build-up of explosive air pressures during wetting of moulded soil could expose new soil surfaces to water; the new exposed surfaces may have enhanced the differential swelling process more so than would have occurred under reduced air pressures. A higher wetting rate might therefore be expected to occur when using water as the wetting liquid at an air pressure of 1000 hPa. Also it is likely that water can move with less resistance (i.e. the hydraulic conductivity may be higher) toward the wetting front if micro-cracks, as shown in Plate 6-1, have been produced between the point of wetting and the wetting front. The above explanations, although speculative, seem reasonable inasmuch as it was already demonstrated in **SECTION 6.2** that higher wetting rates are consistent with greater structure generation (cf. Figures 6-5a & 6-5b). The decreasing mellowing ratios which generally occur with increasing atmospheric pressures (Table 6-4a) also lend some support to the idea. Further research is necessary, however, to reconcile the fact that the wetting rates using cyclohexane followed the same trend

TABLE 6-4a

Ambient Air pressure (hPa)	Urrbrae soil Wetting Rate ($kgkg^{-1}s^{-1}$)	Urrbrae soil MR$ (NN^{-1})	Wiesenboden Wetting Rate ($kgkg^{-1}s^{-1}$)	Wiesenboden MR$ (NN^{-1})
1000	1.98×10^{-5}	0.66**	1.06×10^{-5}	0.53**
500	1.85×10^{-5}	0.94 ns	0.65×10^{-5}	0.62**
250	1.58×10^{-5}	0.84 ns	0.59×10^{-5}	0.57**

Table 6-4a. Wetting rates (using water) and mellowing Ratios, MR, resulting from different ambient air pressures prior to wetting.

TABLE 6-4b

Ambient Air pressure (hPa)	Urrbrae soil Wetting Rate ($kgkg^{-1}s^{-1}$)	Urrbrae soil MR$ (NN^{-1})	Wiesenboden Wetting Rate ($kgkg^{-1}s^{-1}$)	Wiesenboden MR$ (NN^{-1})
1000	1.57×10^{-5}	0.97 ns	1.72×10^{-5}	1.16 ns
500	1.38×10^{-5}	1.07 ns	1.52×10^{-5}	1.00 ns
250	1.15×10^{-5}	0.95 ns	0.95×10^{-5}	1.03 ns

$ Values of MR marked with the superscript ** are significantly different from 1.00 at P=0.05; Values of MR marked with the superscript ns are not significantly different from 1.00 at P=0.05.

Table 6-4b. Wetting rates (using cyclohexane) and mellowing Ratios, MR, resulting from different ambient air pressures prior to wetting.

with reduced atmospheric pressures without having any effect on the tensile strength of the subsequently dried soil (Table 6-4b).

6.3.3 Conclusions

It seems that the forces of air-entrapment, on their own during wetting, do not generate sufficient stresses to induce mellowing. The forces created by differential swelling, alone during wetting, also have limited ability to induce mellowing. The degree of mellowing due to swelling appears to be related to the clay content and possibly the organic matter content, as illustrated by the fact that only the Wiesenboden (high clay and organic carbon contents) experienced mellowing when wetted under vacuum. Only two soils were used in this study, so it may be only circumstantial that the Wiesenboden soil, which mellowed when wetted with water under vacuum, also had higher clay and organic matter contents than the Urrbrae soil. Future research should include a wider range of soils and address the roles of clay and organic matter in resisting the stresses generated by air entrapment and differential swelling. The most significant result of this study has been the ability to quantitatively demonstrate, in terms of tensile strength, the separate and synergistic roles of air entrapment and different swelling in the mellowing process, which have previously only been hinted at in the literature.

SECTION 7. FRACTURE SURFACE RUGOSITY USING NON-CONTACT LASER SCANNING

7.1 Introduction

The method of fracture surface rugosity as used in **SECTIONs 3** through **6** of this thesis is simple in theory, yet its measurement was found to be rather tedious and time consuming. The impregnation and hardening of samples required 24 hours. The sectioning procedure was relatively messy because it involved a kerosene-lubricated diamond saw, and the kerosene had to be wiped off and the samples allowed to dry afterward. The scanning procedure and computer programming for the calculation of σ_R-values was also time-consuming, requiring approximately ten minutes per sample, and there were thousands of samples involved. Furthermore, the measurement relied on the assumption that the soil features being bisected are structurally isotropic, so that the single transect made on each sample could be considered to be representative of the surrounding soil. This was reasonable for the soil clods and disks used in the studies of this thesis, but for structurally anisotropic soil surfaces, a technique is needed which can provide rapid, three dimensional information, with the minimum of labour and time. For these reasons, a potentially simpler and more versatile method was investigated for use in measuring the fracture surface rugosity.

In recent years, laser technology has become much more sophisticated and available for general research purposes. Measurement of the surface topography of soils at a scale of centimetres, for example, is now quite common in tillage and erosion studies in the U.S.A. and Europe (eg. Römkens, et al., 1986; Caussignac and Morel, 1987; Bertruzzi and Stengel, 1988, and Römkens, et al., 1988). In Australia, (at the C.S.I.R.O., Division of Environmental Mechanics, Canberra) an optical noncontact laser system has been used recently by Huang, et al. (1988), for measuring the soil surface topography along parallel transects across an entire three-dimensional surface. The resolution of Huang et al's laser beam and detecting

system (0.1 mm) is practically the same as that obtained by the computer-scanning procedure described in **SECTION 3**.

The C.S.I.R.O. laser-scanner was made available in September 1987 for measuring fracture surface elevations in the following study designed (1) to test the accuracy of the original procedure outlined in **SECTION 3**, and (2) to extend the method of fracture surface rugosity from a two-dimensional analysis to a three-dimensional analysis.

7.2 Multiple Transect (MT) Method

The original procedure outlined in **SECTION** 3 for measuring soil fracture surface rugosity using a single transect-profile will be referred to in this **SECTION** as the Single Transect (**ST**) method. The laser scanning method, which measures topography in three dimensions by using multiple, parallel two dimensional transects will be referred to as the Multiple Transect (**MT**) method.

An optical noncontact laser system (Huang et al., 1988) is used to repeatedly measure the soil surface topography along parallel transects of the entire soil fracture surface. In this study, a 1 mW HeNe laser functions as the light source, and a 35 mm SLR camera, fitted with a photodiode array is used as the light detector (Figure **7-1**). The laser beam is directed normally onto the soil surface and the camera's lens system focuses the image of the interception point (centre reference, CR) onto a photodiode array. Movement of the image on the array is thus a function of the fracture surface topography.

The range of elevation, R, possible with the system is calculated as:

$$R = \frac{(1 + x^2)^{1/2} - 1}{xy} \qquad [7-1]$$

where $x = S\cos\alpha\left(\frac{L - F\sin\alpha}{LF\sin\alpha}\right)$

$$y = \left(\frac{\cos\alpha\ \sin\alpha}{2L}\right)$$

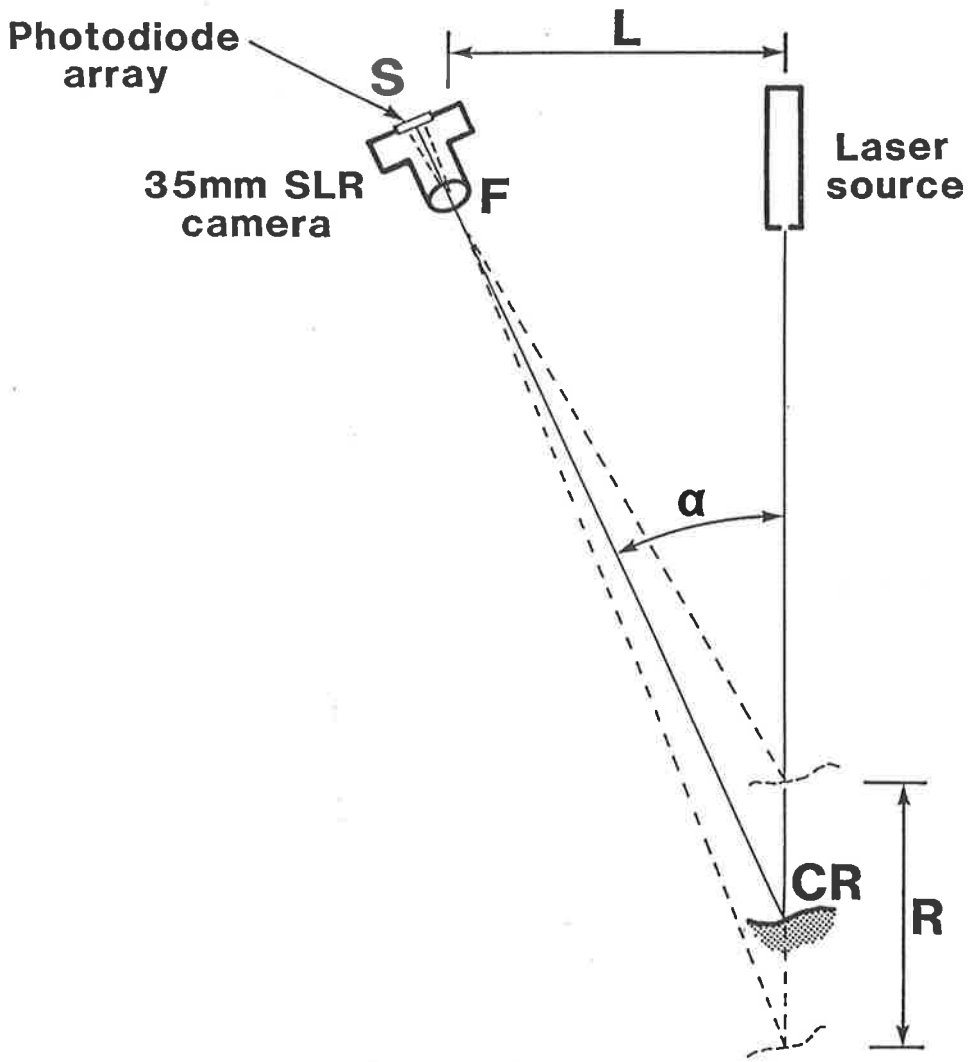

Figure 7-1. Laser scanner for fracture surface analysis (symbols are in text)

S = length of sensing region on diode array
α = angle between laser beam and the optical axis of the lens
L = distance between lens and laser source
F = focal length of lens

The soil fracture face is placed directly, without pretreatment, onto a traversing stage (Micro-Controle Electronique, Model UT100-125PP) which for this work moved at 4 mms^{-1} in increments of 0.1 mm. The sample is passed under the laser beam as described above and after each complete transect of the soil surface, the stage shifts the sample sideways by 0.1 mm and returns in the other direction to produce another transect exactly parallel to the first one. The scanning continues until the entire fracture surface has been scanned. In this way, a large number of fracture surface profiles (instead of just one) may be obtained very quickly on each sample, and with a minimum of effort.

7.3 Experimental Comparison of ST- and MT-Methods

The **MT**-method has a considerable advantage over the **ST**-method because it requires no sample preparation and the scanning procedure can be completed in a fraction of the time. Before considering the replacement of the **ST**-method with the **MT**-method, however, it was considered important to determine the extent to which these two techniques produced the same results. To this end, a series of experiments was conducted to measure σ_R using both techniques on the same soil samples.

7.3.1 Materials and Methods

Three different agricultural topsoils (see Table **7- 1**) were moulded at water contents at or below their lower plastic limits into disk shapes 25 mm in diameter and 10 mm thick. For the Wiesenboden, 16 disks were air dried, then rapidly wetted on sintered glass plates held at a suction of zero hPa. For the Urrbrae and Portneuf soils, 10 disks were air dried, then oven dried (105°C for 24 hours) as control samples, while other groups of 10 disks sealed air-tight and aged at constant water content and temperature (20°C) for seven and fourteen days. After ageing, all

Table 7- 1

Soil (Location)	Water content at moulding ($kgkg^{-1}$)	Lower Plastic Limit ($kgkg^{-1}$)	Clay Content (< 2 μm)
Wiesenboden (South Australia)	0.25	0.30	38%
Urrbrae (South Australia)	0.15	0.20	17%
Portneuf (Idaho, U.S.A.)	0.15	0.21	25%

Table **7-1**. Water contents at moulding, **w**, lower plastic limits, **PL**, and clay contents (< 2 μm) for the three soils used in **SECTION 7.**

samples were air dried, and oven dried (105°C, 24 hours), then fractured into halves using the indirect tension test (described in previous **SECTION**s of this thesis), from which tensile strengths were determined. In addition, maximum penetration resistance at 5mm penetration was measured on the disks of Urrbrae and Portneuf soils using the penetrometer described in previous **SECTION**s. The **ST-** method was used to measure σ_R on one half of each disk, while the **MT-** method was used on the other half of the disk (Figure **7- 2**). While only a single transect was made on each hemi-disk using the **ST-** method, there were from 50 to 80 transects made using the **MT-** method. Calculation of σ_R was done using a running mean, **M**, of length 4mm, as described previously in **SECTION 3**.

7.3.2 Results and Discussion

Data for this experiment are listed in Appendix **5**, Table **A5-1**. It was found that rapid wetting of the Wiesenboden disks resulted in a significant reduction in mean bulk density (non-wetted =1680 ± 10 kgm^{-3}; wetted =1510 ± 10 kgm^{-3}) as well as in mean tensile strength (non-wetted =903.2 ± 29.5 kPa; wetted =178.4 ± 7.1 kPa). The mellowing ratio, **MR**, for this rapid wetting experiment is:

$$MR = \frac{178.4}{903.2} = 0.20 \qquad [7-2]$$

As indicated in **SECTION 6** of this thesis and in Dexter (1983), the very low **MR-** value indicates that significant disruption of the soil matrix has resulted from the passage of a wetting front through the soil.

Rapid wetting of the Wiesenboden also caused a significant increase in the mean values of fracture surface rugosity, σ_R, using both the **ST-**method and the **MT-**method (Table **7- 2a**). The increase in σ_R caused by wetting is consistent with the results of **SECTION 6** which indicate that internal microcracking is almost always detectable whenever the wetting rate is sufficiently high to reduce the tensile strength of the soil.

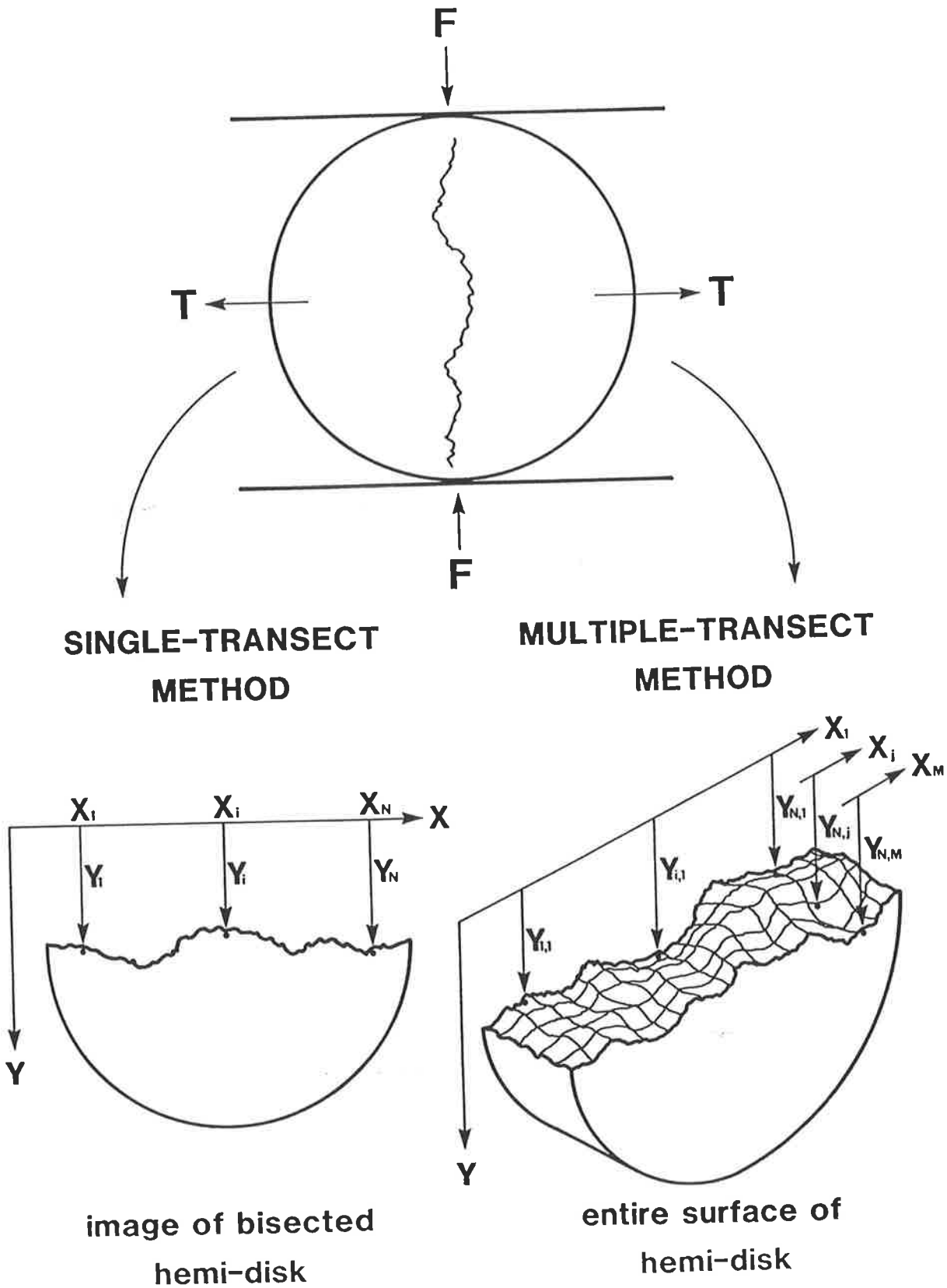

Figure 7-2. Fracture under indirect tension, T, of soil disk (into halves) by applying compressive force, F, between parallel plates. Image of bisected hemi-disk is shown on left (for ST-method); entire surface of corresponding hemi-disk is shown on right (for MT-method).

Table **7- 2a**

Soil	Wetting Treatment	Mean Rugosity (mm) ST- Method σ_R (± s.e.)	n	MT- Method σ_R (± s.e.)	n	
Wiesen-	Not Wetted	0.144 (±0.008)	16	0.129 (±0.006)	16	**
boden	Rapidly Wetted	0.200 (±0.012)	15	0.185 (±0.006)	16	**

Table **7- 2b**

Soil	Ageing Time	Mean Rugosity (mm) ST- Method σ_R (± s.e.)	n	MT- Method σ_R (± s.e.)	n	
Urrbrae	Aged 0 days	0.123 (± 0.008)	7	0.114 (±0.006)	8	**
	7	0.113 (± 0.010)	10	0.105 (±0.006)	10	**
	14	0.116 (± 0.009)	9	0.098 (±0.006)	10	**
Portneuf	0	0.125 (± 0.010)	10	0.108 (± 0.002)	10	**
	7	0.129 (± 0.008)	9	0.109 (± 0.004)	10	**
	14	0.134 (± 0.006)	9	0.107 (± 0.004)	10	**

** The value of **n** represents the number of soil disks, but with the **MT**-method, there were between 50 and 80 transects on each disk, whereas there was only 1 transect per disk with the **ST**-method.

Table **7-2.** Mean fracture surface rugosity, σ_R, from the single transect (**ST**) method, and the multiple transect (**MT**) method for (**a**) the not-wetted and rapidly wetted Wiesenboden, and (**b**) the Urrbrae and Portneuf soils at different ageing times.

It was proposed in **SECTION 3** that the rugosity of a fractured soil surface, σ_R, is directly related to the spacing between the weakest flaws in the soil. To understand the relation between σ_R and the distance between weakest flaws in the present **SECTION**, emphasis should be placed on the **magnitude** of the weakest flaws (i.e. the dispersion of flaw strengths). If the average tensile strength of the soil reflects the average strengths of the weakest flaws, then the weakest flaws in the control disks are approximately five times stronger than those of the wetted soil (i.e. $\frac{1}{MR} = 5.0$). In the control soil, which is relatively homogeneous, the weakest flaws (though much stronger than for the wetted soil disks) are probably distributed according to the spacing between soil mineral particles. Hence the fracture surfaces for the control disks are considerably smoother than for the wetted disks, whose weakest flaws consist of large cracks (very weak flaws) generated during rapid wetting. In cases where significant differences in dispersion of flaw strengths exist, it is therefore important to couple the measurement of σ_R with measurements of tensile strength.

The age hardening experiments (particularly in the Portneuf soil) caused no significant changes (at P=0.10) in the fracture surface rugosity (Table **7- 2b)** , although the trend in the Urrbrae soil (with both **ST-** and **MT-**methods) is toward smoother fracture surfaces after ageing. If the explanation given for the changes in σ_R in the rapid wetting experiment is valid, then the σ_R-results from the age hardening experiments need to be considered in light of the tensile strength data (Table **7- 3a)** . Ageing caused the tensile strength (and penetrometer resistance, Table **7- 3b)** of both soils (particularly the Urrbrae soil) to increase, and this has also been found to occur in other studies (eg Utomo and Dexter, 1981a; Kemper, et al, 1987; Dexter et al, 1988). The changes in strength, however, are relatively small (in comparison to the difference between rapidly wet and non-wetted soil) and the mechanism of strength-change is totally different. The changes in strength due to age hardening were mainly thixotropic in this experiment (constant water content, constant temperature; Mitchell, 1976) and therefore caused by spontaneous re-arrangement of particles into

Table 7-3a

Soil	Time (day)	Mean ρ_b ($kg\,m^{-3}$) (± s.e.)	Mean Tensile Strength (dry; kPa)	Mean w (aged) ($kg\,kg^{-1}$)	Samples (n)
Urrbrae	0	1670 (±2)	244.5 (±22.6)	0.146 (±0.001)	8
	7	1710 (±10)	311.1 (±15.0)	0.147 (±0.001)	10
	14	1740 (±10)	365.4 (±13.0)	0.150 (±0.001)	10
Portneuf	0	1600 (±1)	224.3 (±17.9)	0.153 (±0.002)	10
	7	1610 (±10)	281.2 (±17.4)	0.142 (±0.002)	9
	14	1580 (±10)	273.5 (±19.5)	0.144 (±0.001)	10

Table 7-3b

Soil	Time (day)	Mean Q_p (kPa) (± s.e.)	Mean Water Content ($kg\,kg^{-1}$) (± s.e.)	Samples (n)
Urrbrae	0	2450 (±227)	0.144 (±0.0004)	5
	7	3191 (±70)	0.142 (±0.0002)	5
	14	2605 (±301)	0.144 (±0.001)	5
Portneuf	0	4363 (±151)	0.146 (±0.002)	5
	7	6162 (±428)	0.139 (±0.001)	5
	14	5945 (±500)	0.142 (±0.001)	5

Table 7-3. (a) Mean values of bulk density, tensile strength and gravimetric water content for the Urrbrae and Portneuf soil disks at different ageing times. (b) Mean values of penetrometer resistance and gravimetric water content for the Urrbrae and Portneuf soil disks at different ageing times.

positions of lower free energy after moulding. It has been suggested by Emerson (1977) that the process of re-arrangement of particles from the wet moulded state may involve syneresis, a phenomenon which leaves tiny pores between flocculated clay particles. So while the overall strength of the soil is increased by age hardening, the introduction of tiny pores in the soil allows for the short-circuiting of the fracture pathway in tensile failure. This results in smoother fracture surfaces, and may be similar to the smoothing-effect of calcium on soil fracture surfaces outlined in **SECTION 4.**

On average, the **MT-** method produced slightly lower values of σ_R than the **ST-** method (mean difference = 0.016 mm). Furthermore, due to the very high number of fracture surface profiles generated with the **MT-** method on each hemi-disk, the estimates of σ_R for each treatment were generally less variable than with the **ST-** method (lower standard errors, s.e., for results of **MT-** method in Table **7- 2a** and **7- 2b**). Despite the slight overall mean difference in σ_R between the two methods, the individual mean values of σ_R from the two methods correlate reasonably well on a disk-by-disk basis as shown in (Figure **7- 3**). The small difference in overall mean values of σ_R from the **ST-** method may be simply an artefact of the sample preparation, wherein the fracture surface may have been altered slightly by disturbance caused during the pouring and hardening of the Araldite epoxy around the soil.

7.3.3 Conclusions from Comparison of ST- and MT-Methods

In addition to comparing the two methods of measuring fracture surface rugosity, the experiments have revealed an important relation between σ_R and the distance between weakest flaws in the soil. The magnitude of the weakest flaw strengths (estimated by the tensile strength and penetrometer resistance of the soil) appears to exert considerable control over the fracture pathway, and so it is concluded that measurements of σ_R should always be accompanied by measurements of soil strength.

The results of the comparative study outlined in this **SECTION** indicate that the new laser technique (**MT-**method) provides very similar results of fracture surface

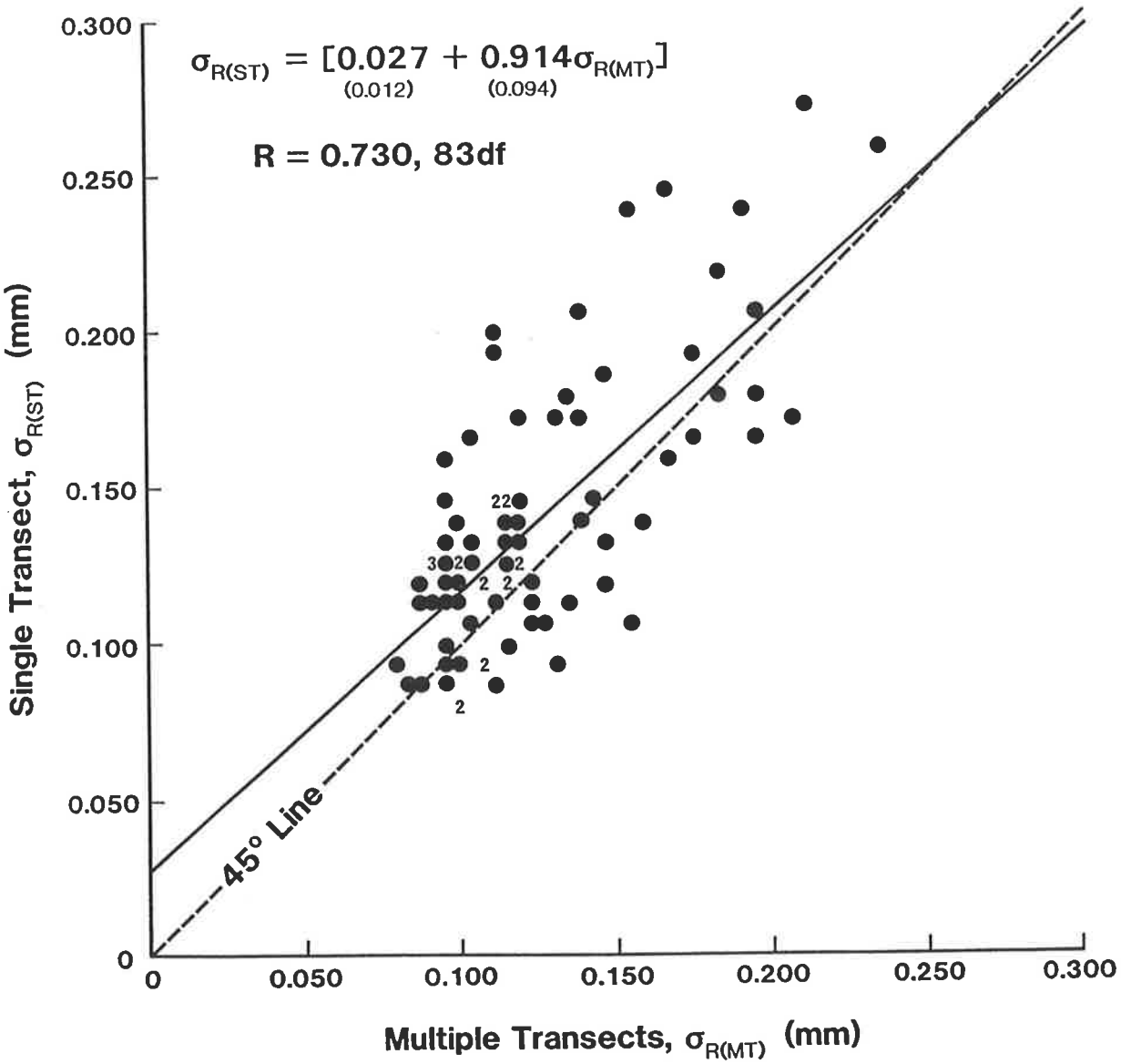

Figure 7-3. Correlation of mean values of fracture surface rugosity, σ_R, between ST-method and MT-method, relative to a 45° line (perfect correlation).

rugosity, σ_R, to those from the original technique (ST-method) introduced in SECTION 3 (i.e. the σ_R-values correlate very well). Furthermore the laser method generates more precise estimates of rugosity (lower standard errors), and is therefore potentially more capable of detecting differences in fracture surface rugosity in the sorts of studies outlined in this thesis.

7.4 Rugosity From Semi-variance Analysis

7.4.1 Introduction

Most of the studies in this thesis, used the parameter, σ_R, (defined in equation [3-4]) to measure of the rugosity (or degree of brokenness) of soil fracture surfaces. It was indicated in SECTION 3, however, that there may be other useful techniques for characterizing the rugosity of transect-data series, one of which is semi-variance analysis (eg. Matheron, 1963). Semi-variograms have recently been used by Lehrsch, et al (1987, 1988), and Dexter and Horn (1988) to examine soil surface roughness at larger scales.

Semi-variograms describe the spatial dependence of data in a series and can reveal information about the spatial distribution of structural features in the data (Campbell, 1978). They are also ideally suited for the analysis of anisotropic structural features. Typically, they are plotted as variance (or semi-variance, $\gamma(l)$) on the ordinate, and equally-spaced distance (or spatial lag, l) on the abscissa. The lag may be expressed in terms of p points, such that $p = \frac{l}{\Delta x}$, where Δx (mm) is the distance between consecutive points in the x direction. The semi-variance, $\gamma(p)$, is calculated after Dexter and Horn (1988) as:

$$\gamma(p) = \frac{1}{2(N-p)} \sum_{i=1}^{i=N-p} \{y(i)-y(i+p)\}^2 \qquad [7-3]$$

where $y(i)$= fracture surface elevation at point i.
p = lag distance between points.
N = total number of points in the data series.

Various models exist to interpret semi-variograms, among which the spherical and linear models are quite common. The spherical model predicts that $\gamma(p) = 0$ at l=0 (i.e. variance of identical points is zero) and increases with increasing **p**, until **p** reaches some critical lag at which the data points become independent of one another. At this critical lag, the variance ideally becomes relatively constant and the semi-variogram levels off. This lag may correspond to the separation distance between dominant soil structural features. The linear model is similar to the spherical model, except that the semi-variance does not level off at large lag distances.

7.4.3 Experimental

The **MT**-data from the fracture surfaces of the disks used in **SECTION 7.3** were used for semi-variance analysis. Both one-dimensional and two dimensional semi-variance analyses were done in order to characterize any anisotropy of the fracture surfaces. Each of the scans (between 50 and 80 of them) per disk with the laser produced a semi-variogram, all of which were averaged at each lag to produce an overall semi-variogram for every disk. The average semi-variogram for each disk was then averaged again at each lag to produce a semi-variogram for each of the treatments. Computations were done using a VAX 11/730 (VMS) computer. Slopes of the log-transformed semi-variograms, $\frac{\delta \log \gamma(p)}{\delta \log p}$, were calculated for the average semi-variograms and used to compute the fractal dimension, **D**, of the fracture surfaces from the equation given by Burrough (1981):

$$\frac{\delta \log \gamma(p)}{\delta \log p} = 4 - 2D \qquad [7-4]$$

7.4.2 Results and Discussion

The one dimensional (1-D) analysis of semi-variance for the rapid wetting experiment (Wiesenboden disks) is expressed in terms of spatial lag, **l** (mm), and is shown in Figure **7-4**. The semi-variance for the non-wetted control lies below that

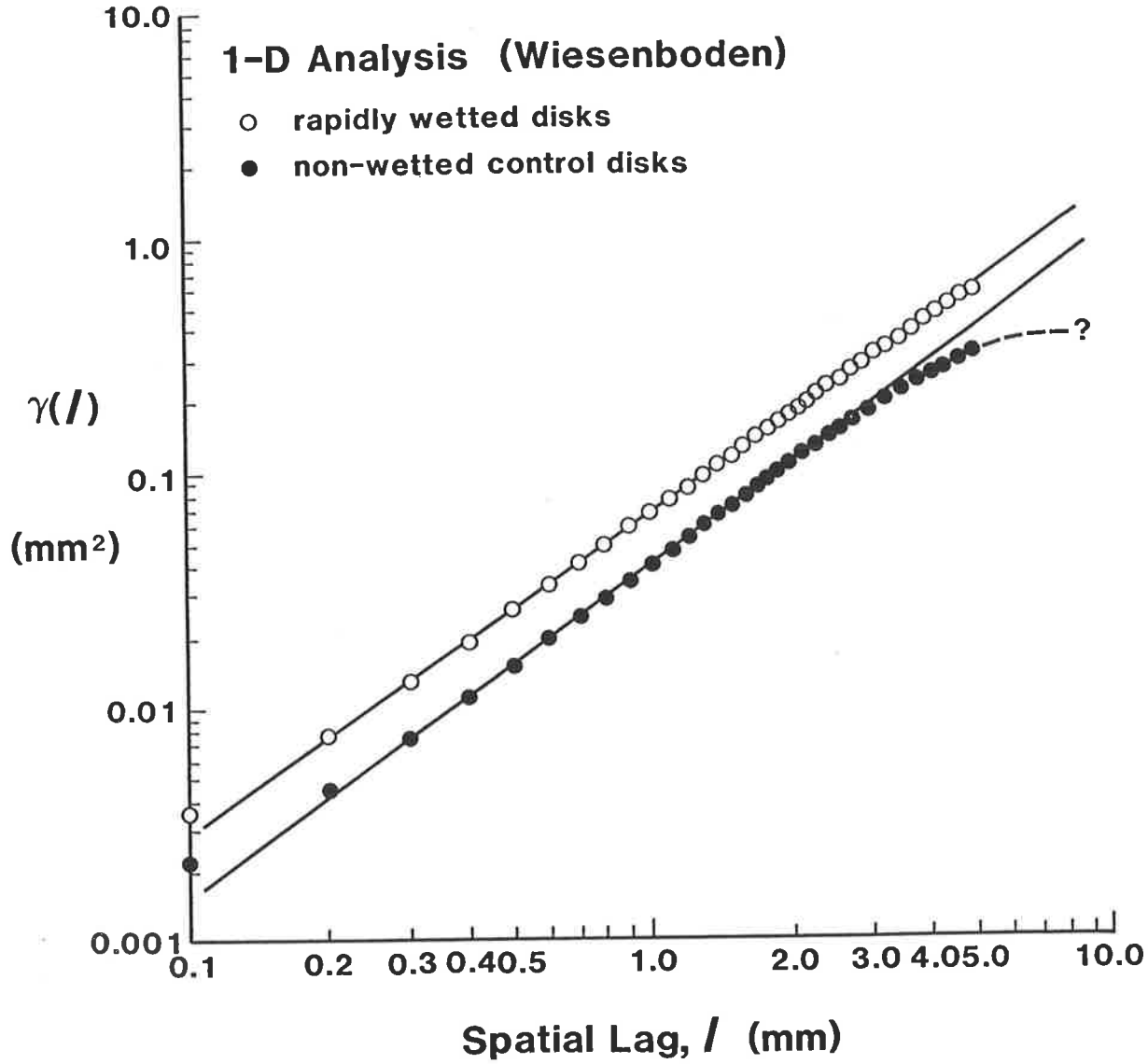

Figure 7-4. One-dimensional autocorrelogram for rapidly wetted and non-wetted moulded Wiesenboden disks.

for the rapidly-wetted disks at all spatial lags. The slopes of the 1-D semi-variograms are 1.41 $\frac{mm^2}{mm}$ and 1.35 $\frac{mm^2}{mm}$, respectively, for the control disks and the rapidly wetted disks. These slopes are not very different, and the corresponding fractal dimensions from equation **[7-4]** are therefore also similar, being 1.30 and 1.33. The semi-variogram for the non-wetted control disks appears to start levelling-off at a spatial lag of approximately 3-4 mm, corresponding to a semivariance of 0.2 mm^2. The semi-variogram for the rapidly wetted disks did not level off.

At infinite lag, the semi-variogram should level-off to the total variance of the data series, σ^2, which is simply the square of the fracture surface rugosity, σ_R. Taking the square root of the $\gamma(l)$-value corresponding to the value of l= 3.2 mm in Figure **7-4** (where the semi-variogram begins to level-off) gives the approximate, unfiltered estimate of the fracture surface rugosity to be $\sigma = (0.2)^{1/2}$ = 0.447 mm, which is approximately three times larger than the filtered value, σ_R = 0.129 mm, shown for the Wiesenboden control disks in Table **7-2a**. This agrees quite well with results from **SECTION 3** (Table **3-5**) which show that the use of a running mean of length 4mm reduces the estimate of rugosity by a factor of approximately three.

The two dimensional (2-D) results for the Wiesenboden rapid wetting experiments show a much greater contrast between the rapidly wetted and the control disks. In Figure **7-5**, the 1-D results (from Figure **7-4**) are superimposed over the 2-D results to show the change in semi-variance which occurs when the variance is examined in two dimensions. The slope as well as the intercept of the semi-variogram for the rapidly wetted disks increase for the 2-D analysis. The control results, on the other hand, should be the same in both dimensions because the soil was moulded and should have a reasonably isotropic structure. This accords with the data shown in Figure **7-5**, which show the control results to remain fairly constant in the analyses for both one and two dimensions. The rapidly wetted disks had very marked structural features (**V**-shaped pattern) like those shown in Plate **6-2**. It is therefore not

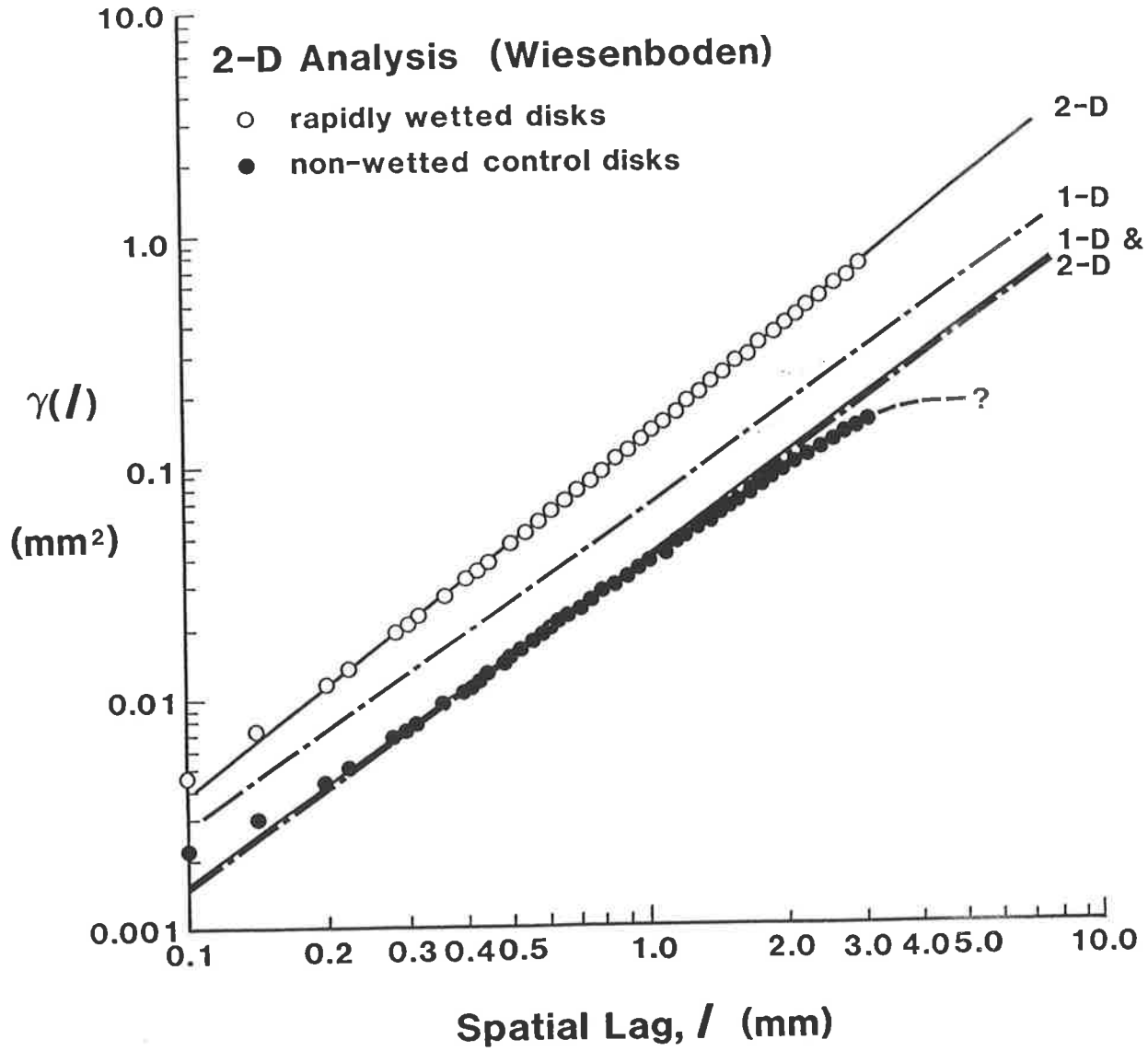

Figure 7-5. Two-dimensional autocorrelogram for rapidly wetted and non-wetted moulded Wiesenboden disks. (Dashed lines are the 1-D values from Figure 7-4).

Table 7-4

Soil and Treatment	$\frac{\delta \log \gamma(l)}{\delta \log l}$ *	Fractal Dimension
Wiesenboden (1-D)		
-Rapidly Wetted	1.35	1.33
-Control	1.41	1.30
Wiesenboden (2-D)		
-Rapidly Wetted	1.52	1.24
-Control	1.42	1.29
Urrbrae (1-D)		
-Not Aged	1.46	1.27
-Aged 7 days	1.37	1.32
-Aged 14 days	1.37	1.32
Portneuf (1-D)		
-Not Aged	1.49	1.25
-Aged 7 days	1.52	1.24
-Aged 14 days	1.40	1.30

* slopes calculated using lines drawn (by eye) through the semi-variograms.

Table **7-4.** Slopes of semi-variograms, and fractal dimensions, **D**, for the experiments oultined in **SECTION 7.**

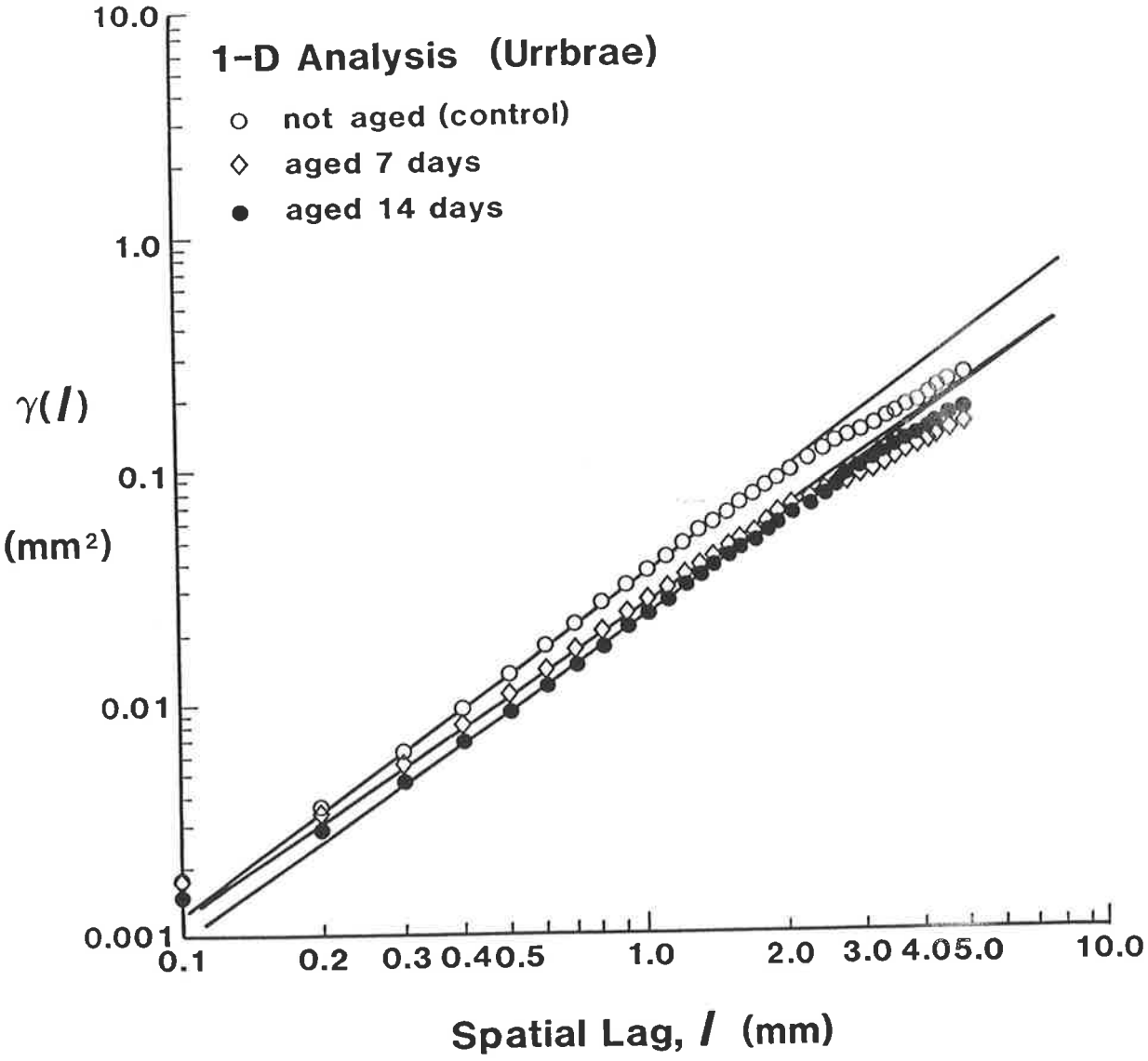

Figure 7-6. One-dimensional autocorrelogram for aged and not-aged moulded Urrbrae soil disks.

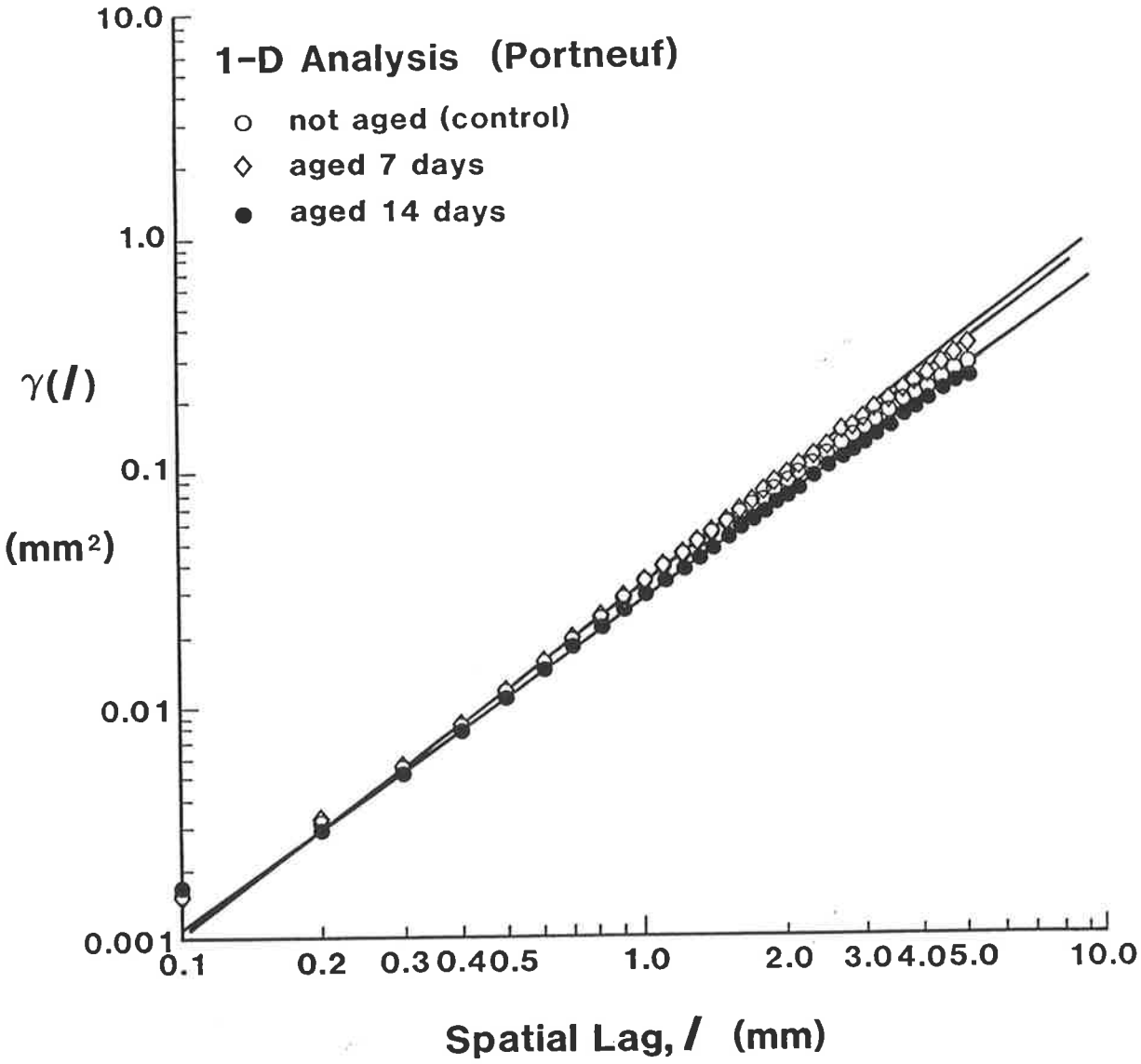

Figure 7-7. One-dimensional autocorrelogram for aged and not-aged moulded Portneuf soil disks.

surprising that an analysis of the structure in two dimensions should reveal that greater spatial variability occurs in the rapidly wetted soil disks.

The semi-variance analysis for the age-hardening experiments revealed essentially the same as the σ_R-results in Table **7- 2b**. For the Urrbrae soil, the fracture surfaces became smoother upon ageing ('aged' lines lower than 'control' line in Figure **7- 6**). The Portneuf soil showed no effect of ageing at all (same as the σ_R-results shown in Table **7- 2b**) as can be seen by the fact that the three semi-variograms in Figure **7- 7** are virtually indistinguishable from one another.

The slopes of the semi-variograms and the corresponding fractal dimensions for all the experiments in this study are shown in Table **7- 4**, and these appear to reveal very little about the structural changes caused by the treatments. This is not altogether surprising, because the slopes are based on an 'average' line (drawn by eye), and does not take into account the degree of bending from the straight lines that occurs to different degrees for each treatment. The only distinguishing feature appears to be the degree of separation of the semi-variograms (different intercepts), but an analysis of this possibility has not been attempted here.

7.4.4. Conclusions

The technique of non-contact laser scanning is a rapid technique which provides multiple-scanning on a scale of 0.1mm. Because of the large amount of data that it produces in three dimensions, it is particularly well-suited to studies on anisotropy of soil structure (eg. semi-variance analysis). The technique offers significant advantages over other techniques in that it requires no sample preparation, and can be adapted to most personal computer equipment. Furthermore, laser sources are now readily available and are relatively inexpensive.

In this set of experiments, the semi-variograms appeared to offer little information about the soil structure that was not already available from σ_R-results. This does not mean, however, that semi-variograms would not be useful in general for the study of soil structural features. On the contrary, semi-variograms can reveal

much about the structural nature of soils having different workabilities, as shown recently in Dexter and Horn (1988). The values of σ_R give only an overall indication of the rugosity of soil fracture surfaces, whereas semi-variograms give more detailed information about the sizes and spatial separation of the structural features. Bumps and curves in a semi-variogram, for example, show that different surface elevations recur at regular separation distances, or lags.

SECTION 8. GENERAL DISCUSSION AND CONCLUSIONS

8.1 Introduction

The various studies outlined in this thesis were designed to improve our understanding of the brittle fracture of unsaturated soils exposed to tensile stresses. They were also designed to investigate the use of natural forces (drying, followed by rapid wetting) for improving the structural condition of degraded (hard-setting, compacted, puddled) soils. This **SECTION** integrates the conclusions from the research and identifies future research needs. The conclusions may be summarized in two main areas: (1) brittle fracture of unsaturated soils under tensile stress, and (2) soil mellowing from natural forces.

8.2 Brittle Fracture of Unsaturated Soils Under Tensile Stress

8.2.1 Tensile Strength

The work of Snyder and Miller (1985), which gives a comprehensive theory for the tensile strength of unsaturated, freshly moulded soils was found to be unsuitable for predicting the tensile strength of age hardened soils (both natural clods and moulded, aged disks). They suggested that in unsaturated, uncemented soils that the weakest flaws in the soil are the air-filled pores. Application of their model to the soils in the present study, however, made unsatisfactory predictions of tensile strength. For example, when the soil was close to saturation ($s > 0.70$) the tensile strength of natural soil clods tended to be higher than predicted by Snyder and Miller's theory. This appears to be the result of age hardening and cementation processes, which occur with time in the field and in the laboratory, and which can impart significant tensile strength to the soil, even in the completely saturated state. When the soil was drier than approximately $s = 0.70$, on the other hand, Snyder and Miller's theory over-estimated the measured tensile strength considerably. This was a result of the fact that aggregation in natural soil causes water to be held mainly in intra-aggregate pores, rather than in inter-aggregate pores. As a consequence, less

water occurs as films and menisci to bind particles together than would be predicted from **s**. Predictions of tensile strength based on the model of Snyder and Miller need therefore to be restricted to coarse textured soils that have been recently moulded, so that neither cementation nor aggregation modify the role of water menisci in response to tensile stresses.

It is apparent that much work needs to be done on the theory of tensile strength in age-hardened, and finer textured soil materials. Future work could perhaps incorporate a cementation function, **f(c)**, into the theory of Snyder and Miller, as well as another function, **g(a)**, which reduces the importance placed upon the degree of pore saturation in drier soils. The function, **g(a)**, might include as a variable the aggregate size distribution of the soil. This would give information about the distribution of water in the soil (whether it is within or between soil aggregates) and would therefore reflect the amount of water present as water menisci, and contributing to the tensile strength of the soil. For natural soil clods, a general working model for the tensile strength might therefore need to be

$$TS = f(c) + g(a)\left(\frac{\chi\ \Psi}{2}\right) \qquad [8-1]$$

This sort of a model could be more useful in predicting the dynamics of brittle failure in real soils, because it relies less on the drainage of water (distance between air-filled pores) for the establishment of crack patterns.

8.2.2 Fracture Surface Rugosity

One of the criticisms of current techniques for studying the brittle fracture of soils (eg. drop shatter test (Hadas and Wolf, 1984a) and soil friability (Utomo and Dexter, 1981b)) is that they are extremely time-consuming. A more rapid method such as the one developed in this thesis has been needed for some time now. With the use of the non-contact laser system, fracture surface analysis is probably the

fastest, most informative method now available for studying the brittle fracture of soils.

The experimental work on fracture surfaces in this thesis is based on the idea of Braunack, et al (1978) that the tensile strength of unsaturated soils is controlled by the distribution of weakest flaw-strengths in the soil. They indicated that when tensile stresses are applied to a soil aggregate, strain energy will be reversibly stored in the soil until a sufficiently large tensile stress develops. Brittle fracture occurs by the activation of one or more of the weakest flaws in the aggregate, and strain energy is then irreversibly lost with the formation of a new fracture surface. This builds on the concept introduced by Hadas (1987) that the soil structure is hierarchical in nature, the largest aggregates and clods being at the top of the hierarchy. The strength of the bonds between compound particles of any hierarchical order is simply the strength of the compound particles of the next lower order in the structural hierarchy (Dexter, 1988a). As a consequence of different particle size distributions and degrees of aggregation different soils contain different levels of structural organization and therefore differ in the concentration of flaws and points of weakness.

It was hypothesized that soil fracture surfaces created under tensile stresses contain a 'blueprint' of the fracture pathway, and further that the topography of the fracture surfaces contains information about the distance between the weakest flaws in the soil. The fracture surface rugosity, σ_R, was proposed as a simple measure of this distance. Factors which increase the density of weakest flaws in the soil (or reduce the spacing between them) will increase the value of σ_R.

The results of **SECTION 3** indicate that there is a strong correlation between the value of σ_R and the average distance between air-filled pores in the soil. The wetter the soil, the greater the distance between the pores that are drained, and the larger is the value of σ_R. The measured values of σ_R , however, were found to be smaller than the distances predicted to lie between air-filled pores, and this indicated that other factors also influence the fracture pathway.

Some clue as to what some of these other factors might be are suggested from the tensile strength results for natural soil clods in **SECTION 3**. The tensile strength of natural soil clods, particularly in wetter soils, was found to be higher than could be predicted on the basis of cohesion due to water menisci alone. It was concluded from this result that the additional cohesive strength of the clods must be the result of cementitious bonding which had developed from age hardening processes and long term wetting and drying in the field. The tensile strength is therefore also a function of the number of interparticle contacts (Kemper, 1958) as well as the strength of the cementitious material binding them together (Ingles, 1962c). So while the distribution of air-filled pores influences the fracture pathway (and probably controls the overall morphology of the fracture surface) there are many interparticle bonds between air-filled pores that modify and reduce the value of σ_R.

Interparticle bonding can be strengthened by the addition of calcium compounds, and as shown in **SECTION 4**, this will influence the distribution of weakest flaws in the soil, and hence the fracture surface morphology. With larger additions of calcium, the values of σ_R tend to decrease, although this may have been related to the difference in size scales between the features detected by the scanning procedure ($\geq$ 0.1mm) and the sizes of the particles that are stabilized by calcium ($<<$ 0.1mm).

Interparticle bonding can also be strengthened by organic carbon in the soil. (Carr and Greenland, 1972). The organic carbon content, however, also influences a host of other soil properties such as the brittle and plastic behaviour of soil under stresses, the bulk density and the water content of the soil. The effect of organic carbon on the dispersion of flaw strengths in the soil was shown in **SECTION 5** to be inseparably tied to the soil water content. The lower plastic limit of the soil may be used to standardize the water contents of different soils, and it has a major influence on the fracture characteristics of the soil. For example, if soils having very different organic carbon contents and bulk densities are fractured at their respective plastic limits, then they can produce similar values of soil strength (Greacen,

1960), and identical values of σ_R. At higher water contents, the σ_R-values increase but at a slower rate than for low-OC soils. This is attributed to the greater macroporosity (more air-filled pores) in high-OC soils, which has the effect of increasing the concentration of weakest flaws over that of soils having lower amounts of organic carbon. At water contents below the plastic limit the trend is reversed so that σ_R-values tend to be lower for high-**OC** soils than for low-**OC** soils. This is probably related to changes in the dispersion of weakest flaw-strengths as the soil dries out, causing the low-**OC** soil to increase in strength more rapidly than the high-**OC** soil. Such changes in the relative strengths of soils having different organic carbon contents have been noted by Davies (1985).

The experiments outlined in **SECTIONS 6 & 7** demonstrate how drastically the distribution of flaws in the soil can change after rapid wetting. Results indicate that internal structure generation occurs almost invariably whenever wetting is sufficiently rapid to reduce the tensile strength of the soil. In studies where drastic changes in the soil structure are induced, an interpretation of σ_R-values needs to be accompanied by information on the tensile strength of the soil because it is the magnitude of the weakest flaws which controls the overall strength of the soil as well as the fracture pathway.

The fracture surface rugosity, σ_R, is ideally suited to the study of cracking patterns in different soils. For example, the single-wetting experiments shown in **SECTION 6** indicate that the Urrbrae soil often had larger values of σ_R than did the Wiesenboden. The reason for this is unknown, and could be investigated by taking both of the soils through a series of wetting and drying cycles and observing the changes that occur in σ_R. The age hardening experiments outlined in **SECTION 7**, showed that the moulded Urrbrae soil (which slakes easily and forms a surface crust) had σ_R-values which were quite similar in magnitude to those of the moulded Portneuf soil (which is known to crumble nicely during tillage and to form an ideal seedbed). Perhaps after a few wetting and drying cycles, however, the differences in soil workability might be detectable from σ_R-values.

Studies such as those mentioned above could give clues about whether characteristic distributions of weakest flaws exist in different soils which may be responsible for differences in soil structure and workability. Experiments comparing soils that are known to be self-mulching with soils that are known to be hard-setting and difficult-to-work would be particularly useful in this regard. Fracture surface analysis on natural soil clods has been recently used by Dexter and Horn (1988) to investigate differences in soil workability between several West German soils.

Additional work also needs to be done relating σ_R to soil resiliency. For example, the question of whether there is a relation between fracture surface rugosity and the ability of the soil to resist compaction and subsidence after tillage needs to be addressed. It has been suggested by Cruse, et al (1980) that seedbeds made up of smoother particles are less able to withstand crusting, densification and tillage-induced plow-pans. Rugosity therefore may be related to the packing geometry, infiltration and water run-off. It may also affect the growth of roots in undisturbed soils. The works of Whiteley, et al (1981), Whiteley and Dexter (1983) and Dexter (1986), for examples, all describe the importance of the surface roughness of aggregates and cracks in promoting root penetration.

From the results of the studies outlined in **SECTIONS 3** to **7**, it is apparent that a given value of σ_R may arise from a large number of combinations of, among other things, the water content, bulk density, organic carbon content, and calcium content. This is partly because the fracture surface rugosity, σ_R, is an overall average measure of the structural condition of soil surfaces. The factors which control σ_R , however, may actually produce different fracture surface morphologies. That is, they may produce features of different angularity and shape. If this were the case, the differences in morphology could probably be distinguished using better techniques than those used here. For example, if high-resolution equipment were used, (perhaps combined with digital filtering techniques to adjust for appropriate scales of observation) the differences in morphology could become quite visible. The

proposed explanation presented at the end of **SECTION 4** (supported by the work of Loveday and Scotter, 1966) could be investigated (viz: that at a scale of resolution of say 10μm, calcium applications will increase the fracture surface rugosity).

If the contributions to σ_R of the different factors discussed in this thesis could be more clearly separated, this would provide a huge step forward for soil structure research. As an example, fracture surface analysis has the potential to replace much of the very tedious, time-consuming and expensive work on thin sections. This could be the case particularly when measurements from thin sections are simply correlated with other measured physical properties (see for example, Kooistra, et al, 1985; Bouma and Kooistra, 1987).

8.3 Soil Mellowing from Natural Forces

An explosion of research on the subject of tillage and on the response of soils and crops to different tillage systems has occurred in the past twenty years. This explains the launching of various new journals (eg. *Soil & Tillage Research*) which cater to this area of research. During this period, there has been a general move toward reduced cultivation (on suitable soils) in order to reduce compaction and structural deterioration (eg. Ellis et al, 1982). It is only relatively recently, however, that significant emphasis has been placed upon research that takes advantage of natural forces in the regeneration of soil structure (eg. Monnier and Goss, 1987; Dexter, 1988c).

The use of natural forces (eg. drying, followed by rapid wetting) was investigated in this thesis with the view of determining limits to which soil must be dried before exposure to water will cause mellowing (generation of micro-cracks) in moulded soil. Generating micro-cracks is a first step toward developing soil structure that is suitable for tillage in compacted and puddled soils. Water under certain conditions can play a major role in generating these cracks, even in soils of relatively low clay content, as shown recently by Stengel (1988).

For the soils used in this study, it was found that mellowing could be induced if the soil was dried to at least a matric potential of -1 to -1.5 MPa and then exposed to free water. Several cycles of wetting and drying would undoubtedly show a more dramatic effect than found here. Only one exposure of the soil to rapid wetting was planned in this thesis in order to establish the lower limits of effectiveness of the wetting process in mellowing. In many parts of the world, more than one cycle of rapid wetting may not be possible due to the short time available to establish seedbeds between seasons.

The rapid wetting experiments in this thesis have looked mainly at the extent to which soils must be dried (at constant temperature) before being wetted, but has not looked at how the rate of drying influences the mellowing process. Drying in this thesis was conducted slowly enough to prevent visible crack-formation. Preliminary work, not presented in this thesis, indicates that the rate of drying may also be important in the mellowing process. The rate of drying (controlled by temperature, relative humidity, wind speed, etc.) changes in the field on a daily basis and will obviously affect the intensity of crack-formation. Some soils crack more than others under different conditions of drying, thus making them more susceptible to the mellowing process during rapid wetting.

There is a great deal of room for more research to be done using natural forces, such as wetting and drying, to ameliorate soil structure problems. The recent works of Towner (1987a,b; 1988), for example, provide the basis for a whole new area of research which has previously only been hinted at by others (eg. van de Graaf, 1978; Koolen and Kuipers, 1983). That is the study of shrinkage and cracking around incompressible particles (eg. sand grains). There is a huge potential for the application of this sort of research to the problems of regenerating structure in compacted, puddled and hard-setting soils. Shrinking and cracking around sand grains may, in fact, be strongly involved in the self-mulching process, which is peculiar to some of the vertisolic soils around the world.

8.4 Summary of Conclusions

1. The prediction of the tensile strength of natural (i.e. age hardened) unsaturated soil is far from being understood, particularly in well-aggregated, finer-textured soils, where aggregation and cementation processes contribute to the strength. Future work needs to incorporate the influence of these processes in such a way as to reduce the importance normally placed on the degree of pore saturation.

2. Soil fracture surfaces that are produced by brittle fracture under tensile stress contain a 'blue print' of the failure pathway. The topography of this failure surface is a result of brittle failure through the joining up of the weakest flaws closest to the plane of major tensile stress in the soil.

3. Fracture surface rugosity, σ_R, is a measure of the distance between the weakest flaws in the soil, although it cannot be directly equated to that distance. Factors reducing the distance between weakest flaws will reduce the value of σ_R measured on fracture surfaces created under tensile stress.

4. The value of σ_R is directly related to the distance between air-filled pores in soil which is otherwise homogeneous. This distance is greatest at near-saturation and decreases during drainage. This suggests that the ends of air-filled pores are points of stress-concentration in brittle soils.

5. The value of σ_R is sensitive to structural improvements caused by the application of calcium to the soil. It was found that σ_R (measured at a scale of 0.1mm) decreased with greater additions of calcium. The scale of measurement, however, probably has a strong influence on the magnitude of σ_R, and requires further investigation. Micro-probe technology may be useful in future research for determining whether differences in rugosity at different scales are related to differences in chemical properties between crack-surfaces and the bulk soil.

6. The value of σ_R is influenced by the soil organic carbon content, but at this stage, it is concluded that the effects are indirect. The reason for this is that organic

carbon influences other factors which control σ_R (eg. water content, bulk density, plasticity).

7. If moulded soils that have different organic carbon contents are fractured at water contents corresponding to their respective lower plastic limits, they will produce very similar values of tensile strength, **TS**, as well as fracture surface rugosity, σ_R. Higher levels of organic carbon tend to reduce the slope of the σ_R against relative water content, $\frac{w}{PL}$, curves. Consequently, higher organic carbon contents produce larger values of σ_R (relative to lower organic carbon contents) at water contents below the plastic limit, and vice versa at water contents above the plastic limit.

8. The non-contact laser system (multiple-transect method) for measuring fracture surface topography, while providing similar results to the single-transect method, appears to provide many advantages. The most significant advantages are that the laser system is faster (requiring no sample preparation), and the multiple scanning offers the opportunity to study anisotropic structural features.

9. The generation of soil structure during rapid wetting is not restricted to dry soils. A maximum matric potential in the order of -1 to -1.5 MPa may be the upper limit for initial water potentials at which mellowing during wetting can still be induced. Internal structure generation as measured by fracture surface rugosity, σ_R, occurs almost invariably whenever wetting is sufficiently rapid to reduce the tensile strength of the soil.

10. The forces of air entrapment on their own during wetting, do not induce mellowing. The forces created by differential swelling, alone during wetting, also have limited ability to induce mellowing. The forces only cause significant mellowing when they act synergistically at the same time.

REFERENCES

Adams, W.A. 1973. The effect of organic matter on the bulk and true densities of some uncultivated podzolic soils. Journal of Soil Science, 24: 10-17.

Adu, J.K. and Oades, J.M. 1978a. Physical factors influencing decomposition of organic materials in soil aggregates. Soil Biology and Biochemistry, 10: 109-115.

Adu, J.K. and Oades, J.M. 1978b. Utilization of organic materials in soil aggregates by bacteria and fungi. Soil Biology and Biochemistry, 10: 117-122.

Aitchison, G.D. 1957. The strength of quasi-saturated and unsaturated soils in relation to the pressure deficiency in pore water. Proceedings Fourth International Conference on Soil Mechanics and Foundation Engineering, I: 135-139.

Aitchison, G.D. 1961. Relationships of moisture stress and effective stress functions in unsaturated soils. pp. 47-52 (plus discussion pp. 63-74 and 143-151) in Pore Pressure and Suction in Soils. Proceedings Conference of the International Society of Soil Mechanics and Foundation Engineering. March 30-31,1960. Butterworths, London.

Allen, N.H.E. 1984. Instability index: a method of measuring the soil structural stability of cultivated seedbeds. M.Sc. thesis. University of Guelph, Guelph, Ontario, Canada. Catalogue Number CAZONUF 74-84A44ENG.

Arca, M.N. and Weed, S.B. 1966. Soil aggregation and porosity in relation to contents of free iron oxide and clay. Soil Science, 101: 164-170.

Arndt, W. 1964. Investigations of some physical problems of Katherine soils leading to proposals for considering new systems of cultivation for the summer rainfall environment. Commonwealth Scientific and Industrial Research Organization, Division of Land Research and Regional Survey. Technical Memorandum 64/3. Progress Report, July, 1963.

Arndt, W. 1965. The nature of the mechanical impedance to seedlings by soil surface seals. Australian Journal of Soil Research, 3: 45-54.

Arnold, P.W. 1978. Surface-electrolyte interactions. pp. 355-405 in D.J. Greenland and M.H.B. Hayes (Eds.) The Chemistry of Soil Constituents.. John Wiley, New York.

Aspiras, R.B., Allen, O.N., Harris, R.F. and Chesters, G. 1971. Aggregate stabilization by filamentous microorganisms. Soil Science, 112: 282-284.

Atterberg, A. 1911. Die plastizitat der tone. Int. Mitteilungen Bodenkunde, 1: 10-43. (In German).

Aylmore, L.A.G. and Quirk, J.P. 1967. The micropore size distributions of clay mineral systems. Journal of Soil Science, 18: 1-17.

Aylmore, L.A.G. and Sills, I.D. 1978. Pore structure and mechanical strength of soils in relation to their constitution. pp. 69-78. in W.W. Emerson, R.D. Bond and A.R. Dexter (Eds.) Modification of Soil Structure. John Wiley, Toronto.

Aylmore, L.A.G. and Sills, I.D. 1982. Characterization of soil structure and stability using modulus of rupture-exchangeable sodium percentage relationships. Australian Journal of Soil Research, 20: 213-224.

Bakker, A.C., Emerson, W.W. and Oades, J.M. 1973. The comparative effects of exchangeable calcium, magnesium, and sodium on some physical properties of Red-Brown Earth subsoils. I. Exchange reactions and water contents for dispersion of Shepparton soil. Australian Journal of Soil Research, 11: 143-150.

Barley, K.P. 1959. Earthworms and soil fertility. IV. The influence of earthworms on the physical properties of a red-brown earth. Australian Journal of Agricultural Research, 10: 371-376.

Barley, K.P. 1961. The abundance of earthworms in agricultural land and their possible significance in agriculture. Advances in Agronomy, 13: 249-268.

Bayramli, E., Abou-obeid, A. and Van de Ven, T.G.M. 1987. Liquid bridges between spheres in a gravitational field. Journal of Colloid and Interface Science, 116: 490-502.

Bennett, J.G. 1936. Broken coal. Journal of the Institute of Fuel, 10: 22-39.

Bennett, J.G. and Brown, R.L. 1941. Broken coal-IV. The mechanics of partial degradation. Journal of the Institute of Fuel, 14: 135-143.

Bennett, J.G., Brown, R.L. and Crone, H.G. 1941. Broken coal-II. The relation between size distribution and breakage process. Journal of the Institute of Fuel, 14: 111-128.

Bennett, O.L., Ashley, D.A. and Doss, B.D. 1964. Methods of reducing soil crusting to increase cotton seedling emergence. Agronomy Journal, 56: 162-165.

Bernard, J.R.L. 1986. The Macquarie Thesaurus. Macquarie Library Proprietary Limited. Chatswood, New South Wales.

Berry, J.P. 1960a. Some kinetic considerations of the Griffith criterion for fracture-I. Equations of motion at constant force. Journal of the Mechanics and Physics of Solids, 8:194-206.

Berry, J.P. 1960b. Some kinetic considerations of the Griffith criterion for fracture-II. Equations of motion at constant deformation. Journal of the Mechanics and Physics of Solids, 8: 207-216.

Bertruzzi, P. and Stengel, P. 1988. Measuring effects of tillage implements on soil surface geometry with a laser reliefmeter. Proceedings 11th Conference of International Soil Tillage Research Organization, Edinburgh. I: 7-12.

Bishop, A.W. 1961. The measurement of pore pressure in the triaxial test. pp. 38-46 (plus discussion pp. 63-74, and 143-151) in Pore Pressure and Suction in Soils. Proceedings Conference of the International Society of Soil Mechanics and Foundation Engineering. March 30-31, 1960. Butterworths, London.

Blackman, R.B. and Tukey, J.W. 1958. The Measurement of Power Spectra. Dover Publications. New York.

Blackmore, A.V. 1981. Self mulching soil. Soils News, 48(July): p. 4. Australian Society of Soil Science.

Blake, B.R. 1965. Bulk density. pp. 384-399. in C.A. Black (Ed.) Methods of Soil Analysis. Part 1. Physical and Mineralogical Properties, Including Statistics of Measurement and Sampling. American Society of Agronomy. Madison, Wisconsin.

Blake, G.R. and Gilman, R.D. 1970. Thixotropic changes with ageing of synthetic aggregates. Soil Science Society of America Proceedings, 34: 561-564.

Blakey, F.A. 1964. Mechanisms of deformation and failure in bonded, discrete particle systems: Failure sources in heterogenous systems. D4: 1-4. in "Mechanisms of Soil Stabilization". Proceedings of a Colloquium convened by the Soil Mechanics Section, Commonwealth Scientific and Industrial Research Organization, Syndal, Victoria, April 6-8, 1964.

Bodman, G.B. and Rubin, J. 1948. Soil puddling. Soil Science Society of America Proceedings, 13: 27-36.

Boekel, P. 1959. Evaluation of the structure of clay soils by means of soil consistency. Mededelingen van de Landbouwhogeschool en de Opzoekingsstations van de Staat te Gent, 24(1): 363-367. (Proceedings of the International Symposium on Soil Structure, Ghent, May 28-31, 1958.) (In English).

Boekel, P. 1965. Karakterisering van de slempigheid van zavelgronden door bepaling van de consistentie. Landbouwkundig Tijdschrift, 77(7): 306-311. (In Dutch with English figures and summary).

Boekel, P. 1979. The workability of the soil in spring in relation to moisture content and moisture transport. Proceedings of Eighth Conference of International Soil Tillage Research Organization, 1: 293-298.

Bolt, G.H. and Koenigs, F.F.R. 1972. Physical and chemical aspects of the stability of soil aggregates. Mededelingen van de Faculteit Landbouwwetenschappen Rijksuniversiteit Gent, 37: 955-973. (Proceedings of the Symposium on Soil Conditioning, Ghent 1972). (In English)

Bolton, F.R. and De Datta, S.K. 1979. Dry soil mulching in tropical rice. Soil Science and Plant Nutrition, 25: 173-181.

Bond, R.D. and Harris, J.R. 1964. The influence of the microflora on physical properties of soils I. Effects associated with filamentous algae and fungi. Australian Journal of Soil Research, 2: 111-122.

Bonneau, M. and Levy, G. 1982. Assembly and physical organization of particles. pp. 268-287. in M. Bonneau and B. Souchier (Eds). Constituents and Properties of Soils. Academic Press, London.

Bouma, J. and Kooistra, M.J. 1987. Soil morphology and soil water movement. pp. 507-511. in N. Fedoroff, L.M. Bresson and M.A. Courty (Eds.) Micromorphology des Sols. Actes de la 7th Reunion Internationale de micromorphologie des soils. Paris, July, 1985.

Bouyoucos, G.J. 1925. The effect of the colloidal content upon the physical properties of soils. Journal of the American Society of Agronomy, 17: 284-294.

Brace, W.F. and Bombolakis, E.G. 1963. A note on brittle crack growth in compression. Journal of Geophysical Research, 68: 3709-3713.

Braunack, M.V. and Dexter, A.R. 1978. Compaction of aggregate beds. pp 119-126. in W.W. Emerson, R.D. Bond and A.R. Dexter (Eds.) Modification of Soil Structure. John Wiley. London.

Braunack, M.V., Hewitt, J.S. and Dexter, A.R. 1979. Brittle fracture of soil aggregates and the compaction of aggregate beds. Journal of Soil Science, 30: 653-667.

Brewer, R. and Blackmore, V. 1956. The effects of entrapped air and optically oriented clay on aggregate breakdown and soil consistence. Australian Journal of Applied Science, 7: 59-68.

Briones, A.A., and Uehara, G. 1977a. Soil elastic constants: I. Calculations from sound velocities. Soil Science Society of America Journal, 41: 22-25.

Briones, A.A., and Uehara, G. 1977b. Soil elastic constants: II. Application to analysis of soil cracking. Soil Science Society of America Journal, 41: 26-29.

Brown, R.L. 1941. Broken coal-III. Generalized law of size distribution. Journal of the Institute of Fuel, 14: 129-134.

Brunauer, S., Emmett, P.H., and Teller, E. 1938. The adsorption of gases in multimolecular layers. Journal of American Chemical Society, 60: 309-316.

Bullock, M.S., Kemper, W.D. and Nelson, S.D. 1988. Soil cohesion as affected by freezing, water content, time and tillage. Soil Science Society of America Journal, 52: 770-776.

Burrough, P.A. 1981. Fractal dimensions of landscapes and other environmental data. Nature, 294: 240-242.

Campbell, J.B. 1978. Spatial variation of sand content and pH within single contiguous delineations of two soil mapping units. Soil Science Society of America Journal, 42: 460-464.

Carman, P.C. 1941. Capillary rise and capillary movement of moisture in fine sands. Soil Science, 52: 1-14.

Carr, C.E., and Greenland, D.J. 1972. Preliminary results of an empirical study of the movement of polymers through soil and their effect on dispersion of clay from aggregates. Mededelingen van de Faculteit Landbouwwetenschappen Rijksuniversiteit Gent, 37(3): 982-992.

Caussignac, J.M. and Morel, G. 1987. Méthode de relevé sans contact de la rugosité d'une surface plane. Laboratoire Central des Ponts et Chaussées, Internal Report F.A.E.R., 1.65.10: 1-24.

Cernuda, C.F., Smith, R.M. and Vicente-Chandler, J. 1954. Influence of initial soil moisture condition on resistance of macroaggregates to slaking and to water-drop impact. Soil Science, 77: 19-27.

Chapman, J.E. 1927. The effects of organic matter on the tillage of a clay soil. Proceedings First International Congress of Soil Science, 1: 443-445.

Chartres, C.J., Green, R.S., Ford, G.W. and Rengasamy, P. 1985. The effects of gypsum on macroporosity and crusting of two red duplex soils. Australian Journal of Soil Research, 23: 467-479.

Chassin, P. 1979. Détermination de l'angle de contact acides humiques-solutions aqueuses de diols. Conséquencés sur l'importance relative des mécanismes de destruction des agrégats. Annales Agronomiques, 30(6): 481-491. (In French with English figures, table and summary).

Chatterjee, R.K. and Jain, J.K. 1970. Studies on aggregate formation with reference to cementing substances. Soil Science and Plant Nutrition, 16: 231-233.

Chittleborough, D.J. and Oades, J.M. 1980. The development of a Red-brown earth. III. The degree of weathering and translocation of clay. Australian Journal of Soil Research, 19: 383-393.

Chepil, W.S. 1955. Factors that influence clod structure and erodibility of soil by wind: IV. sand, silt and clay. Soil Science, 80: 155-162.

Christiansen, J.E. 1944. Effect of entrapped air upon the permeability of soils. Soil Science, 58: 355-365.

Clapp, C.E. and Emerson, W.W. 1965a. The effect of periodate oxidation on the strength of soil crumbs: I. Qualitative studies. Soil Science Society of America Proceedings, 29: 127-130.

Clapp, C.E. and Emerson, W.W. 1965b. The effect of periodate oxidation on the strength of soil crumbs: II. Quantitative studies. Soil Science Society of America Proceedings, 29: 130-134.

Clarke, A.L., Greenland, D.J. and Quirk, J.P. 1967. Changes in some physical properties of the surface of an impoverished red-brown earth under pasture. Australian Journal of Soil Research, 5: 59-68.

Clough, K.S. and Sutton, J.C. 1976. Direct observation of fungal aggregates in sand-dune soil. Canadian Journal of Microbiology, 24: 326-333.

Collis-George, N., and Bond, W.J. 1981. Ponded infiltration into simple soil systems: 2. Pore air pressures ahead of and behind the wetting front. Soil Science, 131: 263-270.

Collis-George, N., and Lal, R. 1971. Infiltration and structural changes as influenced by initial moisture content. Australian Journal of Soil Research, 9: 107-116.

Concaret, J. 1967. Étude des mécanismes de la destruction des agrégats de terre au contact de solutions aqueuses. Annales Agronomiques, 18: 65-144. (In French).

Coughlan, K.J. 1984. The structure of vertisols. pp87-96. in J.W. McGarity, E.H. Hoult and H.B. So (Eds.) The Properties and Utilization of Cracking Clay Soils. (Reviews in Rural Science 5). Proceedings Symposium held at University of New England, Armidale, New South Wales. 24-28 August, 1981.

Coughlan, K.J. and Fox, W.E. 1977. Measurement of aggregate size. Australian Journal of Soil Research, 15: 211-219.

Coughlan, K.J. , Fox, W.E. and Hughes, J.D. 1973. Aggregation in a swelling clay soils. Australian Journal of Soil Research, 11: 133-141.

Craggs, J.W. 1960. On the propagation of a crack in an elastic-brittle material. Journal of the Mechanics and Physics of Solids, 8: 66-75.

Cruse, R.M., Cassel, D.K. and Averette, F.G. 1980. Effect of particle surface roughness on densification of coarse-textured soil. Soil Science Society of America Journal, 40: 692-697.

Czeratzki, W. and Frese, H. 1958. Importance of water in formation of soil structure. pp. 200-211. in H.F. Winterkorn (Ed.) Water and Its Conduction in Soils. Highway Research Board, Special Report 40. Washington, D.C.

Dalrymple, J.B. and Jim, C.Y. 1984. Experimental study of soil microfabrics induced by isotropic stresses of wetting and drying. Geoderma, 34: 43-68.

Davidson, J.L. and Quirk, J.P. 1961. The influence of dissolved gypsum on pasture establishment on irrigated sodic clays. Australian Journal of Agricultural Research, 12: 100-110.

Davidson, J.M. and Evans, D.D. 1960. Turbidimeter technique for measuring the stability of soil aggregates in a water-glycerol mixture. Soil Science Society of America Proceedings, 24: 75-79.

Davies, P. 1985. Influence of organic matter content, moisture status and time after reworking on soil shear strength. Journal of Soil Science, 36: 299-306.

Davis, P.F. and Dexter, A.R. 1972. Two methods for quantitative description of soil particle shape. Journal of Soil Science, 23: 448-455.

deBisschop, F.R.E. and Rigole, W.J.L. 1982. A physical model for liquid capillary bridges between adsorptive solid spheres: the nodoid of plateau. Journal of Colloid and Interface Science, 88: 117-128.

Denisov,N.Y. and Reltov, B.F. 1961. The influence of certain processes on the strength of soils. Proceedings Fifth International Conference on Soil Mechanics and Foundation Engineering. (Paris), I: 75-78.

Deresiewicz, H. 1958. Mechanics of granular matter. Advances in Applied Mechanics, 5: 233-306.

Deshpande, T.L., Greenland, D.J. and Quirk, J.P. 1964. Role of iron oxides in bonding of soil particles. Nature (London), 201: 107-108.

Dettmann, M.G. 1958. Water uptake by pure clays and soil crumbs. Journal of Soil Science, 9: 306-315.

Dexter, A.R. 1975. Uniaxial compression of ideal brittle tilths. Journal of Terramechanics, 12: 3-14.

Dexter, A.R. 1977. Effect of rainfall on the surface micro-relief of tilled soil. Journal of Terramechanics, 14: 11-22.

Dexter, A.R. 1979. Prediction of soil structures produced by tillage. Journal of Terramechanics, 16: 117-127.

Dexter, A.R. 1983. Two types of soil anisotropy induced by the passage of a wetting front. Soil Science Society of America Journal, 47: 1060-1061.

Dexter, A.R. 1985. Shapes of aggregates from tilled layers of some Dutch and Australian soils. Geoderma, 35: 91-107.

Dexter, A.R. 1986. Model experiments on the behaviour of roots at the interface between a tilled seed-bed and a compacted sub-soil. II. Entry of pea and wheat roots into sub-soil cracks. Plant and Soil, 95: 135-147.

Dexter, A.R. 1988a. Advances in characterization of soil structure. Soil and Tillage Research, 11: 199-238.

Dexter, A.R. 1988b. Strength of soil aggregates and of aggregate beds. Catena Supplement, 11: 35-52.

Dexter, A.R. 1988c. Soil amelioration by natural processes. pp. 431-448. in Proceedings Symposium entitled: Soil Management '88. held 19-21 September, 1988. Darling Downs Institute of Advanced Education. Toowoomba, Queensland.

Dexter, A.R. and Horn, R. 1988. Effects of land use and clay content on soil structure as measured by fracture surface analysis. Zeitschrift für Pflanzenernährung und Bodenkunde, 151: 325-330. (In English, with German Figures, tables and summary).

Dexter, A.R., Horn, R. and Kemper, W.D. 1988. Two mechanisms for age hardening of soil. Journal of Soil Science, 39: 163-175.

Dexter, A.R. and Kroesbergen, B. 1985. Methodology for determination of tensile strength of soil aggregates. Journal of Agricultural Engineering Research, 31: 139-147.

Dexter, A.R., Kroesbergen, B. and Kuipers, H. 1984. Some mechanical properties of aggregates of topsoils from the IJsselmeer polders. 2. Remoulded soil aggregates and the effects of wetting and drying cycles. Netherlands Journal of Agricultural Science, 32: 215-227.

Dexter, A.R. and Tanner, D.W. 1972. Packing densities of mixtures of spheres with log-normal size distributions. Nature Physical Science, 238(80): 31-32. July 10, 1972.

Dexter, A.R. and Tanner, D.W. 1973. The force on spheres penetrating soil. Journal of Terramechanics, 9: 31-39.

Dexter, A.R. and Woodhead, T. 1985. Soil mechanics in relation to tillage, implements, and root penetration in lowland soils. pp261-281 in Soil Physics and Rice. International Rice Research Institute, Los Baños, Philippines. (Proceedings of International Workshop on "Physical Aspects of Soil Management In Rice-based Cropping Systems" (P.A.S.M.I.R.C.S.)

Dixit, V.K. and Awasthi, R.K. 1971. Effect of wetting and drying on soil aggregation. Labdev Journal of Science and Technology (Part B), 9: 235-236.

Donald, I.B. 1961. Discussion pp.69-70 in Pore Pressure and Suction in Soils. Proceedings Conference of the International Society of Soil Mechanics and Foundation Engineering. March 30-31, 1960. Butterworths, London.

Douglas, A.G. 1967. Tensile strength of granular materials. Nature, 215(5104): 952-953.

Dowdy, R.H. and Larson, W.E. 1971. Tensile strength of montmorillonite as a function of saturating cation and water content. Soil Science Society of America Proceedings, 35:1010-1014.

Ellis, F.B., Christian, D.G. and Cannell, R.Q. 1982. Direct drilling, shallow tine-cultivation and ploughing on a silt loam soil, 1974-1980. Soil and Tillage Research, 2: 115-130.

Emerson, W.W. 1954a. The effect of various grasses and lucerne on the cohesion of soil crumbs. Transactions Fifth Congress of Soil Science. Léopoldville, France, 2: 65-68.

Emerson, W.W. 1954b. The determination of the stability of soil crumbs. Journal of Soil Science, 5: 233-250.

Emerson, W.W. 1955. The rate of water uptake of soil crumbs at low suctions. Journal of Soil Science, 6: 147-159

Emerson, W.W. 1964. The slaking of soil crumbs as influenced by clay mineral composition. Australian Journal of Soil Research, 2: 211-217.

Emerson, W.W. 1968. The dispersion of clay from soil aggregates. Transactions Ninth International Congress of Soil Science, Adelaide, Australia. 1: 617-626.

Emerson, W.W. 1973. Soil tilth and aggregation. pp 39-43. in Physical Aspects of Swelling Clay Soils. Proceedings of symposium held at University of New England, Armidale, New South Wales, February, 1972.

Emerson, W.W. 1977. Physical properties and structure. pp 78-104. in J.S. Russell and E.L. Greacen (Eds.) Soil Factors in Crop Production in a Semi-Arid Environment. University of Queensland Press. St. Lucia, Queensland.

Emerson, W.W. 1979. Interparticle bonding in soil colloids. pp 4.1-4.11. in D.E. Yates (Ed.) Colloids in Soils- Principles and Practices. Proceedings of Symposium held by Royal Australian Chemical Institute, Division of Colloid and Surface Chemistry; at the Waite Agricultural Research Institute, Adelaide. September 27-28, 1979.

Emerson, W.W. and Dettmann, M.G. 1959. The effect of organic matter on crumb structure. Journal of Soil Science, 10: 227-234.

Emerson, W.W. and Grundy, G.M.F. 1954. The effect of rate of wetting on water uptake and cohesion of soil crumbs. Journal of Agricultural Science, 44: 249-253.

Fagi, A.M. and De Datta, S.K. 1983. Physical properties of rainfed wetland rice soils as affected by cropping system and crop residue management. Field Crops Research, 6: 189-204.

Farrell, D.A., Greacen, E.L. and Larson, W.E. 1967. The effect of water content on axial strain in a loam soil under tension and compression. Soil Science Society of America Proceedings, 31:445-450.

Fippin, E.O. 1910. Some causes of soil granulation. Proceedings of the American Society of Agronomy, 2: 106-121.

Fisher, R.A. 1926. On the capillary forces in an ideal soil; correction of formulae given by W.B. Haines. Journal of Agricultural Science, 16: 492-505.

Fisher, R.A. 1928. Further note on the capillary forces in an ideal soil. Journal of Agricultural Science, 18: 406-410.

Foster, R.C. 1981. Polysaccharides in soil fabrics. Science, 214: 665-667.

Fountaine, E.R. 1954. Investigation into the mechanism of soil adhesion. Journal of Soil Science, 5: 251-263.

Frydman, S. 1964. The applicability of the Brazilian (indirect tension) test to soils. Australian Journal of Applied Science, 15: 335-343.

Fujioka, Y., and Sato, K. 1968a. On the drying of clayey paddy field I. Transactions of the Japanese Society of Irrigation, Drainage and Rural Engineering, September 1968: 21-26. (In Japanese with English figures and summary).

Fujioka, Y., and Sato, K. 1968b. On the drying of clayey paddy field II.Transactions of the Japanese Society of Irrigation, Drainage and Rural Engineering, December, 1968: 1-14. (In Japanese with English summary).

Gerard, C.J. 1965. The influence of soil moisture, soil texture, drying conditions and exchangeable cations on soil strength. Soil Science Society of America Proceedings, 29: 641-645.

Gerard, C.J., Cowley, W.R., Burleson, C.A. and Bloodworth, M.E. 1962. Soil hardpan formation as affected by rate of moisture loss, cyclic wetting and drying and surface applied forces. Soil Science Society of America Proceedings, 26: 601-605.

Gifford, R.O. and Thran, D.F. 1974. Bonding mechanisms for soil crusts. Part II. Strength of silica cementation. pp. 28-30 in J.W. Cary and D.D. Evans (Eds.) Soil Crusts. University of Arizona Agricultural Research Station, Technical Bulletin 214.

Gill, W.R. 1959. The effects of drying on the mechanical strength of Lloyd clay. Soil Science Society of America Proceedings, 23: 255-257.

Gill, W.R. 1971. Economic assessment of soil compaction. pp 431-458. in K.K. Barnes, W.M. Carleton, H.M. Taylor, R.I. Throckmorton and G.E. Vanden Berg (Eds.) Compaction of Agricultural Soils. American Society of Agricultural Engineers, Monograph. St. Joseph, Michigan.

Gill, W.R. and McCreery, W.F. 1960. Relation of size of cut to tillage tool efficiency. Agricultural Engineering, 41:372-374, 381.

Gilmore, R.E. and Nicholls, J.H.H. 1937. Significance of friability and size stability tests on coal. Proceedings of the American Society for Testing Materials, 37: 421-440.

Giovanni, G. and Sequi, P. 1976. Iron and aluminium as cementing substances of soil aggregates I. Acetylacetone in benzene as an extractant of fractions of soil iron and aluminium. Journal of Soil Science, 27: 140-147.

Gobran, G.R., Dufey, J.E. and Laudelout, H. 1982. The use of gypsum for preventing soil sodification: Effect of gypsum particle size and location in the profile. Journal of Soil Science, 33: 309-316.

Gramberg, J. 1966. The axial cleavage fracture-1. Axial cleavage fracturing, a significant process in mining geology. Engineering Geology, 1: 31-72.

Grant, C.D., Kay, B.D., Groenevelt, P.H., Kidd, G.E., and Thurtell, G.W. 1985. Spectral analysis of micropenetrometer data to characterize soil structure. Canadian Journal of Soil Science, 65: 789-804.

Graton, L.C. and Fraser, H.J. 1935. Systematic packing of spheres- with particular relation to porosity and permeability. Journal of Geology, 43(8/1): 785-908.

Greacen, E.L. 1958. The soil structure profile under pastures. Australian Journal of Agricultural Research, 9: 129-137.

Greacen, E.L. 1960. Aggregate strength and soil consistence. Transactions Seventh International Congress of Soil Science, Madison, U.S.A., 1: 256-264.

Greacen, E.L. 1983. Tillage research in a semi-arid environment. Soil and Tillage Research, 3: 107-109.

Green, R. 1967. The spectrum of a set of measurements along a profile. Engineering Geology, 2: 163-168.

Green, W.H. and Ampt, G.A. 1911. Studies on soil physics. Part I. The flow of air and water through soils. Journal of Agricultural Science, 4: 1-24.

Greenland, D.J. 1977. Soil damage by intensive arable cultivation: temporary or permanent?. Philosophical Transactions of the Royal Society, London. Series B. 281: 193-208.

Greenland, D.J. 1979. Structural organization of soils and crop production. pp. 47-56. in R. Lal and D.J. Greenland (Eds.). Soil Physical Properties and Crop Production in the Tropics. John Wiley. New York.

Greenland, D.J. 1981. Soil management and soil degradation. Journal of Soil Science, 32: 301-322.

Greenland, D.J., Lindstrom, G.R. and Quirk, J.P. 1962. Organic materials which stabilize natural soil aggregates. Soil Science Society of America Proceedings, 26: 366-371.

Grevers, M.C.J. and Bomke, A.A. 1986. Tillage practices on a northern clay soil: Effects of sod breaking methods on crop production and soil physical properties. Canadian Journal of Soil Science, 66: 385-395.

Griffith, A.A. 1921. The phenomena of rupture and flow in solids. Philisophical Transactions of the Royal Society of London. Series A, 221: 163-198.

Griffith, A.A. 1924. The theory of rupture. Proceedings First Congress for Applied Mechanics, Delft, 1924: 55-63. (Edited by C.B. Biezeno and J.M. Burgers).

Groenevelt, P.H. and Kay, B.D. 1981. On pressure distribution and effective stress in unsaturated soils. Canadian Journal of Soil Science, 61: 431-443.

Hadas, A. 1987. Long term tillage practice effects on soil aggregation modes and strength. Soil Science Society of America Journal, 51: 191-197.

Hadas, A. and Wolf, D. 1983. Energy efficiency in tilling dry clod-forming soils. Soil and Tillage Research, 3: 47-59.

Hadas, A. and Wolf, D. 1984a. Refinement and re-evaluation of the drop-shatter soil fragmentation method. Soil and Tillage Research, 4: 237-249.

Hadas, A. and Wolf, D. 1984b. Soil aggregates and clod strength dependence on size, cultivation and stress load rate. Soil Science Society of America Journal, 48: 1157-1164.

Haines, W.B. 1925. Studies in the physical properties of soils. II. A note on the cohesion developed by capillary forces in an ideal soil. Journal of Agricultural Science, 15: 529-535.

Håkansson, I. 1985. Swedish experiments on subsoil compaction by vehicles with high axle load. Soil Use and Management, 1(4): 113-116.

Håkansson, I., and Danfors, B. 1981. Effects of heavy traffic on soil conditions and crop growth. Proceedings Seventh International Conference of the International Society for Terrain-Vehicle Systems, 1: 239-253.

Håkansson, I., Voorhees, W.B., Elonen, P., Raghavan, G.S.V., Lowery, B., Van Wijk, A.L.M., Rasmussen, K. and Riley, H. 1987. Soil and Tillage Research, 10: 259-268.

Hallaire, V. 1988. La fissuration d'un soil argileux au cours du dessechement. II. Modélasation morphologique. (Cracking of a clayey soil during shrinkage. II. Morphological Model). Agronomie, 8: 273-280. (In French with English summary, figures and appendix).

Hallet, F.R., Speight, P.A. and Stinson, R.H. 1977. Introductory Biophysics. Methuen, Toronto.

Hamblin, A.P. and Davies, D.B. 1977. Influence of organic matter on the physical properties of some East Anglian soils of high silt content. Journal of Soil Science, 28: 11-22.

Hanks, R.J. and Thorp, F.C. 1957. Seedling emergence of wheat, grain sorghum, and soybeans as influenced by soil crust strength and moisture content. Soil Science Society of America Proceedings, 21: 357-359.

Harris, R.F., Allen, O.N., Chesters, G. and Attoe, O.J. 1963. Evaluation of microbial activity in soil aggregate stabilization and degradation by the use of artificial aggregates. Soil Science Society of America Proceedings, 27: 542-545.

Harris, R.F., Chesters, G., Allen, O.N. and Attoe, O.J. 1964. Mechanisms involved in soil aggregate stabilization by fungi and bacteria. Soil Science Society of America Proceedings, 28: 529-532.

Hayes, M.H.B. and Swift, R.S. 1978. The chemistry of soil organic colloids. pp 179-320. in D.J. Greenland and M.H.B. Hayes (Eds.) The Chemistry of Soil Constituents. John Wiley, New York.

Heinonen, R. 1954. Moisture conditions in Finnish topsoils. Agrogeologisia Fulk., 62: 1-82.

Heinonen, R. 1982. Alleviation of soil compaction by natural forces and cultural practices. 24p. in Proceedings of the International Conference on Land Clearing and Development, at the International Institute of Tropical Agriculture, Ibadan, Nigeria. November 23-26, 1982.

Hénin, S. 1936. Etude sur la régénération des 'éléments structuraus' des sols de limon. (Study on the regeneration of soil structure in loams). Annales Agronomiques (old series), 6: 455-472. (In French).

Hettiaratchi, D.R.P. and O'Callaghan, J.R. 1980. Mechanical behaviour of agricultural soils. Journal of Agricultural Engineering Research, 25: 239-259.

Hillel, D. 1980. Fundamentals of Soil Physics. Academic Press. New York.

Huang, C., White, I., Thwaite, E.G. and Bendeli, A. 1988. A noncontact laser system for measuring soil surface topography. Soil Science Society of America Journal, 52: 350-355.

Hubbell, D.S. and Chapman, J.E. 1946. The genesis of structure in two calcareous soils. Soil Science, 62: 271-281.

Hubble, G.D. 1984. The cracking clay soils: definition, distribution, nature, genesis and use. pp 3-13. in J.W. McGarity, E.H. Hoult and H.B. So (Eds.) The Properties and Utilization of Cracking Clay Soils. (Reviews in Rural Science 5). Proceedings Symposium held at University of New England, Armidale, New South Wales. 24-28 August, 1981.

Hundal, S.S. and De Datta, S.K. 1984. Water table and tillage effects on root distribution, soil water extraction, and yield of sorghum grown after wetland rice in a tropical soil. Field Crops Research, 9: 291-303.

Hunter, R.J. 1987. Foundations of Colloid Science. Volume I. Clarendon Press, Oxford.

Ibanga, I.J., Bidwell, O.W., Powers, W.L., Feyerherm, A.M. and Williams, W.W. 1980. Soil consistence: effect of particle size. Soil Science Society of America Journal, 44: 1124-1126.

Ingles, O.G. 1962a. Bonding forces in soils. I. Natural soils- The physical factors responsible for cohesive strength. Proceedings of the Australian Road Research Board, I(2): 999-1013.

Ingles, O.G. 1962b. Bonding forces in soils. II. Stabilized soils- The chemical and physical reactions responsible for strength development. Proceedings of the Australian Road Research Board, I(2): 1014-1024.

Ingles, O.G. 1962c. Bonding forces in soils. III. A theory of tensile strength for stabilized and naturally coherent soils. Proceedings of the Australian Road Research Board, I(2): 1025-1047.

Ingles, O.G. 1963. The shatter test as an index of strength for soil aggregates. Tewksbury Symposium on Fracture. 1963: 284-303. Commonwealth Scientific and Industrial Research Organization, Syndal, Victoria.

Ingles, O.G. 1964. The nature and strength of interparticle bonds in natural and stabilized soils. D3:9-16 in "Mechanisms of Soil Stabilization". Proceedings of a colloquium convened by the Soil Mechanics Section, Commonwealth Scientific and Industrial Research Organization, Syndal, Victoria. April 6-8, 1964.

Ingles, O.G. 1968. Advances in soil stabilization, 1961-1976. Reviews of Pure and Applied Chemistry, 18: 291-310.

Ingles, O.G. 1970. Mechanisms of clay stabilization with inorganic acids and alkalis. Australian Journal of Soil Research, 8: 81-95.

Ingles, O.G. and Frydman, S. 1963. An examination of some methods for strength measurement in soils. Proceedings Fourth Australia-New Zealand Conference on Soil Mechanics and Foundation Engineering. Adelaide. August 19-23, 1963. 213-219.

Ingles, O.G. and Frydman, S. 1966. The effect of cement and lime on the strength of some soil minerals, and its relevance to the stabilization of Australian soils. Proceedings Third Conference of the Australian Road Research Board, 3(2): 1504-1528.

Ingles, O.G. and Lafeber, D. 1966. The influence of volume defects on the strength and strength-isotropy of stabilized clays. Engineering Geology, 1: 305-310.

Ingles, O.G. and Lafeber, D. 1967. "The initiation and development of crack and joint systems in granular masses". Paper No. 7 of the Proceedings of the Symposium on Stress and Failure Around Underground Openings, held at the Department of mining engineering, University of Sydney. March 1-2, 1967. Commonwealth Scientific and Industrial Research Organization, Research Paper No. 97: 22p.

Inglis, C.E. 1913. Stresses in a plate due to the presence of cracks and sharp corners. Transactions of the Institution of Naval Architects, 55(1): 219-230 (with discussion pp231-241).

Innes, W.B. 1957. Use of a parallel plate model in calculation of pore size distribution. Analytical Chemistry, 29: 1069-1073.

I.R.R.I., 1978. Soils and Rice. International Rice Research Institute. Los Baños, Philippines.

Irwin, G.R. 1957. Analysis of stresses and strains near the end of a crack traversing a plate. Journal of Applied Mechanics, 24: 361-364.

Jaeger, J.C. 1956. Elasticity, Fracture and Flow. (with Engineering and Geological Applications. Methuen, London.

Jeffrey, D.W. 1970. A note on the use of ignition loss as a means for the approximate estimation of soil bulk density. Journal of Ecology, 58: 297-299.

Jenkins, G.M. and Watts, D.G. 1968. Spectral Analysis and its Application. Second Edition. Holden-Day. San Francisco.

Johnson, W.C. 1962. Controlled soil cracking as a possible means of moisture conservation on wheatlands of the southwestern great plains. Agronomy Journal, 54: 323-325.

Johnston, J.R. and Hill, H.O. 1944. A study of the shrinking and swelling properties of Rendzina soils. Soil Science Society of America Proceedings, 9: 24-29.

Jones, R. and Kaplan, M.F. 1957. The effect of coarse aggregate on the mode of failure of concrete in compression and flexure. Magazine of Concrete Research, August: 89-94.

Jumikis, A.R. 1984. Soil Mechanics. Krieger Publishing Co., Malabar, Florida.

Kahlweit, M. 1975. Ostwald ripening of precipitates. Advances in Colloid and Interface Science, 5: 1-35.

Kaplan, M.F. 1961. Crack propagation and the fracture of concrete. Journal of the American Concrete Institute, 58: 591-610.

Kay, B.D., Grant, C.D. and Groenevelt, P.H. 1985. Significance of ground freezing on soil bulk density under zero tillage. Soil Science Society of America Journal, 49: 973-978.

Keer, L.M. 1966. A note on shear and combined loading for a penny-shaped crack. Journal of the Mechanics and Physics of Solids, 14: 1-6.

Kemper, W.D. 1958. Structural implications of moisture retention by clay-size soil materials. Soil Science Society of America Proceedings, 22: 5-8.

Kemper, W.D., Evans, D.D. and Hough, H.W. 1974. Crust strength and cracking. Part I. Strength. pp. 31-38. in J.W. Cary and D.D. Evans (Eds.) Soil Crusts. University of Arizona Agricultural Research Station, Technical Bulletin 214.

Kemper, W.D. and Rosenau, R.C. 1984. Soil cohesion as affected by time and water content. Soil Science Society of America Journal, 48: 1001-1006.

Kemper, W.D., Rosenau, R.C. and Dexter, A.R. 1987. Cohesion development in disrupted soils as affected by clay and organic matter content and temperature. Soil Science Society of America Journal, 51: 860-867.

Kirkham, D., DeBoodt, M.F. and DeLeenheer, L. 1959. Modulus of rupture determination on undisturbed soil core samples. Soil Science, 87: 141-144.

Koenigs, F.F.R. 1963. The puddling of clay soils. Netherlands Journal of Agricultural Science, 11: 145-156.

Kolodny, L. and Joffe, J.S. 1939. Soil aggregation and permeability: the relation between moisture content and the micro-aggregation or the degree of dispersion in soil. Soil Science Society of America Proceedings, 4: 7-12.

Kooistra, M.J., Bouma, J., Boersma, O.H. and Jager, A. 1985. Soil structure differences and associated physical properties of some loamy typic Fluvaquents in the Netherlands. Geoderma, 36: 215-228.

Koolen, A.J. and Kuipers, H. 1983. Agricultural Soil Mechanics. Springer-Verlag. New York.

Koolen, A.J. and Vaandrager, P. 1984. Relationships between soil mechanical properties. Journal of Agricultural Engineering Research, 29: 313-319.

Kousaka, Y., Okuyama, K. and Payatakes, A.C. 1981. Physical meaning and evaluation of dynamic shape factor of aggregate particles. Journal of Colloid and Interface Science, 84: 91-99.

Kruyer, S. 1958. The penetration of mercury and capillary condensation in packed spheres. Transactions of the Faraday Society, 54: 1758-1767.

Kuipers, H. 1980. Processes in physical soil degradation in mechanized agriculture. pp7-18 in D. Boels, D.B. Davies and A.E. Johnston (Eds.). Soil Degradation. Proceedings of the land use seminar on soil degradation. Wageningen. October13-15, 1980. A.A. Bakema. Rotterdam.

Kuipers, H. 1984. The challenge of soil cultivations and soil water problem. Journal of Agricultural Engineering Research, 29: 177-190.

Kurtay, T. and Reece, A.R. 1970. Plasticity theory and critical state soil mechanics. Journal of Terramechanics, 7: 23-56.

Lachenbruch, A.H. 1961. Depth and spacing of tension cracks. Journal of Geophysical Research, 66: 4273-4292.

Larson, W.E. and Allmaras, R.R. 1971. Management factors and natural forces as related to compaction. pp. 367-427. in K.K. Barnes, W.M. Carleton, H.M. Taylor, R.I. Throckmorton and G.E. Vanden Berg (Eds.) Compaction of Agricultural Soils. American Society of Agricultural Engineers, Monograph. St. Joseph, Michigan.

Lehrsch, G.A., Whisler, F.D. and Römkens, M.J.M. 1987. Soil surface roughness as influenced by selected soil physical properties. Soil and Tillage Research, 10: 197-212.

Lehrsch, G.A., Whisler, F.D. and Römkens, M.J.M. 1988. Spatial variation of parameters describing soil surface roughness. Soil Science Society of America Journal, 52: 311-319.

Litchfield, W.H. 1951. Soil survey of the Waite Agricultural Research Institute. Commonwealth Scientific and Industrial Research Organization, Division of Soils, Divisional Report 2/51.

Loveday, J. 1974. Recognition of gypsum responsive soils. Australian Journal of Soil Research, 12: 87-96.

Loveday, J. 1976. Relative significance of electrolyte and cation exchange effects when gypsum is applied to a sodic clay soil. Australian Journal of Soil Research, 14: 361-371.

Loveday, J., Saunt, J.E., Fleming, P.M. and Muirhead, W.A. 1970. Soil and cotton responses to tillage and ameliorant treatments in a brown clay soil. I. Soil responses and water use. Australian Journal of Experimental Agriculture and Animal Husbandry, 10: 313-324.

Loveday, J. and Scotter, D.R. 1966. Emergence response of subterranean clover to dissolved gypsum in relation to properties and evaporative conditions. Australian Journal of Soil Research, 4: 55-68.

Low, A.J. 1955. Improvement of the structural state of soils under leys. Journal of Soil Science, 6: 179-199.

Low, A.J. 1972. The effect of cultivation on the structure and other physical characteristics of grasslands and arable soils (1945-1970). Journal of Soil Science, 23: 363-380.

MacEwen, D.M.C. 1948. Adsorption by montmorillonite, and its relation to surface adsorption. Nature, 162: 935-936.

MacEwen, D.M.C. 1954. Short-range electrical forces between charged colloid particles. Nature, 174: 39-40.

Madelung, E. 1918. Das elektrische feld in systemen von regelmäßig angeordmeten punktladungen. Physikalische Zeitschrift, Leipzig, 19(23): 524-533. (In German).

Mandal, L.N. 1984. Soil research in relation to rice. Journal of the Indian Society of Soil Science, 32: 575-582.

Mandelbrot, B.B. 1977. Fractals. Freeman and Co. San Francisco.

Marshall, T.J. and Quirk, J.P. 1950. Stability of structural aggregates of dry soil. Australian Journal of Agricultural Research, 1: 266-275.

Martin, J.P. 1945. Microorganisms and soil aggregation: I. Origin and nature of some of the aggregating substances. Soil Science, 59: 163-174.

Martin, J.P. 1946. Microorganisms and soil aggregation: II. Influence of bacterial polysaccharides on soil structure. Soil Science, 61: 157-162.

Martin, J.P., Martin, W.P., Page, J.B., Raney, W.A. and De Mint, J.D. 1955. Soil aggregation. Advances in Agronomy, 7: 1-37.

Matheron, G. 1963. Principles of geostatistics. Economic Geology, 58: 1246-1266.

Mazurak, A.P. 1950. Effect of gaseous phase on water-stable synthetic aggregates. Soil Science, 69: 135-148.

McDonald, D.C. and Julian, R. 1966. Quantitative estimation of soil total porosity and macro-porosity as part of the pedological description. New Zealand Journal of Agricultural Research, 8: 927-946.

McGeorge, W.T. 1937. Studies on soil structure: Some physical characteristics of puddled soils. University of Arizona Agricultural Experiment Station, Technical Bulletin 67: 127-177.

McGowan, M., Wellings, S.R. and Fry, G.J. 1983. The structural improvement of damaged clay subsoils. Journal of Soil Science, 34: 233-248.

McHenry, J.R. and Russell, M.B. 1943. Soil aggregation: Elementary mechanics of aggregation of puddled materials. Soil Science Society of America Proceedings, 8: 71-78.

McKenzie, B.M. and Dexter, A.R. 1985. Mellowing and anisotropy induced by wetting of moulded soil samples. Australian Journal of Soil Research, 23: 37-47.

McKenzie, B.M. and Dexter, A.R. 1988a. Axial pressures generated by the earthworm *Aporrectodea rosea*. Biology and Fertility of Soils, 5: 323-327.

McKenzie, B.M. and Dexter, A.R. 1988b. Radial pressures generated by the earthworm *Aporrectodea rosea*. Biology and Fertility of Soils, 5: 328-332.

Mehta, N.C., Streuli, H., Müller, M. and Deuel, H. 1960. Role of polysaccharides in soil aggregation. Journal of the Science of Food and Agriculture, 11: 40-47.

Miller, E.E. and Miller, R.D. 1956. Physical theory for capillary flow phenomena. Journal of Applied Physics, 27: 324-332.

Misra, R.K., Dexter, A.R. and Alston, A.M. 1986. Maximum axial and radial growth pressures of plant roots. Plant and Soil, 95: 315-326.

Mitchell, J.K. 1960. Fundamental aspects of thixotropy in soils. Journal of the Soil Mechanics and Foundations Division, American Society of Civil Engineers, 86(SM3): 19-52. (Paper No. 2522).

Mitchell, J.K. 1976. Fundamentals of Soil Behaviour. John Wiley, New York.

Molope, M.B., Grieve, I.C. and Page, E.R. 1985. Thixotropic changes in the stability of molded soil aggregates. Soil Science Society of America Journal, 49: 979-983.

Monnier, G. and Goss, M.J. 1987. (Eds.) Soil Compaction and Regeneration. Proceedings of the workshop on "Soil Compaction: Consequences and Structural Regeneration Processes". held in Avignon, September 17-18, 1985. A.A. Balkema. Rotterdam.

Moormann, F.R. and van Breemen, N. 1978. Rice: Soil, Water, Land. International Rice Research Institute. Los Baños, Philippines.

Mualem, Y. and Morel-Seytoux, H.J. 1979. Capillary Pressure. pp49-61. in R.W. Fairbridge and C.W. Finkl, Jnr. (Eds.). The Encyclopaedia of Soil Science, Part 1, Physics, Chemistry, Biology, Fertility, and Technology. Dowden, Hutchinson and Ross. Stroudsburg, Pennsylvania.

Mullins, C.E. and Panayiotopoulos, K.P. 1984. The strength of unsaturated mixtures of sand and kaolin and the concept of effective stress. Journal of Soil Science, 35: 459-468

Murray, R.S. and Quirk, J.P. (in press) Interparticle forces in relation to the stability of soil aggregates. International Soil Science Society, Commission II. The Nature and Properties of Soil Colloids. Ghent, Belgium. 1984.

Nagahori, K. and Sato, K. 1970. On the slaking behaviour of the sea bottom clayey soil after receiving repeated drying and wetting. I. The Scientific Reports of the Faculty of Agriculture, Okayama University, 35: 81-87. Okayama, Japan. (In Japanese with English summary and figures).

Nagahori, K. and Sato, K. 1974. Effect on the structural characteristics of mud soil as the cyclic drying and wetting, and the concentration of soil salt -- Studies on agricultural land consolidation of the mud soil area after land drainage of Kasaoka bay polder I. Transactions of the Japanese Society of Irrigation, Drainage and Rural Engineering, December 1974: 1-5. (In Japanese with English summary and figures).

Nichols, M.L. 1931. The dynamic properties of soil. I. An explanation of the dynamic properties of soils by means of colloidal films. Agricultural Engineering, 12: 259-264.

Nikiforoff, C.C. 1941. Morphological classification of soil structure. Soil Science, 52: 193-207.

Oades, J.M. 1976. Prevention of crust formation in soils by poly(vinyl alcohol). Australian Journal of Soil Research, 14: 139-148.

Oades, J.M. 1984. Soil organic matter and structural stability: mechanisms and implications for management. Plant and soil, 76: 319-337.

Oades, J.M. 1986. Associations of colloidal materials in soils. Transactions Thirteenth International Society of Soil Science, Hamburg, West Germany, 6: 660-674.

O'Callaghan, J.F. and Loveday, J. 1973. Quantitative measurement of soil cracking patterns. Pattern Recognition, 5: 83-98.

Odell, R.T., Thornburn, T.H. and McKenzie, L.J. 1960. Relationships of Atterberg limits to some other properties of Illinois soils. Soil Science Society of America Proceedings, 124: 297-300.

Ojeniyi, S.A. and Dexter. A.R. 1979. Soil factors affecting the macrostructures produced by tillage. Transactions of the American Society of Agricultural Engineers, 22: 339-343.

Olson, R.E. 1963. Effective stress theory of soil compaction. Journal of the Soil Mechanics and Foundations Division, Proceedings of the American Society of Civil Engineers, 89(SM2): 27-45.

Panabokke, C.R. and Quirk, J.P. 1957. Effect of initial water content on stability of soil aggregates in water. Soil Science, 83: 185-195.

Penner, E. 1968. Particle size as a basis for predicting frost action in soils. Soils and Foundations, 8: 21-29.

Perry, C. and Gillott, J.E. 1977. The influence of mortar-aggregate bond strength on the behaviour of concrete in uniaxial compression. Cement and Concrete Research, 7: 553-564.

Peterson, J.B. 1943. Formation of water-stable structure in puddled soils. Soil Science, 55: 289-300.

Peterson, J.B. 1947. Calcium linkage, a mechanism in soil granulation. Soil Science Society of America Proceedings, 12: 29-34.

Pillsbury, A.F. and Appleman, D. 1945. Factors in permeability changes of soils and inert granular material. Soil Science, 59: 115-123.

Porter, L.K., Kemper, W.D., Jackson, R.D. and Stewart, B.A. 1960. Chloride diffusion in soils as influenced by moisture content. Soil Science Society of America Proceedings, 24: 460-463.

Probert, M.E., Fergus, I.F., Bridge, B.J., McGarry, D., Thompson, C.H., and Russell, J.S. 1987. The properties and management of vertisols. Commonwealth Agricultural Bureau International. 36p.

Puri, A.N., Asghar, A.G. and Dua, A.N. 1940. Physical characteristics of soils: VI. Influence of clay, exchangeable bases, and hygroscopic moisture on soil cohesion. Soil Science, 49: 239-249.

Quirk, J.P. 1950. The water stability of soil aggregates in relation to the water content at time of wetting. Commonwealth Scientific and Industrial Research Organization, Division of Soils, Report 12/50. pp7.

Quirk, J.P. 1960. Negative and positive adsorption by kaolinite. Nature, 188: 253-254.

Quirk, J.P. 1963. The role of surface forces in determining the physical behaviour of soils and clays. Proceedings Fourth Australia-New Zealand Conference on Soil Mechanics and Foundation Engineering. 205-212.

Quirk, J.P. and Panabokke, C.R. 1962. Incipient failure of soil aggregates. Journal of Soil Science, 13: 60-70.

Quirk, J.P. and Schofield, R.K. 1955. The effect of electrolyte concentration on soil permeability. Journal of Soil Science, 6: 163-178.

Rengasamy, P. 1983. Clay dispersion in relation to changes in the electrolyte composition of dialysed red-brown earths. Journal Soil Science, 34: 723-732.

Rengasamy, P., Greene, R.S.B. and Ford, G.W. 1984. The role of clay fraction in the particle arrangement and stability of soil aggregates- A review. Clay Research, 3: 53-67.

Richards, L.A. 1953. Modulus of rupture as an index of crusting of soil. Soil Science Society of America Proceedings, 17: 321-323.

Robinson, D.O. and Page, J.B. 1950. Soil aggregate stability. Soil Science Society of America Proceedings, 15: 25-29.

Rogowski, A.S. and Kirkham, D. 1976. Strength of soil aggregates: influence of size, density and clay and organic matter content. In M. deBoodt and D. Gabriels (Eds.) Third International Symposium on Soil Conditioning, Gent, Sept. 8-12, 1975. Mededelingen van de Faculteit Landbouwwetenschappen Rijksuniversiteit Gent 41(1): 85-100.

Rogowski, A.S., Moldenhauer, W.C. and Kirkham, D. 1968. Rupture parameters of soil aggregates. Soil Science Society of America Proceedings, 32:720-724.

Römkens, M.J.M., Singarayar, S., and Gantzer, C.J. 1986. An automated noncontact surface profile meter. Soil and Tillage Research, 6: 193-202.

Römkens, M.J.M., Wang, J.Y. and Darden, R.W. 1988. A laser microreliefmeter. Transactions American Society Agricultural Engineers, 31: 408-413.

Rowe, P.W. 1962. The stress-dilatancy relation for static equilibrium of an assembly of particles in contact. Proceedings of the Royal Society of London, Series A, 269: 500-527.

Russell, E.W. 1938. Soil Structure. Imperial Bureau of Soil Science. Technical Communication, Number 37: 1-40. Harpenden, England.

Russell, E.W. and Tamhane, R.V. 1940. The determination of the size distribution of soil clods and crumbs. Journal of Agricultural Science, 30: 210-234.

Salter, R.M. 1925. Climatic agencies in their relation to soil colloids. Journal of the American Society of Agronomy, 17: 294-307.

Sanchez, P.A. 1973. Puddling tropical rice soils:I. Growth and nutritional aspects. Soil Science, 115: 149-158.

Sanchez, P.A. 1973. Puddling tropical rice soils. II. Effects of soil water losses. Soil Science, 115: 303-308.

Sanchez, P.A. 1979. Puddling. pp 406-409. in R.W. Fairbridge and C.W. Finkl, Jr. (Eds.). The Encyclopaedia of Soil Science. Part 1. Physics, Chemistry, Biology, Fertility and Technology. Dowden, Hutchinson and Ross. Stroudsburg, Pennsylvania.

Sato, K. 1969. Changes of the shrinkage and slaking properties of clayey soils as an effect of repeated drying and wetting. Transactions of the Japanese Society of Irrigation, Drainage and Rural Engineering, June 1969: 12-16. (In Japanese, with English summary and figures).

Schofield, R.K. and Samson, H.R. 1954. Flocculation of kaolinite due to the attraction of oppositely charged crystal faces. Discussions of the Faraday Society, 18: 135-145.

Sequi, P. 1978. Soil structure: an outlook. Agrochimica, 22: 403-425.

Shanmuganathan, R.T. and Oades, J.M. 1983a. Influence of anions on dispersion and physical properties of the A horizon of a red-brown earth. Geoderma, 29: 257-277.

Shanmuganathan, R.T. and Oades, J.M. 1983b. Modification of soil physical properties by addition of calcium compounds. Australian Journal of Soil Research, 21: 285-300.

Sharma, P.K. and De Datta, S.K. 1986. Physical properties and processes of puddled rice soils. Advances in Soil Science, 5: 139-178.

Sharma, R.B. and Verma, G.P. 1977. Characterization of shrinkage cracks in medium black clay soil of Madhya Pradesh. I. Pattern and size of cracking in relation to vegetative covers. Plant and Soil, 48: 323-333.

Sideri, D.I. 1936. On the formation of structure in soil: II. Synthesis of aggregates; on the bonds uniting clay with sand and clay with humus. Soil Science, 42: 461-481.

Skempton, A.W. 1960. Significance of Terzaghi's concept of effective stress. pp.42-53 in From Theory to Practice in Soil Mechanics (Selections from the Writings of Karl Terzaghi). John Wiley, New York.

Skempton, A.W. 1961. Effective stress in soils, concrete and rocks. pp. 4-16 in Pore Pressure and Suction in Soils. Proceedings Conference of the International Society of Soil Mechanics and Foundation Engineering. March 30-31, 1960. Butterworths, London.

Sleeman, J.R. 1963. Cracks, peds, and their surfaces in some soils of the Riverine Plain, New South Wales. Australian Journal of Soil Research, 1: 91-102.

Smekal, A. 1936. The nature of the mechanical strength of glass. Journal of the Society of Glass Technology, 20: 432-448.

Smith, C.W., Hadas, A., Dan, J. and Koyumdjisky, H. 1985. Shrinkage and Atterberg limits in relation to other properties of principal soil types in Israel. Geoderma, 35: 47-65.

Smith, R.M. and Browning, D.R. 1946. Influence of evacuation upon laboratory percolation rates and wetting of undisturbed soil samples. Soil Science, 62: 243-253.

Smith, W.O., Foote, P.D. and Busang, P.F. 1929. Packing of homogeneous spheres. Physical Review (Series 2) 34: 1271-1274.

Snyder, V.A. and Miller, R.D. 1985. Tensile strength of unsaturated soils. Soil Science Society of America Journal, 49: 58-65.

Spoor, G. and Godwin, R.J. 1979. Soil deformation and shear strength characteristics of some clay soils at different moisture contents. Journal of Soil Science, 30: 483-498.

Stace, H.C.T., Hubble, G.D., Brewer, R., Northcote, K.H., Sleeman, J.R., Mulcahy, M.J. and Hallsworth, E.G. 1972. A Handbook of Australian Soils. Relim Publications. Glenside, South Australia.

Stafford, J.V. and Geikie, A. 1987. An implement configuration to loosen soil by inducing tensile failure. Soil and Tillage Research, 9: 363-376.

Stakman, W.P. and Bishay, B.G. 1976. Moisture retention and plasticity of highly calcareous soils in Egypt. Netherland Journal of Agricultural Science, 24: 43-57.

Stauffer, L.H. 1927. Measurement of physical characteristics of soils. Soil Science, 24: 373-379.

Stengel, P. 1988. Cracks formation during swelling: effects on soil structure regeneration after compaction. Proceedings Eleventh International Conference of International Soil Tillage Research Organization. Edinburgh, Scotland. 1: 147-152.

Stengel, P. and Bourlet, M. 1987. Fissuration d'un sol argileux gonflant apres compactage: Effet de l'humectation. (Effect of wetting on cracks formation in a compacted clay soil) in G. Monnier and M.J. Goss (Eds.) Soil Compaction and Regeneration. Proceedings Workshop on "Soil Compaction: Consequences and Structural Regeneration Processes", Avignon, September 17-18, 1985. (In French with English summary).

Stone, J.A., Allen, N.H.E. and Grant, C.D. 1985. Corn fertility treatments and the surface structure of a poorly drained soil. Soil Science Society of America Journal, 49: 1001-1004.

Stroh, A.N. 1960. A simple model of a propagating crack. Journal of the Mechanics and Physics of Solids, 8: 119-122.

Stroosnyder, L. and Koorevaar, P. 1972. Air pressure within soil aggregates during quick wetting and subsequent 'explosion'. Mededelingen van de Faculteit Landbouwwetenschappen Rijkuniversiteit Gent, 37(3): 1095-1106. (Proceedings of the Symposium on Soil Conditioning, Ghent, 1972).

Telfair, D., Garner, M.R., and Miars, D. 1957. The restoration of a structurally degenerated soil. Soil Science Society of America Proceedings, 21: 131-134.

Tessier, D., Pédro, G. and Camara, L. 1980. Sur le comportement hydrique et l'évolution de l'organization des argiles (kaolinites et smectites) au cours de la dessiccation et de la réhumectation. Comptes Rendus de l'Acadamie des Sciences. Paris. 290(May 5, 1980): Series D: 1169-1172. (In French with English summary).

Tisdall, J.M. and Oades, J.M. 1979. Stabilization of soil aggregates by the root systems of ryegrass. Australian Journal of Soil Research, 17: 429-441.

Tisdall, J.M. and Oades, J.M. 1980a. The management of ryegrass to stabilize aggregates of a red-brown earth. Australian Journal of Soil Research, 18: 415-422.

Tisdall, J.M. and Oades, J.M. 1980b. The effect of crop rotation on aggregation in a red-brown earth. Australian Journal of Soil Research, 18: 423-433.

Tisdall, J.M. and Oades, J.M. 1982. Organic matter and water-stable aggregates in soils. Journal of Soil Science, 33: 141-163.

Towner, G.D. 1987a. The mechanics of cracking of drying clay. Journal of Agricultural Engineering Research, 36: 115-124.

Towner, G.D. 1987b. The tensile stress generated in clay through drying. Journal of Agricultural Engineering Research, 37: 279-289.

Towner, G.D. 1988. The influence of sand- and silt-size particles on the cracking during drying of small clay-dominated aggregates. Journal of Soil Science, 39: 347-356.

Towner G.D. and Childs, E.C. 1972. The mechanical strength of unsaturated porous granular material. Journal of Soil Science, 23: 481-498.

Trangmar, B.B., Yost, R.S. and Uehara, G. 1985. Application of geostatistics to spatial studies of soil properties. Advances in Agronomy, 38: 45-94.

Tschebotarioff, G.P., Ward, E.R. and DePhilippe, A.A. 1953. The tensile strength of disturbed and recompacted soils. Proceedings Third International Conference on Soil Mechanics and Foundation Engineering, I: 207-210.

Uehara, G. and Jones, R.C. 1974. Bonding mechanisms for soil crusts. Part I. Particle surfaces and cementing agents. pp. 17-28 in J.W. Cary and D.D. Evans (Eds.). Soil Crusts. University of Arizona Agricultural Research Station, Technical Bulletin 214.

University of Adelaide. 1988. Meteorological Records. p 221. Waite Agricultural Research Institute Biennial Report for 1986-87. Adelaide, South Australia.

U.S.D.A. 1985. Report on the VII workshop on soil taxonomy and agrotechnology transfer. Part I. Recommendations. Soil Taxonomy News, 10(April): 7-14. Soil Management Support Services. Soil Conservation Service, United States Department of Agriculture.

Utomo, W.H. and Dexter, A.R. 1981a. Age hardening of agricultural topsoils. Journal of Soil Science, 32: 335-350.

Utomo, W.H. and Dexter, A.R. 1981b. Soil friability. Journal of Soil Science, 32: 203-213.

Utomo, W.H. and Dexter, A.R. 1981c. Tilth mellowing. Journal of Soil Science, 32: 187-201.

Utomo, W.H. and Dexter, A.R. 1981d. Effect of ageing on compression resistance and water stability of soil aggregates disturbed by tillage. Soil and Tillage Research, 1: 127-137.

Utomo, W.H. and Dexter, A.R. 1982. Changes in soil aggregate water stability induced by wetting and drying cycles in non-saturated soils. Journal of Soil Science, 33: 623-637.

Van de Graaf, R.H.M. 1978. Size of subsoil blocky peds in relation to textural parameters, depth and drainage. pp. 89-96. in W.W. Emerson, R.D. Bond and A.R. Dexter (Eds.) Modification of Soil Structure. John Wiley, Brisbane.

Van Shaik, J.C., Kemper, W.D., and Olsen, S.R. 1966. Contribution of adsorbed cations to diffusion in clay-water systems. Soil Science Society of America Proceedings, 30: 17-22.

Vilensky, D.G. 1937. Recent investigations on the process of soil aggregation. Pochvovedenie (Pedology), 1937(9): 1361-1373. (In Russian).

Vilensky, D.G. 1940. Studies on the process of soil aggregation. Pochvovedenie (Pedology), 1940(8): 28-37. (In Russian).

Vilensky, D.G. 1945. Aggregation of Soil: Its Theory and Practical Application. Academy of Sciences, Moscow. Translated from Russian into English by A. Howard, Commonwealth Scientific and Industrial Research Organization, Melbourne, 1949.

Vilensky, D.G. and Germanova, V. 1934. Experimental study of the problem of structure formation. Pochvovedenie (Pedology), 1934(1): 34-60. (In Russian with English figures, tables, plates and summary).

Vomocil, J.A. and Chancellor, W.J. 1967. Compressive and tensile failure strengths of three agricultural soils. Transactions of the American Society of Agricultural Engineers, 10: 741-744, 779.

Vomocil, J.A. and Waldron, L.J. 1962. Effect of moisture content on tensile strength of unsaturated glass bead systems. Soil Science Society of America Proceedings, 26: 409-412.

Voorhees, W.B. 1983. Relative effectiveness of tillage and natural forces in alleviating wheel-induced soil compaction. Soil Science Society of America Journal, 47: 129-133.

Waldron, L.J. 1977. The shear resistance of root-permeated homogeneous and stratified soil. Soil Science Society of America Journal, 41: 843-849.

Waldron, L.J. and Dakessian, S. 1981. Soil reinforcement by roots: calculation of increased soil shear resistance from root properties. Soil Science, 132: 427-435.

Waldron, L.J., McMurdie, J.L. and Vomocil, J.A. 1961. Water retention by capillary forces in an ideal soil. Soil Science Society of America Proceedings, 25: 265-267.

Walls, J.H., Houbolt, J.C. and Press, H. 1954. Some measurements and power spectra of runway roughness. National Advisory Committee for Aeronautics, Technical Note No. 3305. Langley Aeronautical Laboratory, Langley Field, VA, USA.

Warkentin, B.P. 1982. Clay soil structure related to soil management. Tropical Agriculture (Trinidad), 59(2): 82-91.

Webster, R. 1977. Spectral analysis of gilgai soil. Australian Journal of Soil Research, 15: 191-204.

Webster, R. 1985. Quantitative spatial analysis of soil in the field. Advances in Soil Science, 3: 1-70.

White, E.M. 1966. Subsoil structure genesis: theoretical considerations. Soil Science, 101: 135-141.

White, E.M. 1967. Soil age and texture factors in subsoil structure genesis. Soil Science, 103: 288-298.

Whiteley, G.M. and Dexter, A.R. 1983. Behaviour of roots in cracks between soil peds. Plant and Soil, 74: 153-162.

Whiteley, G.M., Utomo, W.H. and Dexter, A.R. 1981. A comparison of penetrometer pressures and the pressures exerted by roots. Plant and Soil, 61: 351-364.

Williams, C.H. 1981. Chemical properties. pp. 47-61. in J.M. Oades, D.G. Lewis and K. Norrish (Eds.) Red-brown Earths of Australia. (Waite Agricultural Research Institute/ Commonwealth Scientific and Industrial Research Organization, Division of Soils. Adelaide, South Australia.

Williams, B.G., Greenland, D.J. and Quirk, J.P. 1967. The tensile strength of soil cores containing polyvinyl alcohol. Australian Journal of Soil Research, 5: 85-92.

Williams, B.G., Greenland, D.J. and Quirk, J.P. 1968. The water stability of natural clay aggregates containing polyvinyl alcohol. Australian Journal of Soil Research, 6: 59-66.

Winne, D.H., and Wundt, B.M. 1958. Application of the Griffith-Irwin theory of crack propagation to the bursting behaviour of disks, including analytical and experimental studies. Transactions of the American Society of Mechanical Engineers, 80: 1643-1658.

Winterkorn, H.F. 1942. Mechanism of water attack on dry cohesive soil systems. Soil Science, 54: 259-273.

Winterkorn, H.F. 1955. The science of soil stabilization. pp 1-24 in H.F. Winterkorn (Ed.) Soil and Soil-Aggregate Stabilization. Highway Research Board Bulletin 108. National Research Council. Washington, D.C.

Wolf, D. and Luth, H.J. 1977. Tillage equipment for clod-forming soils. Paper No. 77-1008. : 9p. American Society of Agricultural Engineers. Raleigh, North Carolina.

Wolkewitz, H. 1958. Reßbilder trocknender tone und ihre deutung. (Cracking of drying clays and its significance). Zeitschrift für Pflanzenernährung Düngung Bodenkunde, 82: 17-33. (In German).

Yoder, R.E. 1936. A direct method of aggregate analysis of soils and a study of the physical nature of erosion losses. Journal American Society Agronomy, 28: 337-351.

Zasadzinski, J.A.N., Sweeney, J.B., Davis, H.T. and Scriven, L.E. 1987. Finite element calculations of fluid menisci and thin-films in a model porous media. Journal of Colloid and Interface Science, 119: 108-116.

sample variance $s^2 = \dfrac{\sum_{i=1}^{n} (X_i - \bar{X})^2}{n-1}$

sample standard deviation $s = \sqrt{s^2}$

sample standard error $s.e. = \sqrt{\dfrac{s^2}{n}}$

Appendix 1. Effect of Running Mean on the Variance Spectra of a Random Function f(x)

Differences between data values and running- or local-means are often used in communications engineering to filter 'unwanted' low frequency (long wavelength) data. a common misconception, however, is that a running mean of length **M** will remove all 'unwanted' variance at wavelengths $\lambda > M$, yet will have no effect on the (desired) variance occurring at shorter wavelengths, $\lambda \leq M$. It may be important to understand the attenuating effects, which occur at wavelengths above and below $\lambda = M$. When it is seen that the application of a running mean is actually equivalent to multiplying the variance spectra by the attenuation function

$$|K(\lambda)|^2 = \left(1 - \frac{\sin \frac{\pi M}{\lambda}}{\frac{\pi M}{\lambda}} \right)^2 \qquad [A\text{-}1]$$

the usefulness of this filter for a given set of data may be more readily assessed. The derivation outlined below is an expanded and modified version of the excellent, but rather obscure work of Walls, Houbolt and Press (1954).

Let the random function **f(x)** be the elevations along a transect of a soil fracture surface. The centred local, or running mean of **f(x)** over the interval **M** is:

$$g(x) = \frac{1}{M} \int_{x-\frac{M}{2}}^{x+\frac{M}{2}} f(x)\,dx \qquad [A\text{-}2]$$

The difference between the elevation, **f(x)** and its running-mean elevation, **g(x)**, is of primary interest because it provides information unbiased by overall trends (i.e.

long wavelength variance). The difference between **f(x)** and **g(x)** is:

$$h(x) = f(x) - g(x) \qquad \textbf{[A-3]}$$

or by substitution,

$$h(x) = f(x) - \frac{1}{M} \int_{x-\frac{M}{2}}^{x+\frac{M}{2}} f(x)\,dx \qquad \textbf{[A-4]}$$

The finite Fourier transform of **h(x)**, as a function of frequency may be written in complex-value form as:

$$H(\Omega) = \int_{-X}^{X} h(x) e^{-i\Omega x}\,dx \qquad \textbf{[A-5]}$$

where $\Omega = 2\pi f$ ('reduced' frequency) or $\frac{2\pi}{\lambda}$, and **f** = frequency (inverse of wavelength, λ). Substituting equation **[A-3]** into equation **[A-5]** gives:

$$H(\Omega) = \int_{-X}^{X} f(x) e^{-i\Omega x}\,dx - \int_{-X}^{X} g(x) e^{-i\Omega x}\,dx \qquad \textbf{[A-6]}$$

which is the same as

$$H(\Omega) = \int_{-X}^{X} f(x) e^{-i\Omega x}\,dx - \frac{1}{M} \int_{-X}^{X} \int_{x-\frac{M}{2}}^{x+\frac{M}{2}} f(n) e^{-i\Omega x}\,dn\,dx \qquad \textbf{[A-7]}$$

By interchanging the order of integration for the double integral term (to enable the

x-integral of the second term to be evaluated) it is found that:

$$H(\Omega) = \int_{-X}^{X} f(x)\, e^{-i\Omega x}\, dx - \frac{1}{M} \int_{n-\frac{M}{2}}^{n+\frac{M}{2}} \int_{-X}^{X} f(n) e^{-i\Omega x}\, dn\, dx \qquad [A\text{-}8]$$

and

$$H(\Omega) = \int_{-X}^{X} f(x)\, e^{-i\Omega x}\, dx - \left(\frac{\sin \frac{\Omega M}{2}}{\frac{\Omega M}{2}} \right) \int_{-X}^{X} f(n) e^{-i\Omega n}\, dn \qquad [A\text{-}9]$$

which reduces to

$$H(\Omega) = \left(1 - \frac{\sin \frac{\Omega M}{\lambda}}{\frac{\Omega M}{\lambda}} \right) F(\Omega) \qquad [A\text{-}10]$$

where $F(\Omega)$ is simply the finite Fourier transformation of the original random function $f(x)$:

$$F(\Omega) = \int_{-X}^{X} f(x)\, e^{-i\Omega x}\, dx \qquad [A\text{-}11]$$

The variance spectrum of $h(x)$ is described in the equation:

$$\phi_h(\Omega) = \lim_{x \to \infty} \frac{1}{2\pi x} |H(\Omega)|^2 \qquad [A\text{-}12]$$

which is equal to

$$\phi_h(\Omega) = \lim_{x \to \infty} \frac{1}{2\pi x} H(\Omega)\, H(-\Omega) \qquad [A\text{-}13]$$

and by substitution for $H(\Omega)$ we get:

$$\phi_h(\Omega) = \left(1 - \frac{\sin \frac{\Omega M}{\lambda}}{\frac{\Omega M}{\lambda}} \right)^2 \lim_{x \to \infty} \frac{1}{2\pi x} F(\Omega)\, F(-\Omega) \qquad [A\text{-}14]$$

$$= \left(1 - \frac{\sin \frac{\Omega M}{\lambda}}{\frac{\Omega M}{\lambda}} \right)^2 \phi_f(\Omega) \qquad [A\text{-}15]$$

The term $\left(1 - \frac{\sin \frac{\Omega M}{\lambda}}{\frac{\Omega M}{\lambda}} \right)^2$ is the function responsible for the attenuation of the variance spectrum when a running mean is employed, such as that defined by **h(x)** in equation **[A-4]**. By replacing $\frac{\Omega M}{2}$ with $\frac{\pi M}{\lambda}$, the attenuation function can be expressed in terms of wavelengths or structural unit sizes.

$$|K(\lambda)|^2 = \left(1 - \frac{\sin \frac{\pi M}{\lambda}}{\frac{\pi M}{\lambda}} \right)^2 \qquad [A\text{-}16]$$

A plot of $|K(\lambda)|^2$ versus the dimensionless ratio, $\frac{\lambda}{M}$, is instructive (Figure **A1-1**) in that $\frac{\lambda}{M}$ describes the structural feature size relative to the length of the running mean. There is no effect on the variance of structural features that are the same size as **M** (i.e. $\frac{\lambda}{M} = 1.0$). The variance of all structural features **>** **M** (i.e. $\frac{\lambda}{M} > 1.0$) is rapidly attenuated to smaller than 20%. There is, however, some magnification of the variance of structural features for $0.5 < \frac{\lambda}{M} < 1.0$.

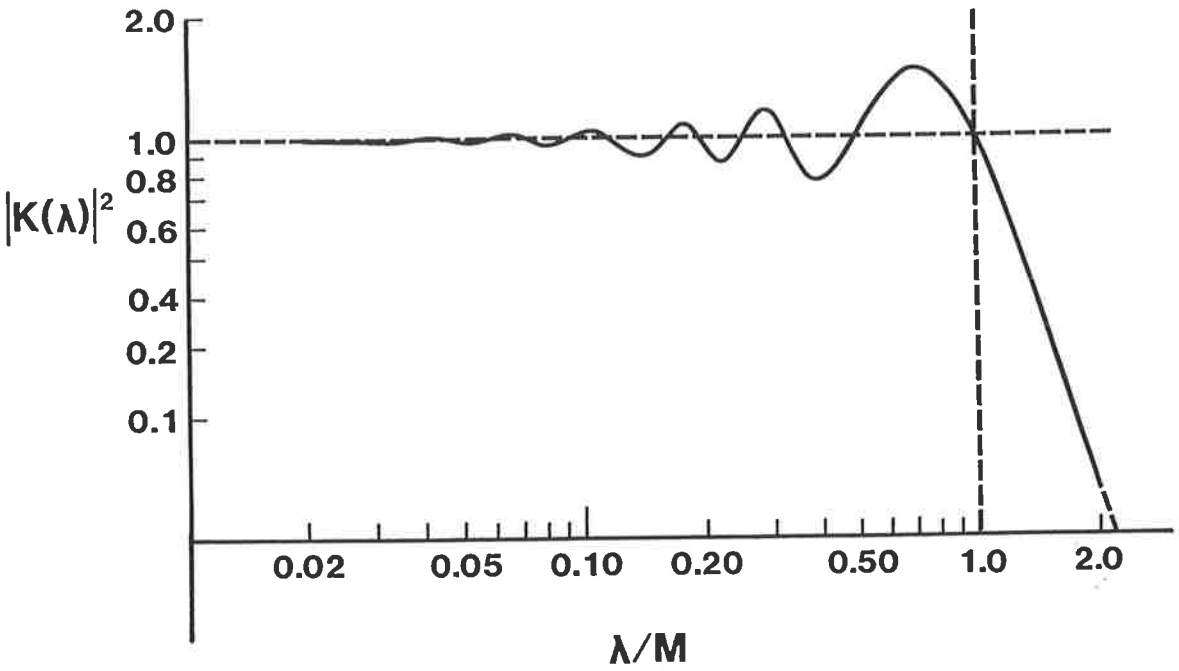

Figure A1-1. Running-mean attenuation function, $|K(\lambda)|^2$, plotted against the relative size of soil features, λ/M, where M is the length of the running mean, and λ is the soil feature size.

Choice of Running-Mean Length

A running mean of length **M**=4 mm was used in all parts of this thesis. Although the choice of **M**=4 mm was somewhat arbitrary, it was controlled by the length of the fractured soil surfaces (only 23 mm). Its choice also reflected the need to filter the variance introduced by tilting of the sample either under the video camera (or under the laser scanner) and to filter that caused by large-scale features, while at the same time preventing the significant loss of information that occurs when values of **M** become too large. Loss of variance begins to occur when **M** becomes larger than approximately 15% of the length of the data series (Blackman and Tukey, 1958).

An example illustrating how the length of the running mean, **M**, influences the fracture surface rugosity, σ_R, is shown in Figure **A1-2** for the natural soil clods (at three of five different water suctions) that were discussed in **SECTION 3.5.3.1**, and which were illustrated in Figure **3-10**. It can be seen in Figure **A1-2** that the value of σ_R increases as the length of the running mean increases, although due to the limited length of sample (constant scanning length of 23 mm) the slope of the line begins to decrease for **M** >4 mm. The point at which the slope begins to decrease is indicated by the vertical arrow in Figure **A1-2** at **M** = 4 mm. A running mean length of 4 mm represents 17% of the length of each sample, and is therefore the maximum possible value that should be used in accordance with Blackman and Tukey's (1958) criteria. The selection of **M** = 4 mm is therefore suitable for use in this study because it provides σ_R-values which filter out a large amount of large scale variance without losing the required information about structural features smaller than 4 mm. When a running mean is not used for calculating the standard deviation, the values of σ can be much larger and much more variable. For example, the values of σ (no running mean) corresponding to the three lines shown in Figure **A1-2** are σ = 1.019 ± 0.035 mm for Ψ = 0.5 kPa, σ = 0.796 ± 0.069mm for Ψ = 5 kPa, and σ = 0.873 ± 0.047 mm for Ψ = 50kPa.

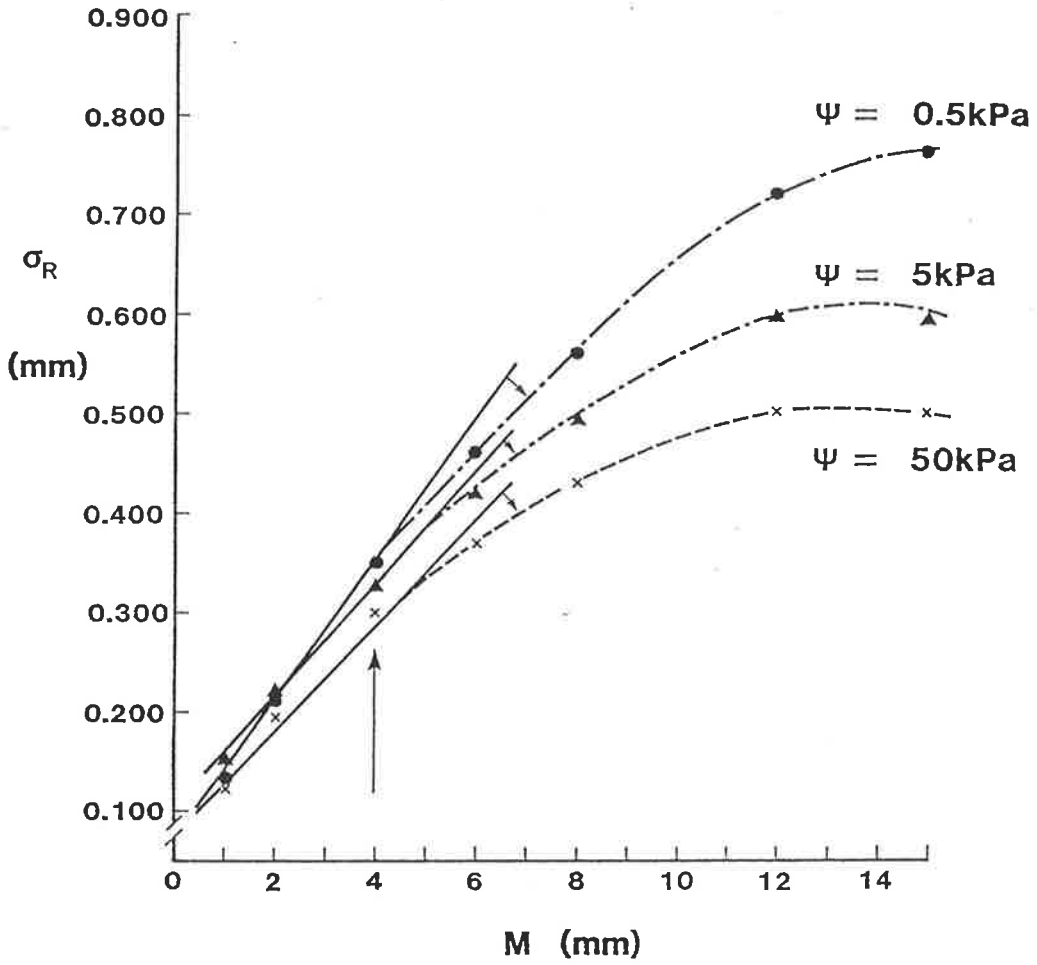

Figure A1-2. Fracture surface rugosity (σ_R, mm) of undisturbed Urrbrae soil clods as a function of the length of the running mean (M, mm) for three of the five different water suctions (Ψ, kPa) used for establishing water contents (cf. Figure 3-10).

Appendix 2. Raw Data for SECTION 3

Appendix **2** consists of two Tables, both of which are needed for the calculation of data used in **SECTION 3**.

Table **A2-1** presents gravimetric water contents, **W**, on a clod-by-clod basis for soil clods taken from Field W-10 (Waite Institute) and brought from saturation to equilibrium using water suctions of 5, 10, 50, 100 & 500 hPa (1hPa ≈ 1cm water). Values of W_Q are water contents from pieces of clod on which penetrometer resistance was determined, and values of W_{TS} are those from pieces on which tensile strengths were determined ($\bar{W}$ is the mean of W_Q & W_{TS}). The values of $\bar{W}$ in Table **A2-1** are the values used in Table **3-2** for the calculation of the volumetric water contents, θ.

Table **A2-2** presents the penetrometer resistance, Q_p, and tensile strength, **TS**, data on a clod-by-clod basis for the same clods listed in Table **A2-1**.

Appendix Table A2-1

Water Suction h (hPa)	Clod #	Water Content for Q_p-clod W_Q (kgkg^{-1})	Water Content for TS-clod W_{TS} (kgkg^{-1})	Average Water Content $\bar{W}$ (kgkg^{-1})	Group Averages (±s.e.), n
5	1	0.241	0.246	0.244	0.245
"	2	0.266	0.245	0.256	(± 0.006)
"	3	0.285	0.278	0.282	n=8
"	4	0.240	0.236	0.238	
"	5	0.231	0.236	0.234	
"	6	0.223	0.238	0.231	
"	7	0.240	0.225	0.233	
"	8	0.246	0.242	0.244	
10	1	0.232	0.228	0.230	0.224
"	2	0.220	0.206	0.213	(± 0.004)
"	3	0.218	0.208	0.213	n=8
"	4	0.219	0.204	0.212	
"	5	0.237	0.228	0.233	
"	6	0.225	0.222	0.224	
"	7	0.237	0.217	0.227	
"	8	0.231	0.252	0.242	
50	1	0.199	0.205	0.202	0.214
"	2	0.211	0.206	0.209	(± 0.007)
"	3	0.207	0.202	0.205	n=9
"	4	0.248	-	0.248	
"	5	0.194	0.185	0.190	
"	6	0.192	0.191	0.192	
"	7	0.229	0.232	0.231	
"	8	0.230	0.221	0.226	
"	9	0.225	0.228	0.227	
100	1	0.186	-	0.186	0.203
"	2	0.202	0.206	0.204	(± 0.003)
"	3	0.184	0.193	0.189	n=9
"	4	0.215	0.205	0.210	
"	5	0.206	0.221	0.214	
"	6	0.218	0.215	0.217	
"	7	0.207	0.205	0.206	
"	8	0.197	0.202	0.200	
"	9	0.212	0.188	0.200	
500	1	0.178	0.177	0.178	0.183
"	2	0.182	0.189	0.186	(± 0.183)
"	3	0.183	0.193	0.188	n=8
"	4	0.187	0.189	0.188	
"	5	0.164	0.162	0.163	
"	6	0.196	0.188	0.192	
"	7	0.188	0.170	0.179	
"	8	0.192	0.185	0.189	

Appendix Table A2-2

Water Suction h (hPa)	Clod #	Penetrometer Resistance Q_p (kPa)	Mean Q_p (kPa)	Tensile Strength (kPa)	Mean TS (kPa)
5	1	168.45	110.79	2.82	2.53
"	2	47.42	(± 20.98)	1.70	(± 0.414)
"	3	15.22	n=8	1.64	n=8
"	4	92.09		2.68	
"	5	119.17		5.14	
"	6	141.75		2.12	
"	7	108.93		2.59	
"	8	193.28		1.53	
10	1	394.18	368.38	3.68	3.50
"	2	415.14	(± 72.70)	2.32	(± 0.313)
"	3	482.90	n=8	5.09	n=8
"	4	77.61		3.74	
"	5	298.35		3.01	
"	6	753.92		4.14	
"	7	163.84		2.59	
"	8	361.11		3.42	
50	1	2153.70	917.89	4.50	5.17
"	2	1345.00	(± 217.52)	7.11	(± 0.571)
"	3	571.37	n=9	4.38	n=8
"	4	206.51		--.--	
"	5	1284.49		7.93	
"	6	1319.17		5.67	
"	7	279.13		3.18	
"	8	329.42		4.31	
"	9	772.26		4.28	
100	1	2641.09	1016.60	12.80	6.09
"	2	823.30	(± 228.19)	3.30	(± 0.903)
"	3	1028.69	n=9	5.63	n=9
"	4	665.58		5.54	
"	5	675.31		7.19	
"	6	227.85		4.97	
"	7	938.10		5.01	
"	8	1389.30		5.07	
"	9	760.16		5.33	
500	1	1754.53	1693.05	7.03	6.94
"	2	1582.71	(± 258.63)	5.04	(± 0.312)
"	3	1125.27	n=8	7.95	n=8
"	4	1287.11		7.33	
"	5	1413.13		7.06	
"	6	2915.61		6.46	
"	7	2645.84		7.58	
"	8	820.18		7.06	

Appendix 3. Water Desorption Data for Natural Soil Clods from the Permanent Rotation Plots, Waite Institute.

The effects of organic matter on brittle fracture (outlined in **SECTION 5**) were investigated using soil from the Permanent Rotation Plots at the Waite Agricultural Research Institute. Differences in fracture surface rugosity may be related to differences in the macro-porosity of the different soils. Information on the pore size distribution, particularly the macroporosity, may be inferred from water release curves, and so it was considered important to determine these for soil from the ten Rotation Plots discussed in **SECTION 5** of this thesis.

For this purpose, a number of fist-size natural clods were collected in July, 1988 from each of the plots. The clods were brought to the laboratory where they were saturated and then drained on porous ceramic plates at suctions of 3, 5, 10, 30, 50, 100, 300, and 500 hPa water over a period of five months. As the soil was progressively drained, water contents were determined on the same large clod each time by cutting a chunk of moist soil from each clod while it remained on the ceramic plate.

Presented in Appendix-Table **A3-1** are the average gravimetric water contents, with standard errors and numbers of samples for each plot, at each of the eight suctions listed above. These are plotted in Appendix-Figure **A3-1**. Using average bulk densities from Table **5-2**, and assuming an average particle density of 2650 kgm^{-3} the volumetric water contents were calculated and are presented in Appendix-Table **A3-2(a)**. These data were plotted as desorption curves, and linear equations in the form of

$$\theta = a + b\,(\log_{10} h) \qquad \textbf{[A3- 1]}$$

were calculated and the regression coefficients are presented in the Appendix-Table **A3-2(b)** along with data on **%OC** and ρ_b. The same analysis was done on the Rotation Groups as shown in Appendix-Table **A3-3**, and these are plotted in Appendix-Figure **A3-2**.

Table A3-1

Gravimetric Water Contents ($kgkg^{-1}$) at Different Suctions

Plot #		Water Suctions (hPa) 3	5	10	30	50	100	300	500
5	w	0.2172	0.2012	0.1990	0.1929	0.1930	0.1874	0.1753	0.1681
	(± s.e.)	(± 0.0071)	(± 0.0068)	(± 0.0059)	(± 0.0027)	(± 0.0061)	(± 0.0050)	(± 0.0044)	(± 0.0035)
	n	5	5	5	4	4	5	6	6
6	w	0.2268	0.2231	0.2180	0.2012	0.1970	0.1942	0.1761	0.1575
	(± s.e.)	(± 0.0063)	(± 0.0058)	(± 0.0037)	(± 0.0016)	(± 0.0027)	(± 0.0043)	(± 0.0055)	(± 0.0052)
	n	5	5	5	4	4	5	5	6
7	w	0.2086	0.2182	0.2313	0.2101	0.1974	0.1944	0.1727	0.1575
	(± s.e.)	(± 0.0049)	(± 0.0068)	(± 0.0076)	(± 0.0035)	(± 0.0067)	(± 0.0052)	(± 0.0055)	(± 0.0053)
	n	5	5	5	4	4	5	5	6
17	w	0.2361	0.2362	0.2228	0.2256	0.2166	0.2046	0.1916	0.1773
	(± s.e.)	(± 0.0141)	(± 0.0107)	(± 0.0073)	(± 0.0061)	(± 0.0056)	(± 0.0093)	(± 0.0040)	(± 0.0047)
	n	5	5	5	4	4	5	6	6
18	w	0.2634	0.2490	0.2496	0.2295	0.2166	0.2116	0.1991	0.1925
	(± s.e.)	(± 0.0100)	(± 0.0019)	(± 0.0054)	(± 0.0067)	(± 0.0071)	(± 0.0053)	(± 0.0036)	(± 0.0071)
	n	5	4	5	4	4	5	6	5
19	w	0.2517	0.2558	0.2589	0.2290	0.2198	0.2127	0.1957	0.1901
	(± s.e.)	(± 0.0076)	(± 0.0044)	(± 0.0101)	(± 0.0031)	(± 0.0022)	(± 0.0029)	(± 0.0032)	(± 0.0052)
	n	5	5	5	4	4	5	6	5
20	w	0.2338	0.2394	0.2419	0.2199	0.2064	0.2101	0.1934	0.1871
	(± s.e.)	(± 0.0041)	(± 0.00628)	(± 0.0039)	(± 0.0046)	(± 0.0037)	(± 0.0064)	(± 0.0040)	(± 0.0053)
	n	5	5	5	4	4	5	6	6
29	w	0.3584	0.3891	0.3211	0.2689	0.2841	0.2742	0.2288	0.2389
	(± s.e.)	(± 0.0202)	(± 0.0235)	(± 0.0168)	(± 0.0061)	(± 0.0241)	(± 0.0159)	(± 0.0217)	(± 0.0207)
	n	5	5	5	4	4	5	4	6
34	w	0.2138	0.2182	0.2469	0.2172	0.2018	0.1995	0.1599	0.1500
	(± s.e.)	(± 0.0044)	(± 0.0096)	(± 0.0159)	(± 0.0102)	(± 0.0049)	(± 0.0052)	(± 0.0059)	(± 0.0055)
	n	5	5	5	5	5	5	6	6
35	w	0.2139	0.2152	0.2088	0.1960	0.1930	0.1784	0.1540	0.1429
	(± s.e.)	(± 0.0089)	(± 0.0070)	(± 0.0051)	(± 0.0070)	(± 0.0061)	(± 0.0026)	(± 0.0064)	(± 0.0050)
	n	5	5	5	5	5	5	6	6

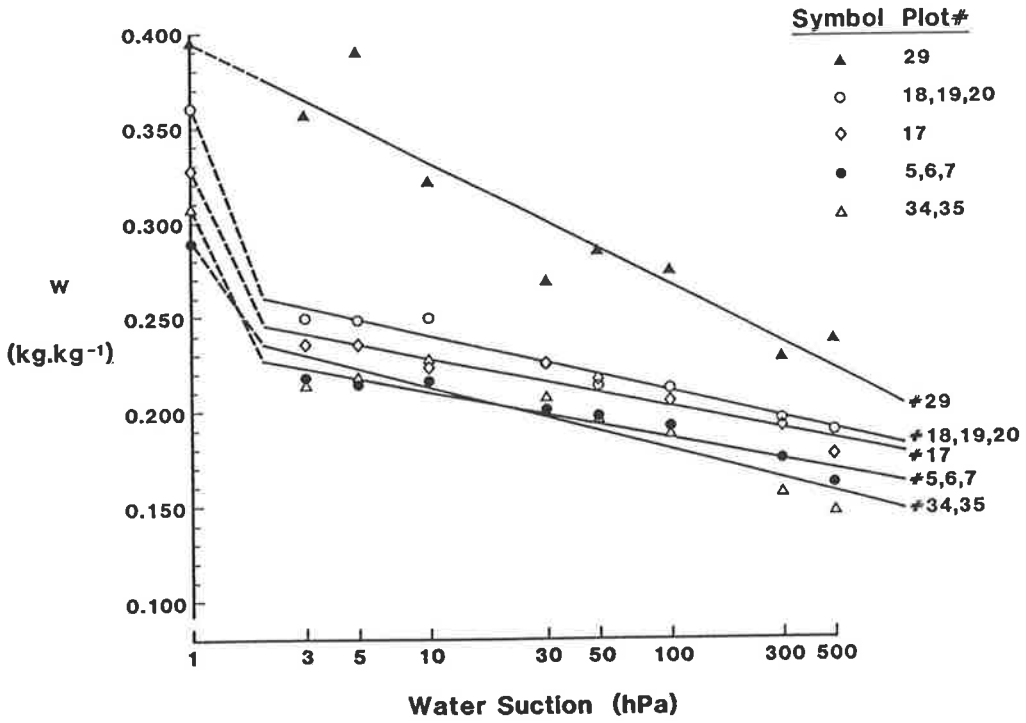

Figure A3-1. Gravimetric water contents, **w**, (grouped by rotation) plotted as functions of the applied water suction, **h**.

Table A3-2(a)

Volumetric Water Contents (by plot)

Plot #	Water Suctions (hPa) 3	5	10	30	50	100	300	500
5	0.4083	0.3783	0.3741	0.3627	0.3628	0.3523	0.3296	0.3160
6	0.4241	0.4172	0.4077	0.3762	0.3684	0.3632	0.3293	0.2945
7	0.3963	0.4146	0.4395	0.3992	0.3751	0.3694	0.3281	0.2993
17	0.4203	0.4204	0.3966	0.4016	0.3855	0.3642	0.3410	0.3156
18	0.4530	0.4283	0.4293	0.3947	0.3726	0.3640	0.3425	0.3311
19	0.4203	0.4272	0.4324	0.3824	0.3671	0.3552	0.3268	0.3175
20	0.3951	0.4046	0.4088	0.3716	0.3488	0.3551	0.3268	0.3162
29	0.5770	0.6265	0.5170	0.4329	0.4574	0.4415	0.3684	0.3846
34	0.3934	0.4015	0.4543	0.3996	0.3713	0.3671	0.2942	0.2760
35	0.3936	0.3960	0.3842	0.3606	0.3483	0.3283	0.2834	0.2629

Table A3-2(b)

Regression Coefficients (by plot)

Plot #	%OC*	ρ_b* (kgm^{-3})	Regression Coefficients a	b	r**
5	0.97	1880	0.4142	-0.0343	0.964
6	1.07	1870	0.4571	-0.0540	0.978
7	1.18	1900	0.4552	-0.0495	0.876
17	1.29	1780	0.4506	-0.0447	0.959
18	1.80	1720	0.4742	-0.0541	0.990
19	2.01	1670	0.4628	-0.0537	0.969
20	2.04	1690	0.4304	-0.0412	0.950
29	2.45	1610	0.6392	-0.1044	0.930
34	0.98	1840	0.4652	-0.0610	0.841
35	0.97	1840	0.4391	-0.0603	0.975

* %OC and ρ_b are from Table 5-2

** r is the regression correlation coefficient, for which n=8 points

Table A3-3(a)

Volumetric Water Contents (by rotation)

Plot #	Water Suctions (hPa) 3	5	10	30	50	100	300	500
5,6,7	0.4096	0.4034	0.4071	0.3794	0.3688	0.3616	0.3290	0.3033
17	0.4203	0.4204	0.3966	0.4016	0.3855	0.3642	0.3410	0.3156
18,19,20	0.4228	0.4200	0.4235	0.3829	0.3628	0.3581	0.3320	0.3216
29	0.5770	0.6265	0.5170	0.4329	0.4574	0.4415	0.3684	0.3846
34,35	0.3935	0.3988	0.4193	0.3801	0.3598	0.3477	0.2888	0.2695

Table A3-3(b)

Regression Coefficients (by rotation)

Plot #	%OC	Regression Coefficients a	b	r**
5,6,7	1.07	0.4422	-0.0459	0.967
17	1.29	0.4506	-0.0447	0.959
18,19,20	1.95	0.4558	-0.0497	0.980
29	2.45	0.6392	-0.1044	0.930
34,35	0.97	0.4522	-0.0607	0.921

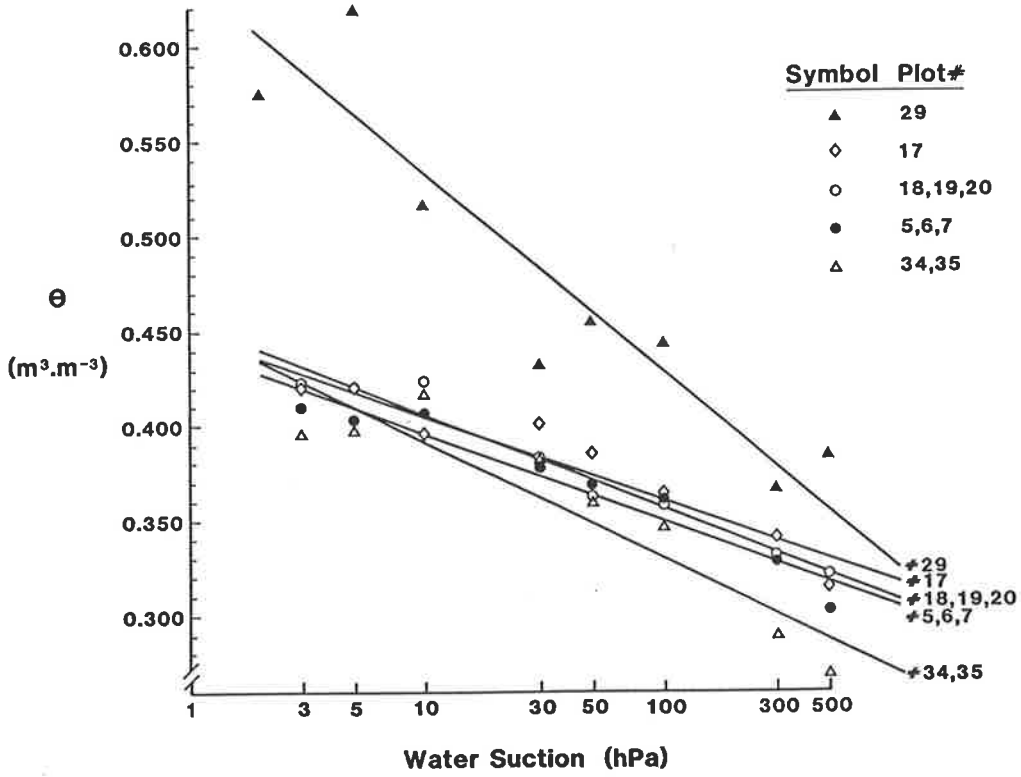

Figure A3-2. Volumetric water contents, θ, (grouped by rotation) plotted as functions of the applied water suction, h.

As suggested in **SECTION 3** the model of soil cubes for predicting the distance between air-filled cracks needs to be improved and tested on a wider range of soils. When such a model is developed, the data presented in this Appendix are ideally suited for testing because of the wide range of pore sizes shown on a soil differing only in the organic carbon content.

Appendix 4. Raw Data For SECTION 5

Appendix 4 consists of four Tables, each needed for the calculation of data presented in **SECTION 5.**

Table **A4-1** presents, on a clod-by-clod basis for each of the ten plots used in the Permanent Rotation Experiment, the bulk density, ρ_b, the penetrometer resistance, Q_p (and its corresponding gravimetric water content, w_Q), the tensile strength, **TS** (and its corresponding water content, w_{TS}), the mean water content, $\bar{w}$, the fracture surface rugosity by direct and by indirect fracture methods ($\sigma_{R(d)}$, and $\sigma_{R(ind)}$), and the mean $\bar{\sigma}_R$. The data from Table **A4-1** are used mainly in reference to **SECTION 5.3.**

Table **A4-2** presents, on a disk-by-disk basis for each of the ten plots used in the Permanent Rotation Experiment, the bulk density, ρ_b, the gravimetric water content, **w**, the tensile strength, **TS**, and the fracture surface rugosity, σ_R, of disks held at a constant water suction of 50 kPa. The data from Table **A4-2** are used mainly in reference to **SECTION 5.4.**

Table **A4-3** presents, on a disk-by-disk basis for plot #35 and #29 from the Permanent Rotation Experiment, the bulk density, ρ_b, the gravimetric water content, **w**, the penetrometer resistance, Q_p, &/or the tensile strength, **TS**, and the fracture surface rugosity, σ_R, for soil disks brought to seven different water suctions (**h** = 0.1, 1.0, 5.0, 10.0, 50.0, 10^7 (air dry), and 10^8 (oven dry) kPa). The data from Table **A4-3** are used mainly in reference to **SECTION 5.5.**

Table **A4-4** presents, on a clod-by-clod basis for each of the ten plots used in the Permanent Rotation Experiment, the bulk density, ρ_b, gravimetric water content, **w**, the tensile strength, **TS**, and the fracture surface rugosity, σ_R for (**a**) air dry clods and for (**b**) oven dry clods. The data from Table **A4-4** are used mainly in reference to **SECTION 5.6.**

Table A4-1

Plot #5

Clod #	OC %	ρ_b (kgm^{-3})	Q_p (kPa)	w_Q ($kgkg^{-1}$)	TS (kPa)	w_{TS} ($kgkg^{-1}$)	$\bar{w}$ ($kgkg^{-1}$)	$\sigma_{R(d)}$ (mm)	$\sigma_{R(ind)}$ (mm)	$\bar{\sigma}_R$ (mm)
1	1.28	1570	920.38	0.179	10.54	0.171	0.175	0.242	0.279	0.261
2	1.36	1690	2729.56	0.178	7.22	0.175	0.177	0.217	0.248	0.233
3	0.91	1620	814.44	0.158	8.42	0.164	0.161	0.238	0.202	0.220
4	0.76	1610	3146.33	0.161	5.14	0.163	0.162	0.264	-.---	0.264
5	0.84	1680	1990.37	0.160	5.86	0.158	0.159	0.258	0.228	0.243
6	0.77	1600	1833.64	0.163	7.93	0.156	0.160	0.239	0.210	0.225
7	0.89	1640	2398.65	0.170	5.57	0.164	0.167	0.295	0.210	0.253
8	0.93	1650	3652.81	0.162	3.16	0.159	0.161	-.---	0.131	0.131
9	1.06	1650	933.48	0.170	4.97	0.160	0.165	-.---	0.181	0.181
10	1.01	1590	1660.82	0.170	5.42	0.171	0.171	0.205	0.296	0.251
11	0.84	1530	1424.24	0.171	3.37	0.160	0.166	0.350	-.---	0.350
Mean	0.97	1620	1954.97	0.167	6.15	0.164	0.166	0.256	0.221	0.228
± se	±0.06	±10	±284.41	±0.002	±0.67	±0.002	±0.002	±0.015	±0.017	±0.012
n	11	11	11	11	11	11	11	9	9	11

Plot #6

Clod #	OC %	ρ_b (kgm^{-3})	Q_p (kPa)	w_Q ($kgkg^{-1}$)	TS (kPa)	w_{TS} ($kgkg^{-1}$)	$\bar{w}$ ($kgkg^{-1}$)	$\sigma_{R(d)}$ (mm)	$\sigma_{R(ind)}$ (mm)	$\bar{\sigma}_R$ (mm)
1	1.41	1530	1250.55	0.194	6.61	0.183	0.189	0.301	0.284	0.293
2	1.03	1630	979.02	0.181	7.32	0.162	0.172	0.292	0.405	0.349
3	1.50	1540	1094.57	0.194	5.19	0.189	0.192	0.289	0.305	0.297
4	0.79	1630	770.39	0.163	4.28	0.161	0.162	0.245	-.---	0.245
5	1.40	1550	2458.17	0.192	6.86	0.194	0.193	0.318	0.221	0.270
6	0.77	1570	832.53	0.172	4.51	0.174	0.173	0.311	0.254	0.283
7	0.77	1650	1299.08	0.153	6.25	0.152	0.153	0.267	-.---	0.267
8	0.78	1600	1295.84	0.164	6.25	0.157	0.161	0.191	-.---	0.191
9	1.51	1500	1005.48	0.198	7.01	0.190	0.194	0.371	0.232	0.302
10	0.81	1570	1380.57	0.161	4.18	0.161	0.161	0.243	0.152	0.198
11	0.99	1630	1955.55	0.168	5.64	0.174	0.171	0.203	0.219	0.211
Mean	1.07	1600	1301.98	0.176	5.83	0.172	0.175	0.276	0.259	0.264
± se	±0.10	±10	±151.09	±0.005	±0.34	±0.004	±0.005	±0.016	±0.026	±0.015
n	11	11	11	11	11	11	11	11	8	11

(continued.....)

(...Table A4-1, cont'd)

Plot #7

Clod #	OC %	ρ_b (kgm^{-3})	Q_p (kPa)	w_Q ($kgkg^{-1}$)	TS (kPa)	w_{TS} ($kgkg^{-1}$)	$\bar{w}$ ($kgkg^{-1}$)	$\sigma_{R(d)}$ (mm)	$\sigma_{R(ind)}$ (mm)	$\bar{\sigma}_R$ (mm)
1	0.81	1620	1472.78	0.169	4.51	0.182	0.176	0.332	-.---	0.332
2	0.81	1610	1491.74	0.169	4.54	0.169	0.169	0.370	-.---	0.370
3	1.01	1500	1141.74	0.177	5.41	0.179	0.178	0.202	0.279	0.241
4	1.49	1630	1459.30	0.176	10.80	0.177	0.177	0.222	0.171	0.197
5	1.49	1590	1518.95	0.177	6.89	0.172	0.175	0.326	0.267	0.297
6	1.02	1590	726.22	0.176	5.45	0.177	0.177	0.191	0.243	0.217
7	1.51	1570	2429.84	0.176	8.56	0.175	0.176	0.201	0.150	0.176
8	0.98	1620	1914.37	0.167	6.83	0.168	0.168	0.286	0.203	0.245
9	0.81	1640	2580.08	0.157	3.53	0.169	0.163	0.629	0.293	0.461
10	1.48	1600	1983.25	0.185	7.98	0.186	0.186	0.235	0.250	0.243
11	1.59	1630	1892.16	0.181	6.68	0.178	0.180	0.198	0.222	0.210
Mean	1.18	1600	1691.86	0.174	6.47	0.176	0.175	0.290	0.231	0.272
± se	±0.10	±10	±162.79	±0.002	±0.63	±0.002	±0.002	±0.039	±0.016	±0.026
n	11	11	11	11	11	11	11	11	9	11

Plot #17

Clod #	OC %	ρ_b (kgm^{-3})	Q_p (kPa)	w_Q ($kgkg^{-1}$)	TS (kPa)	w_{TS} ($kgkg^{-1}$)	$\bar{w}$ ($kgkg^{-1}$)	$\sigma_{R(d)}$ (mm)	$\sigma_{R(ind)}$ (mm)	$\bar{\sigma}_R$ (mm)
1	1.38	1600	1348.12	0.189	6.88	0.174	0.182	0.459	0.257	0.358
2	0.96	1600	1173.06	0.170	7.66	0.168	0.169	0.333	0.352	0.343
3	0.92	1650	761.28	0.169	6.19	0.170	0.170	0.200	0.402	0.301
4	1.40	1620	448.71	0.180	9.87	0.175	0.178	0.255	-.---	0.255
5	0.98	1620	1075.35	0.170	6.58	0.165	0.168	0.330	0.182	0.256
6	1.38	1600	974.03	0.177	7.82	0.178	0.178	0.235	0.569	0.402
7	1.41	1630	1996.98	0.173	10.58	0.175	0.174	0.285	0.176	0.231
8	1.40	1630	1520.32	0.180	9.12	0.176	0.178	0.245	0.224	0.235
9	1.35	1590	2230.19	0.176	7.76	0.179	0.178	0.171	0.350	0.261
10	1.62	1610	1685.65	0.192	7.79	0.191	0.192	0.284	0.261	0.273
11	1.40	1570	1293.34	0.193	8.65	0.173	0.183	0.207	0.176	0.192
Mean	1.29	1610	1318.82	0.197	8.17	0.175	0.177	0.273	0.295	0.282
± se	±0.07	±10	±157.67	±0.003	±0.43	±0.002	±0.002	±0.024	±0.040	±0.019
n	11	11	11	11	11	11	11	11	10	11

(continued.....)

(...Table A4-1, cont'd)

Plot #18

Clod #	OC %	ρ_b (kgm^{-3})	Q_p (kPa)	w_Q ($kgkg^{-1}$)	TS (kPa)	w_{TS} ($kgkg^{-1}$)	$\bar{w}$ ($kgkg^{-1}$)	$\sigma_{R(d)}$ (mm)	$\sigma_{R(ind)}$ (mm)	$\bar{\sigma}_R$ (mm)
1	1.84	1530	1253.42	0.189	8.08	0.179	0.184	0.374	0.300	0.337
2	1.92	1550	1755.90	0.188	5.85	0.182	0.185	0.205	-.---	0.205
3	2.12	1510	1152.97	0.198	9.90	0.198	0.198	0.362	0.396	0.379
4	0.81	1510	357.96	0.212	5.64	0.216	0.214	0.457	-.---	0.457
5	1.90	1570	2837.50	0.185	10.45	0.192	0.189	0.503	-.---	0.503
6	1.90	1570	2633.11	0.182	11.67	0.177	0.180	0.430	0.302	0.366
7	1.85	1570	532.56	0.189	9.54	0.187	0.188	0.402	-.---	0.402
8	1.99	1510	3245.78	0.197	6.29	0.198	0.198	0.343	0.369	0.356
9	1.65	1510	978.03	0.187	5.37	0.190	0.189	0.334	-.---	0.334
10	1.93	1540	974.91	0.197	10.86	0.190	0.194	0.295	-.---	0.295
11	1.91	1550	1839.88	0.187	11.49	0.188	0.188	0.263	0.408	0.336
Mean	1.80	1540	1598.18	0.192	8.65	0.191	0.192	0.361	0.355	0.361
± se	±0.10	±10	±288.01	±0.003	±0.75	±0.003	±0.003	±0.026	±0.023	±0.024
n	11	11	11	11	11	11	11	11	5	11

Plot #19

Clod #	OC %	ρ_b (kgm^{-3})	Q_p (kPa)	w_Q ($kgkg^{-1}$)	TS (kPa)	w_{TS} ($kgkg^{-1}$)	$\bar{w}$ ($kgkg^{-1}$)	$\sigma_{R(d)}$ (mm)	$\sigma_{R(ind)}$ (mm)	$\bar{\sigma}_R$ (mm)
1	1.96	1550	1984.38	0.187	6.70	0.196	0.192	0.353	0.384	0.369
2	1.81	1610	1612.03	0.192	9.11	0.198	0.195	0.299	0.250	0.275
3	1.92	1590	2005.34	0.206	8.16	0.203	0.205	0.175	0.423	0.299
4	2.27	1660	1112.79	0.188	7.77	0.193	0.191	0.143	0.465	0.304
5	1.83	1570	895.05	0.187	7.34	0.193	0.190	0.351	0.307	0.329
6	2.07	1550	2256.77	0.205	12.67	0.200	0.203	0.241	0.192	0.217
7	2.08	1550	1266.39	0.200	17.08	0.189	0.195	0.440	0.300	0.370
8	2.01	1520	3680.01	0.197	8.42	0.190	0.194	0.208	0.490	0.349
9	1.92	1680	1787.60	0.190	12.33	0.184	0.187	0.187	0.131	0.159
10	1.88	1590	1532.67	0.188	9.76	0.189	0.189	0.142	0.220	0.181
11	2.33	1510	2319.66	0.219	8.60	0.203	0.211	0.273	0.333	0.303
Mean	2.01	1580	1859.34	0.196	9.81	0.194	0.196	0.256	0.318	0.287
± se	±0.12	±20	±228.30	±0.003	±0.92	±0.002	±0.002	±0.029	±0.035	±0.022
n	11	11	11	11	11	11	11	11	11	11

(continued.....)

(...Table A4-1, cont'd)

Plot #20

Clod #	OC %	ρ_b (kgm^{-3})	Q_p (kPa)	w_Q ($kgkg^{-1}$)	TS (kPa)	w_{TS} ($kgkg^{-1}$)	$\bar{w}$ ($kgkg^{-1}$)	$\sigma_{R(d)}$ (mm)	$\sigma_{R(ind)}$ (mm)	$\bar{\sigma}_R$ (mm)
1	2.06	1630	2398.27	0.195	12.27	0.194	0.195	0.215	0.184	0.200
2	2.14	1560	3499.83	0.212	--.--	-.---	0.212	0.357	-.---	0.357
3	1.94	1610	3295.07	0.187	9.62	0.196	0.192	0.249	0.232	0.241
4	2.28	1530	3530.90	0.210	8.83	0.212	0.211	0.283	0.211	0.247
5	1.80	1580	2189.51	0.192	7.37	0.184	0.188	0.218	-.---	0.218
6	1.86	1650	2000.35	0.186	15.37	0.187	0.187	0.298	0.121	0.210
7	2.29	1500	1226.96	0.204	8.64	0.226	0.215	-.---	-.---	-.---
8	1.99	1580	1870.70	0.188	6.54	0.201	0.195	0.210	0.189	0.200
9	2.08	1590	2658.31	0.195	13.46	0.201	0.198	0.231	0.350	0.291
10	2.19	1600	4005.56	0.195	10.59	0.197	0.196	-.---	0.254	0.254
11	1.79	1600	2228.57	0.185	5.59	0.195	0.190	0.148	0.409	0.279
Mean	2.04	1580	2627.64	0.195	9.83	0.199	0.198	0.245	0.244	0.250
± se	±0.05	±10	±256.80	±0.003	±0.94	±0.004	±0.003	±0.020	±0.033	±0.016
n	11	11	11	11	10	10	11	9	8	10

Plot #29

Clod #	OC %	ρ_b (kgm^{-3})	Q_p (kPa)	w_Q ($kgkg^{-1}$)	TS (kPa)	w_{TS} ($kgkg^{-1}$)	$\bar{w}$ ($kgkg^{-1}$)	$\sigma_{R(d)}$ (mm)	$\sigma_{R(ind)}$ (mm)	$\bar{\sigma}_R$ (mm)
1	2.71	1540	4739.52	0.213	5.92	0.228	0.221	0.243	0.216	0.230
2	2.31	1530	1621.52	0.221	8.64	0.209	0.215	0.248	0.316	0.282
3	1.94	1470	3003.45	0.234	8.74	0.228	0.231	0.209	0.228	0.219
4	1.94	1550	1854.36	0.205	5.26	0.194	0.200	0.201	0.344	0.273
5	2.58	1430	1773.38	0.271	4.66	0.233	0.252	0.242	0.426	0.334
6	1.64	1580	1877.07	0.187	12.63	0.179	0.183	0.342	0.319	0.331
7	3.20	1450	2535.78	0.255	5.42	0.256	0.256	0.309	0.213	0.261
8	2.12	1570	3078.32	0.186	3.57	0.211	0.199	0.234	0.542	0.388
9	2.51	1450	2789.21	0.224	6.90	0.221	0.223	0.247	0.291	0.269
10	3.20	1400	1786.60	0.257	8.44	0.240	0.249	0.232	0.274	0.253
11	2.78	1540	3513.80	0.192	11.78	0.253	0.223	0.224	0.167	0.196
Mean	2.45	1540	2597.55	0.222	7.45	0.223	0.223	0.248	0.303	0.276
± se	±0.15	±20	±289.59	±0.009	±0.87	±0.007	±0.007	±0.013	±0.032	±0.017
n	11	11	11	11	11	11	11	11	11	11

(continued.....)

(...Table A4-1, cont'd)

Plot #34

Clod #	OC %	ρ_b (kgm^{-3})	Q_p (kPa)	w_Q ($kgkg^{-1}$)	TS (kPa)	w_{TS} ($kgkg^{-1}$)	$\bar{w}$ ($kgkg^{-1}$)	$\sigma_{R(d)}$ (mm)	$\sigma_{R(ind)}$ (mm)	$\bar{\sigma}_R$ (mm)
1	0.76	1700	664.58	0.171	2.21	0.162	0.167	0.275	0.237	0.256
2	0.76	1640	1427.73	0.156	4.49	0.148	0.152	0.325	0.191	0.258
3	2.07	1600	1721.71	0.173	7.06	0.179	0.176	0.280	0.230	0.255
4	0.80	1580	671.32	0.169	4.09	0.165	0.167	0.397	0.250	0.324
5	0.86	1640	1157.21	0.164	3.90	0.160	0.162	0.266	0.166	0.216
6	0.95	1570	1044.16	0.172	2.99	0.167	0.170	0.357	0.281	0.319
7	0.75	1630	1266.27	0.161	4.14	0.170	0.166	0.352	-.---	0.352
8	0.96	1600	850.87	0.173	3.96	0.173	0.173	0.400	0.294	0.347
9	0.92	1620	1425.61	0.169	4.20	0.170	0.170	0.253	0.297	0.275
10	0.94	1610	1390.05	0.174	3.34	0.178	0.176	0.297	0.384	0.341
Mean	0.98	1620	1161.95	0.168	4.04	0.167	0.168	0.320	0.259	0.294
± se	±0.12	±10	±111.31	±0.002	±0.40	±0.003	±0.002	±0.017	±0.022	±0.015
n	10	10	10	10	10	10	10	10	9	10

Plot #35

Clod #	OC %	ρ_b (kgm^{-3})	Q_p (kPa)	w_Q ($kgkg^{-1}$)	TS (kPa)	w_{TS} ($kgkg^{-1}$)	$\bar{w}$ ($kgkg^{-1}$)	$\sigma_{R(d)}$ (mm)	$\sigma_{R(ind)}$ (mm)	$\bar{\sigma}_R$ (mm)
1	1.65	1510	2555.37	0.182	9.11	0.178	0.180	0.430	0.165	0.298
2	1.46	1580	2622.88	0.174	7.01	0.166	0.170	0.166	0.154	0.160
3	0.87	1660	2463.16	0.161	4.05	0.157	0.159	0.199	0.312	0.256
4	0.69	1640	3684.50	0.147	7.46	0.146	0.147	0.263	-.---	0.263
5	0.87	1610	768.15	0.156	3.75	0.154	0.155	0.264	0.293	0.279
6	0.86	1650	2880.05	0.155	3.66	0.154	0.155	0.264	0.358	0.311
7	0.81	1680	3449.17	0.157	6.14	0.153	0.155	0.240	0.199	0.220
8	0.83	1690	728.47	0.159	7.72	0.150	0.155	0.176	0.145	0.161
9	0.94	1700	3038.39	0.157	6.16	0.156	0.157	0.201	-.---	0.201
10	0.73	1700	3629.73	0.142	6.34	0.143	0.143	0.224	0.174	0.199
Mean	0.97	1640	2581.99	0.159	6.14	0.156	0.158	0.243	0.225	0.235
± se	±0.10	±20	±335.07	±0.004	±0.58	±0.003	±0.003	±0.024	±0.029	±0.017
n	10	10	10	10	10	10	10	10	8	10

- (END OF TABLE A4 - 1) -

Table A4-2

Plot #5

Disk #	ρ_b ($kg\,m^{-3}$)	w ($kg\,kg^{-1}$)	TS (kPa)	$\sigma_{R(ind)}$ (mm)
1	----	-----	-----	-----
2	1930	0.158	45.05	0.210
3	1850	0.157	44.92	0.185
4	1890	0.167	35.51	0.351
5	1810	0.160	41.96	0.166
6	1850	0.170	32.65	0.177
7	1920	0.159	39.01	0.214
8	1890	0.167	37.16	0.195
9	1880	0.171	30.31	0.167
10	1880	0.176	28.12	0.322
Mean	1880	0.165	37.19	0.221
(± s.e.)	(± 10)	(± 0.002)	(± 2.04)	(± 0.023)
n	9	9	9	9

Plot #6

Disk #	ρ_b ($kg\,m^{-3}$)	w ($kg\,kg^{-1}$)	TS (kPa)	$\sigma_{R(ind)}$ (mm)
1	1970	0.161	40.41	0.135
2	1870	0.167	37.69	0.228
3	1870	0.168	43.66	0.258
4	1870	0.169	34.21	0.206
5	1970	0.164	45.37	0.159
6	1870	0.161	46.74	0.197
7	1850	0.164	37.59	0.186
8	1880	0.163	40.91	0.163
9	1780	0.174	27.64	0.224
10	1800	0.177	27.75	0.198
Mean	1870	0.167	38.20	0.195
(± s.e.)	(± 20)	(± 0.002)	(± 2.12)	(± 0.012)
n	10	10	10	10

(continued.....)

(...Table A4-2, cont'd)

Plot #7

Disk #	ρ_b ($kg\,m^{-3}$)	w ($kg\,kg^{-1}$)	TS (kPa)	$\sigma_{R(ind)}$ (mm)
1	1910	0.159	33.81	0.233
2	1880	0.163	43.84	0.197
3	1910	0.166	40.07	0.261
4	1950	0.163	44.99	0.152
5	1940	0.165	41.33	0.152
6	1850	0.172	35.80	0.276
7	1980	0.161	45.46	0.183
8	1860	0.160	39.56	0.252
9	1800	0.173	27.66	0.253
10	1910	0.171	38.60	0.252
Mean	1900	0.165	39.11	0.221
(± s.e.)	(± 20)	(± 0.002)	(± 1.74)	(± 0.015)
n	10	10	10	10

Plot #17

Disk #	ρ_b ($kg\,m^{-3}$)	w ($kg\,kg^{-1}$)	TS (kPa)	$\sigma_{R(ind)}$ (mm)
1	1810	0.170	36.38	0.260
2	1680	0.171	29.64	0.209
3	1830	0.185	32.61	0.143
4	1750	0.182	33.03	0.185
5	1790	0.180	33.50	0.222
6	1800	0.178	38.15	0.266
7	1740	0.172	35.03	0.272
8	1760	0.172	34.61	0.218
9	1820	0.184	29.32	0.276
10	1780	0.178	37.01	0.155
Mean	1780	0.177	33.93	0.221
(± s.e.)	(± 10)	(± 0.002)	(± 0.93)	(± 0.015)
n	10	10	10	10

(continued.....)

(...Table A4-2, cont'd)

Plot #18

Disk #	ρ_b ($kg\,m^{-3}$)	w ($kg\,kg^{-1}$)	TS (kPa)	$\sigma_{R(ind)}$ (mm)
1	1700	0.195	41.46	0.235
2	1700	0.190	46.95	0.153
3	1690	0.199	42.94	0.204
4	1700	0.201	33.72	0.182
5	1760	0.199	37.58	0.200
6	1720	0.192	43.28	0.226
7	1710	0.185	46.00	0.186
8	1710	0.190	40.83	0.301
9	1750	0.205	32.87	0.312
10	1710	0.203	34.10	0.228
Mean	1720	0.196	39.97	0.223
(± s.e.)	(± 10)	(± 0.002)	(± 1.62)	(± 0.016)
n	10	10	10	10

Plot #19

Disk #	ρ_b ($kg\,m^{-3}$)	w ($kg\,kg^{-1}$)	TS (kPa)	$\sigma_{R(ind)}$ (mm)
1	1730	0.201	41.97	0.112
2	1720	0.197	41.28	0.162
3	1700	0.204	41.39	0.189
4	1670	0.206	34.51	0.207
5	1730	0.209	34.74	0.216
6	1710	0.208	40.26	0.157
7	1670	0.192	44.44	0.214
8	1750	0.196	45.24	0.178
9	1270	0.208	29.48	0.242
10	1720	0.204	44.83	0.342
Mean	1670	0.203	39.82	0.202
(± s.e.)	(± 40)	(± 0.002)	(± 1.65)	(± 0.019)
n	10	10	10	10

(continued.....)

(...Table A4-2, cont'd)

Plot #20

Disk #	ρ_b ($kg\,m^{-3}$)	w ($kg\,kg^{-1}$)	TS (kPa)	$\sigma_{R(ind)}$ (mm)
1	1700	0.202	40.14	0.174
2	1690	0.199	41.16	0.218
3	1630	0.207	34.69	0.172
4	1740	0.205	37.88	0.155
5	1670	0.215	29.42	0.241
6	1680	0.215	37.47	0.223
7	1710	0.200	43.51	0.235
8	1730	0.199	43.40	0.167
9	1670	0.213	34.49	0.179
10	1700	0.202	36.67	0.189
Mean	1690	0.206	37.88	0.195
(± s.e.)	(± 10)	(± 0.002)	(± 1.39)	(± 0.010)
n	10	10	10	10

Plot #29

Disk #	ρ_b ($kg\,m^{-3}$)	w ($kg\,kg^{-1}$)	TS (kPa)	$\sigma_{R(ind)}$ (mm)
1	1560	0.218	33.01	0.233
2	1610	0.226	34.66	0.177
3	1570	0.237	32.03	0.245
4	1670	0.233	26.94	0.173
5	1560	0.235	29.66	0.230
6	1630	0.238	35.73	0.174
7	1580	0.228	40.75	0.256
8	1610	0.225	32.22	0.299
9	1650	0.227	32.81	0.210
10	1640	0.227	34.74	0.147
Mean	1610	0.229	33.25	0.214
(± s.e.)	(± 10)	(± 0.002)	(± 1.17)	(± 0.015)
n	10	10	10	10

(continued.....)

(...Table A4-2, cont'd)

Plot #34

Disk #	ρ_b ($kg\,m^{-3}$)	w ($kg\,kg^{-1}$)	TS (kPa)	$\sigma_{R(ind)}$ (mm)
1	1920	0.115	29.39	0.286
2	1850	0.156	34.14	0.159
3	1880	0.160	29.17	0.231
4	1880	0.167	30.25	0.228
5	1740	0.166	25.71	0.250
6	1860	0.167	28.03	0.183
7	1830	0.155	29.40	0.187
8	1810	0.159	24.59	0.118
9	1750	0.183	29.96	0.123
10	1840	0.159	28.97	0.237
Mean	1840	0.163	28.96	0.200
(± s.e.)	(± 20)	(± 0.003)	(± 0.82)	(± 0.018)
n	10	10	10	10

Plot #35

Disk #	ρ_b ($kg\,m^{-3}$)	w ($kg\,kg^{-1}$)	TS (kPa)	$\sigma_{R(ind)}$ (mm)
1	1810	0.160	33.20	0.197
2	1820	0.159	30.76	0.315
3	1840	0.167	32.02	0.164
4	1790	0.164	37.90	0.180
5	1860	0.172	31.72	0.183
6	1890	0.166	38.30	0.252
7	1890	0.160	39.89	0.214
8	1780	0.163	37.35	0.184
9	1930	0.164	26.00	0.219
10	1800	0.172	26.61	0.276
Mean	1840	0.165	33.37	0.218
(± s.e.)	(± 20)	(± 0.001)	(± 1.54)	(± 0.015)
n	10	10	10	10

- (END OF TABLE A4- 2) -

Table A4-3

Suction = 0.1 kPa
Plot #29

Disk #	ρ_b ($kg\,m^{-3}$)	w ($kg\,kg^{-1}$)	Q_p (kPa)	TS (kPa)	$\sigma_{R(ind)}$ (mm)
1	1640	0.273	118.60	--.--	0.220
2	1630	0.273	114.61	--.--	0.252
3	1630	0.278	120.41	--.--	0.227
4	1660	0.275	168.20	--.--	0.221
5	1700	0.283	116.36	--.--	0.138
6	1650	0.273	157.72	--.--	0.207
7	1670	0.280	110.37	--.--	0.477
8	1670	0.271	144.50	--.--	0.181
9	1700	0.274	137.51	--.--	0.107
10	1640	0.280	125.28	--.--	0.203
Mean	1660	0.276	131.36	--.--	0.223
(± s.e.)	(± 10)	(± 0.001)	(± 6.26)	--.--	(±0.031)
n	10	10	10		10

Suction = 0.1 kPa
Plot #35

Disk #	ρ_b ($kg\,m^{-3}$)	w ($kg\,kg^{-1}$)	Q_p (kPa)	TS (kPa)	$\sigma_{R(ind)}$ (mm)
1	1830	0.199	8.92	--.--	0.080
2	1860	0.201	9.92	--.--	0.370
3	1830	0.200	12.73	--.--	0.213
4	1830	0.207	21.46	--.--	0.124
5	1880	0.206	14.23	--.--	0.286
6	1820	0.203	24.83	--.--	0.232
7	1890	0.200	14.04	--.--	0.178
8	1850	0.200	27.89	--.--	0.423
9	1850	0.196	60.71	--.--	0.221
10	1830	0.201	28.51	--.--	0.201
Mean	1850	0.201	22.32	--.--	0.233
(± s.e.)	(± 10)	(± 0.001)	(± 4.82)	--.--	(±0.033)
n	10	10	10		10

(continued.....)

(...Table A4-3 cont'd)

Suction = 1.0 kPa
Plot #29

Disk #	ρ_b ($kg\,m^{-3}$)	w ($kg\,kg^{-1}$)	Q_p (kPa)	TS (kPa)	$\sigma_{R(ind)}$ (mm)
1	1640	0.267	358.24	--.--	0.181
2	1610	0.272	358.62	--.--	0.240
3	1660	0.257	341.40	--.--	0.180
4	1680	0.260	345.45	--.--	0.182
5	1680	0.259	423.88	--.--	0.173
6	1670	0.260	317.19	--.--	0.153
7	1660	0.270	232.09	--.--	0.181
8	1650	0.262	246.82	--.--	0.297
9	1620	0.268	287.62	--.--	0.172
10	1600	0.279	277.89	--.--	0.197
Mean	1650	0.265	318.92	--.--	0.196
(± s.e)	(± 10)	(± 0.002)	(± 18.49)	--.--	(±0.013)
n	10	10	10		10

Suction = 1.0 kPa
Plot #35

Disk #	ρ_b ($kg\,m^{-3}$)	w ($kg\,kg^{-1}$)	Q_p (kPa)	TS (kPa)	$\sigma_{R(ind)}$ (mm)
1	1870	0.186	53.16	--.--	0.212
2	1850	0.192	55.47	--.--	0.163
3	1850	0.193	24.27	--.--	0.163
4	1810	0.192	44.24	--.--	0.195
5	1800	0.192	35.56	--.--	0.238
6	1790	0.185	100.51	--.--	0.256
7	1810	0.189	36.50	--.--	0.320
8	1790	0.188	50.35	--.--	0.193
9	1780	0.186	49.48	--.--	0.116
10	1850	0.189	39.24	--.--	0.285
Mean	1820	0.189	48.88	--.--	0.214
(± s.e)	(± 10)	(± 0.001)	(± 6.48)	--.--	(±0.020)
n	10	10	10		10

(continued.....)

(...Table A4-3 cont'd)

Suction = 5.0 kPa
Plot #29

Disk #	ρ_b (kg m^{-3})	w (kg kg^{-1})	Q_p (kPa)	TS (kPa)	$\sigma_{R(ind)}$ (mm)
1	1610	0.251	616.41	--.--	0.137
2	1630	0.254	549.28	--.--	0.120
3	1680	0.249	428.62	--.--	0.187
4	1650	0.250	533.37	--.--	0.118
5	1650	0.252	556.77	--.--	0.291
6	1620	0.255	659.28	--.--	0.168
7	1690	0.244	593.89	--.--	0.197
8	1680	0.249	576.17	--.--	0.173
9	1630	0.249	518.84	--.--	0.122
10	1680	0.249	549.59	--.--	0.246
Mean	1650	0.250	558.22	--.--	0.176
(± s.e.)	(± 10)	(± 0.001)	(± 19.53)	--.--	(±0.018)
n	10	10	10		10

Suction = 5.0 kPa
Plot #35

Disk #	ρ_b (kg m^{-3})	w (kg kg^{-1})	Q_p (kPa)	TS (kPa)	$\sigma_{R(ind)}$ (mm)
1	1790	0.188	61.08	--.--	0.121
2	1820	0.185	92.40	--.--	0.164
3	1830	0.181	94.40	--.--	0.282
4	1840	0.184	77.49	--.--	0.330
5	1800	0.185	147.93	--.--	0.213
6	1830	0.184	158.47	--.--	0.126
7	1750	0.193	104.19	--.--	0.167
8	1800	0.178	218.05	--.--	0.190
9	1760	0.186	126.90	--.--	0.226
10	1780	0.183	219.24	--.--	0.242
Mean	1800	0.185	130.02	--.--	0.206
(± s.e.)	(± 10)	(± 0.001)	(± 17.55)	--.--	(±0.021)
n	10	10	10		10

(continued...)

(...Table A4-3 cont'd)

Suction = 10.0 kPa
Plot #29

Disk #	ρ_b ($kg\,m^{-3}$)	w ($kg\,kg^{-1}$)	Q_p (kPa)	TS (kPa)	$\sigma_{R(ind)}$ (mm)
1	1660	0.241	684.92	--.--	0.165
2	1660	0.234	1005.17	--.--	0.204
3	1610	0.244	740.20	--.--	0.145
4	1590	0.248	771.33	--.--	0.137
5	1610	0.248	591.77	--.--	0.230
6	1680	0.241	884.94	--.--	0.225
7	1680	0.245	438.42	--.--	0.163
8	1600	0.243	1237.51	--.--	0.221
9	1690	0.241	608.05	--.--	0.239
10	1610	0.249	661.58	--.--	-.---
Mean	1640	0.243	762.39	--.--	0.192
(± s.e.)	(± 10)	(± 0.001)	(± 72.60)	--.--	(±0.013)
n	10	10	10		9

Suction = 10.0 kPa
Plot #35

Disk #	ρ_b ($kg\,m^{-3}$)	w ($kg\,kg^{-1}$)	Q_p (kPa)	TS (kPa)	$\sigma_{R(ind)}$ (mm)
1	1830	0.175	99.83	--.--	0.198
2	1800	0.175	157.34	--.--	0.151
3	1860	0.176	95.39	--.--	0.160
4	1820	0.177	137.94	--.--	0.221
5	1800	0.174	208.07	--.--	0.219
6	1860	0.180	86.72	--.--	0.163
7	1860	0.176	65.01	--.--	0.163
8	1800	0.175	128.77	--.--	0.234
9	1860	0.176	69.00	--.--	0.152
10	1860	0.179	165.52	--.--	0.150
Mean	1840	0.176	121.36	--.--	0.181
(± s.e.)	(± 10)	(± 0.001)	(± 14.66)	--.--	(±0.011)
n	10	10	10		10

(continued...)

(...Table A4-3 cont'd)

Suction = 50.0 kPa
Plot #29

Disk #	ρ_b ($kg\,m^{-3}$)	w ($kg\,kg^{-1}$)	Q_p (kPa)	TS (kPa)	$\sigma_{R(ind)}$ (mm)
1	1600	0.191	4749.00	--.--	0.177
2	1670	0.187	4629.84	--.--	0.254
3	1660	0.186	4874.28	--.--	0.153
4	1720	0.184	5960.12	--.--	0.195
5	1650	0.187	5779.19	--.--	0.176
6	1600	0.187	4632.77	35.52	0.133
7	1630	0.186	4155.92	37.21	0.161
8	1680	0.186	5159.78	40.59	0.161
9	1650	0.184	5326.23	36.08	0.180
10	1650	0.184	5019.28	40.03	0.143
Mean	1650	0.186	5028.64	37.89	0.173
(± s.e.)	(± 10)	(± 0.001)	(± 173.73)	(±1.03)	(±0.011)
n	10	10	10	5	10

Suction = 50.0 kPa
Plot #35

Disk #	ρ_b ($kg\,m^{-3}$)	w ($kg\,kg^{-1}$)	Q_p (kPa)	TS (kPa)	$\sigma_{R(ind)}$ (mm)
1	1820	0.150	2211.48	--.--	0.198
2	1800	0.152	4299.55	--.--	0.131
3	1810	0.149	2325.90	--.--	0.192
4	1820	0.150	3098.04	--.--	0.166
5	1800	0.149	2962.40	--.--	0.234
6	1830	0.147	3600.47	32.70	0.134
7	1810	0.147	2993.16	43.97	0.146
8	1840	0.146	3216.52	38.34	0.202
9	1870	0.148	4038.63	46.79	0.161
10	1870	0.147	4279.02	37.77	0.144
Mean	1830	0.149	3302.52	39.92	0.171
(± s.e.)	(± 10)	(± 0.001)	(± 235.30)	(±2.48)	(±0.011)
n	10	10	10	5	10

(continued...)

(...Table A4-3 cont'd)

Suction = AIR DRY
Plot #29

Disk #	ρ_b ($kg\,m^{-3}$)	w ($kg\,kg^{-1}$)	Q_p (kPa)	TS (kPa)	$\sigma_{R(ind)}$ (mm)
1	1600	0.016	--.--	261.30	0.176
2	1610	0.017	--.--	209.29	0.127
3	1630	0.017	--.--	253.83	0.112
4	1560	0.018	--.--	226.90	0.183
5	1620	0.016	--.--	297.08	0.177
6	1640	0.017	--.--	273.51	0.143
7	1590	0.017	--.--	241.60	0.110
8	1650	0.017	--.--	248.24	0.139
9	1600	0.017	--.--	265.19	0.156
10	1620	0.016	--.--	250.74	0.090
Mean	1610	0.017	--.--	252.77	0.141
(± s.e)	(± 10)	(± 0.0002)	--.--	(±7.70)	(±0.010)
n	10	10		10	10

Suction = AIR DRY
Plot #35

Disk #	ρ_b ($kg\,m^{-3}$)	w ($kg\,kg^{-1}$)	Q_p (kPa)	TS (kPa)	$\sigma_{R(ind)}$ (mm)
1	1810	0.012	--.--	293.50	0.116
2	1760	0.012	--.--	298.75	0.127
3	1790	0.012	--.--	347.15	0.133
4	1760	0.013	--.--	270.49	0.108
5	1780	0.013	--.--	279.29	0.147
6	1760	0.012	--.--	256.18	0.116
7	1740	0.013	--.--	305.42	0.138
8	1760	0.012	--.--	291.26	0.104
9	1750	0.013	--.--	278.02	0.217
10	1740	0.013	--.--	315.52	0.108
Mean	1770	0.013	--.--	293.56	0.131
(± s.e)	(± 10)	(± 0.0002)	--.--	(±8.10)	(±0.011)
n	10	10		10	10

(continued...)

(...Table A4-3 cont'd)

Suction = OVEN DRY
Plot #29

Disk #	ρ_b ($kg\,m^{-3}$)	w ($kg\,kg^{-1}$)	Q_p (kPa)	TS (kPa)	$\sigma_{R(ind)}$ (mm)
1	1590	0	--.--	344.48	0.139
2	1600	"	--.--	297.27	0.086
3	1610	"	--.--	348.55	0.131
4	1610	"	--.--	346.73	0.165
5	1610	"	--.--	322.19	0.100
6	1620	"	--.--	297.13	0.117
7	1600	"	--.--	298.56	0.131
8	1620	"	--.--	340.22	0.128
9	1610	"	--.--	356.74	0.139
10	1590	"	--.--	292.56	0.094
Mean	1610	0	--.--	324.44	0.123
(± s.e)	(± 3)	--	--.--	(±8.13)	(±0.008)
n	10	10		10	10

Suction = OVEN DRY
Plot #35

Disk #	ρ_b ($kg\,m^{-3}$)	w ($kg\,kg^{-1}$)	Q_p (kPa)	TS (kPa)	$\sigma_{R(ind)}$ (mm)
1	1780	0	--.--	350.23	0.178
2	1760	"	--.--	380.20	0.172
3	1780	"	--.--	430.49	0.100
4	1740	"	--.--	356.21	0.152
5	1740	"	--.--	375.98	0.138
6	1780	"	--.--	400.63	0.175
7	1760	"	--.--	361.08	0.168
8	1800	"	--.--	453.56	0.087
9	1710	"	--.--	403.31	0.135
10	1720	"	--.--	360.09	0.144
Mean	1760	0	--.--	387.18	0.145
(± s.e)	(± 10)	--	--.--	(±10.87)	(±0.010)
n	10	10		10	10

- (END OF TABLE A4 - 3) -

Table A4 - 4

Suction = AIR DRY
Plot #5

Clod #	ρ_b* ($kg\,m^{-3}$)	w ($kg\,kg^{-1}$)	TS (kPa)	$\sigma_{R(ind)}$ (mm)
1	1560	0.009	83.73	0.252
2	1750	0.009	26.40	0.248
3	1710	0.008	57.59	0.206
4	1540	0.010	31.58	0.301
5	1550	0.017	71.87	0.177
6	1670	0.012	33.80	0.286
7	1550	0.013	35.70	0.223
8	1710	0.011	54.27	0.281
9	1710	0.010	60.02	0.222
Mean	1640	0.011	50.55	0.244
(± s.e.)	(± 30)	(± 0.001)	(± 6.62)	(± 0.014)
n	9	9	9	9

Suction = AIR DRY
Plot #6

Clod #	ρ_b* ($kg\,m^{-3}$)	w ($kg\,kg^{-1}$)	TS (kPa)	$\sigma_{R(ind)}$ (mm)
1	1690	0.010	75.27	0.226
2	1700	0.010	50.07	0.201
3	1650	0.014	106.41	0.155
4	1920	0.011	82.77	0.250
5	1620	0.011	51.75	0.197
6	1640	0.011	58.61	0.194
7	1850	0.013	92.32	0.156
8	1800	0.015	86.35	0.193
9	1600	0.015	69.26	0.236
10	1660	0.011	87.45	0.219
11	1650	0.012	71.30	0.214
12	1550	0.012	61.21	0.168
Mean	1690	0.012	74.90	0.201
(± s.e.)	(± 30)	(± 0.001)	(± 4.80)	(± 0.009)
n	12	12	12	12

* Values of bulk density were estimated from the measured geometric mean diameter and oven dry mass of each clod, assuming that the clods were roughly spherical in shape.

(continued.....)

(...Table A4-4 cont'd)

Suction = AIR DRY
Plot #7

Clod #	ρ_b* ($kg\,m^{-3}$)	w ($kg\,kg^{-1}$)	TS (kPa)	$\sigma_{R(ind)}$ (mm)
1	1640	0.010	55.84	0.207
2	1690	0.012	63.72	0.252
3	1550	0.011	61.00	0.175
4	1560	0.010	57.98	0.240
5	1900	0.010	90.38	0.111
6	1770	0.011	146.74	- . - - -
7	1880	0.010	79.79	0.268
8	1760	0.011	93.73	0.329
9	1550	0.010	42.78	0.171
Mean	1700	0.011	76.88	0.219
(± s.e.)	(± 50)	(± 0.0002)	(± 10.37)	(± 0.024)
n	9	9	9	8

Suction = AIR DRY
Plot #17

Clod #	ρ_b* ($kg\,m^{-3}$)	w ($kg\,kg^{-1}$)	TS (kPa)	$\sigma_{R(ind)}$ (mm)
1	1490	0.015	97.94	0.122
2	1470	0.013	27.37	- . - - -
3	1670	0.011	37.21	- . - - -
4	1830	0.011	81.18	0.193
5	1570	0.014	19.68	0.222
6	1590	0.014	56.72	0.242
7	1740	0.013	82.88	0.243
8	1750	0.010	30.10	0.289
9	1510	0.013	46.23	0.226
10	1790	0.013	46.37	0.251
11	1530	0.013	43.74	0.236
12	1680	0.014	57.54	0.111
13	1760	0.017	91.30	0.199
14	1600	0.011	68.87	0.162
15	1770	0.013	67.54	0.129
16	1610	0.010	55.84	0.167
17	1810	0.013	108.53	0.231
Mean	1660	0.013	59.94	0.202
(± s.e.)	(± 30)	(± 0.0004)	(± 6.26)	(± 0.014)
n	17	17	17	15

* Values of bulk density were estimated from the measured geometric mean diameter and oven dry mass of each clod, assuming that the clods were roughly spherical in shape.

(continued.....)

(...Table A4-4 cont'd)

Suction = AIR DRY
Plot #18

Clod #	ρ_b* ($kg\,m^{-3}$)	w ($kg\,kg^{-1}$)	TS (kPa)	$\sigma_{R(ind)}$ (mm)
1	1740	0.018	88.18	- . - - -
2	1610	0.017	76.06	0.157
3	1620	0.015	41.22	0.129
4	1570	0.017	65.93	0.243
5	1470	0.014	34.97	0.329
6	1570	0.018	81.10	0.137
7	1790	0.017	133.53	0.208
8	1590	0.017	66.70	0.244
Mean	1620	0.017	73.46	0.207
(± s.e.)	(± 40)	(± 0.0005)	(± 10.79)	(± 0.027)
n	8	8	8	7

Suction = AIR DRY
Plot #19

Clod #	ρ_b* ($kg\,m^{-3}$)	w ($kg\,kg^{-1}$)	TS (kPa)	$\sigma_{R(ind)}$ (mm)
1	1730	0.017	37.68	0.237
2	1590	0.020	82.05	0.122
3	1710	0.017	69.09	0.129
4	1720	0.018	69.84	0.151
5	1650	0.016	58.07	0.344
6	1330	0.016	43.24	0.306
7	1690	0.017	67.39	0.240
8	1420	0.017	33.38	0.224
9	1920	0.018	115.19	0.140
10	1370	0.017	67.19	- . - - -
11	1530	0.015	57.49	0.164
12	1560	0.020	65.61	0.193
13	1470	0.024	42.29	0.244
14	1630	0.014	79.90	0.167
15	1420	0.017	71.20	0.123
16	1460	0.016	54.78	0.255
17	1480	0.017	61.24	0.210
Mean	1570	0.017	63.27	0.203
(± s.e.)	(± 40)	(± 0.001)	(± 4.71)	(± 0.017)
n	17	17	17	16

* Values of bulk density were estimated from the measured geometric mean diameter and oven dry mass of each clod, assuming that the clods were roughly spherical in shape.

(continued.....)

(...Table A4-4 cont'd)

Suction = AIR DRY
Plot #20

Clod #	ρ_b* ($kg\,m^{-3}$)	w ($kg\,kg^{-1}$)	TS (kPa)	$\sigma_{R(ind)}$ (mm)
1	1480	0.012	46.37	- . - - -
2	1510	0.013	45.77	0.204
3	1570	0.013	60.44	0.140
4	1580	0.013	69.04	0.199
5	1810	0.013	81.89	0.116
6	1560	0.016	74.91	0.128
7	1690	0.013	52.93	- . - - -
8	1840	0.016	86.85	0.265
Mean	1630	0.014	64.78	0.175
(± s.e.)	(± 50)	(± 0.0005)	(± 5.61)	(± 0.023)
n	8	8	8	6

Suction = AIR DRY
Plot #29

Clod #	ρ_b* ($kg\,m^{-3}$)	w ($kg\,kg^{-1}$)	TS (kPa)	$\sigma_{R(ind)}$ (mm)
1	1600	0.018	83.12	0.178
2	1590	0.017	48.49	- . - - -
3	1710	0.018	132.04	0.138
4	1550	0.017	53.35	0.270
5	1670	0.021	86.94	0.182
6	1470	0.021	44.58	0.399
7	1510	0.016	71.33	0.204
8	1350	0.021	61.93	0.294
9	1300	0.018	55.47	0.250
10	1500	0.020	54.42	0.187
11	1440	0.017	54.85	0.235
12	1630	0.016	44.63	- . - - -
13	1400	0.016	44.84	0.280
14	1590	0.018	48.40	0.307
15	1420	0.018	41.03	- . - - -
Mean	1520	0.018	61.69	0.244
(± s.e.)	(± 30)	(± 0.0005)	(± 6.17)	(± 0.021)
n	15	15	15	12

* Values of bulk density were estimated from the measured geometric mean diameter and oven dry mass of each clod, assuming that the clods were roughly spherical in shape.

(continued.....)

(...Table A4-4 cont'd)

Suction = AIR DRY
Plot #34

Clod #	ρ_b* ($kg\,m^{-3}$)	w ($kg\,kg^{-1}$)	TS (kPa)	$\sigma_{R(ind)}$ (mm)
1	1540	0.009	65.66	0.191
2	1650	0.010	33.86	0.159
3	1800	0.009	38.38	0.137
4	1640	0.010	52.59	0.287
5	1620	0.010	53.93	0.131
6	1730	0.009	41.83	- . - - -
7	1650	0.009	22.48	0.325
8	1750	0.010	71.17	- . - - -
9	1560	0.009	30.12	0.179
10	1920	0.011	83.56	0.129
Mean	1680	0.010	49.36	0.192
(± s.e.)	(± 40)	(± 0.0002)	(± 6.19)	(± 0.026)
n	10	10	10	8

Suction = AIR DRY
Plot #35

Clod #	ρ_b* ($kg\,m^{-3}$)	w ($kg\,kg^{-1}$)	TS (kPa)	$\sigma_{R(ind)}$ (mm)
1	1810	0.011	49.26	0.206
2	1670	0.010	71.94	- . - - -
3	1660	0.013	68.63	- . - - -
4	1340	0.018	73.36	0.305
5	1500	0.017	132.87	0.300
6	1650	0.011	46.12	0.198
7	1860	0.010	89.03	- . - - -
8	1670	0.013	77.94	- . - - -
9	1510	0.017	100.93	0.191
10	- - - -	0.017	181.23	0.196
11	1850	0.016	135.38	0.146
12	1860	0.014	159.67	0.293
13	1810	0.010	90.71	- . - - -
14	1750	0.014	38.60	0.186
15	1770	0.014	110.78	- . - - -
16	1890	0.014	155.23	0.135
Mean	1710	0.014	98.85	0.216
(± s.e.)	(± 40)	(± 0.001)	(± 10.81)	(± 0.020)
n	15	16	16	10

* Values of bulk density were estimated from the measured geometric mean diameter and oven dry mass of each clod, assuming that the clods were roughly spherical in shape.

(...Table A4-4 cont'd)

Suction = OVEN DRY
Plot #5

Clod #	W ($kg kg^{-1}$)	TS (kPa)	$\sigma_{R(ind)}$ (mm)
1	0	50.71	0.180
2	"	130.72	0.160
3	"	73.67	-.---
4	"	63.02	0.282
5	"	48.87	0.214
6	"	79.61	-.---
7	"	53.88	0.236
8	"	45.41	0.141
9	"	58.22	0.283
Mean	0	67.12	0.214
(± s.e.)	-	(± 8.81)	(± 0.021)
n	9	9	9

Suction = OVEN DRY
Plot #6

Clod #	W ($kg kg^{-1}$)	TS (kPa)	$\sigma_{R(ind)}$ (mm)
1	0	44.74	0.217
2	"	90.44	0.231
3	"	108.20	0.171
4	"	84.94	0.341
5	"	76.55	-.---
6	"	100.78	0.152
7	"	118.05	0.181
8	"	110.51	-.---
9	"	39.78	0.234
10	"	64.41	0.157
11	"	90.01	0.154
12	"	133.46	-.---
Mean	0	88.49	0.204
(± s.e.)	-	(± 8.23)	(± 0.020)
n	12	12	9

(continued.....)

(...Table A4-4 cont'd)

Suction = OVEN DRY
Plot #7

Clod #	w ($kg\,kg^{-1}$)	TS (kPa)	$\sigma_{R(ind)}$ (mm)
1	0	80.42	0.224
2	"	61.32	0.164
3	"	80.25	0.199
4	"	67.35	0.106
5	"	74.43	0.171
6	"	43.49	0.141
7	"	54.85	0.290
8	"	143.55	0.295
9	"	135.18	-.---
Mean	0	82.32	0.199
(± s.e.)	-	(± 11.51)	(± 0.024)
n	9	9	8

Suction = OVEN DRY
Plot #17

Clod #	w ($kg\,kg^{-1}$)	TS (kPa)	$\sigma_{R(ind)}$ (mm)
1	0	74.20	0.145
2	"	85.88	0.263
3	"	46.45	0.135
4	"	77.73	0.287
5	"	47.60	0.194
6	"	97.02	0.340
7	"	131.82	0.196
8	"	117.91	0.184
9	"	85.82	0.110
10	"	54.07	0.342
11	"	94.27	-.---
12	"	40.99	0.116
13	"	72.63	0.144
14	"	71.24	-.---
15	"	96.39	0.140
16	"	88.07	0.118
17	"	37.39	0.281
Mean	0	77.62	0.200
(± s.e.)	-	(± 6.44)	(± 0.021)
n	17	17	15

(continued.....)

(...Table A4-4 cont'd)

Suction = OVEN DRY
Plot #18

Clod #	w ($kg\,kg^{-1}$)	TS (kPa)	$\sigma_{R(ind)}$ (mm)
1	0	89.34	0.164
2	"	81.92	0.185
3	"	66.43	0.247
4	"	76.42	0.234
5	"	71.76	0.261
6	"	77.85	0.133
7	"	69.47	- . - - -
8	"	90.74	0.166
Mean	0	77.99	0.199
(± s.e.)	-	(± 3.15)	(± 0.018)
n	8	8	7

Suction = OVEN DRY
Plot #19

Clod #	w ($kg\,kg^{-1}$)	TS (kPa)	$\sigma_{R(ind)}$ (mm)
1	0	74.57	0.106
2	"	90.37	0.240
3	"	107.42	0.098
4	"	33.88	0.283
5	"	56.32	0.326
6	"	60.85	0.306
7	"	31.94	- . - - -
8	"	66.38	0.340
9	"	60.56	- . - - -
10	"	55.45	- . - - -
11	"	39.22	0.310
12	"	83.31	0.221
13	"	129.10	- . - - -
14	"	94.87	0.142
15	"	56.37	0.171
16	"	79.25	0.159
17	"	41.15	0.309
Mean	0	68.29	0.232
(± s.e.)	-	(± 6.49)	(± 0.024)
n	17	17	13

(continued.....)

(...Table A4-4 cont'd)

Suction = OVEN DRY
Plot #20

Clod #	W ($kg\,kg^{-1}$)	TS (kPa)	$\sigma_{R(ind)}$ (mm)
1	0	62.09	0.171
2	"	78.98	0.182
3	"	40.91	0.255
4	"	41.13	0.380
5	"	46.77	0.113
6	"	142.08	0.257
7	"	56.12	0.187
8	"	83.31	0.220
Mean	0	68.92	0.221
(± s.e.)	-	(± 11.89)	(± 0.028)
n	8	8	8

Suction = OVEN DRY
Plot #29

Clod #	W ($kg\,kg^{-1}$)	TS (kPa)	$\sigma_{R(ind)}$ (mm)
1	0	68.78	0.214
2	"	33.79	0.221
3	"	57.49	0.230
4	"	84.16	0.202
5	"	40.91	0.178
6	"	35.60	-.---
7	"	94.92	0.158
8	"	51.26	0.296
9	"	85.48	-.---
10	"	78.04	0.226
11	"	116.89	-.---
12	"	93.24	0.159
13	"	94.00	0.319
14	"	61.37	0.339
15	"	47.31	-.---
Mean	0	69.55	0.231
(± s.e.)	-	(± 6.50)	(± 0.019)
n	15	15	11

(continued.....)

(...Table A4-4 cont'd)

Suction = OVEN DRY
Plot #34

Clod #	w ($kg\,kg^{-1}$)	TS (kPa)	$\sigma_{R(ind)}$ (mm)
1	0	85.07	0.220
2	"	51.97	0.172
3	"	113.82	0.163
4	"	58.48	0.344
5	"	52.66	0.144
6	"	58.44	-.---
7	"	61.03	-.---
8	"	87.93	0.100
9	"	52.66	0.233
10	"	96.72	-.---
Mean	0	71.88	0.197
(± s.e.)	-	(± 7.01)	(± 0.030)
n	10	10	7

Suction = OVEN DRY
Plot #35

Clod #	w ($kg\,kg^{-1}$)	TS (kPa)	$\sigma_{R(ind)}$ (mm)
1	0	79.59	0.169
2	"	160.18	-.---
3	"	134.58	0.223
4	"	68.55	0.152
5	"	139.73	-.---
6	"	121.32	0.141
7	"	112.69	0.243
8	"	52.11	0.188
9	"	67.51	0.160
10	"	128.84	0.193
11	"	55.67	0.144
12	"	115.15	-.---
13	"	96.18	0.127
14	"	148.33	-.---
15	"	190.91	0.202
16	"	192.38	0.203
Mean	0	116.48	0.179
(± s.e.)	-	(± 11.10)	(± 0.010)
n	16	16	12

- (END OF TABLE A4 - 4) -

Appendix 5. Raw Data For SECTION 7

Appendix 5 consists of several Tables, each of which contains the raw data needed for the calculation of mean values listed in **SECTION 7.3.** For the rapid wetting experiments data are tabulated on bulk density, ρ_b, tensile strength, **TS**, fracture surface rugosity, σ_R, from the single-transect (**ST**) method, and mean fracture surface rugosity, $\bar{\sigma}_R$, resulting from the multiple-transect (**MT**) method, using laser scanning.

Table A5-1

Soil: Wiesenboden
Treatment: Rapidly Wetted

Disk #	ρ_b* ($kg kg^{-3}$)	TS (kPa)	σ_R-ST (mm)	$\bar{\sigma}_R$-MT (mm)	(± s.e.) (mm)	laser scans
1	1500	185.89	0.104	0.154	(± 0.0039)	76
2	1520	205.78	0.243	0.155	(± 0.0051)	81
3	1530	203.67	0.244	0.168	(± 0.0041)	81
4	1480	153.73	0.138	0.161	(± 0.0036)	81
5	1530	235.00	- . - - -	0.192	(± 0.0027)	81
6	1530	189.65	0.240	0.191	(± 0.0040)	76
7	1460	142.75	0.161	0.169	(± 0.0060)	81
8	1500	167.50	0.170	0.176	(± 0.0025)	81
9	1520	179.74	0.183	0.195	(± 0.0040)	81
10	1480	173.45	0.260	0.237	(± 0.0054)	81
11	1520	188.83	0.220	0.183	(± 0.0041)	81
12	1510	175.62	0.181	0.182	(± 0.0088)	81
13	1540	193.36	0.176	0.208	(± 0.0075)	71
14	1460	115.30	0.204	0.197	(± 0.0078)	66
15	1500	150.56	0.194	0.176	(± 0.0050)	81
16	1530	193.36	0.276	0.211	(± 0.0060)	76
Mean	1510	178.39	0.200	0.185		
(± s.e.)	(± 10)	(± 7.1)	(± 0.012)	(± 0.006)		
n	16	16	15	16		

*calculated after wetted disks were oven dried

Soil: Wiesenboden
Treatment: Non-Wetted Control

Disk #	ρ_b ($kg kg^{-3}$)	TS (kPa)	σ_R-ST (mm)	$\bar{\sigma}_R$-MT (mm)	(± s.e.) (mm)	laser scans
17	1690	825.32	0.166	0.103	(± 0.0030)	71
18	1670	926.59	0.139	0.140	(± 0.0069)	76
19	1660	920.58	0.119	0.123	(± 0.0042)	66
20	1660	1041.84	0.205	0.140	(± 0.0033)	76
21	1690	978.70	0.104	0.126	(± 0.0060)	71
22	1710	836.53	0.143	0.121	(± 0.0026)	76
23	1690	956.88	0.107	0.124	(± 0.0020)	71
24	1650	713.24	0.117	0.116	(± 0.0037)	76
25	1690	908.22	0.200	0.112	(± 0.0016)	71
26	1680	928.79	0.176	0.130	(± 0.0040)	81
27	1680	847.41	0.172	0.141	(± 0.0033)	76
28	1660	712.03	0.134	0.094	(± 0.0013)	76
29	1670	962.95	0.128	0.115	(± 0.0040)	76
30	1700	984.42	0.091	0.132	(± 0.0033)	71
31	1720	1050.80	0.164	0.195	(± 0.0023)	71
32	1640	756.89	0.133	0.148	(± 0.0042)	76
Mean	1680	903.20	0.144	0.129		
(± s.e.)	(± 10)	(± 29.47)	(± 0.008)	(± 0.006)		
n	16	16	16	16		

(continued.....)

(...Table A5-1 cont'd.)

Soil: Urrbrae
Treatment: Non-Aged Control

Disk #	ρ_b ($kgkg^{-3}$)	w ($kgkg^{-3}$)	TS (kPa)	σ_R-ST (mm)	$\bar{\sigma}_R$-MT (mm)	(± s.e.) (mm)	laser scans	Q_p (kPa)	w ($kgkg^{-3}$)
33	1680	0.149	282.20	-.---	0.112	(± 0.0027)	81	-.-	-.-
34	1610	0.147	193.86	0.133	0.120	(± 0.0022)	81	-.-	-.-
35	1610	0.150	160.16	0.147	0.145	(± 0.0034)	76	-.-	-.-
36	1680	0.146	201.78	0.150	0.120	(± 0.0022)	76	-.-	-.-
37	1670	0.146	248.30	0.124	0.118	(± 0.0026)	81	-.-	-.-
38	1700	0.141	212.57	0.113	0.101	(± 0.0015)	81	-.-	-.-
39	1700	0.142	314.50	0.103	0.114	(± 0.0041)	71	-.-	-.-
40	1730	0.146	342.84	0.094	0.081	(± 0.0024)	81	-.-	-.-
I	----	-.---	---.--	-.---	-.---	-.---	-	2189.27	0.144
II	----	-.---	---.--	-.---	-.---	-.---	-	3264.25	0.142
III	----	-.---	---.--	-.---	-.---	-.---	-	2146.97	0.144
IV	----	-.---	---.--	-.---	-.---	-.---	-	2619.13	0.144
V	----	-.---	---.--	-.---	-.---	-.---	-	2028.80	0.144
Mean	1670	0.146	244.53	0.123	0.114			2449.68	0.144
s.e.	(±20)	(±0.001)	(±22.57)	(±0.008)	(±0.006)			(±226.81)	(±0.0004)
n	8	8	8	7	8			5	5

Soil: Urrbrae
Treatment: Aged 7 Days

Disk #	ρ_b ($kgkg^{-3}$)	w ($kgkg^{-3}$)	TS (kPa)	σ_R-ST (mm)	$\bar{\sigma}_R$-MT (mm)	(± s.e.) (mm)	laser scans	Q_p (kPa)	w ($kgkg^{-3}$)
41	1730	0.149	325.87	0.128	0.118	(± 0.0030)	81	-.-	-.-
42	1670	0.147	371.11	0.077	0.100	(± 0.0029)	61	-.-	-.-
43	1740	0.148	294.74	0.113	0.087	(± 0.0007)	81	-.-	-.-
44	1690	0.146	298.45	0.093	0.106	(± 0.0012)	51	-.-	-.-
45	1730	0.148	322.96	0.093	0.096	(± 0.0025)	81	-.-	-.-
46	1720	0.152	397.95	0.187	0.149	(± 0.0049)	81	-.-	-.-
47	1640	0.152	279.51	0.115	0.092	(± 0.0017)	76	-.-	-.-
48	1770	0.147	298.25	0.088	0.094	(± 0.0019)	81	-.-	-.-
49	1660	0.140	293.35	0.117	0.097	(± 0.0021)	81	-.-	-.-
50	1710	0.144	228.91	0.120	0.114	(± 0.0016)	81	-.-	-.-
I	----	-.---	---.--	-.---	-.---	-.---	-	3167.04	0.142
II	----	-.---	---.--	-.---	-.---	-.---	-	3112.76	0.143
III	----	-.---	---.--	-.---	-.---	-.---	-	3370.06	0.142
IV	----	-.---	---.--	-.---	-.---	-.---	-	2987.61	0.142
V	----	-.---	---.--	-.---	-.---	-.---	-	3319.40	0.142
Mean	1710	0.147	311.11	0.113	0.105			3191.37	0.142
s.e.	(±10)	(±0.001)	(±14.97)	(±0.010)	(±0.006)			(±69.50)	-.---
n	10	10	10	10	10			5	5

(continued.....)

(...Table A5-1 cont'd.)
Soil: Urrbrae
Treatment: Aged 14 Days

Disk #	ρ_b (kgkg^{-3})	w (kgkg^{-3})	TS (kPa)	σ_R-ST (mm)	$\bar{\sigma}_R$-MT (mm)	(± s.e.) (mm)	laser scans	Q_p (kPa)	w (kgkg^{-3})
51	1790	0.147	310.17	-.---	0.090	(± 0.0032)	81	-.-	-.-
52	1710	0.151	349.37	0.113	0.095	(± 0.0020)	81	-.-	-.-
53	1680	0.153	316.03	0.085	0.084	(± 0.0010)	71	-.-	-.-
54	1790	0.147	334.06	0.162	0.097	(± 0.0021)	81	-.-	-.-
55	1740	0.145	400.51	0.080	0.098	(± 0.0016)	81	-.-	-.-
56	1770	0.156	423.54	0.119	0.089	(± 0.0010)	81	-.-	-.-
57	1680	0.150	361.81	0.123	0.148	(± 0.0038)	81	-.-	-.-
58	1740	0.146	345.27	0.144	0.096	(± 0.0029)	81	-.-	-.-
59	1730	0.147	413.40	0.129	0.090	(± 0.0017)	81	-.-	-.-
60	1780	0.153	399.81	0.089	0.089	(± 0.0020)	76	-.-	-.-
I	----	-.---	---.--	-.---	-.---	-.---	-	1548.27	0.146
II	----	-.---	---.--	-.---	-.---	-.---	-	3214.71	0.144
III	----	-.---	---.--	-.---	-.---	-.---	-	2588.19	0.143
IV	----	-.---	---.--	-.---	-.---	-.---	-	2512.45	0.142
V	----	-.---	---.--	-.---	-.---	-.---	-	3162.18	0.143
Mean	1740	0.150	365.40	0.116	0.098			2605.16	0.144
s.e.	(±10)	(±0.001)	(±13.02)	(±0.009)	(±0.006)			(±300.64)	(±0.001)
n	10	10	10	9	10			5	5

Soil: Portneuf
Treatment: Non-Aged Control

Disk #	ρ_b (kgkg^{-3})	w (kgkg^{-3})	TS (kPa)	σ_R-ST (mm)	$\bar{\sigma}_R$-MT (mm)	(± s.e.) (mm)	laser scans	Q_p (kPa)	w (kgkg^{-3})
91	1580	0.147	213.77	0.191	0.111	(± 0.0020)	81	-.-	-.-
92	1600	0.149	255.94	0.096	0.108	(± 0.0025)	81	-.-	-.-
93	1620	0.150	155.63	0.119	0.098	(± 0.0021)	81	-.-	-.-
94	1600	0.152	234.60	0.147	0.113	(± 0.0025)	81	-.-	-.-
95	1610	0.164	213.62	0.144	0.110	(± 0.0021)	76	-.-	-.-
96	1610	0.156	292.29	0.112	0.113	(± 0.0040)	81	-.-	-.-
97	1610	0.150	300.31	0.100	0.097	(± 0.0012)	81	-.-	-.-
98	1560	0.153	271.57	0.087	0.112	(± 0.0034)	81	-.-	-.-
99	1590	0.151	154.95	0.149	0.116	(± 0.0023)	81	-.-	-.-
100	1640	0.159	150.64	0.109	0.103	(± 0.0023)	76	-.-	-.-
I	----	-.---	---.--	-.---	-.---	-.---	-	4546.61	0.148
II	----	-.---	---.--	-.---	-.---	-.---	-	4866.42	0.144
III	----	-.---	---.--	-.---	-.---	-.---	-	4225.55	0.140
IV	----	-.---	---.--	-.---	-.---	-.---	-	4105.51	0.149
V	----	-.---	---.--	-.---	-.---	-.---	-	4073.07	0.147
Mean	1600	0.153	224.33	0.125	0.108			4363.43	0.146
s.e.	(±7)	(±0.002)	(±17.93)	(±0.010)	(±0.002)			(±151.06)	(± 0.002)
n	10	10	10	10	10			5	5

(continued.....)

(...Table A5-1 cont'd.)
Soil: Portneuf
Treatment: Aged 7 Days

Disk #	ρ_b ($kg\,kg^{-3}$)	w ($kg\,kg^{-3}$)	TS (kPa)	σ_R-ST (mm)	$\bar{\sigma}_R$-MT (mm)	(± s.e.) (mm)	laser scans	Q_p (kPa)	w ($kg\,kg^{-3}$)
101	1620	0.142	254.88	0.179	0.134	(± 0.0028)	81	-.-	-.-
102	1600	0.149	315.04	0.126	0.096	(± 0.0014)	81	-.-	-.-
103	1620	0.152	214.33	0.124	0.104	(± 0.0024)	81	-.-	-.-
104	1550	0.139	312.39	0.116	0.124	(± 0.0029)	81	-.-	-.-
105	1650	0.151	312.38	0.129	0.091	(± 0.0023)	71	-.-	-.-
106	1590	0.131	316.21	0.139	0.117	(± 0.0021)	81	-.-	-.-
107	1610	0.140	330.71	0.135	0.115	(± 0.0017)	81	-.-	-.-
108	----	-.---	---.--	-.---	0.105	(± 0.0019)	81	-.-	-.-
109	1640	0.138	292.34	0.095	0.100	(± 0.0020)	81	-.-	-.-
110	1620	0.136	182.31	0.119	0.107	(± 0.0019)	81	-.-	-.-
I	----	-.---	---.--	-.---	-.---	-.---	-	4487.09	0.139
II	----	-.---	---.--	-.---	-.---	-.---	-	6322.60	0.139
III	----	-.---	---.--	-.---	-.---	-.---	-	6803.01	0.142
IV	----	-.---	---.--	-.---	-.---	-.---	-	6751.85	0.140
V	----	-.---	---.--	-.---	-.---	-.---	-	6443.64	0.135
Mean	1610	0.142	281.18	0.129	0.109			6161.64	0.139
s.e.	(±10)	(±0.002)	(±17.41)	(±0.008)	(±0.004)			(±428.33)	(±0.001)
n	9	9	9	9	10			5	5

Soil: Portneuf
Treatment: Aged 14 Days

Disk #	ρ_b ($kg\,kg^{-3}$)	w ($kg\,kg^{-3}$)	TS (kPa)	σ_R-ST (mm)	$\bar{\sigma}_R$-MT (mm)	(± s.e.) (mm)	laser scans	Q_p (kPa)	w ($kg\,kg^{-3}$)
111	1560	0.144	323.45	0.137	0.101	(± 0.0010)	71	-.-	-.-
112	1600	0.147	264.28	0.147	0.114	(± 0.0016)	81	-.-	-.-
113	1510	0.146	177.03	0.175	0.120	(± 0.0018)	81	-.-	-.-
114	1550	0.146	199.66	0.113	0.135	(± 0.0026)	76	-.-	-.-
115	1670	0.152	326.36	0.127	0.093	(± 0.0018)	81	-.-	-.-
116	1550	0.142	286.18	0.127	0.101	(± 0.0030)	81	-.-	-.-
117	1570	0.140	242.59	0.127	0.101	(± 0.0013)	81	-.-	-.-
118	1550	0.139	228.10	0.121	0.107	(± 0.0020)	81	-.-	-.-
119	1600	0.146	320.84	0.135	0.102	(± 0.0018)	81	-.-	-.-
120	1590	0.139	366.94	-.---	0.095	(± 0.0006)	81	-.-	-.-
I	----	-.---	---.--	-.---	-.---	-.---	-	5264.47	0.144
II	----	-.---	---.--	-.---	-.---	-.---	-	5098.51	0.144
III	----	-.---	---.--	-.---	-.---	-.---	-	7537.96	0.142
IV	----	-.---	---.--	-.---	-.---	-.---	-	6714.41	0.136
V	----	-.---	---.--	-.---	-.---	-.---	-	5108.49	0.143
Mean	1580	0.144	273.54	0.134	0.107			5944.77	0.142
s.e.	(±10)	(±0.001)	(±19.52)	(±0.006)	(±0.004)			(±500.45)	(± 0.001)
n	10	10	10	9	10			5	5

-(END OF TABLE A5-1)-